Biggs, Manus Jonathan Paul (2009) The influence of nanotopographical structures on osteoblast adhesion formation and the functional response of mesenchymal stem cell populations. PhD thesis

http://theses.gla.ac.uk/552/

The Influence of Nanotopographical Structures on Osteoblast Adhesion Formation and the Functional Response of Mesenchymal Stem Cell Populations

Manus Jonathan Paul Biggs

For the degree of PhD at the University of Glasgow, UK

November 2008

AO Research Institute,
Clavadelerstrasse
CH 7270 Davos
Switzerland

Centre for Cell Engineering,
Division of Infection and Immunity,
University of Glasgow, G12 8QQ
United Kingdom

It is predicted that the percentage of persons over 50 years of age affected by bone diseases will double by 2020 (Navarro *et al.*, 2008). Clearly this represents a need for permanent, temporary or biodegradable orthopaedic devices that are designed to substitute or guide bone repair. Polymeric medical devices are widely used in orthopaedic surgery and play a key role in fracture fixation and in areas of orthopaedic implant design. Initial uncertainty regarding the adequacy of polymeric materials to withstand functional stresses obliged clinicians to implement these biomaterials in non-load-bearing applications such as fixation of the maxillofacial skeleton. Strategies to guide bone repair, have included topographical modification of these devices in an attempt to regulate cellular adhesion, a process fundamental in the initiation of osteoinduction and osteogenesis.

Advances in fabrication techniques have evolved the field of surface modification and, in particular, nanotechnology has allowed the development of experimental nanoscale substrates for the investigation into cell-nanofeature interactions. This thesis is concerned with the study of nanotopographical structures on osteoblast adhesion and mesenchymal stem cell (MSC) function, with an aim to improving the functionality of orthopaedic craniomaxillofacial devices.

In this study primary human osteoblast (HOBs) were cultured on nanoscale topographies fabricated by lithographic and phase separation techniques in poly(methyl methacrylate) (pMMA). Adhesion subtypes in HOBs were quantified by immunofluorescent microscopy and cell-substrate interactions investigated via immunocytochemistry with scanning electron microscopy. To investigate the effects of these substrates on cellular function 1.7 K microarray analysis was employed to study the changes in gene profiles of enriched MSC populations cultured on these nanotopographies.

Nanotopography differentially affected the formation of adhesions in HOBs and induced significant changes in genetic expression of MSCs on experimental substrates. Nanopit type topographies fabricated by electron beam lithography were shown to inhibit directly the formation of large adhesion complexes in HOBs and induce significant down-regulation of canonical signalling and functional pathways in MSCs. Nanocrater and nanoisland type topographies fabricated by polymer demixing however reduced adhesion formation and induced up-regulation of osteospecific pathways. Nanogrooved

topographies fabricated by photolithography influenced HOB adhesion formation and MSC osteospecific function in a manner dependant on the groove width.

The findings of this study indicate that nanotopographical modification significantly modulates both osteoblast adhesion and MSC function, implicating topographical modification as a viable strategy to enhance orthopaedic device functionality.

Contents

This thesis is dedicated to the memory of my mother Valerie, who was always hugely supportive of my decision to peruse a doctoral degree and who helped to make me the person I am today. I miss you very much.

I would like to thank my supervisors Profs Chris Wilkinson and Geoff Richards for all their invaluable advice. You have both been a great source of expertise and have aided me immensely over the past four years.

I specifically thank my primary supervisor, mentor and friend Dr Matt Dalby. Without whom there would be no hypothesis, no data and no thesis. Your time, patience and guidance throughout my doctoral studies was constant and you have been hugely influential in defining the scientist that I am today, and the future course of my career. I thank you sincerely.

I extend my gratitude to all at CCE especially Adam, Cath, Mathis, Nikolaj and Andy. You have all in your own way been instrumental in the successful completion of my studies at CCE. I would also like to acknowledge all the students working in CCE and AO whom I have befriended on my convoluted path to enlightenment, you have made the PhD process both enjoyable and rewarding, *Bonum amicitia et vinum laetificat cor hominis.*

I acknowledge all involved in the substrate fabrication process, John Pedersen (SDC Dandisc A/S, Denmark) for the organising and preparation of nickel shims and Mrs. Mary Robertson, Ms. Sara McFarlane and Mr. Davie McCloy for their help with embossing and characterisation. This work was funded by the AO Research Fund, Switzerland; Grant Number: 04-D81.

Finally heartfelt thanks to my companion, partner and friend Vanessa Phelan for bringing love, laughter and support to my life when I needed it most. Without your tireless encouragement and devotion this thesis would never have reached completion. I am forever indebted to you.

I hereby declare that the research reported within this thesis is my own work, unless other wise stated, and that at the time of submission is not being considered elsewhere for any other academic qualification.

Manus Biggs

November 1st 2008

A list of abstracts accompanying oral presentations given by the candidate.

Biggs MJ, Richards RG, Gadegaard N, Wilkinson CD, Dalby MJ: Nanoscale Biomimetic Modification of the Cell-Substrate Interface for Bone Tissue Engineering. *United Kingdom Society of Biomaterials, Manchester 2006.*

Biggs MJ, Richards RG, Gadegaard N, Wilkinson CD, Dalby MJ: Nanoscale Biomimetic Modification of the Cell-Substrate Interface for Bone Tissue Engineering. *Tissue and Cell Engineering Society, Sheffield 2006.*

Biggs MJ, Richards RG, Gadegaard N, Wilkinson CD, Dalby MJ: Nanoscale Topographical Modification for Bone Tissue Engineering. *Swiss Bone and Mineral Society, Bern 2006.*

Biggs MJ, Richards RG, Gadegaard N, Wilkinson CD, Dalby MJ: Nanoscale Biomimetic Modification of the Cell-Substrate Interface for Bone Tissue Engineering. *European Society of Biomaterials, Nantes 2006.*

Biggs MJ, Richards RG, Gadegaard N, Wilkinson CD, Dalby MJ: The Influence of Nanoscale Structures on Osteoblast Adhesion. *Society for Experimental Biology, Glasgow 2007.*

Biggs MJ, Richards RG, Gadegaard N, Wilkinson CD, Oreffo ROC, Affrossman S, Dalby MJ: The Influence of Nanoscale Topography on Osteoblast Adhesion and Genetic Expression. *Tissue Engineering and Regenerative Medicine, Toronto 2007.*

Biggs MJ, Richards RG, Gadegaard N, Wilkinson CD, Oreffo ROC, Affrossman S, Dalby MJ: Fabrication of Nanoscale Biomimetic Topographies. *IMCE Kyushu University-England-IMRAM Tohoku University 2nd Joint Workshop. Sendai, Japan 2008.*

Biggs MJ, Richards RG, Gadegaard N, Wilkinson CD, Oreffo ROC, Affrossman S, Dalby MJ: The Influence of Nanoscale Topography on Osteoblast Adhesion and Genetic Expression. *Invited Lecture, Stevens Institute of Technology, New Jersey, USA 2008*

Biggs MJ, Richards RG, Gadegaard N, Wilkinson CD, Oreffo ROC, Affrossman S, Dalby MJ: The Influence of Nanoscale Structures on Cellular Adhesion and Function. *Invited Lecture, Columbia University, New York, USA 2008*

Original research publications authored by the candidate on work relating to this thesis.

Biggs MJ, Richards RG, Gadegaard N, Wilkinson CD, Dalby MJ: Regulation of implant surface cell adhesion: characterization and quantification of S-phase primary osteoblast adhesions on biomimetic nanoscale substrates. *J Orthop Res* 2006, 25(2):273-282.

Dalby MJ, Biggs MJ, Gadegaard N, Kalna G, Wilkinson CD, Curtis AS: Nanotopographical stimulation of mechanotransduction and changes in interphase centromere positioning. *J Cell Biochem* 2006, 100(2):326-338.

Biggs MJ, Richards RG, Gadegaard N, Wilkinson CD, Dalby MJ: The effects of nanoscale pits on primary human osteoblast adhesion formation and cellular spreading. *J Mater Sci; Mater Med 2007,* 18:399-404.

Biggs MJ, Richards RG, Gadegaard N, Wilkinson CD, Oreffo ROC, Affrossman S, Dalby MJ: Adhesion formation of primary human osteoblasts and the functional response of mesenchymal stem cells to 330 nm deep microgrooves. *J R Soc. Interface 2008*, 27(5):1231-1242.

Biggs MJ, Richards RG, Wilkinson CD, Dalby MJ: Focal adhesion interactions with nanostructures: A novel method for immuno-SEM labelling of focal adhesions in S-phase cells. *J Microsc 2008,* 231:28-37.

Biggs MJ, Richards RG, Gadegaard N, Wilkinson CD, Oreffo ROC, Affrossman S, Dalby MJ: Interactions with nanoscale topography: Adhesion quantification and signal transduction in cells of osteogenic and multipotent lineage. *J biomed Mater Res A 2008*.

Chapter I: General Introduction

Chapter II: Materials and Methodology

Chapter III: Protocol Development

Chapter IV: Nanoscale Pits

Chapter V: Random Nanoscale Islands and Craters

Chapter VI: 300 nm Deep Microgrooves

Chapter VII: Discussion

Table index

α-MEM	alpha minimal essential medium
AFM	atomic force microscope (microscopy)
ALP	alkaline phosphotase
ANOVA	analysis of variance
apt1	aperture 1
BrdU	5-bromo-2-deoxyuridine
BSA	bovine serum albumen
BSE	back-scattered electron
cDNA	complementary (signal stranded) DNA
CK1	cytoplasmic casein kinase 1
CMF	craniomaxillofacial
CO_2	carbon dioxide
CPB	Ca^{2+}/cAMP-response elements binding protein
DAPI	4'-6-Diamidino-2-phenylindole
DNA	deoxyribonucleic acid
EBL	electron beam lithography
E. coli	*Escherichia coli*
ECM	extracellular matrix
EDTA	ethylenediaminetetraacetic acid
ERK	extracellular signal-regulated kinases
FA	focal adhesion
FAK	focal adhesion kinase
FCS	foetal calf serum
fig	figure
FITC	fluorescein isothiocyanate
FX	focal complex
g	acceleration due to gravity
G1	growth phase 1
G2	growth phase 2
G-protein	guanine nucleotide-binding proteins
HBSS	HEPES buffered saline solution
HEPES	4-(2-hydroxyethyl)-1-piperazineethanesulfonic acid
HOB	primary human osteoblast
IGF-I	insulin-like growth factor-1
IgG	immunoglobulin G
IgM	immunoglobulin M
IPA	Ingenuity Pathway Analysis
MACS	magnetic activated cell sorting
MAPK	mitogen-activated protein kinase
mDia1	mammalian diaphanous protein 1
mRNA	messenger ribonucleic acid
MSC	mesenchymal stem cell
NF-kB	nuclear factor-kappa B
OGM	osteoblast growth medium
pBrS	poly(bromostyrene)
PBS	phosphate buffered saline

pC	poly(carbonate)
PCNA	proliferating cell nuclear antigen
PDGF	platelet derived growth factor
pDMS	poly(dimethylsiloxane)
pEEK	poly(etheretherketone)
PIPES	piperazine-1,4-bis(2-ethanesulfonic acid)
pMMA	poly(methyl methacrylate)
pS	poly(styrene)
p-value	probability value
Ra	average roughness
RACK1	receptor of activated C-kinase 1
RAR	retinoic acid receptor
RGDS	glycine-aspartic acid-serine motif
RGD	arginine-glycine-aspartic motif
Rmax	maximum roughness
RNA	ribonucleic acid
ROCK	Rho-associated kinase
ROH_2O	reverse osmosis water
rpm	revolutions per minute
RTK	receptor tyrosine kinase
SDS	sodium dodecyl sulfate
SE	secondary electron
SEM	scanning electron microscope (microscopy)
SMA	super-mature adhesion
SOX	sex determining region Y-like, high mobility group box
S-phase	synthesis-phase
SR	self-reinforcing
Src	Src family kinase
SSC	saline sodium citrate
STD	standard deviation
STRO-1	stromal cell surface protein
TAB1	transforming growth factor-β activated kinase-1 binding protein
TEM	transmission electron microscopy
TGF-β	transforming growth factor beta
TGFBR	transforming growth factor beta receptor
Tris	tris(hydroxymethyl)aminomethane
tRNA	transfer RNA
TRP	transient receptor potential
UV	ultraviolet
v/v	volume (of solute) per volume (of solvent)
VEGF	vascular endothelial growth factor
w/v	weight (of solute) per volume (of solvent)
w/w	weight per weight
Wnt	wingless-type mouse mammary tumor virus integration site family member
YFP	yellow fluorescent protein

CHAPTER I

General Introduction

1.1. Introduction

This thesis highlights the importance/development of the physiomechanical processes that regulate early cell/biomaterial interaction and the influence of nanoscale topographical modification on osteoblast adhesion and mesenchymal stem cell (MSC) function, with an aim to developing third generation cranio-facial fixation devices. As materials technology and the field of tissue engineering advances, the role of cellular adhesive mechanisms, in particular the interactions with implantable devices, becomes more relevant in both research and clinical practice.

Biomaterials are never truly inert, being at best biotolerant, and the cell-substratum interface functions as more than a simple boundary of definition between the host and an implanted device, rather it presents primary cues for cellular adhesion and subsequent induction and tissue neogenesis. Indeed, the function and cytocompatibility of a construct can be assessed *in vitro* by the observation of viability and bio-functionality of cells on a materials surface. The range of materials currently in use within biomedical applications and their lack of biofunctionality reflects the increasing need of biomimetic constructs but also indicates the challenges present within the field, i.e. to ultimately control the interactions that occur at the cell-substratum interface.

Biomimetic devices could conceivably present physical and chemical properties, which approach the physicochemical properties of tissues that they are meant to, augment or replace. The key tenet of this technology is to use the exquisite ability of biological systems to respond to topographic features or chemical stimuli in order to help develop next-generation biomaterials. Recently published in Science are the prerequisites for third-generation biomaterials; not only should they support the healing site (as first generation), but they should be bioactive and possibly biodegradable (as second generation and they should influence cell behaviour at the molecular level (Hench & Polak, 2002).

The synthetic surfaces encountered by cells following prosthetic device implantation usually possess an imposed topography from the fabrication processes, perhaps uncharacterised or unknowingly derived from their methods of manufacture (Curtis, 2004). Indeed, at the molecular level, intentionally smooth surfaces are an ideal almost impossible to accurately reproduce on a functional device surface. Topographical

microroughness may or may not be formed intentionally, however micron sized topography has been shown to play an essential role in determining cell adhesion and subsequent cellular function (Clark *et al.*, 1987, Clark *et al.*, 1991, Tanaka *et al.*, 2007).

In order to investigate the reaction elicited by a material *in vivo* an understanding is required of the roles played by the cytoskeleton, cellular membranes, and the extracellular matrix (ECM) following introduction of a foreign material. Increased knowledge of the extra cellular environment, topographical and chemical cues present at the cellular level and how cells react to these stimuli has resulted in the development of functionalised surfaces via topographical modification with an aim to regulate cell attachment and subsequent cellular processes. While microscale topography significantly modulates cellular behaviour *in vitro*, an important consideration in material biophysical modification is the observation that cells *in vivo* contact with nanoscale as well as microscale topographic features, and while single cells are typically tens of microns in diameter, subcellular structures including cytoskeletal elements, transmembrane proteins and filopodia tend towards the nanoscale. Further to this, extracellular supporting tissues also typically present an intricate network of cues at the nanoscale. For instance, basement membranes of various tissues are composed of a complex mixture of nm size (5–200 nm) pits, pores, protrusions, and fibres (Brody *et al.*, 2006, Karuri *et al.*, 2004), suggesting a regulatory role for these structures *in vivo*.

The use of lithographic and dry etching techniques derived from the silicon microelectronics industry has facilitated the investigation into the intricate influence of nanoscale topography on all aspects of cellular function. The focus of this first chapter is on recent *in vitro* studies considering cellular interactions with fabricated nanoscale topographies, with an emphasis on the modulation of cellular adhesion in craniomaxillofacial (CMF) internal fixation. We examined the hypothesis that nanoscale topographies affect both cellular adhesion and adhesion-related cell function by reviewing the state of the art of experimental nanotopographies in relation to cellular adhesion formation, cytoskeletal organisation and the functional response.

Topography will be discussed in greater detail at the end of this chapter.

1.2. Regenerative Medicine

The idea that biological tissues can be induced to undergo enhanced regeneration in the absence of spontaneous repair has at its heart a theme of interdisciplinary cooperation. The successful development of an engineered tissue requires intellectual and practical expertise from engineers and biological science alike, as well as clinicians to voice a want for these advances and to help translate this basic science into clinical solutions (fig.1.1). Indeed tissue engineering can be regarded as the third therapy of regenerative medicine along with the two major clinical therapies, organ transplantation and reconstructive surgery (Tabata, 2001). As understanding of mechanisms and predictive outcomes of specific diseases are developed, so too are the potential therapeutic targets for tissue engineered constructs; this lends new hope for solutions to degenerative disease. Tissue engineering can also been described as life-increasing therapy, a title that can be justified by the potential to engineer new tissues and organs.
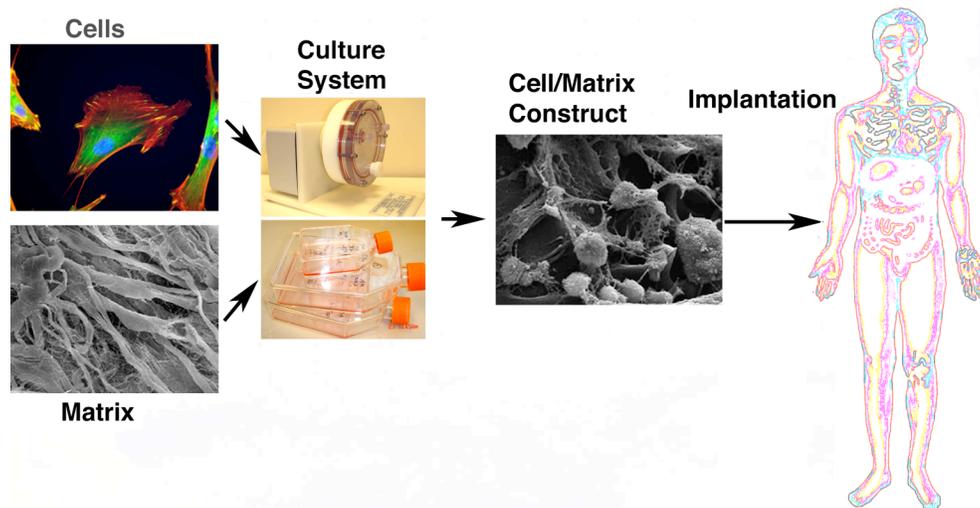
Fig. 1.1. The central dogma of tissue engineering (Biggs, unpublished work). Cells are isolated and combined *in vitro* with a suitable scaffold system. Culture systems are utilised to encourage cellular infiltration and proliferation before being transplanted to a site of disease or compromise.

It is envisaged that new constructs capable of providing the vital biochemical and biophysical milieus to a population of cells could essentially regulate cellular behaviour and function. The repertoire of biomaterials that are currently being used and/or

investigated for the technology and methodology of tissue engineering is constantly being revised and updated. However, the use of these materials varies depending upon their desired application (Tabata, 2004). Since the inception of tissue engineering nearly 20 years ago in reference to the endothelial-like membrane that had adhered to the surface of a polymethylmathacrylate ophthalmic prosthesis (Wolter & Meyer, 1984), the field of biomaterials has seen a consistent growth with a steady introduction of new ideas and productive branches, particularly in the development of small technology encompassing micro and nano materials.

1.3. Bone Tissue Engineering

Bone regeneration represents a major challenge in the field of tissue engineering due to the multifunctional roles carried out by mineralised tissues in homeostasis. Load bearing or bridging biomaterials are typically utilised to repair or replace damaged or diseased bone maintaining structural integrity and allowing new bone formation to occur (Zaffe *et al.*, 2003) (fig 1.2). As the life expectancy of the developed world increases coupled with an increasing ageing population, the need for improved surgical intervention into bone degeneration is increased and so are the challenges for scientists working within this field. Bone resorption associated with osteoporotic remodelling, bone microcrack formation, fatigue and fracture are common problems associated with such an increase in life expectancy, all dramatically reducing the quality of life for such individuals.

Bone associated neoplastic malignancies, often associated with primary tumour site metastases also result in a loss of bone mass and function, commonly resulting in large bone defects, immobilisation and reabsorption of mineralised bone (Coleman, 2006, Kinder *et al.*, 2008, Quattrocchi *et al.*, 2007).
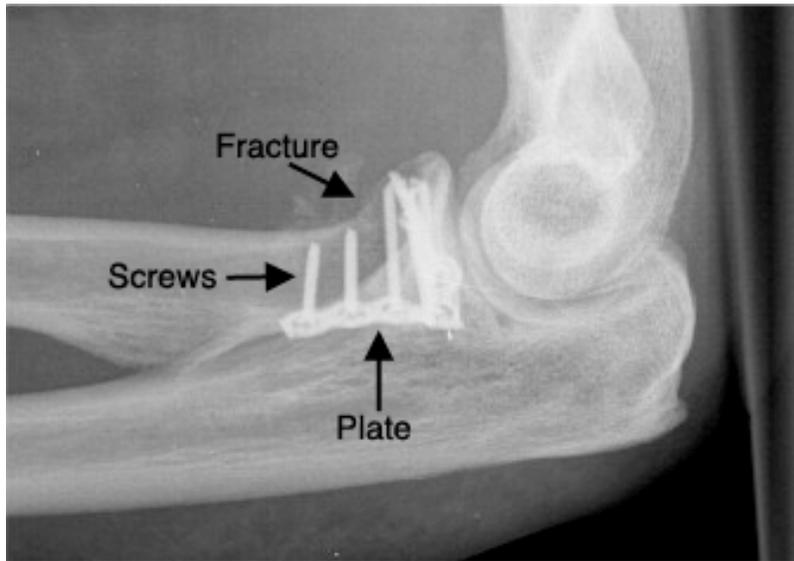
Fig. 1.2 Internal fixation of the proximal radius, adapted from (Ring, 2008). Rigid internal fixation is the technique of choice for surgical intervention in fracture of the radial head as seen above. Opposing fracture surfaces are held firmly in place with steel or titanium plates and screws.

Due to the relatively low levels of stress and compressive forces exerted in the bones of CMF region (mandibular body and rami being the exception), the need for load bearing constructs in CMF repair is replaced by the need for plates and screws which ensure fractured bone remain closely opposed and do not fail under the high tortional forces (Seebeck *et al*., 2005) exerted during implantation. Effective repair of bone defects of the calvaria and maxillo-facial area in response to traumatic, inflammatory or neoplastic lesions still represents a major challenge in neuro and plastic surgery. In the CMF skeleton, osseous fixation techniques most often applied are internal fixation with metal or bioresorbable plate systems (fig. 1.3) (Kosaka *et al*., 2003b).
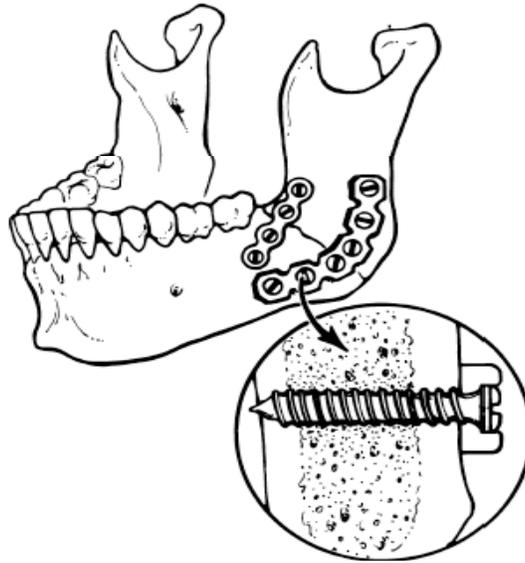
Fig. 1.3. Mandibular plates and screws, adapted from (Gear et al., 2005). Intraoperative maxillomandibular fixation along with rigid internal fixation is the technique of choice for surgical intervention in mandible angle fracture. Opposing fracture surfaces are held firmly in place with steel or titanium plates and screws.

1.4. Biomaterials in Craniomaxillofacial Repair

In the context of implantable biomaterials, bone fracture fixation was addressed early on in the development of the field with therapies reportedly utilising iron wires in 1775 (Laing, 1979). The evolution and progression of the science of cranioplasty has been closely linked to the instance of war injuries and road accidents and the state of the art, as with general fracture fixation, has significantly improved with accelerated research into this area. The primary objective of cranioplastic procedures is ultimately to restore the continuity of the normal bony tissues and pericranial structures in such a way that results in a satisfactory cosmetic outcome. At present this objective is ideally obtained using permanent or durable biologically inert materials, however CMF reconstruction techniques can be traced back to ancient times. Archaeological evidence has unearthed artefacts indicating that prehistoric South Pacific populations used coconut shells to repair gaps in the skull and that even prehistoric Peruvians performed a type of cranioplasty using gold plates (Artico *et al.,* 2003).

The 20th century has introduced an increasing repertoire of alloplastic materials for cranioplastic reconstruction. Aluminium, gold, tantalum, stainless steel, titanium, acrylic

resins, polyethylene, silicone elastomeres, and ceramics have all been investigated as to their suitability for such an application (Buchel *et al.*, 2005, Turvey *et al.*, 2002). However, alloplastic materials are not the best solution to this problem because they present various limitations and complications resulting from the materials mechanical and thermal properties, and from the host's elicited *in vivo* reactions to the materials and their by-products. For example, Kudelska-Mazur *et al.,* have reported on the decreased viability and focal adhesion (FA) formation of osteoblasts cultured on polished surgical steel in relation to polished titanium (Kudelska-Mazur *et al.,* 2005). They argue this is predominantly due to problems associated with steel corrosion products. Clearly the bulk material choice upon to which we wish to impart bioactivity is critical.

A need exists for orthopaedic biomaterials with optimised mechanical and physical properties. Constructs should be capable of stimulating osseoinduction while minimising fibrous capsule formation (when implanted in bone), foreign body mediated inflammation, and musculotendon adhesion. In CMF surgery, bone fixation methods should offer excellent three-dimensional stability for multiple, different sized bone segments. Nonresorbable alloplastic implants usually represent permanent foreign bodies and can be associated with innate complications including infection, extrusion, implant migration, recurrent haemorrhage, and residual diplopia (Shibahara *et al.,* 2002), which may ultimately require removal of the implant, sometimes many years postoperatively. Indeed Kosaka, *et al.* have reported on the tendency of steel wires in cranial surgery to migrate cerebrally which has obvious complications (Kosaka *et al.,* 2003a). These problems may be regulated by the use of bioactive biomaterials, in particular by the new generation of biomimetic materials in development.

The ideal material for primary reconstruction of CMF defects is autogenous bone. There is no need for extensive and costly preoperative planning, and the biocompatibility is uniquely optimal. However, the availability of autogenously bone donor sites in CMF repair is extremely limited, coming predominantly from retromolar tissue or from the iliac crest, a procedure typically requiring a second intervention and introducing an increased risk of complication (Beirne *et al.*, 1996, Kline & Wolfe, 1995, Raghoebar *et al.*, 2001).

The current trend is CMF fixation is towards patient specific implants for large defects produced out of non resorbable polymers. Metal devices can obscure soft and hard tissue integration to implants during evaluation by X-ray or MRI. Poly(etheretherketone) (pEEK) has been used as a replacement for metals in CMF specific implants, due to its radiolucency.

It is therefore the role of osteoinductive biomimetic materials to bridge the gap between the shortage of available osseous donor sites (Ebraheim *et al.,* 2001) where donor site morbidity and other complications can occur and the need for a material possessing bone-like characteristics (Isaac *et al.*, 2008, Kim *et al.*, 2008, Ripamonti *et al.*, 2008). To date numerous strategies have been investigated in an attempt to enhance a biomaterials performance *in vivo* and enhance osteoblast adhesion and bone tissue formation. Osteoconductive hydroxyapatite cement (Wiltfang *et al.,* 2004), titanium modified by topographical microstructural features (Zinger *et al.,* 2004) and immobilisation of bioactive molecules to a substrate surface (Dettin *et al.,* 2005) have all been employed successfully to reduce giant cell recruitment, osteolysis and fibrous capsule formation (Fig 1.4) and promote increased osteoblast adhesion.
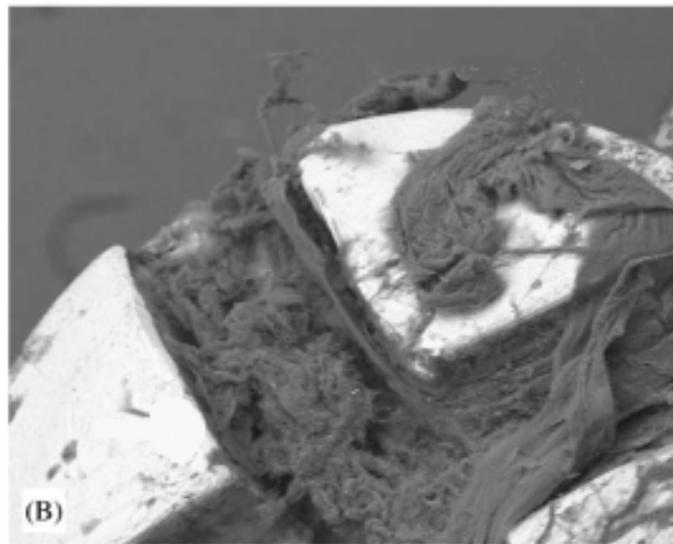
Fig. 1.4. Fibrous tissue deposition on a steel screw head, adapted from (Zaffe et al., 2003). Increased fibroblast activation and the formation of multinucleate giant cells following orthopaedic implantation can result in non-functional tissue deposition and fibrous capsule formation.

1.5. The Micro-Architecture of Bone Tissue

Bone is a viable highly dynamic structural tissue capable of sustained growth and repair throughout adult life. The strength of bone lies in its unique fibrous and trabecular structure that gives osseous tissue a maximum strength to weight ratio. A rigid yet lightweight skeleton makes possible the distribution of force exerted on the body due to gravity, whilst providing the mechanical machinery necessary for locomotion and ensuring adequate protection for the vital organs. In addition, bone is the primary site of haematopoiesis, maintaining the circulating cellular component of the haemolymphoid system by providing a reservoir of developing red and white blood cells. Bone also participates in the maintenance of serum-mineral metabolism and is considered an important component of the immune system.

Bone preserves the generalised organisation of all of the connective tissues as a native population of mesenchymal cells within a fibrous matrix. The term connective tissue is a general one used to describe a group of tissues with a variety of diverse functions. The connective tissue proper develops from embryonic mesenchyme, the derivative of embryonic mesoderm and neural crest ectoderm and serves as a primitive supporting tissue to convey the blood vessels and neurons to supply the mesenchymal cells of bone tissue (George-Weinstein *et al*., 1998, Guarino, 1995). Osteoblasts can be identified as forming aggregates at the bone periphery, where they produce and maintain a specialised ECM known as 'osteoid' (Meyer, 1956, Palumbo *et al*., 2004). Bone formation is directed through one of two ossification pathways. Firstly intramembranous bone formation, characteristic of many flat bones and the skull, occurs within mesenchymal tissue following recruitment of osteocytes and the deposition of osteoid (Bernard & Pease, 1969, Bevelander & Johnson, 1950, Blumer *et al*., 2006). Secondly, endochondral ossification, characteristic of the long bones and vertebral column is accomplished by the ossification of an initially cartilaginous tissue (Watanabe, 1965).

Cortical bone forms a compact bony layer at the bone periphery. It is a dense outer shell, which provides the hard continuous bony surface of mature bones. Cancellous bone is a honeycomb - like structure comprised of many bony trabeculae formed into struts, (fig. 1.5). These structures are typically orientated along lines of force resulting from

mechanical loading. Trabeculae are abridged by perpendicular trabecular projections, strengthening this deep network of anastomosing bony plates.

Viable bone is composed of numerous interconnected units termed Haversian systems. These units are roughly cylindrical in shape and possess a long axis parallel to the long axis of mature bone. The central domain of these Haversian systems is occupied by a single Haversian canal - an aperture containing blood vessels and lymphatic as well as loose connective tissue, surrounded by concentric layers of mineralised matrix termed lamellae, which are established by residing osteoblasts and maintained by entrapped osteocytes as discussed in (Birch de, 1880, Fell & Robison, 1934).
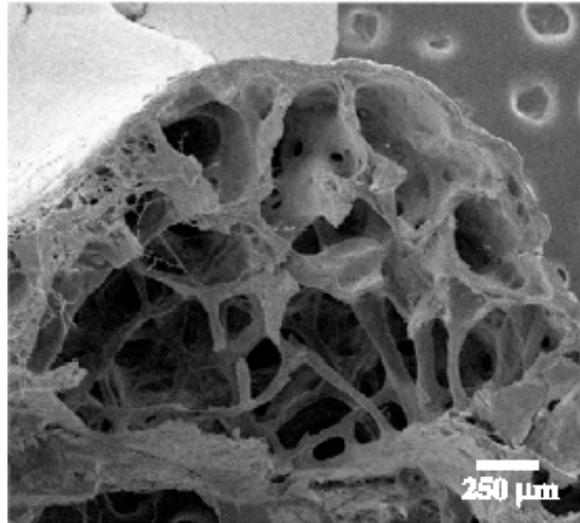
Fig. 1.5. The trabecular mesostrcture of bone, adapted from (Rubin et al., 2004). Cancellous bone is formed by many vertical and transverse interconnecting trabeculae that impart bone with light-weight strength.

Bone extracellular tissue is a natural composite biomaterial with a complex hierarchical structure, composed of a macromolecular network including proteins, glycoproteins, and polysaccharides, providing an environment rich in both biochemical and topographical cues. Cortical bone is composed of elongated, cylindrical osteons of about 10-500 μm in diameter (Rho *et al.*, 1998). Each osteon is a cylinder consisting of multiple concentric lamellae of about 3-7 μm in thickness (Giraud-Guille, 1988). Collagen within each lamellae is arranged into parallel bundles which lie obliquely relative to adjacent lamellae (Rubin *et al.*, 2004), in addition collagen molecules aggregate into highly ordered fibrils,

composed of three protein chains, wound together in a triple helix of about 300 nm length (Wagner & Weiner, 1992) which also present a banded pattern at the ultra structural level composed of 69-nm repeat banding units (Bozec *et al.*, 2005, Brodsky & Persikov, 2005, Rubin *et al.*, 2004), these are permeated within the ECM with nanoscale crystals of apatite (Ricard-Blum & Ruggiero, 2005). Bone tissue itself may be viewed as a dynamic and self-regulated collection of nano and microscale structures (fig. 1.6 & 1.7).
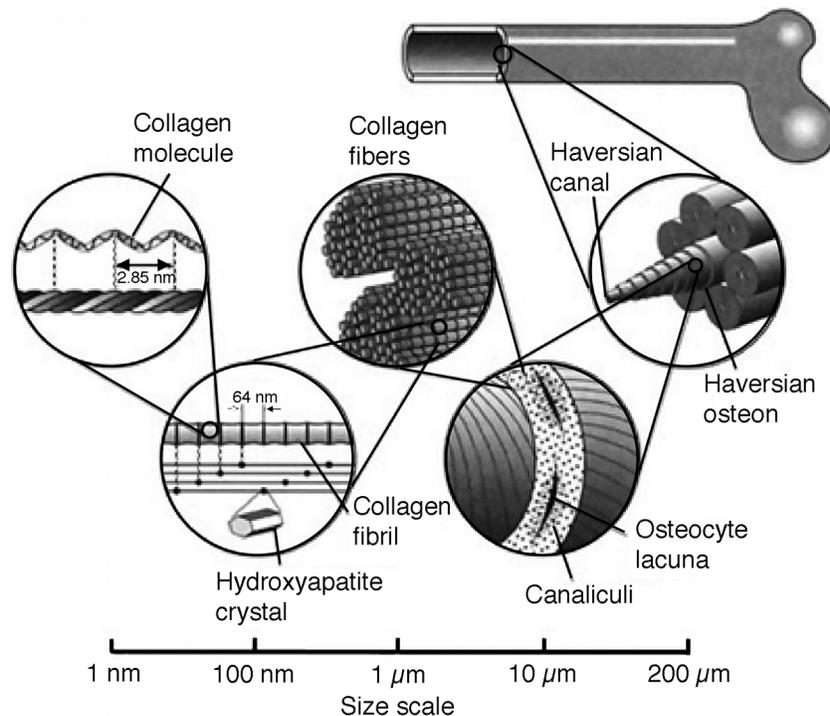
Fig. 1.6. Schematic overview of the nano and micro constituents of bone, adapted from (Ruppel et al., 2008). The hierarchical architecture of bone can be viewed as a complex system of nano and microstructures. Like all composite materials, each constituent of bone has a different, but intimately related, contribution to the overall integrity of the tissue.

Collagen is initially deposited by osteoblasts in an unordered loosely arranged manner termed woven bone, a process recapitulated in developing tissue or fracture healing. Woven bone has been shown to be composed of ECM proteins differing from those of mature lamellar bone, osteocyte number and lacunae size are also seen to be relatively increased (Hernandez *et al.*, 2004). Between the concentric lamellae are located the lacunae and the osteocytes therein. Caniculi containing the processes of these osteocytes, as well as interspaced Volkmann's canals, radiate from the Haversian canal to allow for

the exchange of nutrients between the haematopoietic and osseous fluid systems. (Ricard-Blum & Ruggiero, 2005). Thus in addition to intercellular communication by gap junctions, the cells making up this bony network remain in contact via their common environment - a contiguous proteoglycan filled fluid network (Knothe Tate, 2003).
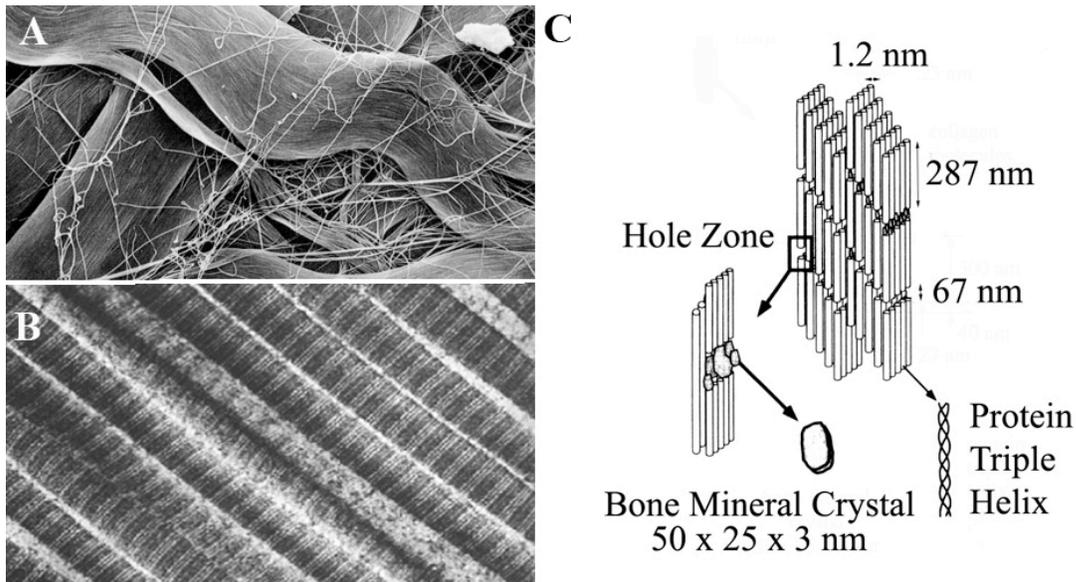
Fig. 1.7. The hierarchical micro and nanoarchitecture of mineralised tissue, adapted from (Rho et al., 1998). (A) Collagen molecules are arranged into large fibril aggregates (B) Individual collagen fibrils demonstrate a regular banding structure composed of 67-nm repeat banding. These are permeated with nanoscale crystals of apatite.

Bone can be considered a specialised connective tissue, differing primarily from connective tissue proper by the large amount of inorganic calcium found within its ECM. Mineralisation is achieved by the deposition of apatite crystals $Ca_{10}(PO_4)_6(OH)_2$, and incorporation of calcium into the ECM collagens and proteoglycans. Like all composite materials, each constituent of bone has a different, but intimately related, contribution to the overall quality of the tissue. A typical bone consists of bone tissue, other connective tissues such as fibrocartillage, epithelial tissue, smooth muscle tissue, and nerve tissue. Bone tissue itself, however, can be described as mineralised connective tissue synthesised and maintained by the three cell types described in detail below.

1.6. The Osteoblast

Osteoblasts reside on all bony surfaces and may either be active or inactive depending on the activity of the tissue, however inactive osteoblasts, termed bone-lining cells, are predominantly localised to the periosteum. They become activated as functional osteoblasts in response to mechanical or biochemical stimuli typically arising from microcrack formation or cell necrosis. A fraction of these cells become embedded within the matrix of the bone proper and remain seconded as osteocytes (Pawlicki, 1975).

The osteoblast is one of the two cell lineages, the other being the osteoclast (see section 1.8), that work together to actively remodel and maintain healthy bone tissue (fig. 1.8). The process of osteoblast differentiation leading to bone mineralisation is a poorly understood series of temporally and spatially coordinated events occurring on the magnitude of weeks and months. A significant endpoint in this process is the creation of a mineralised matrix that consists mainly of collagen, non-collagenous proteins and hydroxyapatite. Osteoblasts, are derived from MSCs, the protagonist cells of skeletogenesis (fig. 1.9).
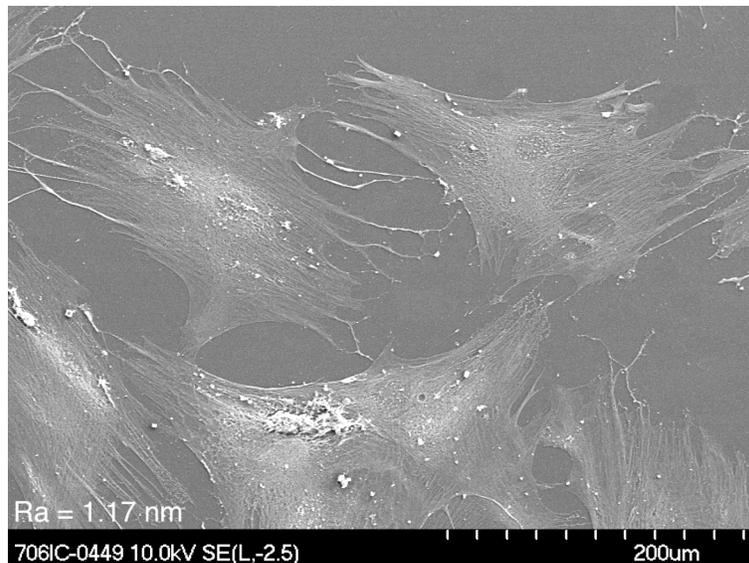
Fig. 1.8. SEM micrograph of human osteoblasts adhering to planar polymeric substrate (Biggs, unpublished work). Isolated osteoblasts appear flattened and well-spread when cultured on a planar substrate. Cell membranes have been removed to reveal the cytoskeletal structure. Note the presence of multiple cellular extensions.

Osteoblast function and proliferation is regulated by both circulating factors (growth factors, cytokines, and steroid hormones) and tissue architecture-related signals (cell–cell contact and cell-substratum adhesion); however, the role of endogenous nanotopography in this process is still unknown. In both normal developing and healing bone, osteoblastic activity is increased relative to that of osteoclast resorption. In mature bone however, there is approximately equal activity between both osteoblastic and osteoclastic lineages (Cool & Nurcombe, 2005).

Mesenchymal Stem Cell

↓ Induction

Osteoprogenitor Cell

Commitment

↓ Proliferation

Pre-Osteoblast Cell

↓ Differentiation

Osteoblast

Maturation
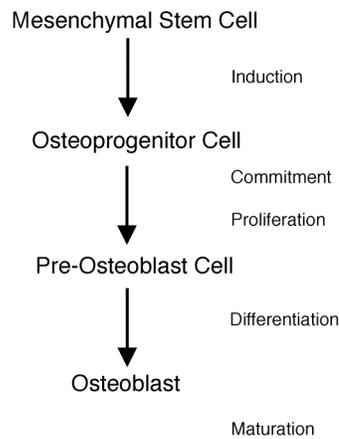
Fig. 1.9. The differentiation pathway of MSCs, adapted from (Cool & Nurcombe, 2005). MSCs become committed in response to external stimuli, i.e. mechanical loading, topography and secreted growth factors.

Osteoblasts in bone are subjected to a complex stress-strain field while residing within the ECM. In response to mechanical loading, this fibrillar collagen network exerts not only normal tensile and compressive forces on the cells but also fluid sheer stresses as a result of bone fluid movements. Indeed Tanaka *et al.* recently reported that fluid sheer stress is the major factor in induced expression of load responsive genes including osteopontin and matrix metalloproteinase 1B (Tanaka *et al*., 2005). These matrix metalloproteinases have been identified as playing a key role in osteoblast mediated bone surface resorption and have been shown to digest unmineralised osteoid. Furthermore, recent data suggest that bone-lining cells are responsible for the removal of the organic residual matrix in lacunae and that this is a matrix metalloproteinase dependent process (Mulari *et al*., 2004).

1.7. The Osteocyte

Bone remodelling is a dynamic process that repairs damaged bone tissue by resorbing and returning it to a homeostatic strain level. Although it is still unknown how mechanical loading of bone induces the highly regulated process of tissue remodelling, osteocyte survival seems to be regulated both by mechanical loading (Mann *et al*., 2006) and sheer stress (Leclerc *et al*., 2006). Bakker *et al* have reported that the absence of external mechanical forces leads to osteocyte apoptosis via the inhibition of Bcl-2 signalling (Bakker *et al*., 2004) which is typically followed by resorption of the surrounding matrix (Knothe Tate, 2003).

Osteocytes possess extensions that are tethered in the peri-cellular space to the caniculi wall via transverse filaments. These extensions contain a central bundle of actin filaments similar in appearance to that present in the microvilli of the brush border enterocyte. Osteocyte processes typically contain 15-20 of these actin filaments surrounded by a 25 nm annulus. These extensions it is argued, are sensitive to external forces in a manner similar to that of the steriocillia of the ear (Han *et al*., 2004), providing the cells with mechanotransductive cues in response to tissue strain. You *et al* have provided an elegant model indicating that this mechanotransduction occurs due to fluid drag on the pericellular matrix which is transmitted to the transverse tethering filaments in the pericellular space, producing a tensile force which is then transmitted to the cell process cytoskeleton by membrane spanning proteins (You *et al*., 2004).

It has been widely accepted that osteocytes play the largest part in the control of bone remodelling (McCreadie *et al*., 2004). These stellate shaped cells lie within mineralised lacuna (lakes) and communicate via cytoplasm extensions with adjacent osteocytes and overlying bone cells (Knothe Tate, 2003, Pawlicki, 1975). The transformation from osteoblast to mature osteocyte takes about 3 days. During this time the cell looses its mobility and becomes trapped within a volume of endogenous ECM three times its own cellular volume (Knothe Tate, 2003).

1.8. The Osteoclast

The osteoclast is a multinucleated bone-resorbing cell derived from pluripotent haematopoietic stem cells (Bar-Shavit, 2007) which reside in: spleen, bone marrow, and the peripheral blood (fig. 1.10). Osteoclasts form a part of the mononuclear phagocyte system and share many morphologic, cytochemical, and functional characteristics with tissue macrophages and macrophage polykaryons. It has been shown that human osteoclast precursors reside in the monocyte fraction and exhibit a monocyte-macrophage phenotype (Husheem *et al.*, 2005). Tissue strain experienced at bony tissues due to human and animal locomotion is typically in the region of 0.2% (Han *et al.*, 2004). Such exerted levels of strain ensure bone resorption is balanced with bone formation, and prevents loss of mineralisation via osteoclast activity, possibly by osteocyte medicated cell signalling.
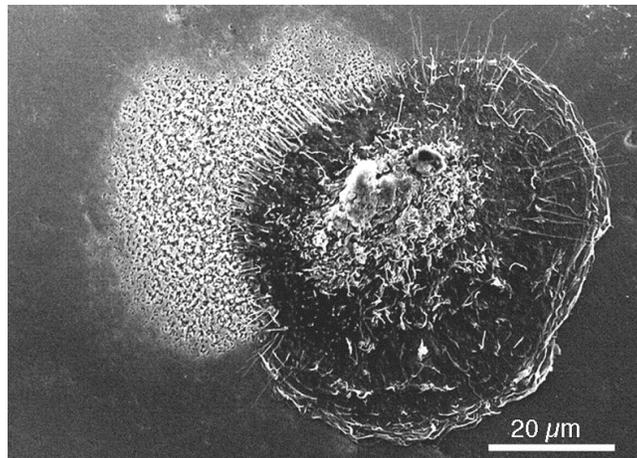
Fig. 1.10. SEM micrograph of an osteoclast creating an absorption lacunae, adapted from (Akisaka et al., 2006). The resorption pit is clearly discernable from the surrounding un-abrided surface. Retraction fibres are evident extending from the resorbed area.

1.9. The Mesenchymal Stem Cell

In the adult, the osteoblast is derived from a marrow stromal fibroblastic stem cell termed the MSC, a non-hematopoietic multipotent stem-like cell, capable of differentiating into both mesenchymal and non-mesenchymal lineages (fig. 1.11). The adult stem cell, first described in the haematopoietic system following an investigation sparked by the

detonation of atomic devices in Nagasaki and Hiroshima has been isolated from virtually every tissue of the body (McCulloch *et al*., 1965). Of greater interest however is the apparent phenomenon that these adult cells, arising from different sources have the inherent potential to spontaneously trans-differentiate into other tissue progenitor cells (Conrad & Huss, 2005).
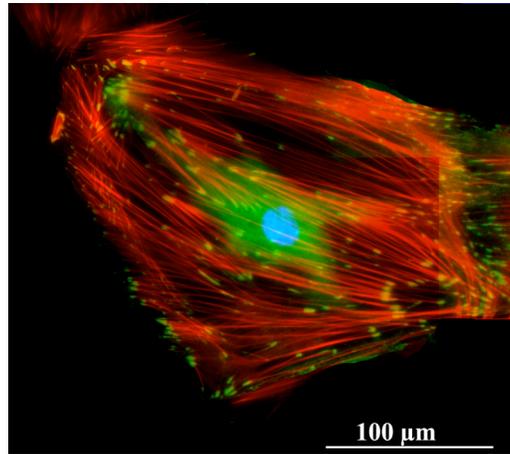
Fig. 1.11. Tri-fluorescent labelling of a STRO-1 selected human mesenchymal stem cell (Biggs, unpublished work). MSCs represent the adherent fraction of bone marrow stromal cells. Morphologically STRO-1 selected cells are large, mononucleated and well adhered cells. Blue: nucleus, Green: vinculin, Red: actin.

Stem cells form uncommitted populations, capable of both self-renewal, differentiation into multiple cell lineages and the capacity for maintained proliferation. Thus a stem cell can be defined as maintaining a supply of undifferentiated progenitor cells (self-renewal) in spite of continual differentiation. The bone marrow serves as a reservoir for a variety of cells including the non-mesenchymal hemopoietic stem cells found in systemic blood and marrow stromal cells, those responsible for bone neogenesis. MSCs, however, only constitute a small percentage (0.01–0.001% of mononuclear cells isolated on ficoll/percoll density gradient) of the total number of bone marrow-populating cells. Interestingly, osteogenic progenitor cells, capable of osteoblast differentiation, are also detected ectopically, notably within the peripheral circulation (Eghbali-Fatourechi *et al*., 2005).

The regenerative capacity of bone has long been recognised and yet, to date, limited

evidence regarding the nature of these multipotent MSC has come to light. This is predominantly owing to their low incidence, variable morphology and, despite nearly four decades of research, indeterminate biochemical phenotype. Friedenstein and colleagues first presented the evidence that marrow stroma contained populations of postnatal stem cells with multil-lineage mesodermal differentiation (McCulloch *et al*., 1965) in the form of fibroblastic colony-forming units able to generate, cartilage, bone, muscle, tendon, ligament, fat and fibrous connective tissue (fig. 1.12) (Friedenstein, 1995).

Progenitor cells derived from stromal stem cells may be multipotent but they are committed to one or more cell lines with a reduced capacity for plasticity or interconversion and thus have a hierarchical position between a stem cell and differentiated progeny. It is important to note therefore that osteogenic progenitors are an intermediate between a stem cell and differentiated progeny (i.e., osteoblast). Although MSCs are multi-differentiational entities, it seems that they most readily differentiate down an osteogenic lineage. When cultured in the presence of mineral inductive medium, MSCs show the capacity to form structurally distinctive mineralised deposits in comparison with other mineral-matrix-forming postnatal stem cells, such as dental pulp stem cells (Gronthos *et al*., 2003, Shi *et al*., 2002).
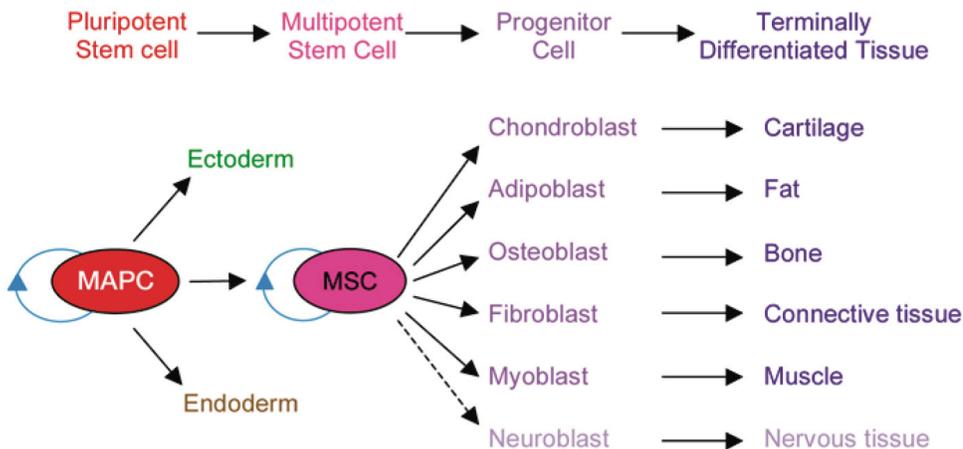
Fig. 1.12. The process of cellular differentiation, adapt ed from (Oreffo et al., 2005). From self-renewing stem cells to generation of all mesenchymal cell lineages, omnipotent cells of embryonic origin progress down highly regulated pathways to become terminally differentiated.

As has been mentioned, due to an increasing aging population, clinical imperatives to augment and facilitate skeletal tissue lost as a consequence of trauma or degeneration have led to increased interest in these progenitor cells and regulating their potential differentiation pathways (Oreffo *et al*., 2005). In recent years, much effort has been directed towards answering the fundamental question of whether MSCs are capable of forming bone for therapeutic purposes. Subsequently experiments with *ex vivo*-expanded human MSCs found that these cells could be successfully used for the treatment of critical size bone defects in long bones (Quarto *et al*., 2001). Isolation and expansion of MSCs *in vitro* has proved a critical process in differentiation studies, undertaken using a restricted panel of monoclonal antibodies, including STRO-1 (Gronthos & Zannettino, 2008) SH-2 (Barry *et al*., 1999) and HOP-26 (Oreffo *et al*., 2005, Zannettino *et al*., 2003).

1.10. The Extracellular Matrix

When compared with the intracellular proteins, ECM proteins are relatively young. ECM proteins evolved approximately 700 million years ago with the emergence of multicellular organisms (Huxley-Jones *et al*., 2007) with a large number of them demonstrating great conservation. The ECM is a complex three-dimensional environment that plays an important roles in tissue and organ morphogenesis, in the maintenance of cell and tissue structure and function, and in the host response to injury (Badylak, 2002). It comprises of a network of self-assembled glycoprotein and collagens in a glycosaminoglycan and proteoglycan ground substance (Little, 1973) which are initially synthesised early in gastrulation (Sathananthan & Trounson, 2005, Zagris, 2001). At the tissue level, cells are continually influenced by a complex system of self-regulation imparted by ECM. The ECM provides the cellular population with dynamic biophysical stimuli, to regulate cellular differentiation and function. Cellular interactions with this matrix have a definitive role in guiding development, maintaining homeostasis and directing regeneration (Hubbell, 2003). This is in addition to directing cellular migration through the modulation of cellular adhesion (Xia *et al*., 2008).

The physical structure of the ECM imparts both rigidity, chemical and topographical information regulated by the density and variation of the constituent glycoproteins and collagens (Schlunck *et al*., 2008). These variables have been shown to influence cytoskeletal structures (Saez *et al*., 2007), protein expression patterns (Karamichos *et al*., 2007), signal transduction (Dalby *et al*., 2007d), and cellular differentiation (Engler *et al*., 2007, Khatiwala *et al*., 2007).

Collagens are by far the most numerous of proteins within the ECM, indeed collagen, being the must abundant protein in the human body, makes up about 30% of the total protein content, while about 90% of the dry weight of the ECM is collagen (Vakonakis & Campbell, 2007). At present approximately 29 different types of collagen are recognised. Collagens are secreted by stromal cells into the ECM as immature isoforms termed tropocollagen. This molecule consists of three polypeptide chains, which form a helical structure 300 nm long, and 1.5 nm in diameter (Steven, 1972). These molecules polymerise within the ECM to form the different collagen types. Type I collagen was the first of the collagens to be identified, and is the major structural component of the ECM in the majority of tissues; here collagen molecules align side by side in a staggered fashion with three quarters of their length in contact with a neighbouring collagen molecule.

Other types of collagen typically exist within the ECM in much lower quantities that collagen type I. The composition of the ECM and the relative amounts of these collagens provides tissues with distinct and individual mechanical properties. Type II, III VI and XI collagens all aggregate to form fibrils; accordingly they all share a common gene coding for their alpha chain (Ottani *et al*., 2002). Type IV collagen does not form fibrils but aggregates of 3-dimensional mesh-like molecules, this type of collagen is important in basement membrane formation. Other collagens such as type IX are not fibril forming *per se*, yet are termed fibril associated, acting to attach collagens to each other and to various other ECM components.

As well as providing strength and structure, the ECM is also responsible for providing a local environment favourable to cell growth and proliferation, while at the same time providing a medium that allows the free diffusion of metabolites and endocrine signalling molecules to and from the cells of a tissue. ECM proteins are macromolecules with

somewhat of a multifunctional role. They are composed of many domains that are frequently repeated within the same molecule or show phylogenetic links to domains in other ECM proteins (Perkins *et al*., 1989). Various specific binding motifs provide sites that serve to regulate cellular function via the coupling of the cytoskeleton to the ECM. Binding of cells to these sites can result in translation and transcription of genes and ultimately the expression of proteins. These sequences, in particular the arginine-glycine-aspartic acid-serine (RGDS) and arginine-glycine-aspartic acid (RGD) motifs interact with the integrins of the plasma membrane, transmembrane receptors that mediate cell-substratum adhesion, discussed in detail below.

Other filamentous components can be found within the ECM, often acting as mediators of adhesion between ECM components and between the ECM and populating cells. These molecules are often found in association with various other ECM fibrillar components. The list of ECM filamentous proteins is constantly being reviewed and updated, particularly in reference to the entactins, perlecan, decoran, aggregan etc. The majority of these fibres are multipurpose, often serving as structural components as well as mediators of ECM and cellular binding. These molecules demonstrate complex secondary and tertiary structure and in particular also possess binding sites for the cell adhesion molecules the integrins.

The cells of the ECM, including MSCs are derived from embryonic mesoderm and are responsible for the secretion and maintenance of its components. Cells present in the embryonic mesoderm begin to deposit ECM molecules early in gastrulation (Zagris 2001), this primitive mesenchyme is central to cellular migration through the primitive node during gastrulation and is the embryonic tissue from which all connective tissues originate (Kimura *et al*., 2006).

Many ECM proteins form large families. For instance there are some 30 genes identified for collagens and 12 identified for laminins. Additional events, such as alternative splicing, proteolytic processing and glycosylation, increase the variation between proteins from the same family and expand the functions of these large, multifunctional molecules. With the identification of many new ECM proteins and elucidation of the exact atomic structure of these proteins by advanced analytical techniques such as X-ray crystallography and nuclear magnetic resonance spectroscopy, advances have been made

in defining the domain structures responsible for ECM – cell and intermolecular binding as well as the higher order architecture of extracellular components. Such approaches have begun to identify the various interactions important in ECM assembly and ECM – cell interactions (Chesnick *et al.*, 2008, Orgel *et al.*, 2006).

1.11. Cell–Substrate Interactions

Cell-substrate interactions can be regarded as the defining factors of a biomaterial performance *in vivo*, ultimately determining the long-term performance of a device *in situ*. It can be reasoned that the integration of exogenous materials can be improved by controlling the associated interfacial reactions, in an attempt to minimise non-functional tissue encapsulation and aseptic loosening. Fibrous encapsulation is known to occur with both metal (Suska *et al.*, 2007) and polymeric biomedical constructs (Andersson *et al.*, 2007), usually with the presence of a fluid filled void between the tissue and implant. This reduced biocompatibility may have many causative origins, however a frequent outcome is diminished cellular adhesion followed by destabilisation of the implant alongside an inhibition of tissue regeneration and repair as well as an increase in the potential for infection (Baxter *et al.*, 2002). Device parameters including surface chemistry, charge, texture and porosity can all be optimised to enhance the tissue response to a device *in vivo* (Dettin *et al.*, 2005, Xu & Siedlecki, 2007). Other approaches utilise the localisation of bioactive molecules either natural or synthetic, to a material surface.

In many situations, enhanced cellular adhesion is a desirable outcome in order to increase implant stability and to reduce device failure. However a body of research suggests that permanent fixation, particularly in internal CMF fixation is not ideal, and the retention of a device following healing may present implant site morbidity. In such a situation surface mediated reduction of cellular adhesion is desirable in order to facilitate device removal and prevent re-fracture upon removal.

Adherent cells are complex, self-sustaining units (Schwarz *et al.*, 2006) that require ECM anchorage in order to proliferate (Triplett & Pavalko, 2006). Modern implants make use of chemical and topographical modification to facilitate cellular adhesion (Dettin *et al.*,

2005, Keselowsky *et al*., 2004) differentiation and tissue deposition (Wan *et al*., 2005) (Marchisio *et al*., 2005, Yamaguchi *et al*., 2004). Following implantation ECM proteins undergo rapid adsorption to a material surface (Oleschuk *et al*., 2000, Suh *et al*., 2004), adhering cells actively probe the physical properties of the ECM; their contractile machinery facilitating both cellular motility and the formation of protrusions termed 'lamellipodia' with which cells move and sense their surroundings *in vitro* (Abercrombie *et al*., 1970, Dalby *et al*., 2004b, Zinger *et al*., 2004). Lamellipodia are associated with fine hair-like protrusions termed 'filopodia' (fig. 1.13), which contain a core of extended actin filament bundles that gather special information and 'sense' the ECM and substrate surface.
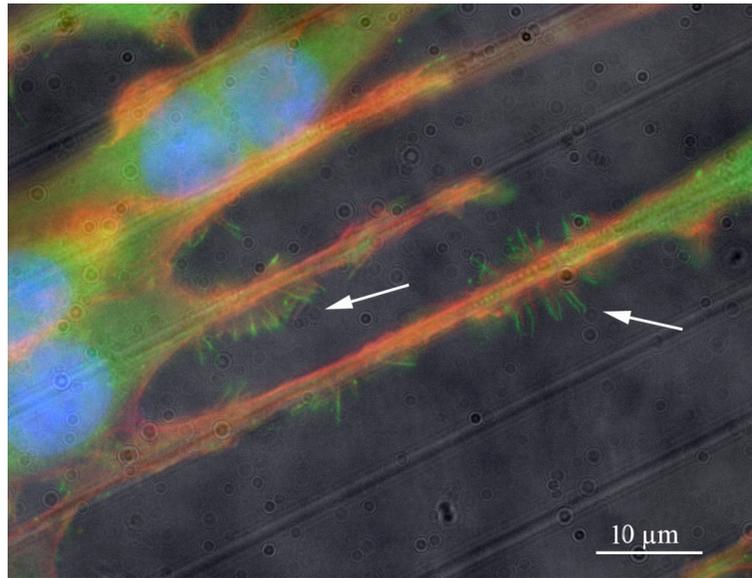
Fig. 1.13. Filopodia formation in endothelial cells on a nanogroove substrate (Biggs unpublished data). Endothelial cells probe the underlying grooved substratum with fine filopodial extensions (arrows) from the leading and trailing free edge.

Filopodia were first described by Gustafson and Wolpert (1961) in cells of the blastocoelic cavity of sea urchins. It was noted these cells appeared to use filopodial extensions to gather spatial information. Once cells locate a topographical site suitable for adhesion, or perhaps an ECM protein motif, a signalling feedback pathway initiates integrin receptor clustering at the plasma membrane and adhesion plaque protein recruitment (Lim *et al*., 2007). These actions require guanine nucleotide-binding proteins

(G-protein) signalling and the development of an integrated cytoskeleton (Carragher & Frame, 2004, Zimerman *et al.*, 2004).

Initial cell tethering and filopodia exploration is followed by lamellipodia-mediated ruffling (Bershadsky *et al.*, 2006b), membrane activity and cellular flattening and spreading (Cavalcanti-Adam *et al.*, 2007, Zimerman *et al.*, 2004) all mediated by the development of cell-substratum points of contact termed focal adhesions (FAs). By progressively sending out these lamellipodial extensions along the leading cell edge, focal complexes (FXs) are made which transmit strong propulsive traction to the cytoskeleton allowing the cell to move across or flatten on a surface (Gupton & Waterman-Storer, 2006, Pollard, 2003).

The attachment and separation of the cell from the surface is controlled by an integrin feedback loop, mediating the leading and trailing cell boundary. It has been shown that fast cellular migration occurs at intermediate ECM concentration and slow migration occurs at low and high ECM concentration (Gupton & Waterman-Storer, 2006). A simple mechanical model has been proposed to explain this observation, in which too little adhesion does not provide sufficient traction whereas too much adhesion renders cells immobile (Gupton & Waterman-Storer, 2006). With time, endogenous matrix is secreted by the cells and matrix assembly sites form on the ventral plasma membrane. It can be reasoned that this reduction in cellular migration, the formation of mature adhesion sites and the onset of ECM synthesis are processes indicative of terminal cellular differentiation.

1.12. The Focal Adhesion

Cells interact and communicate intracellularly via single or multiple chain transmembrane proteins termed integrins. These adhesion receptors are recognised as the central regulators of cell–biomaterial interactions, which mediate adhesion to the extra cellular matrix or to other cells (Cohen *et al.*, 2004). Integrin receptors are composed of non-covalently linked α and β subunits which bind specifically to specific motifs located on ECM molecules e.g. the RGD tripeptide found in the adhesive proteins of the ECM such as fibronectin, vitronectin and laminin (Garcia, 2005). First cloned in 1986 (Tamkun

et al., 1986), integrin proteins are a fundamental initiator of cell and tissue organisation and are preserved throughout evolution, even in the most primitive of metazoan organisms (Adams, 2002, Pancer *et al*., 1997). Integrin-mediated adhesion is a highly regulated and complex process involving receptor-ligand binding as well as post-ligation interactions with multiple intracellular binding partners (Carvalho *et al*., 2003). Integrins therefore are large allosteric machines which are activated both by biochemical (Arnold *et al*., 2004) mechanical (Hirayama & Sumpio, 2007) and topographical cues (Heydarkhan-Hagvall *et al*., 2007) and transmit information in a bi-directional manner from the extracellular environment to the machinery of intracellular transcription.

Upon binding, integrins rapidly associate with motif sequences via their globular head domains and connect the actin microfilaments of the cytoskeleton to ECM components via adaptor proteins, most notably talin. Ligand binding in itself alters integrin conformation and affinity and, in the case of multivalent ligands, integrin clustering. With increased integrin clustering, these early cell–matrix contacts form anchoring FXs at the lamellipodium leading edge. These are discrete supramolecular complexes that contain structural adaptor proteins, such as vinculin, talin, and paxillin (Bershadsky *et al*., 2006b, Burridge *et al*., 1988, Zimerman *et al*., 2004). These transient complexes are observed to have a substrate distance at closest approach of 10 nm, (Curtis, 1964) and mature into larger FA plaques upon increased intracellular and/or extracellular tension.

The regulation of FA formation in adherent cells is highly complex and involves both the turnover of single contacts and the reinforcement of the adhesion plaque by protein recruitment. A second key aspect of regulation is that, once assembled, matrix complexes can be turned over to enable their repositioning or interconversion. FAs emerge as diverse protein networks that provide structural integrity and dynamically link the ECM to intracellular actin (fig. 1.14), directly facilitating cell migration and spreading through continuous regulation and the dynamic interaction with actin. Furthermore, in combination with growth factor receptors, these adhesive clusters activate signalling pathways crucial to cell survival that regulate transcription factor activity, direct cell growth and differentiation.
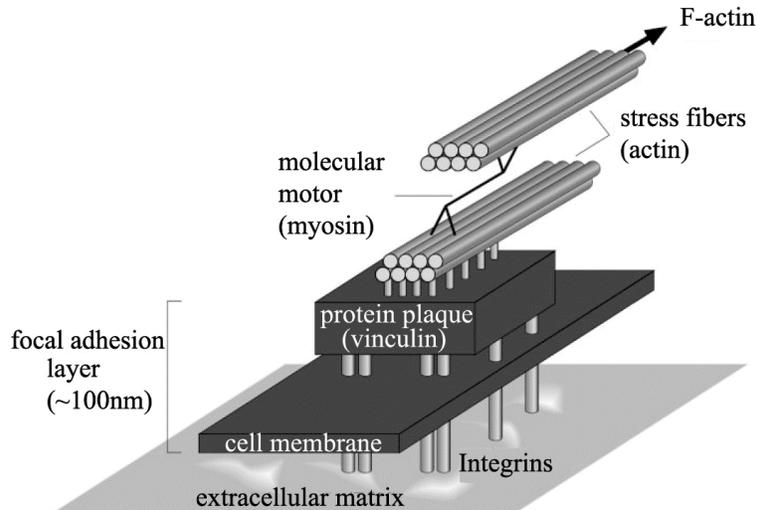
Fig. 1.14. Focal adhesions are intimately associated with filamentous actin of the cytoskeleton, adapted from (Aroush & Wagner, 2006). Intracellular tension is generated by the interaction of actin with molecular motor myosin.

Ward and Hammer developed a model of adhesion strengthening (Ward and Hammer, 1993), which predicts large increases in adhesion strength following increased receptor clustering and adhesion size, marked by an elongation of the adhesion plaque. This process is believed to be due to an increase in tension at the adhesion site as FA size has been shown to be proportional to the force applied to it by the cell (Balaban *et al.*, 2001) indicating adhesion sites act as mechanosensors (Schwarz *et al.*, 2006) and form additional contact points with the underlying substratum in response.

This force must exceed a critical value for adhesion elongation, but when growth occurs it occurs preferentially in an anisotropic manner in the direction of the force (Besser *et al.*, 2006). When a cell adheres to a surface, it exerts traction forces to balance the internal forces generated by cytoskeletal tension (Chicurel *et al.*, 1998). These forces have been measured, and most cells appear to generate traction forces in the range of tens to hundreds of nanonewtons (Jean *et al.*, 2004, Tan *et al.*, 2003). This fixes a minimal value for the force that enables the growth of the FA by anisotropic elongation and indicates the role of substrate stiffness in affecting the size and strength of FAs (Guo *et al.*, 2006). This force threshold depends on the precise chemical nature of the adhesion, however there is an upper limit to the force: very large stresses or a decrease in substrate

rigidity prevent adhesion elongation consistent with the observation of the transformation of FAs into fibrillar adhesions as discussed below (Nicolas *et al*., 2004).

FXs originate as dot-like structures of 0.5 μm^2, which are regulated by the GTPase Rac and precede larger FAs that are regulated by the small G-protein Rho (Wozniak *et al*., 2004). Mature FAs are typically dash shaped, $1 - 5$ μm^2 and contain vinculin, paxillin and talin signalling complexes and mediate integrin function to regulate cellular behaviours such as cell migration (Ziegler *et al*., 2008). Fibrillar type adhesions specifically contain α_5 and β_1 integrins and tensin (Wozniak *et al*., 2004) and play a major role in fibronectin organisation (Fayet *et al*., 2007). Carragher *et al.* suggest that FXs do not simply gradually mature into FAs, but rather indicate that regulated transition of FXs to FAs requires local retraction of lamellipodia to provide a positive stimuli for FA formation (Carragher & Frame, 2004).

When intracellular forces per unit length exceeds a critical threshold at the integrin substrate interface the displacement of the anchoring integrins is sufficient enough to induce a stick-slip motion where the adhesion complex moves rather than deforms. In this scenario changes in protein density around the adhesion plaque are negligible and no further adsorption of proteins to the FA occurs. This progressive recruitment of integrins in the absence of FA proteins results in the formation of tension-insensitive fibrillar adhesions. The assembly of a fibronectin matrix, a structure essential for cell migration during embryogenesis and wound healing is dependant on integrin clustering and fibrillar adhesion formation (Danen *et al*., 2002, De Jong *et al*., 2006). Whilst they are involved in fibronectin organising, fibrillar adhesions are relatively weak contacts, which are morphologically fibrillar by co-alignment with actin stress fibres.

To date studies indicate that tyrosine phosphorylation within FXs occurs after the initial recruitment of focal adhesion kinase (FAK), vinculin and paxillin (Carragher & Frame, 2004). FAK directly influences the survival signalling pathway, and is responsible for negating mitochondria dependant apoptosis (programmed cell death), resulting in the inactivation of caspase 9 and the inhibition of cellular anoikis (apoptosis resulting from insufficient adhesion) (Grigoriou *et al*., 2005) (fig.1.15).
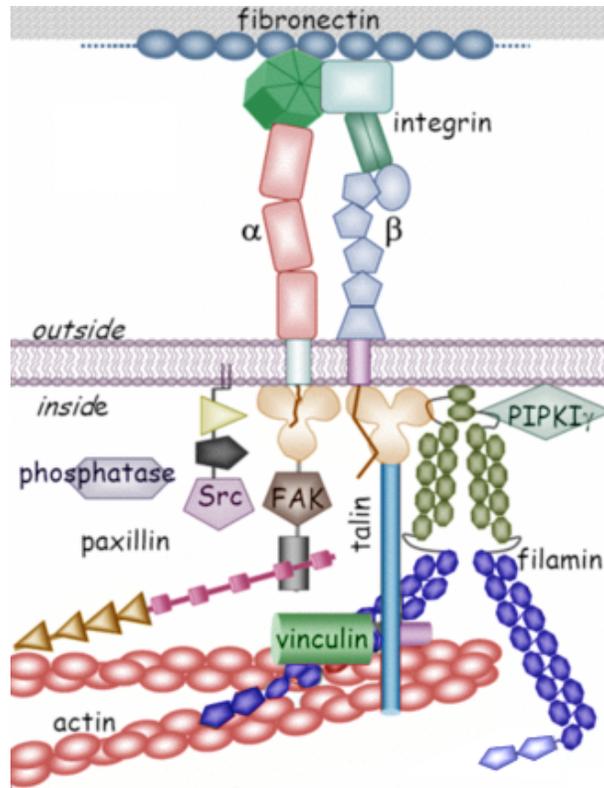
Fig. 1.15. *The proteins of the focal adhesion plaque, adapted from (Campbell, 2008).* A complex aggregation of structural and secondary signalling molecules propagate external forces to both the machinery of mechanical tension (the cell cytoskeleton) and of genetic transcription (molecular signalling).

1.13. The Cell Cytoskeleton

The cytoskeleton exists as an extended interconnecting framework providing eukaryotic cells with a means for locomotion, intracellular protein transport, cell integrity, proliferation and importantly, cell adhesion and flattening relative to a substrate. Three types of cytoskeletal filaments are common to eukaryotic cells and play fundamental roles in cellular spatial organisation.

Microfilaments are prominent cytoskeletal structures, present in most well-spread cultured cells, composed of straight bundles of actin, measuring from just a few microns to tens or even hundreds of microns. Although multicellular organisms contain a wide array of actin assemblies, the actin structures that play fundamental roles in cellular integrity can be roughly subdivided into five categories: (1) lamellipodial actin networks at the leading edge of the cell, (2) unipolar filopodial bundles, (3) the cortical actin shell

beneath the plasma membrane, and (4) the contractile actin ring located at the division plane during cytokinesis and (5) contractile filamentous actin in the cytoplasm tight bundles. These bundles, commonly denoted "stress fibres" are associated at their termini with FAs and maintain an isometric tension, which is applied to the ECM through cellular adhesions (Zimerman *et al.*, 2004) (fig. 1.16).
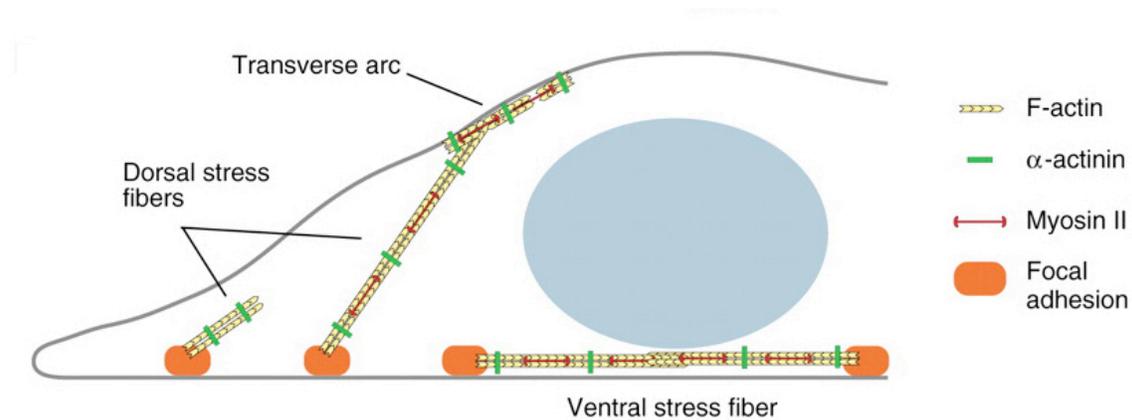
Fig. 1.16. Focal adhesions are intimately associated with filamentous actin of the cytoskeleton, adapted from (Pellegrin & Mellor, 2007). Intracellular tension is generated by the interaction of actin with the molecular motor myosin. Actin polymerisation is regulated by α-actinin.

Microtubules are long hollow cylinders of polymerised tubulin about 24 nm in diameter. Like actin filaments, microtubules are dynamic structures that undergo rapid cycles of assembly and disassembly within the cell, a phenomenon termed dynamic instability (the stochastic switching between phases of growth and shortening). They perform a variety of functions both in determining cell shape and in specialised cellular motility, including some forms of cell locomotion, the intracellular transport of organelles, and the separation of chromosomes during mitosis, extending from the microtubule organising centres such as centrosomes and basal bodies.

Intermediate filaments are cytoskeletal structures with a diameter between that of actin microfilaments and tubulin microtubules. These diverse polymer structures are formed by members of a family of related proteins of which there are about 70 different genes that code for various proteins. Most intermediate filaments measure between 9 and 11 nm in

diameter when fully assembled (Weinger & Holtrop, 1974). Evolutionary diversity has resulted in the description of five types of these cytoskeletal proteins including vimentin – a cytoskeletal protein abundant in both MSCs and osteoblasts.
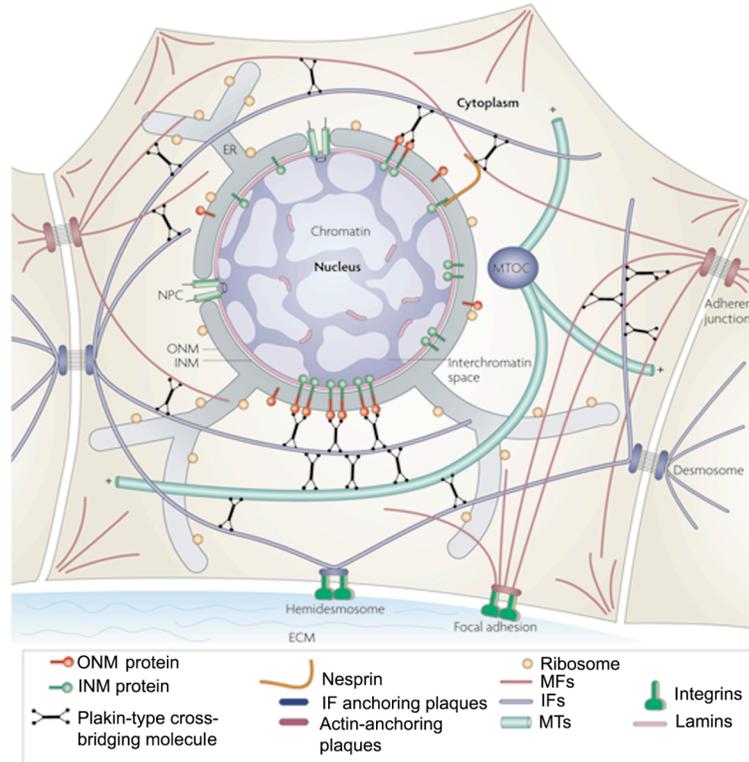
Fig. 1.17. The tensegrity structure, adapted from (Herrmann et al., 2007). Structural integrity of the cell is derived from an interplay of tensional forced imparted by the microfilament system (MFs) and compressive forces from the intermediate filament (IFs) and microtubule (MTs) networks.

1.14. Mechanotransduction and Tensegrity

It is becoming increasingly clear that epigenetic factors, particularly mechanical and topographical cues, have a central role in the regulation of cellular behaviour. Mechanotransduction is based on the ability of specialised cellular mechanotransducer molecules to change their chemical activity state when they are mechanically distorted, converting mechanical energy into biochemical energy by modulating the kinetics of protein-protein or protein-ligand interactions within the cell. However little is known regarding the levels of force required to initiate mechanotransduction or the role of intracellular force transmission on mechanosensor activation of adhesion proteins (Mack

et al., 2004). Indirect (biochemical) mechanotransductive pathways trigger signalling transduction cascades and can convey distinct signals to the cell (Durieux *et al.*, 2007). However, there have been a number of attempts to explain how the cytoskeleton may act as an integrated unit to convey mechanotransductive signals from the extracellular environment. Tensegrity was first described by the architect R. Buckminster Fuller in 1961 as a building principle to explain the possibility of structural stability by continuous tension or `tensional integrity' rather than by continuous compression (e.g. as used in a stone arch). The cellular tensegrity model proposes that the physical interactions between actin microfilaments, microtubules, and cell substrate adhesions govern the shape and stiffness of the cells (Ingber, 2006).

The cellular unit can be viewed as a pre-stressed tensegrity structure, with tensional forces borne by cytoskeletal microfilaments, which are balanced by interconnected structural elements that resist compression, most notably, internal microtubule struts, intermediate filaments and FAs. In this model microtubules bear most of the compressive forces in rounded cells with few anchoring adhesions whereas the actin microfilament and associated ECM molecules bear most of the load such as in well spread cells observed *in vitro* on adhesive substrates (Hu *et al.*, 2004a).

The forces required for stress fibre derived tension and the development of structural anisotropy are produced by the interactions between actin and the molecular motor myosin, resulting in unidirectional contraction (Zimerman *et al.*, 2004). This model of actin mediated cellular tension is described as relying on three major criteria: (i) an activation signal that triggers actin and myosin phosphorylation, (ii) the tension-dependent assembly of the actin and myosin into stress fibres, and (iii) the cross-bridge cycling between the actin and myosin filaments that generates the tension (Deshpande *et al.*, 2006). Intermediate filaments that interconnect at many points along microtubules, microfilaments and the nuclear surface provide mechanical stiffness to the cell through their material properties and their ability to act as cross-bridging stabilisers which can tensionally stiffen both the cytoskeletal and nucleoskeletal networks (fig. 1.17). Integrins/FA sites, cytoskeleton constituents, G-proteins, ion channels, intercellular junction proteins, and membrane biomolecules have all been identified as potential mechanosensors (Mack *et al.*, 2004). Some FA constituents are also found in the nucleus

and display either nuclear localisation or export signals. FA proteins that are known to shuttle to the nucleus include the FA adaptor protein zyxin, which has been shown to affect gene transcription (Cattaruzza *et al*., 2004). The ability of proteins to reside in both the FA and nuclear compartments allows them to facilitate communication between those two subcellular domains. Pavalko *et al*. describe a model whereby multiprotein complexes, called mechanosomes, comprised of adhesion proteins acquired from the FAs as well as zyxin move between the adhesion complexes and the nucleus, thereby regulating gene expression (Pavalko *et al*., 2003).

Pursuit of a complete tensegrity theory and the observation that cytoskeletal development is adhesion mediated has led to the concept that mechanical signals are transferred from the ECM, across sites of FA via the molecular filament networks that form the cytoskeleton. This theory of direct (mechanical) mechanotransduction infers that cytoskeletal structures form the primary load-bearing elements in the cell and provide a potential mechanism to link mechanical stresses applied at the tissue level to changes in molecular dynamics within the cell, distortions of the ECM, or an associated increase in its rigidity, manifest as a distortion or a tug on the FA site and are propagated through the cytoskeleton to the cell interior. Increases in cytoskeletal tension can also feedback to promote structural changes in the surrounding ECM, such as unfolding of peptide domains within fibronectin molecules that promote fibril assembly (Hu *et al*., 2004b) and a reinforcing of the extracellular network.

The observation that a direct mechanical connection exists between the integrins, the cytoskeleton, and the nucleus suggests a possible direct line of force transfer between the surface of the cell and the nucleus, essentially forming a single physical lattice extending from the ECM to the nucleoskeletal network. This is in agreement with Forgacs percolation theory whereby he describes the ECM as the spiders web and changes in stress/strain of the web will be relayed to the spiders body (nucleus) via its legs (cytoskeleton) (Forgacs, 1995). In this sense tensegrity is simply a specialised percolation network with both theories agreeing that an interconnected cytoskeletal network is required for the transmittal of mechanical signals (fig. 1.18).
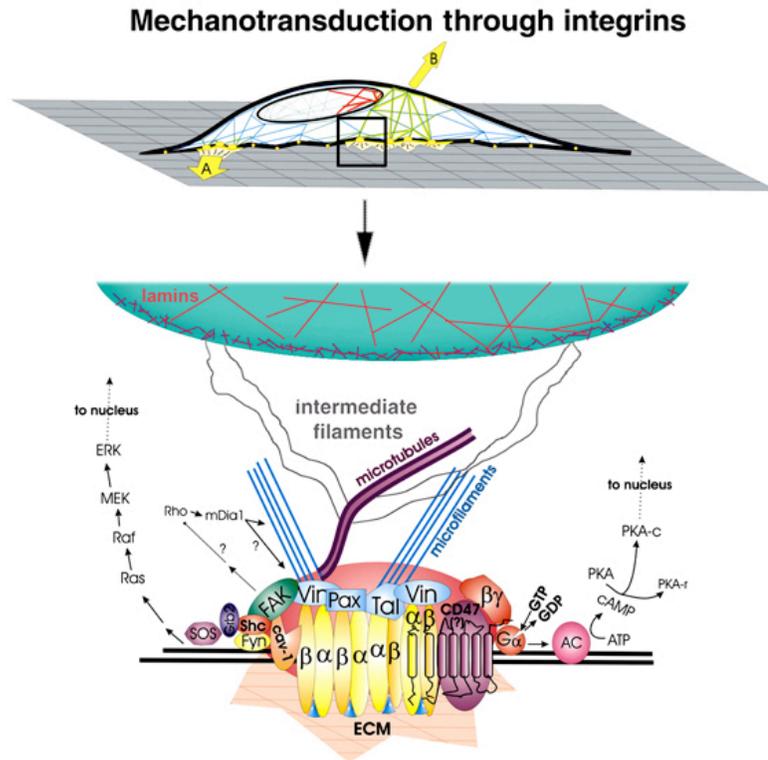
Fig. 1.18. Mechanotransduction through integrins, adapted from (Ingber, 2003). A continuous cytoskeletal network propagates adhesion mediated intracellular tension from the ECM to the nucleus. Secondary signalling molecules are also translocated to the nuclear machinery to influence transcription.

Studies in muscle cells indicate that intermediate filaments can transmit stress signals to the chromatin (Bloom *et al.*, 1996). This signalling could occur through the cytoskeletal intermediate filament interaction with nucleoskeletal intermediate filaments (lamins) and be transmitted to deoxyribonucleic acid (DNA) via the close relationship of lamins and chromatin, specifically chromosome telomeres. Consistent with this is the evidence from Dahl *et al.*, 2004 that the nucleus can expand in response to tension through changes in laminar morphology, but is resistant to compression (Dahl *et al.*, 2004). A key question - assuming that mechanical signals can be transmitted to the nucleus- is *how are these signals translated into genomic changes?*

It is now accepted that interphase chromosomes occupy discrete territories within the nucleus (Cremer & Cremer, 2001). These territories are complex folded structures with interchromatin channels penetrating into the territory interior and allowing diffusion of transcriptional activators (Cremer & Cremer, 2001). The model of direct

mechanotransduction proposes that changes of the mechanical structure of the cell may be involved in changing chromosomal organisation. In support of this concept is a study by Dalby *et al* that shown changes in cell spreading on nano-topography leads to cytoskeletal and nucleoskeletal rearrangements (Dalby *et al*., 2007a). Moreover, adhesion induced modulation of cell shape and associated nuclear tension has been suggested to affect both protein synthesis and gene expression (Dalby *et al*., 2006a, Li *et al*., 2008). Nuclei and cell morphological changes associated with topographical modification has been correlated with changes in gene and protein expression profile (Dalby *et al*., 2003c).

1.15. Substrate Topography

Topographical modification is one method that may be employed to influence cellular adhesion and spreading in an attempt to regulate gene transcription through direct mechanotransduction. The term *topography* is used to describe the morphology arising at a material surface due to its general architecture or surface roughness, factors known to directly influence cell-substratum interactions irrespective of, or in conjunction with the surface chemistry (Liao *et al*., 2003). When describing a material topography it is favourable to differentiate between the relative deviations in scale that may occur at a topographical level, subsequently surface topography is generally subdivided into macro-, micro- and nanoscale surface features.

Macrotopography is concerned with the physical conformation of an object; such parameters usually define the materials function. In a biomedical setting macrotopographical reference may be made to screw threads, stent struts, internal sutures etc. These topographical conformations are vital to the function of such implants and are not in the short-term subject to large-scale remodelling in an *in vivo* environment.

Microtopography may result from surface roughness of texture and typically refers to features varying from 0.5-100 μm in dimension. Qualification of surface roughness involves the presence of spikes or pits that can be of random size distribution and density. The phenomenon of microroughness may result from fabrication processes such as welding or laser cutting (Brabazon *et al*., 2008) or may be intentionally applied to a device in order to regulate cell attachment, i.e. sandblasting or plasma spraying of an

orthopaedic devices to create microroughness has been shown to increase osteoblast adhesion and proliferation (Kim *et al*., 2003). Microroughness is both difficult to reproduce and studies with microrough substrates and the cellular response can often be conflicting. The obvious question is, *why is there such variation in the conclusions drawn by many studies*? Differences in cell types used and the subsequent parameters of analysis, device fabrication, and varying degrees of surface roughness are some of the principle areas from where variation between studies may stem. Definitions are certainly required as to what constitutes a 'rough' surface (millimetres, micrometres, nanometres). For instance, Boyan states that if the average roughness (Ra) of a surface is greater than the size of an individual osteoblast, then essentially this surface may been seen as smooth since the distance between peaks is too great as to be detected (Boyan *et al*., 2003). Microrough surfaces with a similar Ra can be very different in morphological appearance, and unlike the controlled topographical features described below, it can be reasoned some of the success currently associated with implants fabricated to include a microrough surface is attributed to cellular interlocking rather than an altered cellular response to the topographical features (Davies, 2007). Here it is noted that implant stability is predominantly due to microscale surface topography with features in the sub-micron scale-range that promote tissue interlocking (fig. 1.19).
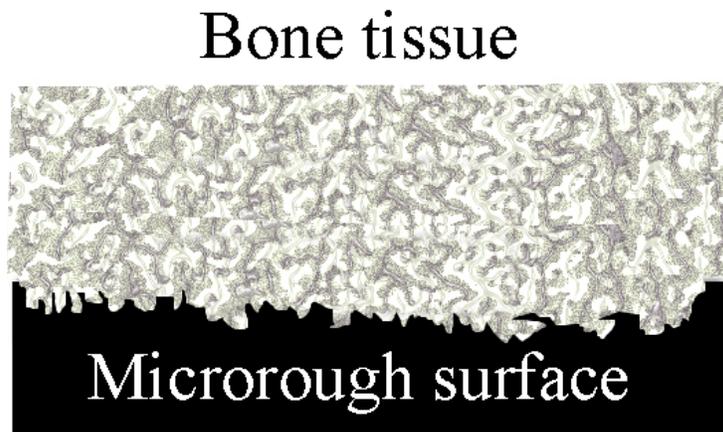
Fig. 1.19. Surface roughening promotes increased tissue interlocking. Cellular adhesion is not increased by surface roughness, rather whole tissue adhesion is increased by bone growth into the topographical microfeatures.

1.16. The Effects of Nanotopography on Adhesion Formation

That nanoscale features can affect cell behaviour is demonstrated in studies with fabricated topographical features, which elicit changes in cellular morphology and function. However, it is unknown at present if cells actually respond directly to nanoscale topographical features or respond to the subsequent changes imparted onto the pre-adsorbed protein layer. Nanotechnology aims to create and use structures and systems in the size range of about 0.1–500 nm covering the atomic, molecular and macromolecular length scales. A range of methods exist for the generation of topographical nanoscale features including chemical vapour deposition, polymer demixing, colloidal lithography, photolithography, electron beam lithography (EBL), etc. For a full review of the methodology for nanoscale fabrication technology in 2006 see (Norman & Desai, 2006).

The general protocols for nanomanufacturing require high resolution and low cost for fabricating devices. With respect to biological investigations, nanotopographies should occur across a large surface area (ensuring repeatability of experiments and patterning of implant surfaces), be reproducible (allowing for consistency in experiments), and preferably, accessible (limiting the requirement for specialist equipment) (Wood, 2007). The extent to which nanotopography influences cell behaviour within an *in vivo* environment still remains unclear. Question being asked in the field of orthopaedic device manufacture is whether surface nanofeatures offer any relevant stimuli to the cellular component of the immediate tissue and if so whether implants could be fabricated to include topographical nanofeatures which do so. Fabricated model surfaces with defined topographies are of great experimental importance in engaging with such issues.

The rationale for developing nanostructured materials for regenerative medicine stems from the complex structure of *in vivo* extracellular tissue, composite nanostructures composed of seemingly random fibrillar ECM molecules, pits and protrusions. The fact that many cell-types are naturally adapted to nanophase topographies has led to a series of studies investigating the cellular response toward synthetic nanostructures. To date the field of cell-substrate interactions has been directed towards the phenomenon of biomimetic nanotopographically induced mechanotransduction with present studies indicating that most cells do react significantly to nanotopographical cues *in vitro* (Smith *et al.*, 2007). The processes that mediate cellular reaction to nanoscale surface structures

however are not well understood and may be direct (Dalby *et al*., 2007d) (a direct result of the influence of the surface topography) or indirect (Martines *et al*., 2005) (where the surface structure has affected the composition, orientation, or conformation of the adsorbed ECM components) (Andersson *et al*., 2003).

That topographical influences can drive contact guidance and cell migration in osteoblast populations is well documented (Hamilton *et al*., 2007, Ismail *et al*., 2007). Nanoscale pits (Teixeira *et al*., 2003), grooves (Lenhert *et al*., 2005, Zhu *et al*., 2005) and protrusions (San Thian *et al*., 2008) promote contact guidance and cellular orientation to varying degrees depending on feature dimension and conformation (Dalby *et al*., 2007d), phenomena shown to increase tissue stability *in vitro* (Zhu *et al*., 2005). Of particular interest in studies examining the effect of these topographies is the reorganisation of the cell cytoskeleton and cell morphology in response to nanofeatures, parameters that have already been established as important mediators of direct mechanotransduction and changes in gene expression. Initiation of this process however is dependant on integrin interactions with the substratum and the topographical regulation of cell adhesion, a process which appear to be dependant on the symmetry and spacing of the underlying nanofeatures (Curtis *et al*., 2001, Sato *et al*., 2008).

1.17. The Effects of Nanoprotrusions on Cell Adhesion

Studies of cell adhesion on nanoscopic protrusions have increased greatly with the development of novel fabrication techniques, which provide robust, high throughput methods for the fabrication of topographic features ranging from the submicron to the true nanoscale. The fabrication of nanoprotrusions has been achieved using various methods including colloidal lithography (Hanarp *et al*., 1999), polymer demixing (Affrosman *et al*., 1996), electrospinning (Frenot & Chronakis, 2003) and EBL (Wilkinson, 2004). Of these, the first three methods provide a surface with random or semi-random nanoprotrusions while EBL can be employed to fabricate highly reproducible ordered nanopatterns.

Nanoprotrusions and raised topographical features are commonly found within the ECM of mineralised tissues (Bozec & Horton, 2006) Recently Dalby *et al*. investigated the

feasibility of modulating the adhesion and behaviour of human bone-marrow cells toward biomaterial surfaces with use of surfaces containing 33 nm high "islands" manufactured with use of polymer demixing. Here osteoblasts were shown to synthesise osteospecific proteins critical for bone formation (Dalby *et al*., 2008a). Conversely, studies by Dalby *et al* using nanoislands with increased height (95 nm) have demonstrated that fibroblasts initially undergo increased cytoskeletal organisation and filopodia formation when compared to cells cultured on flat controls. This initial phase is short-lived however, and fibroblasts begin to dedifferentiate and undergo anoikis due to lack of adhesion and cellular spreading (Dalby *et al*., 2003a). Similarly Berry *et al*. showed that three dimensional constructs with features of a similar dimension also reduced MSC adhesion (Berry *et al*., 2006).

Again, reducing the height of these nanoprotrusions has been shown to increase cellular adhesion in fibroblasts with accompanying up-regulations in proteins critical to cytoskeleton and filopodia dynamics (Dalby *et al*., 2002). Lim *et al* have demonstrated the increased incidence of mature adhesion plaque formation in osteoblasts cultured on nanoislands down to 11 nm in height (Lim *et al*., 2005b), again adhesion and proliferation of osteoblasts on these nanoislands was significantly reduced when island height was increased to 85 nm. Nanoislands fabricated by polymer demixing typically possess feature widths with microscale dimensions however, decreases in fibroblast adhesion formation are observed when cultured on nanocolumn type features with diameters of 100 nm. Again osteoblast adhesion was increased relative to planar control substrates on nanoislands varying from 3 – 30 nm (Lim *et al*., 2005a).

A common theme of cellular adhesion on nanoscale protrusions is the observation of a decrease in cellular adhesion with increasing protrusion height. Studies to date indicate the presence of a "restrictive zone" where nanoprotrusion height perturbs cellular adhesion (table 1.1). As a general rule, this reduction in cellular adhesion seems to be induced by nanoscale features greater than 100 nm, this however is related heavily to feature width, density and substrate chemistry as well as cell type, yet is observable on a wide variety of polymeric substrates fabricated by differing methods with a wide variety of cell types. Recent studies point to the disruption of adhesion elongation (Milner & Siedlecki, 2007), it seems the influential regulation of cellular adhesion stems from the

innate ability of surface protrusions to prevent mature FA formation which can be regulated by controlling interfeature area.

Table 1.1. The influence of nanoscale protrusions on cellular adhesion. Cellular adhesion was reported to decrease on structures measuring approximately 100 nm in height and with microscale widths and pitch. Conversely studies show an increase in adhesion formation when cells are cultured on nanofeatures with lower aspect ratio features as well as on features with increased height.

Study	Cell type	Chemistry	Pitch	Width	Height	Adhesion modulation
(Milner & Siedlecki, 2007)	Human foreskin fibroblast	Poly(L-lactic acid)	590 nm	500-550 nm	250-300 nm	Increased adhesion formation
(Dalby *et al.*, 2003a)	h-TERT fibroblast cells	pS	1.67 μm±0.66 μm	0.99 μm±0.69 μm	95 nm	Reduced cell adhesion
(Berry *et al.*, 2006)	Human Bone marrow stromal cells	pS/poly(n-butyl methacrylate) blend	-	0.99 μm±0.69 μm	90 nm	Reduced adhesion formation
(Lim *et al.*, 2005a)	Human foetal osteoblastic cells	Poly lactic acid/pS blend	-	-	15-45 nm	Increased adhesion formation
(Dalby *et al.*, 2002)	h-TERT fibroblast cells	pS/pBrS blend	527 nm	263 nm	13 nm	Increased adhesion formation
(Lim *et al.*, 2005b)	Human foetal osteoblastic cells	pS/pBrS blend	527 nm	263 nm	11 nm	Increased adhesion formation

1.18. The Effects of Nanopits on Cell Adhesion

As with nanoscale protrusions, the fabrication of nanopit type topographies has benefited greatly from the advent of high resolution writing techniques such as EBL and dip-pen nanolithography. Yet less ordered topographies can be fabricated via self-organisation techniques, such as polymer demixing to produce large area nanotopographic substrates for assessing the cellular response. Nanopores are identified as common constituents of tissues *in vivo*, notably basement membrane of the cornea (Abrams *et al.*, 2000) and the aortic heart valve (Brody *et al.*, 2006) and may be implicated in the regulation of cell behaviour and function. Pitted topographies have been shown to produce differing effects on cellular adhesion, depending on pit diameter and interestingly the order and symmetry of pit positioning (Biggs *et al.*, 2006, Dalby *et al.*, 2008b). The majority of studies investigating cellular adhesion on nanotopographies agree that adhesion is reduced on

ordered or densely arranged nanopit and nanoporous substrates with diameters ranging from nano to the micron scale (Lim *et al.*, 2007).

Studies by Hart *et al* showed that highly ordered arrays of 120 nm wide nanopits, in both hexagonal and square conformation patterns, significantly reduced cell adhesion in osteoprogenitor populations by directly modulating filopodial formation (Hart *et al.*, 2007), indicating the ability of these cells to gather spatial and topographical signals from nanoscale pits, depending on how they are spatially arranged. It is reported that greatest adhesion formation on nanoscale pit arrays is noted in between nanopit features at the interpit region (Dalby *et al.*, 2006a). This suggests modifying the planar interpit area can affect cellular adhesion. Recent studies also indicate the ability of cells to respond significantly to small changes in the order of nanopit spacing and that modulating the order of pit conformation significantly affects both cellular adhesion and cellular function (Biggs *et al.*, 2007, Dalby *et al.*, 2007d) and that it is the degree of order which is critical for these processes not nanopit dimension.

Currently the trends regarding topographical modification of cell adhesion indicate that both protrusion type features and pits significantly affect adhesion when in the nanoscale. This has recently been demonstrated in a study by Lim *et al* which concluded that greater cell adhesion and modified integrin expression was noted when topographic features have ca. 10–20 nm scale z-axis dimension (height or depth), and that this is regardless of topographic shapes (island or pit). Also, this effect deteriorated when nanofeatures reach a height or depth of ca. 100 nm, again indicating the perturbing effects of nanopits and pores on cell adhesion (table 1.2) (Krasteva *et al.*, 2004, Lim *et al.*, 2007). As with nanoscale protrusions, increasing pit dimensions to the microscale has been shown to increase cell spreading, and mature FA formation in endothelial cells, and also increase FA mediated signal transduction by increased tyrosine phosphorylation (Hamilton *et al.*, 2007).

Table 1.2. The influence of nanoscale pits on cellular adhesion. Cellular adhesion was reported to decrease on structures measuring approximately 100 nm in depth and with widths and pitch varying from 35-300 nm. Conversely adhesion is reported to increase when topographical structures exceed or do not meet these critical feature dimensions.

Study	Cell type	Chemistry	Pitch	Width	Depth	Adhesion modulation
(Karuri *et al.*, 2006)	Corneal epithelial cells	Silicone	400 nm	Variable	350 nm	Increased adhesion
(Lim *et al.*, 2007)	Human foetal osteoblastic cells	poly(L-lactic acid)/pS blend	Variable	90 nm	14 nm	Increased adhesion
(Lim *et al.*, 2007)	Human foetal osteoblastic cells	poly(L-lactic acid)/pS blend	Variable	400 nm	45 nm	No modification
(Hart *et al.*, 2007)	Osteoprogenitor cells	poly(carbonate)	300 nm Hexagonal array	120 nm	100 nm	Decreased adhesion formation
(Dalby *et al.*, 2006a)	h-TERT fibroblast cells	pMMA	300 nm Hexagonal array	120 nm	100 nm	Decreased focal and fibrillar adhesion formation
(Curtis *et al.*, 2004)	h-TERT fibroblast cells	polycaprolactone	100 nm	35 nm	-	Decreased adhesion formation
(Curtis *et al.*, 2004)	h-TERT fibroblast cells	polycaprolactone	200 nm	75 nm	-	Decreased adhesion formation

1.19. The Effects of Nanogrooves on Cell Adhesion

Nanogrooved topographies consist of alternating grooves and ridge features differ from both nanoprotrusions and nanopits as they produce very predictable effects on cellular morphology – which can be argued are directly related to cellular alignment through contact guidance (Zhu *et al.*, 2004). Common methods of fabrication include EBL (Diehl *et al.*, 2005), photolithography (Dalby *et al.*, 2006b) and direct laser irradiation (Zhu *et al.*, 2005) which may be employed to yield anisotropic substrates with varying feature widths and depths.

A key fabrication tenet of nanogroove substrates for the study of cellular-interface interactions is that of biomimetic ECM design, an attempt to mimic the topographical cues imparted by the fibrous nature of ECM. Further to this, the elongated morphology and alignment induced by grooved substrates may resemble the natural state of many cell

populations *in vivo*, suggesting that nanogrooved surfaces may induce enhanced tissue organisation and facilitate active self-assembly of ECM molecules to further mediate cell attachment and orientation. A wide range of cell types such as fibroblasts (Dalby *et al.*, 2003c), osteoblast (Lenhert *et al.*, 2005), nerve cells (Yim *et al.*, 2007) and MSCs (Dalby *et al.*, 2006b) respond profoundly to grooved substrates. Further to this cells cultured on nanogrooves have been shown to up-regulate the expression of fibronectin – an initiator of integrin binding (Chou *et al.*, 1995) as well as proteins key in cellular adhesion (Dalby *et al.*, 2008c) and the transduction of mechanical forces (Jin *et al.*, 2008). A study by Dalby *et al* recently demonstrated that cellular alignment and adhesion formation on nanometric grooves is regulated by the receptor of activated protein kinase C1 (RACK1) – an important mediator of indirect mechanotransductive signalling which is thought to regulate integrin-mediated cell migration (Hermanto *et al.*, 2002). Increased RACK1 expression was shown to disrupt contact guidance and promote cellular spreading and adhesion formation (Dalby *et al.*, 2008c).

As with the topographies discussed above, nanogroove features seem to directly influence the formation of FAs in cultured cells, unlike the above however, nanogrooved topographies also influence the orientation of the adhesion plaque (Teixeira *et al.*, 2004). At present no clear conclusions have been reached regarding the absolute dimensions required for cellular and adhesion alignment, more likely this process is cell specific and dependant on whether the cell is isolated or part of a colony (Clark *et al.*, 1990). It is probable that an interplay between groove pitch and groove depth regulates adhesion alignment, yet present studies indicated groove depth as being more influential in adhesion alignment (Clark *et al.*, 1990, Loesberg *et al.*, 2007). Studies show that cell and cytoskeletal alignment in human corneal cells has generally been found to be more pronounced on patterns with ridge widths between 1 and 5 μm than on grooves and ridges with larger lateral dimensions (Karuri *et al.*, 2004, Matsuzaka *et al.*, 2000, Teixeira *et al.*, 2003) and that beyond nanoscale groove widths, FAs are almost exclusively oriented obliquely to the topographic patterns (Teixeira *et al.*, 2006). In many cell types data suggest that cellular function and adhesion is strongly enhanced with decreasing groove feature sizes into the nanometre range (Lu *et al.*, 2008), current studies have indicated however, that contact guidance is not initiated on groove depths below 35 nm or ridge

widths smaller than 100 nm (table 1.3) (Loesberg *et al*., 2007).

Table 1.3. The influence of nanoscale grooves on cellular adhesion. Nanogroove substrates modulate adhesion orientation as well as regulate adhesion frequency. Studies indicate that substrates with a groove pitch below 35 nm and a depth below 70 nm do not initiate contact guidance in most cells.

Study	Cell type	Chemistry	Pitch	Depth/Height	Adhesion modulation
(Loesberg *et al*., 2007)	Rat dermal fibroblasts	pS	100 nm	35 nm	Reduced alignment and adhesion
(Teixeira *et al*., 2006)	Human corneal epithelial cells	Silicon oxide	400 & 4000 nm	70 & 1900 nm	Oblique Adhesion formation
(Lu *et al*., 2008)	Rat aortic endothelial cells	Titanium oxide	750 nm	150 nm	Increase adhesion
(Heydarkhan-Hagvall *et al*., 2007)	Human foreskin fibroblasts	Silicon oxide	230 nm	200-300 nm	Increased Integrin β_3, Adhesion alignment
(Karuri *et al*., 2004)	Human corneal epithelial cells	Silicon oxide	400 nm	250 nm	Adhesions restricted to the tops of the ridges
(Teixeira *et al*., 2006)	Human corneal epithelial cells	Silicon oxide	800-2000 nm	550 -1150 nm	Parallel adhesion formation

Adhesion formation on nanogrooved substrates is shown to occur predominantly on ridge structures (Teixeira *et al*., 2003) or at the groove/ridge boundaries (Wojciak-Stothard *et al*., 1996). Furthermore, it has been suggested that the geometrical dimensions of the FA plaques force propagation on a grooved surface to be orientated parallel to the ridges (Ohara & Buck, 1979). It may be argued that the increased surface area of these topographies can lead to increased topographical sites for adhesion formation and an increase in cellular adhesion. In reality however, nanogroove-induced cellular alignment is associated with a reduction in cellular FA formation relative to planar substrates.

Cell alignment to the long axis of the groove is typically accompanied by the organisation of cytoskeletal elements in an orientation parallel to the grooves. A study published by Teixeira *et al*. (2006) notes that epithelial cells switch from parallel to perpendicular

alignment on grooved substrate when features decreased in pitch size from 4000 to 400 nm, rearranging the FA distribution in a similar manner (Teixeira *et al*., 2006).

1.20. Aims and Objectives

Research on biomaterial surface characteristics and elicited cell response therein has a key role for continued success in the field of orthopaedic design. A material surface *in vivo* functions as more than a simple boundary to the surrounding environment but supports a dynamic extracellular molecular constituent and provides topographical cues that may be perceived by cells as spatial information. Nanotopography has recently been proposed as a contributing factor in the regulation of the cellular response and a valuable tool for modulating functionality, qualities invaluable in the design of orthopaedic devices.

The thesis therefore will examine the hypothesis that biomimetic nanotopographical features can influence both the adhesion of primary human osteoblasts and the functional response of MSCs in a manner complimentary to implant design, and that both cellular adhesion and differentiation may be modulated by topographical modification alone. This will be achieved by the following:

- *The development and fabrication of polymeric substrates possessing defined nanotopographical features in chemically identical polymeric replicas.*

- *An investigation into the effects of these topographies on FA plaque formation in synthesis-phase (S-phase) human osteoblasts.*

- *An investigation into the effects of these topographies on STRO-1+ MSC function and subsequent differentiation.*

CHAPTER II

Materials and Methodology

2.1. General Introduction

This section will further rationalise the hypothesis that drove the experimental studies and the use of the materials in this thesis as well as the methodologies employed to examine the effect of nanoscale topographies on cellular function.

Osteoblast and osteoblast-like cell models from multiple species and sources have been implemented as valuable models in orthopaedic studies, particularly those involving cell-substratum adhesion assays (Dettin *et al*., 2008, Dulgar-Tulloch *et al*., 2008) and experimental modulation of intracellular signalling pathways. To ensure the osteoblasts used in this study retained high levels of functionality primary human cells were used at low passage.

In order to elucidate how nanotopographical cues may effect the general morphology and adhesion formation in osteoblast populations both epifluorescent and SEM microscopical techniques were employed to analyse cellular cytoskeletal elements and FA formation in primary human osteoblasts. Immunofluorescent labelling of vinculin, S-phase nuclei and cytoskeletal elements was developed to facilitate high-throughput adhesion quantification in a synchronised population of cells. Immunocytochemical labelling was also combined with low voltage field emission scanning electron microscopy (SEM) in order to simultaneously visualise the interactions that occur between the low aspect ratio features present on experimental substrates and the FA plaque of adhering cells. This technique improves upon epifluorescent methods by allowing regulation of depth of signal formation, increasing the spatial resolution available.

Live cell imaging was also employed in this thesis to visualise the modulation of adhesion formation in metabolising osteoblasts over a finite time period. Osteoblasts were transfected with plasmid DNA encompassing yellow fluorescent protein (YFP) modified vinculin. YFP is a 27 kDa molecule with an excitation peak of 490 nm and an emission peak of 527 nm *(Prendergast & Mann, 1978)*. These proteins are commonly created by mutating threonine[203] to an aromatic amino acid, typically tyrosine. The resulting π-π stacking and increased local polarisability immediately adjacent to the chromophore are believed to be responsible for the 20 nm shift to longer excitation and emission wave-lengths (Griesbeck *et al*., 2001, Ormo *et al*., 1996, Prendergast & Mann, 1978). Fluorescent proteins have been used in a myriad of applications for biological

systems and have previously been used in studies concerning the role of vinculin in FA dynamics (Cohen *et al*., 2005, Cohen *et al*., 2006).

Human MSCs are increasingly being recognised as crucial in the experimental processes employed to investigate the osteoinductive potential of future biomaterials. In particular, MSCs have been used extensively to determine the effects of topographical modification on osteospecific differentiation and functional modulation (Ciapetti *et al*., 2006, Dalby *et al*., 2007b, Schneider *et al*., 2004).

Although there is currently no assay that can be performed on a single MSCs to determine whether that cell is capable of undifferentiated division, there are surface antigens that can be used to isolate a population of cells that have similar self-renewal and differentiation capacities. Yet MSCs, as a population, typically do not all express all the proposed markers; and it is not certain which ones must be expressed in order for that cell to be classified as of osteogenic lineage. To circumvent some of the issues around the characterisation of the skeletal stem cell, magnetic activated cell sorting (MACS) combined with immunoselecting for the stromal cell surface antigen - STRO-1 was used for the isolation of MSC rich human marrow stromal cell cultures (Oreffo *et al*., 2005, Tare *et al*., 2008).

Gronthos and co-workers found that the heterogeneity of the stromal cell population could be reduced by isolation using a monoclonal antibody to STRO-1, which recognises a trypsin-resistant cell surface antigen present on a subpopulation of bone marrow cells (Gronthos & Zannettino, 2008, Mirmalek-Sani *et al*., 2006). Cells expressing STRO-1 were first identified by Simmons (Simmons & Torok-Storb, 1991) been found to be predominantly adherent, potentially high-growth, colony-forming units which exhibit multipotent differentiation capability (Dennis *et al*., 2002).

To investigate the topographical induction of MSCs differentiation, functional modification was examined by 1.7 K microarray chip analysis. While it seems more appropriate to use large arrays to search for patterns or whole group pathways of gene activity, arrays can also be used to observe individual gene changes. Both approaches were used here in order identify large-scale modulation of MSCs function as well as to locate complex signalling pathways of interest and changes in individual gene expression. Two pathways strongly implemented in the adhesion process and in osteodifferentiation

were dissected and individual gene modulations analysed in depth, namely integrin signalling (Carvalho *et al*., 2003) and wingless-type mouse mammary tumor virus integration site family member (Wnt)/β-catenin signalling respectively (Piters *et al*., 2008).

2.2. Cell Models

2.2.1 Primary Human Osteoblasts

All experiments were performed with adult human osteoblastic cells after 1-4 passages *in vitro*. Primary human osteoblasts (HOBs) were derived from a femoral head biopsy of an 84 year old Caucasian female and a knee biopsy taken from a 74 year old Caucasian female (purchased from *PromoCell®, Heidelberg, Germany*). Osteoblasts were isolated from the spongiosa of hip or knee bone. Briefly, the trabecular bone was cleaned from connective tissue, divided into smaller pieces (approx. 4 mm × 4 mm) and placed into a Petri dish (10-15 pieces per dish) and filled with sufficient osteoblast growth medium (OGM). After about 10-14 days, osteoblasts grew out of the bone into the Petri dish. When the cells reached sub-confluency, the bone pieces were removed from the dish and the cells trypsinised, counted, and re-seeded into new vessels. HOBs were identified as osteoblastic cells on the basis of (a) positive staining for alkaline phosphatase (ALP), (b) increase in ALP expression after 1,25-vitamin D3 treatment, (c) secretion of osteocalcin in the presence of 10^{-10} M 1,25-vitamin D3 and 10^{-8} M vitamin K, (d) secretion of type I procollagen peptide in the presence of 50 μg/ml ascorbic acid, and (e) formation of mineralising nodules in the presence of 10 mM glycerophosphate and 50 μg/ml ascorbic acid, as previously demonstrated (Kasperk *et al*., 1995a). For more information see (Kasperk *et al*., 1995b).

After establishing primary cultures, the cells are frozen in liquid nitrogen in serum-free freezing medium (*PromoCell®, Heidelberg, Germany*), using a computer controlled freezing unit following strict protocol. Proliferating cell cultures were made from cryoconserved cells which have been thawed and cultured for three days at PromoCell's cell culture facility. HOBs were maintained in 75 cm^2 culture flasks in OGM (*PromoCell®, Heidelberg, Germany*) containing 10% foetal calf serum (FCS), and

supplemented with 10^{-10} M 1,25-vitamin D3, 10^{-8} M vitamin K, 50 μg/ml ascorbic acid, 10 mM glycerophosphate as provided by the osteoblast nutrient supplement C-39615 (*PromoCell®, Heidelberg, Germany*). Media was replaced every 2-3 days.

2.2.2 STRO-1 Positive MSCs

STRO-1+ MSCs were provided by Prof Richard Oreffo, University of Southampton. STRO-1+ cells were isolated from bone marrow samples obtained from haematologically normal patients undergoing routine total hip replacement surgery. Only tissue that would have been discarded was used with the approval of the Southampton General Hospital Ethics Committee. A total of 12 samples (five male and seven female of mean age 71±11 years) were prepared.

Marrow cells were harvested using minimal essential medium - α modification (α-MEM) to aspirate cells from trabecular bone marrow samples. Cells were pelleted by centrifugation at 250 *g* for 4 minutes at 4°C. The cell pellet was resuspended in α-MEM and passed through a nylon mesh (70 μm pore size; *Becton–Dickinson, Franklin Lakes, NJ*).

Red blood cells were removed by centrifugation using lymphoprep solution (*Robins scientific, Solihull, UK*). The cells from the buffy layer were resuspended at 1×10^8 cells in 10 ml blocking solution (4-(2-hydroxyethyl)-1-piperazineethanesulfonic acid (HEPES) buffered saline solution (HBSS) with 5% volume per volume (v/v) FCS, 5% (v/v) human normal serum, and 1% weight per volume (w/v) bovine serum albumin (BSA) fraction volume) and incubated with STRO-1 antibody in a hybridoma supernatant (*hybridoma was provided by Dr. J. Beresford, University of Bath*). Cells were incubated with MACS anti-immunoglobulin M beads (*Miltenyi Biotech, Bisley, UK*) after washing the excess STRO-1 antibody with MACS buffer (HBSS containing 1% fraction volume BSA). Labelled cells were then added to an un-magnetised column and collected as control unsorted cells or separated as follows. Antibody incubated cell suspension was added to a column within the magnet and elutant was collected as the STRO-1 negative fraction. The column was then washed and in the absence of the magnet, 1 ml MACS buffer was added and the resultant cell population was eluted as the STRO-1 positive fraction. For

each fraction, five cell counts were performed using a fast read disposable counting chamber (*ISL, Paignton, UK*).

2.3. Experimental and Control Substrate Preparation

Experimental substrate fabrication was exclusively in polymethylmethacralate (pMMA), (a non-biodegradable polymer which has FDA approval for implants) as discussed in detail in the materials and methodology section of chapters 4, 5 and 6. All experimental and control substrates were first subjected to a sterilisation process prior to cell seeding, pMMA substrates were rinsed in 70% ethanol/water solution 3 times for 3 seconds. All pMMA replicates were next rinsed twice in HBSS pH 7.4 for 5 seconds to remove any ethanol residue. Planar pMMA (*Goodfellow, Cambridgeshire, UK*) replicas trimmed to approximately 2 cm^2 were used as control substrates. Planar controls possessed an average roughness (Ra) of 1.2 nm over 10 mm^2 and a maximum roughness (Rmax) of 5.6 nm over 10 mm^2 as deduced by SEM and atomic force microscopy (AFM) analysis. (fig. 2.1).
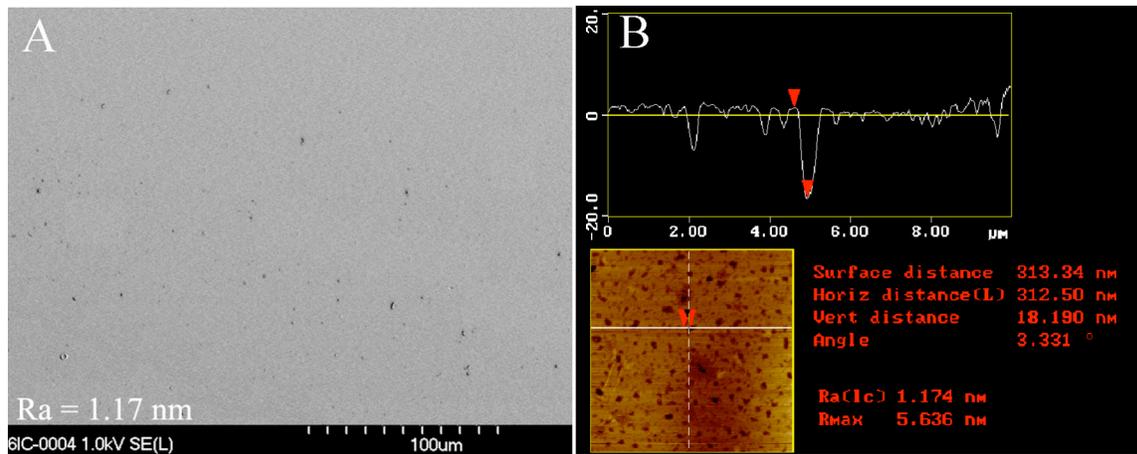
Fig. 2.1. Topographical characterisation of planar pMMA. (A,B) SEM and AFM analysis revealed ultra-smooth pMMA substrates possessed a planar topography with an Ra of 1.2 over 10 mm^2

2.4. Fixation for Immunocytochemical - SEM

The immunolabelling method was a modified version of that first described by Richards *et al.* (Richards *et al.*, 2001b). Cells were rinsed for 2 minutes in 0.1M Piperazine-1,4-

bis(2-ethanesulfonic acid) (PIPES) buffer, pH 7.4 before being permeabilised with buffered 0.5% Triton X-100 (4 × 1 minutes) (10.3 g sucrose, 0.292 g NaCl, 0.06 g MgCl$_2$, 0.476 g HEPES, 0.5 ml Triton X 100, in 100 ml water, pH 7.2) to remove the cell membrane. Cells were then stabilised in 4% paraformaldehyde with 1% sucrose in 0.1 M PIPES, pH 7.4 buffer, for 5 minutes and rinsed three times for 2 minutes in 0.1 M PIPES buffer to remove unreacted aldehyde. Non-specific binding sites were blocked with 1% BSA and 0.1% polysorbate 20 (Tween 20) in 0.1 M PIPES buffer, pH 7.4 for 15 minutes. Cells were then incubated with anti-vinculin monoclonal anti-human immunoglobulin G (IgG) raised in mouse, clone hVin-1 (*1:200, Sigma, Poole, UK*) in PIPES buffer/1% BSA /0.1% Tween 20 for 2 hours at 37°C. Cells were rinsed six times for 2 minutes in PIPES/ 1% BSA/0.1% Tween 20. Non-specific binding sites were blocked with 5% goat serum/ 1% BSA/0.1% Tween 20 in PIPES buffer for 15 minutes. The cells were labelled with goat anti-mouse 5 nm gold conjugate (*1:200, BB International, Cardiff, UK*) in PIPES buffer/1% BSA/0.1%. Tween 20 overnight for 12 hours at 22°C. All samples were then rinsed six times for 2 minutes in PIPES buffer. Samples were fixed permanently in 2.5% glutaraldehyde for 5 minutes in PIPES buffer and rinsed three times for 2 minutes in PIPES buffer. Gold probes were silver-enhanced with a silver developing solution for 7 minutes (*BBI International, Cardiff, UK*). Samples were immediately rinsed twice in ultra-pure water to remove any unreacted enhancer. Additional contrasting of the cell was accomplished by staining the cells with 1% osmium tetroxide in PIPES pH 6.8 for 1 hour followed by a final rinsing six times for 2 minutes in PIPES buffer.

2.5. Post-Fixation Processing for Immunocytochemical-SEM

The HOBs were next dehydrated through an ethanol series (50, 60, 70, 80, 90, 96, and 100%) followed by a fluorisol/ethanol series (25, 50, 75, and 100%) (fluorisol—1,1,2 trichloro,1,2,2, trifluoro ethane). The samples were then completely dehydrated with a SPI-DRY^{TM} critical point dryer (*Structure Probe Inc., Leicestershire, UK*), mounted on aluminium stubs and coated with a 12 nm layer of carbon using a Baltec CED030 carbon thread evaporator. (*Baltec, FL*). Samples (both with and without cells) were imaged using a Hitachi S-4700 field emission SEM fitted with an Autrata yttrium aluminium garnet

backscattered electron (BSE) scintillator type detector. The images were taken in both the secondary electron (SE) and BSE modes, with accelerating voltages between 2-10 kV. BSE images were taken with an emission current of 50 μA, an aperture of 100 μm (apt1) and working distances of 10-12 mm to allow low voltage imaging (Richards & Ap Gwynn, 1995).

2.6. Plasmid Expansion and Cellular Transfection

2.6.1. Bacterial Transformation

The complementary DNA (cDNA) starter - a plasmid with an inserted code for vinculin plus a YFP tag, was generated and generously provided by Prof Susan Craig (Johns Hopkins University School of Medicine) as DNA spotted onto filter paper. The spotted region was isolated and placed in 50 μl of a 10 mM tris(hydroxymethyl)aminomethane (Tris) solution in an ependorff tube for 15 mins. A 50 μl aliquot of one shot top 10 chemically competent *Escherichia coli (E. coli)* cells was placed in ice to thaw from -80°C. The ependorff tube containing the plasmid DNA was centrifuged at 16000 *g* for 30 sec and 5 μl of DNA solution was introduced into the bacterial aliquot and left in the icebox for 30 minutes. The *E. coli* aliquot was subsequently heat-shocked for 30 seconds at 42°C before being returned to the icebox for another 2 minutes.

2.6.2. Plasmid Expansion and Isolation

A 200 μl solution of super-optimal catabolite media (20 g bacto tryptone, 5 g yeast extract, 0.58 g NaCl, 0.186 g KCl in 1 L of water) (*Invitrogen, Carlsbad, California*) was added to the bacterial cell suspension for 1 hour at 30°C on a shaker table. The bacterial suspension was subsequently spread onto a lysogeny broth plate containing 25 μg/ml kanamycin (5 g tryptone, 5 g NaCl, 2.5 g yeast extract, 1.5 g of agar in 500 ml de-ionized water ph 7.5, 12.5 mg ampicillin).

Following 24 hours incubation at 37°C a colony was selected from the lysogeny broth plate and transferred to 500 ml of lysogeny broth media containing 25 μg/ml kanamycin (5 g tryptone, 5 g NaCl, 2.5 g yeast extract in 500 ml de-ionized water ph 7.5, 12.5 mg kanamycin). This bacteria suspension was incubated at 37°C for a further 24 hours to

allow bacterial expansion of the plasmid. High copy plasmid DNA was purified from this bacterial suspension using a QIAGEN plasmid midi kit and resuspended in a 10 Mm Tris buffer, pH 8.5 according to manufacturer protocols.

2.6.3. HOB Transfection

HOBs were expanded to passage 4 following 5 weeks of culture and approx. 70% confluency. The media was subsequently replace by 10 mls of HBSS for 1 minute which was removed prior to trypsinisation in 3 mls of 0.04% trypsin/0.03% ethylenediaminetetraacetic acid (EDTA) (*PromoCell®, Heidelberg, Germany*). Cellular transfection was accomplished with a human MSC nucleofector® kit VPE-1001 (*Amaxa AG, Cologne, Germany*). Cells were isolated by centrifugation at 250 *g* for 4 minutes before being resuspended in 100 µl of human MSC nucleofector® solution (*Amaxa AG, Cologne, Germany*) at 22°C and a final density of 5×10^5 cells per 100 µl. The cellular suspension was loaded into the specialised cuvette (*Amaxa AG, Cologne, Germany*) and 3 µl of the YFP-vinculin plasmid solution was added before mixing via gentle pipetting. Electroporation and plasmid nucleofection was accomplished with a Nucleofector® II system AAD-101N (*Amaxa AG, Cologne, Germany*) using the MSC transfection setting according to manufacture protocol. Cells were resuspended in 20 mls of OGM, warmed to 37°C and allowed to adhere for 10 hours in a 75 cm^2 culture flask. HOBs were then trypsinised as described above and seeded onto planar and experimental substrates at a final density of approx. 1×10^3 cells per ml to allow single cell imaging.

2.6.4. Live Cell Imaging

HOBS on planar and experimental substrates were transferred aseptically to preconstructed live-cell imaging conduits (fig. 2.2) for viewing with a Zeiss Axiovert 200 M microscope with a Zeiss Plan Neofluor 40 × (0.75 NA) lens, an analogue regulated environmental stage (*Zeiss, Hertfordshire, UK*) and a evolution™ QEi monochrome digital Camera (*Media Cybernetics, Bethesda, MD*). HOBs were maintained for 36 hours in nutrient mixture F-10 HAM (*Sigma, Poole, UK*) encompassing 10% FCS and supplemented with 10^{-10} M 1,25-vitamin D3, 10^{-8} M vitamin K, 50 µg/ml ascorbic acid,

10 mM glycerophosphate as provided by the osteoblast nutrient supplement C-39615 (*PromoCell®, Heidelberg, Germany*).

Conduits were fabricated from bi-sected 50 ml polypropylene centrifuge tubes (*Corning, Poole, UK*). These were sawed to approximately 10 mls in volume and attached via a polydimethylsiloxane (pDMS) seal to an underlying microscopy coverslip measuring 35 mm × 64 mm (*Agar scientific, Essex, London*). Conduits were sterilised by filling to the brim with 70% ethanol three times for 1 minute followed by washing with HBSS.
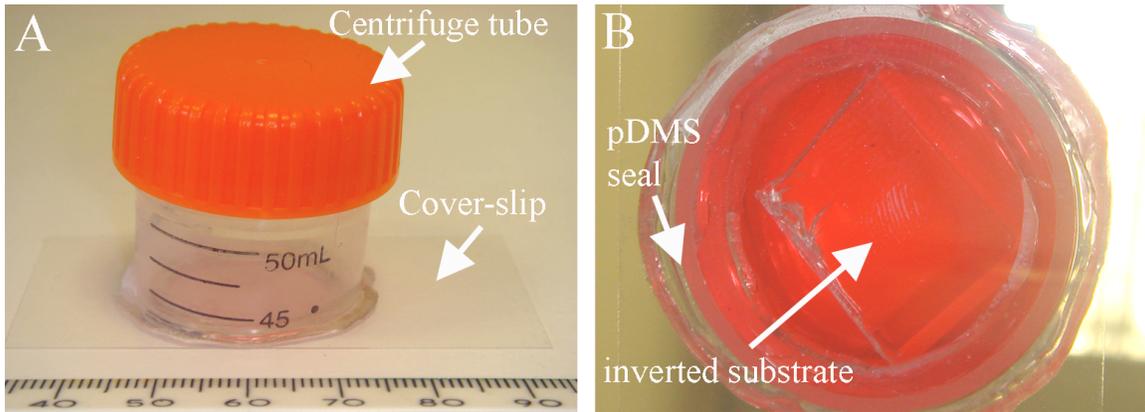
Fig. 2.2. The apparatus of YFP-vinculin live-cell imaging. (A) Live-cell imaging was conducted within airtight sterile conduits fabricated from polypropylene centrifuge tubes fused to an underlying coverslip. (B) Substrates were inverted to accommodate high-magnification live-cell imaging.

2.7. RNA Isolation and Microarray Analysis

STRO-1+ cells were seeded onto experimental and planar control substrates at a final density of 1×10^6 cells per ml to facilitate high-density cell adhesion and increase ribonucleic acid (RNA) yield. Cells were maintained at 37°C with a 5% CO_2 atmosphere in α-MEM (*Invitrogen, Carlsbad, California*) containing 10% FCS, which was replaced every 2 days.

Cells were cultured up to approximately 90% confluency (21 days in culture) so as to allow sufficient quantities of RNA to be extracted for microarray hybridisation. Cells were lysed and total RNA was extracted using a Stratagene Absolutely RNA Miniprep Kit according to manufacturer's protocols (*Agilent Technologies, Cheshire, UK*). OGM was removed and each sample was rinsed in 600 μm of a lysis buffer encompassing 0.7%

β-mercaptoethanol. STRO-1+ MSC lysate was collected via a rubber cell-scraper into a 2 ml prefiltered receptacle tube and centrifuged with an Eppendorf minispin (*Sigma, Poole, UK*) at 14,000 *g* for 5 minutes.

The resulting filtrate was retained and diluted with 500 µm of 70% ethanol before being mixed thoroughly with a vortex rotamixer (*Hook & Tucker, Croydon, UK*). Approximately 700 µm of this mixture was transferred to an RNA binding prefiltered receptacle tube and centrifuged at 14,000 *g* for 1 minute. This process was repeated with the remaining filtrate mixture. The filtrate was subsequently discarded and the filter rinsed by the addition of 600 µl of low salt wash buffer and centrifuging at 14,000 *g* for 1 minute. This process was repeated and all filtrate discarded.

The filter was incubated for 15 minutes at 37°C with 55 µm of DNase buffer encompassing 10% lyophilised DNase-I. The filter was washed with 600 µl of high salt wash buffer and centrifuged at 14,000 *g* for 1 minute. This process was repeated with a low salt wash buffer. Following washing all filtrate was discarded and the filter subjected to a further washing with 300 µl of low salt wash buffer followed by centrifuging at 14,000 *g* for 2 minutes.

The dried filter was transferred to a 1 ml Eppendorf tube and incubated for 2 minutes at 22°C with 40 µl of elution buffer. The tube and filter were subsequently centrifuged at 14,000 *g* for 1 minute. This elution process was then repeated and the filtrate retained.

Measurement of extracted RNA yields was performed with a NanoDrop® ND-1000 UV-Vis Spectrophotometer at ratios of 230/260 nm and 260/280 nm. From this 2 µg of RNA from each sample was used to make cyanine 3 or cyanine 5 - (*Amersham Biosciences, Uppsala, Sweden*) labelled cDNA using Superscript II reverse transcriptase with a poly-T messenger ribonucleic acid (mRNA) primer (*Invitrogen, Carlsbad, California*). The number of microarray chips and RNA sample replicates used was 5, thus giving 5 control and 5 test RNA isolates.

Samples were prepared for hybridisation by combining fragmented salmon sperm DNA (*0.5 µg/µl; Invitrogen, Carlsbad, California*) and yeast transfer RNA (tRNA) (*0.5 µg/µl; Invitrogen, Carlsbad, California*) in EasyHyb solution (*Roche Diagnostics, East Sussex, UK*). Samples were hybridised for 16 hours at 37°C onto three cDNA microarrays containing 1,718 known human expressed sequence tags. Arrays were next washed three

times at room temperature with 0.1% (v/v) saline sodium citrate (SSC) containing 0.1% (v/v) sodium dodecyl sulfate (SDS) followed by one wash with 0.1% SSC alone. Fluorescence intensities were captured using a Packard Scanarray Lite (*Perkin Elmer, Boston, MA*) laser confocal scanner. Data was exported into a spreadsheet where the mean gene changes were calculated.

This data was up-loaded to the Ingenuity® Pathways Analysis (IPA) server, (Ingenuity® Systems, www.ingenuity.com). The functional and canonical analyses were then generated through the use of IPA. Up and down regulated genes were associated with canonical pathways in the Ingenuity® Pathways knowledge base. The significance of the association between the data set and the canonical pathway was measured in 2 ways: 1) The so-called canonical or classical activation pathways were described as a ratio of the number of genes from the microarray analysis that map to the pathway divided by the total number of genes that map to the canonical pathway. 2). Right-tailed Fischer's exact t test (Fisher, 1922) was used to calculate a probability value (p-value) determining the probability that the association between the genes affected by experimental topographies and the canonical pathway is explained by chance alone. The smaller the p-value is, the less likely that the association is random, and the more significant the association.

In general, p-values less than 0.05 indicate a statistically significant, non-random association. In this method, the p-value for a given function, pathway, or list is calculated by considering (1) the number of focus molecules that participate in that function, pathway, or list and (2) the total number of molecules that are known to be associated with that function, pathway, or list in the Ingenuity® knowledge base. The more focus molecules involved, the more likely the association is not due to random chance, and thus the more significant the p-value. Similarly, the larger the total number of molecules known to be associated with the process, the greater the likelihood that an association is due to random chance, and the p-value accordingly becomes less significant. In short, the p-value identifies statistically significant over-representation of focus molecules in a given function, pathway, or list. Over-represented functions, pathways, or lists have more focus molecules associated with them than expected by chance. Regarding the experimental work described within this thesis, increased statistical significance emerges from increased numbers of genes measured which are specific to a particular pathway,

greatly reducing the possibility that changes in pathway functions are due to chance alone.

2.8. Discussion

Throughout the body of this work pMMA was used as the material of choice for the fabrication of experimental and planar control polymeric replicate. Its qualities of relative biocompatibility, reliability, relative ease of manipulation, and low toxicity have been extensively characterised and incorporated by many different medical specialties. pMMA has been used for bone cements, contact and intraocular lens, screw fixation in bone, filler for bone cavities and skull defects and vertebrae stabilisation in osteoporotic patients. Although numerous novel alloplastic polymers show promise, the versatility and reliability of pMMA cause it to remain a popular and frequently used in cell biology assays (Hautamaki *et al.*, 2008, Race *et al.*, 2008). Acrylic bone cements have played and still play a key role in the anchorage of prostheses to the surrounding bone in cemented arthroplasties. Charnley introduced the self-polymerising pMMA bone cement into contemporary orthopaedics (Charnley, 1960). Owing to the nature of the pMMA bone cement, it provides an excellent primary fixation of the prosthesis, but without further modification, (chemical or topographical) it does not promote a biological secondary fixation.

Although cell culture has proved invaluable in the study of bone biology, *in vitro* model systems cannot reproduce the complex three-dimensional micro and nanoenvironment that constitutes bone tissue. Nonetheless, despite the limitations of the various systems, *in vivo* culture systems with primary osteoblasts or osteoblast-like cell lines have provided significant and important contributions to our understanding of the normal processes leading to bone formation, remodeling and resorption.

It is likely that primary cells derived from human bone tissue contain osteoblasts at all stages of differentiation, including osteoprogenitor cells that proliferate before undergoing a series of maturational steps to become differentiated osteoblasts capable of forming mineralised nodules in culture (Aubin, 1998; Malavalk *et al.*, 1999). Work carried out with primary cell cultures have provided much insight into the phenotypic

characteristics of cells of the bone microenvironment, and the factors governing their development and function. Moreover primary cultures are widely used to study the progression of differentiation *in vitro*, while the great majority of osteoblast-like cell lines do not mineralise in culture. Although it is not yet possible to grow functional bone tissue in the laboratory, much knowledge has been generated from the characterisation and isolation of primary cells regarding the processes of bone formation and resorption and the factors that regulate the fine balance essential for skeletal homeostasis.

When studying MSC differentiation cell origin and phenotype are essential aspects in bone tissue engineering. This has been recapitulated by different articles, particularly in the field concerning bone marrow-derived stem cells (Fang *et al*., 2008, Steinhardt *et al*., 2008). As only one in every 100,000 nucleated cells derived from bone marrow is a stem cell, a procedure of isolation is required to decrease the inclusion of non-MSCs (Montjovent *et al*., 2004). Here selective STRO-1+ sorting was undertaken to ensure a population of cells with multilineage potential. STRO-1+ selection has repeatedly been shown to be a reliable robust method of MSC isolation (Gronthos & Zannettino, 2008), further to this, STRO-1+ cells show effective hard tissue formation *in vivo* (Yang *et al*., 2008).

One important consideration regarding the function of HOB and STRO-1+ MSC populations is that of mean donor age. During aging, cells of different organs undergo several cellular and genetic changes leading to impairment of their performance both *in vitro* and *in vivo* (Kveiborg *et al*., 2001, Narayanan *et al*., 1996), an age-related decrease in signals needed for optimal function of osteoblasts however has also been demonstrated (e.g. growth hormone and insulin-like growth factor-1 (IGF-I) (Kveiborg *et al*., 2000, Pfeilschifter *et al*., 1993). It has previously been shown however that the number of MSCs present in human bone marrow is maintained during aging suggesting that the bone forming potential of the individual osteoblasts is the rate limiting step during bone formation (Stenderup *et al*., 2001).

Advances in microarray bioinformatics, such as IPA, as used here, have allowed a move away from gene fishing and the problems associated with microarray reliability. Rather, it is now possible to consider gene responses as comparative functional changes. To do this, primary statistics are first generated, which considers fold-change, false discovery rate

and array spot quality and are used to feed robust changes into pathway and functional databases, thus changes in single gene expression may be complied into a comprehensive and integrative schematic of changes in cellular signalling pathways and function.

In order to examine the modulation of this signalling system in STRO-1+ MSCs, functional analysis of integrin signalling was chosen for individual gene analysis, the role of which is discussed in section 1.12.

As well as integrin signalling pathways, Wnt/β-catenin signalling has previously been shown to be regulated by cellular adhesion and to control the ubiquitination and stability of the FA protein paxillin. More importantly Wnt/β-catenin signalling pathways have been shown to be important in osteogenesis (Deng *et al*., 2008, Piters *et al*., 2008). Studies by Day *et al* demonstrated the association of genetic ablation of β-catenin in the developing mouse embryo with the formation of chondrocytes at the expense of osteoblast differentiation during both intramembranous and endochondral ossification. Conversely, ectopic up-regulation of the canonical Wnt signalling led to suppression of chondrocyte formation and enhanced ossification (Day & Yang, 2008).

Chapter III

Adhesion Quantification and Protocol

Development

3.1. General Introduction

This chapter describes the development of a tailored protocol to allow high-throughput adhesion quantification of S-phase cells. It is noted that at this initial stage, the substrate materials described in this chapter were chosen purely for ready availability. HOBs were cultured on 120 nm diameter, 300 nm centre-centre spacing, and 100 nm deep pit arrays. A master pattern was produced by EBL and deep reactive etching of silicon in a near–square symmetry (see section 4.2.1). A Ni replica of the Silicon master was made and Experimental substrates were injection moulded via this Ni intermediary into poly(carbonate) (pC).

Quantification of FA number and area is accepted as one method for measuring total cell adhesion and to help determine cytocompatibility. Richards *et al*. (Richards *et al*., 1993) developed electron microscopical analysis of vinculin labelled cells as an assay of the cytocompatibility of metal surfaces used for biomedical devices. Here large *intra*-sample variation of FA density measurements made accurate adhesion assessment difficult. Davies *et al*. (Davies *et al*., 1993) comments that the numbers of FA sites can vary by up to 10% in a population of metabolising cells. To address this problem it is favourable to quantify adhesion formation in a single phase of the cell cycle.

The period of nuclear replication of total DNA, or S-phase, was identified originally by Howard & Pelc (1951) (Everhart & Rubin, 1974, Howard & Pelc, 1951, Pelc & Howard, 1952) by tracing the incorporation of radioactive phosphorus into the nucleus. Cross & ap Gwynn observed cell flattening during S-phase of the cell cycle and then rounding-up of cells when approaching mitosis (Cross & ap Gwynn, 1987). Further to this, Hunter *et al* observed that FAs were most developed and numerous in flattened cells (Hunter *et al*., 1995), it was also noted that the adhesion strength of cells flattened relative to the substratum was greater (Ingber *et al*., 1995, Lotz *et al*., 1989, Meredith *et al*., 2004), leading to the hypothesis that cells possessing the greatest cell-substratum adhesion are found during S-phase of the cell cycle. During this stage of the cell cycle, cells demonstrate distinct morphological and physiological characteristics, which can be exploited in their identification.

Previous studies using electron microscopical imaging of vinculin have attempted to identify S-phase cells by the incorporation of tritated thymidine into the nucleus of cells

entering S-phase and so accumulating amino acids from the media (Meredith *et al*., 2004, Owen *et al*., 2002).

Owen used a combination of autoradiography and immunolabelling to enable simultaneous identification of both S-phase cells and their FAs with SEM. S-phase cells were radio-labelled with a pulse of tritiated thymidine, selectively incorporated into cells actively synthesising DNA. The cells were immunogoldlabelled for vinculin, prepared for autoradiography, and embedded in resin, which was polymerised before removing the substrate, to expose the embedded cell under-surface. Electron-energy 'sectioning' of the sample allowed separate S-phase cell identification in one electron-energy 'section' and visualisation of the immunogold label in another 'section', within the same cell, therefore enabling accurate FA quantification. Unfortunately though the technique worked well, it required weeks for the excitation within the autoradiography. Here, in order to develop a more rapid methodology, 5-Bromodeoxyuridine (BrdU), another thymidine analogue, was used to label HOBs cultured on the nano-pitted pC within S-phase. This S-phase labelling has been twinned with fluorescence protocols to allow much faster sample throughput than electron microscopy and it has been shown previously by Meredith *et al* that the measurement accuracy with fluorescence protocols with large numbers of cells matches that of SEM methods which usually uses smaller numbers of cells.

To identify S-phase cells, HOBs were initially subjected to serum starvation followed by serum supplementation to induce S-phase (possessing a synchronised nuclear cycle) in the cell population. Incorporation of BrdU into the nucleus of cells undergoing increased DNA synthesis was subsequently fluorescently labelled. FAs were also labelled in these cells via vinculin detection, a major linker-protein of the FA plaque. This has allowed for the rapid quantification of single-phase cells to allow for assessment of adhesion to materials without artefact relating to cell cycle phase.

3.2. Materials and Methodology

3.2.1. Substrate Fabrication

Near-square arrays of nanopits measuring 120 nm in diameter, with an average inter-pit pitch of 300 nm ± 50 nm and a depth of 100 nm were fabricated by EBL according to methodology described in section 4.2.1 and injection moulded in pC. Near-square substrates had reduced order. The location of the pits was changed from perfectly square by shifting the position of each pit by p × 5 nm, where p is a random integer between 0 and 9, in both the x and y directions (fig. 3.1). Planar pC was used as a control substrate as described in section 2.3.
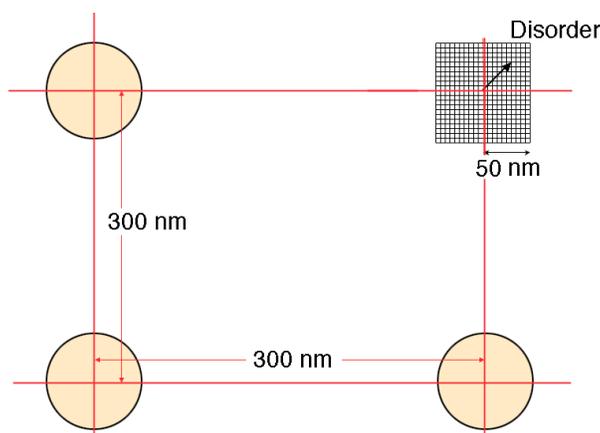
Fig. 3.1. Schematic representation of the generation of pit disorder. The red lines are on a 300 by 300 grid. The centre of the dots is displaced by 5p nm where p is a random integer between -10 and +10.

3.2.2. Cell Culture

Methodology for osteoblast isolation and culture was as that described in section 2.2.1. HOBs were expanded to passage 4 following 5 weeks of culture. The media was subsequently replace by 10 mls of HBSS for 1 minute which was removed prior to trypsinisation in 3 mls of 0.04% trypsin/0.03% EDTA (*PromoCell®, Heidelberg, Germany*). The cell suspension was diluted in HBSS to a final volume of 10 ml and pelleted by centrifugation at 250 *g* for 7 minutes before being resuspended in OGM and seeded onto untreated experimental and planar control pMMA substrates at a final density of 1×10^5 cells per ml to allow single cell imaging. Cells were maintained at 37^oC with a 5% CO_2 atmosphere in PromoCell® OGM containing 10% FCS (*PromoCell®,*

Heidelberg, Germany) which was replaced every 2 days. Following 7 days of culture HOBs were maintained for 4 days without changing the media, inducing a brief period of serum starvation. OGM encompassing 10% FCS was subsequently introduced to the culture following 4 days of serum starvation and HOBs allowed to metabolise for 17 hours, giving rise to a population of cells possessing a synchronised nuclear cycle. Following this period HOBs were cultured in OGM containing 10 µM BrdU for 3 hours.

3.2.3. Immunocytochemistry for Adhesion Quantification

HOBs were fixed in 4% paraformaldehyde in phosphate buffered saline solution (PBS), with 1% sucrose at 37°C for 15 minutes. Once fixed, the samples were washed with PBS. Samples were permeabilised with buffered 0.5% Triton X-100 (10.3 g sucrose, 0.292 g NaCl, 0.06 g MgCl$_2$, 0.476 g HEPES, 0.5 ml Triton X-100, in 100 ml water, pH 7.2) at 4°C for 5 minutes. Non-specific binding sites were blocked with 1% BSA in PBS at 37°C for 5 minutes and samples were subsequently subjected to one of two immunolabelling protocols:

1.   Samples were incubated for 30 minutes with a solution of 2 M HCl followed by incubation in anti-BrdU monoclonal anti-human IgG raised in mouse, clone BU-33 (*1:100, Sigma, Poole*)*,* in a 1% BSA PBS solution for 1 hour (37°C). Samples were then incubated for 2 hours (37°C) with anti-vinculin monoclonal anti-human IgG raised in mouse, clone hVin-1 (*1:200, Sigma, Poole, UK*), in a 1% BSA PBS solution encompassing rhodamine conjugated phalloidin (*1:50, Molecular Probes, Oregon, USA*).

2.   Samples were incubated for 2 hours in a solution encompassing anti-BrdU/DNase-I solution RPN2001 cell proliferation kit, (*1:100, Amersham Biosciences Uppsala, Sweden*), anti-vinculin monoclonal anti-human IgG raised in mouse, clone hVin-1 (*1:200, Sigma, Poole, UK*) and rhodamine conjugated phalloidin (*1:50, Molecular Probes, Oregon, USA*) at 37°C.

After either protocol, samples were neutralised with 0.5% Tween 20/PBS (5 minutes × 3) to minimise background labelling from charge association. A secondary, biotin conjugated antibody monoclonal horse anti-mouse in 1% BSA/PBS was added for 1 hour (37°C) (*1:50, Vector Laboratories, Peterborough, UK*) followed by subsequent washing as above. Fluorescein isothiocyanate (FITC) conjugated streptavidin was added, in 1%

BSA/PBS, (*1:50, Vector Laboratories, Peterborough, UK*) 4°C for 30 minutes, and given a final wash.

Samples were mounted in Vectorshield mountant for fluorescence containing 4'-6-Diamidino-2-phenylindole for DNA staining (*Vector Laboratories, Peterborough, UK*), then viewed with a Zeiss Axiovert 200M microscope with a Zeiss Plan Neofluor 40 × (0.75 NA) lens. Image manipulation in Adobe® Photoshop was then used to superimpose the colour channels to show adhesion complexes (vinculin) in green, actin in red and S-phase nuclei in blue.

Samples prepared for S-phase nuclei imaging using an HCl denaturing process (protocol 1) were seen to possess reduced FA labelling. Adhesion site immunofluorescent labelling intensity was low and the cell periphery appeared damaged and fragmented. Nuclear labelling was diffuse and individual small deposits of nuclear FITC present (fig. 3.2A). DNA scission using DNase-I (protocol 2) resulted in increased adhesion labelling intensity. Cells appeared morphologically unaffected by this process and nuclear labelling was dense and increased in intensity (fig. 3.2B), on this basis, method 2, DNase-I treatment was selected as the preferred methodology.
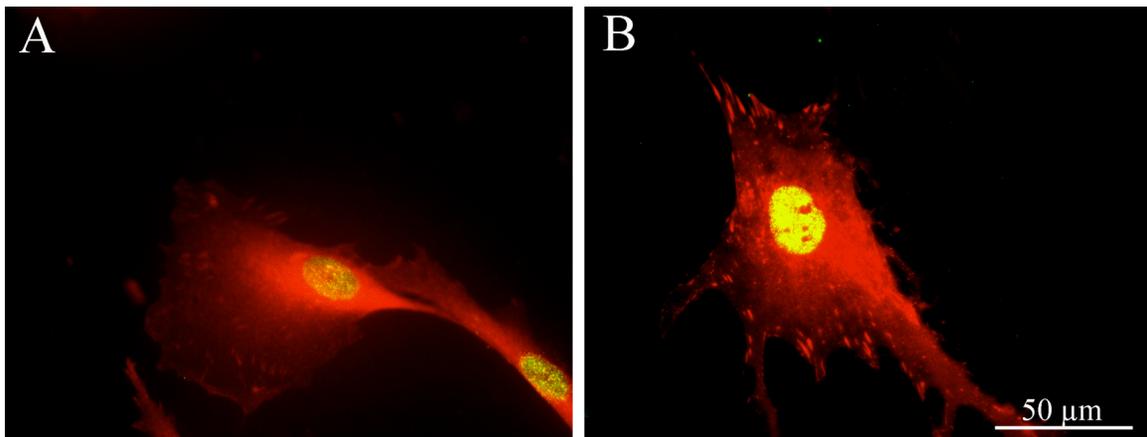
Fig. 3.2. Fluorescent imaging of vinculin labelling in S-phase HOBs cultured on planar surfaces. (A) DNA denaturation with HCL was associated with destruction of vinculin epitopes and reduced labelling intensity. Nuclear labelling was also diffuse. (B) DNA scission accomplished with DNase-I resulted in increased nuclear and FA labelling intensity. Red = vinculin, Yellow = S-phase nuclei.

3.2.4. Image Analysis

Experimental and planar control substrates were replicated 3 times and fluorescent images captured from individual HOBs on each (n = 15 per replicate), these were exported to ImageJ and adhesion complex number per cell and adhesion length were analysed according to a schematic threshold analysis (fig. 3.3). The adhesion frequency was measured as the average number of adhesions per cell that had a given adhesion length pertaining to an adhesion subtype. The bin size was 0.5 µm. Criteria for adhesion classification was according to length scales described in current literature (Bershadsky *et al*., 2006a, Bershadsky *et al*., 1985). Adhesion complexes measuring less than 2 µm were assigned as FXs, while those from 2 – 5 µm were designated as FAs. Adhesion complexes over 5 µm in length were classified as a third adhesion subtype initially identified here – the super-mature adhesion (SMA) that will be discussed throughout this thesis. Data was $\log_2$ normalised and analysed using Tukey analysis of variance (ANOVA). Results of $p < 0.05$ were considered significant.
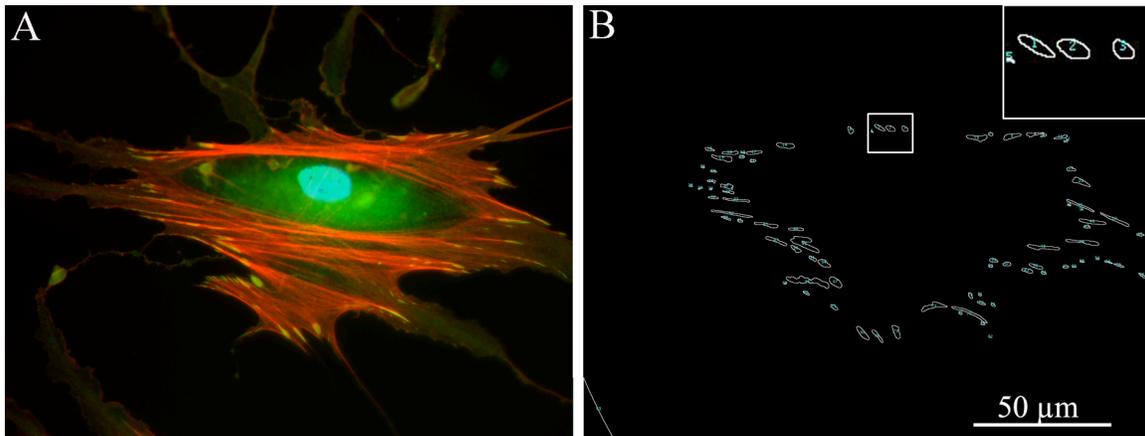
Fig. 3.3. Adhesion complex scoring and the quantification procedure in S-phase HOBs cultured on planar surfaces. (A) Adhesion sites and S-phase cells were identified by vinculin and BrdU immunofluorescent detection respectively. (B) Adhesion quantification was according to a schematic threshold analysis. Red = actin, Green = vinculin, Light blue = S-phase nuclei.

3.3. Results

3.3.1. Characterisation of Fabricated Substrate Topography

The injection moulding process resulted in the fabrication of nanopit arrays measuring 120 nm in diameter, with an average inter-pit pitch of 300 ± 50 nm and a depth of 100 nm. Substrates appeared morphologically unaffected by the processing process, and free from polymer crazing. Near-square substrates had reduced order, by shifting the pits from perfectly square by ± 50 nm in the x or y direction (fig. 3.4B). An area of 1 cm^2 was imprinted. The percentage of this area composed of pits was 14.2%. The planar controls had an Ra of 1.2 nm over 10 μm^2.
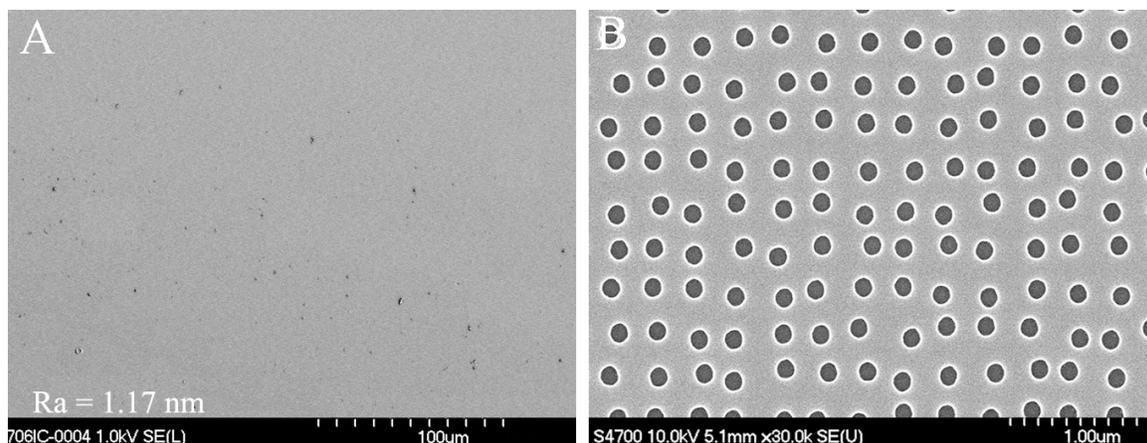
Fig. 3.4. SEM image of a planar control substrate and an original near-square nanopit array substrate. (A) Planar control substrates possessed an Ra of 1.2 nm over 10 μm^2 (B) Arrays of near ordered nanopits in pC substrates produced by EBL and injection moulding possessed square arrays of nanopits displaced by ± 50 nm.

3.3.2. Osteoblast Morphology and Cytoskeletal Organisation

Initial imaging of HOB morphology and cytoskeleton revealed cell morphology to be preserved on both control and the experimental topography. On planar controls and near-square substrates S-phase HOBs were well spread with large lamellae and cytoplasmic processes and an organised cytoskeleton (fig. 3.5).
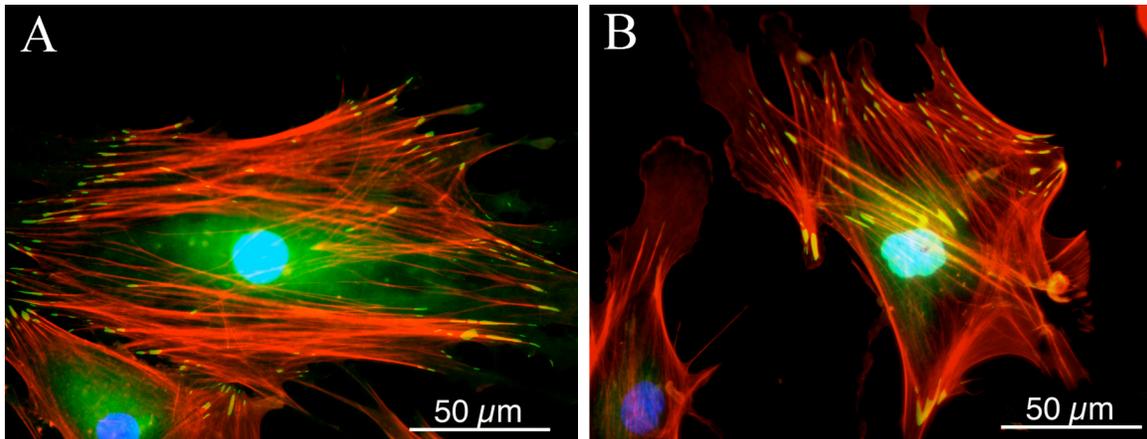
Fig. 3.5. Fluorescent image of adhesion formation and stress fibre organisation of S-phase HOBs on near-square substrates. (A, B) S-phase HOBs cultured on control and experimental substrates respectively were well-spread and possessed large and numerous adhesions and stress fibres. Red = actin, Green = vinculin, Light Blue = S-phase nuclei, Dark Blue = non-S-phase nuclei.

3.3.3. Adhesion Quantification

Quantification of vinculin localised within adhesion complexes revealed significant differences in adhesion formation between S-phase HOBs cultured on control and near-square arrays of nanopits (fig. 3.4). HOBs cultured on both substrates demonstrated maximum FX frequency between 1.5 – 2 μm in length. HOBs cultured on control substrates however possessed greater numbers of FXs measuring 1.5 μm relative to HOBs cultured on near-square substrates. Frequency of adhesion formation in HOBs on all substrates began to decrease in the FA range (fig. 3.6A). The Frequency of SMAs over 10.5 μm in length decreased on planar control substrates relative to near-square substrates, here adhesions complexes were noted up to 20 μm in length (fig. 3.6B).
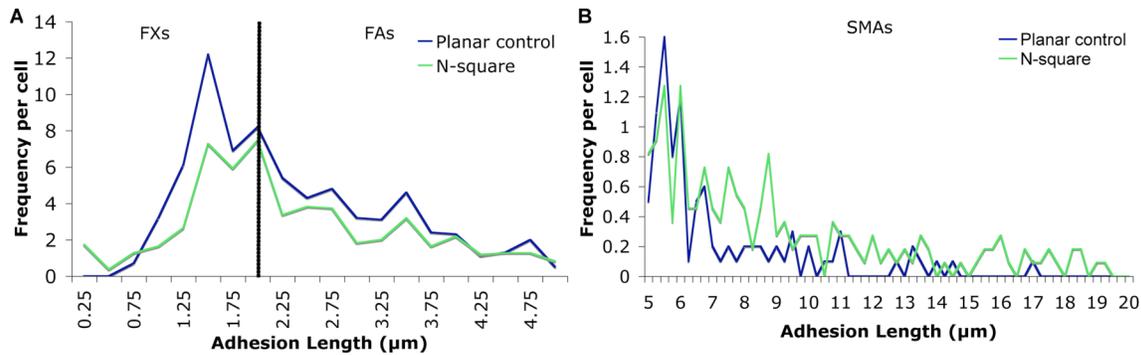
Fig. 3.6. Quantification of adhesion complex distribution in S-phase HOBs on near-square substrates*.
(A). FX formation was increased on planar controls relative to near-square (N-square) substrates. FA distribution decreased as adhesion length increased on both substrates. (B) Frequency of SMAs over approx. 10.5 µm in length decreased on planar control substrates relative to near-square substrates. A significant number of adhesions complexes on near-square arrays were observed to approach 20 µm in length.*

3.3.4. Adhesion Length

Mean FX length (adhesion complexes measuring less than 2 µm) in S-phase HOBs was approx. 1.3 µm on both substrates. Mean FA length (adhesion complexes measuring between 2 µm and 5µm) was approx. 3 µm on both substrates. Intersubstrate variation of FX and FA length was low (fig. 3.7). SMA formation in HOBs cultured on near-square substrates was significantly increased relative to HOBs cultured on planar control substrates. The mean length of SMAs in HOBs cultured on control substrates was 7.2 µm, yet this increased to 11 µm in HOBs on near-square substrates.

3.3.5. Adhesion Number

Differences in the total number of FXs, FAs and SMAs in S-phase HOB cells were found to be more pronounced than topographically induced variation in adhesion length. HOBs cultured on near-square substrates formed reduced numbers of FXs and FAs relative to planar control substrates (25 and 27 respectively), but formation of SMAs was significantly increased in cells on the near-square, with a mean value of 17 per cell (fig. 3.8), compared to 10 per cell in HOBs on the planar control substrates.
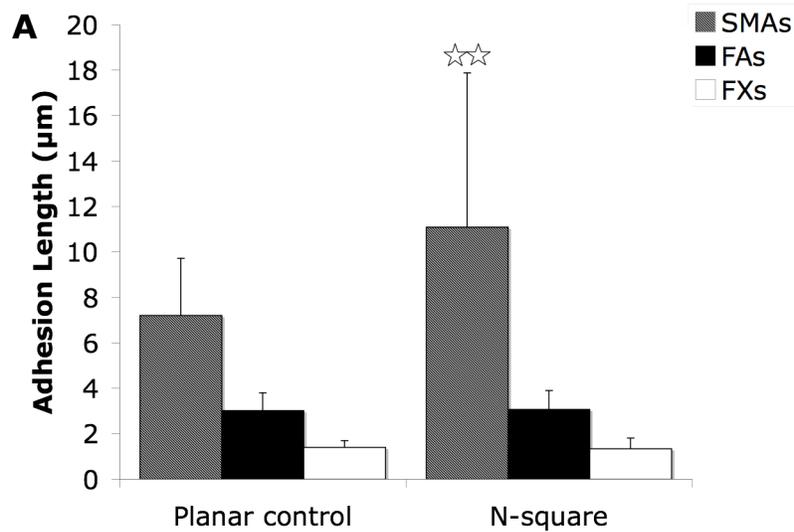
Fig. 3.7. Quantification of adhesion complex length in S-phase HOBs on near-square substrates. Mean adhesion length for FXs and FAs was conserved in HOBs cultured on both substrates. Cells cultured on near-square substrates (N-square) showed a marked increase in SMA length. Difference of p < 0.01 denoted by ★★. Results are mean ± SD.
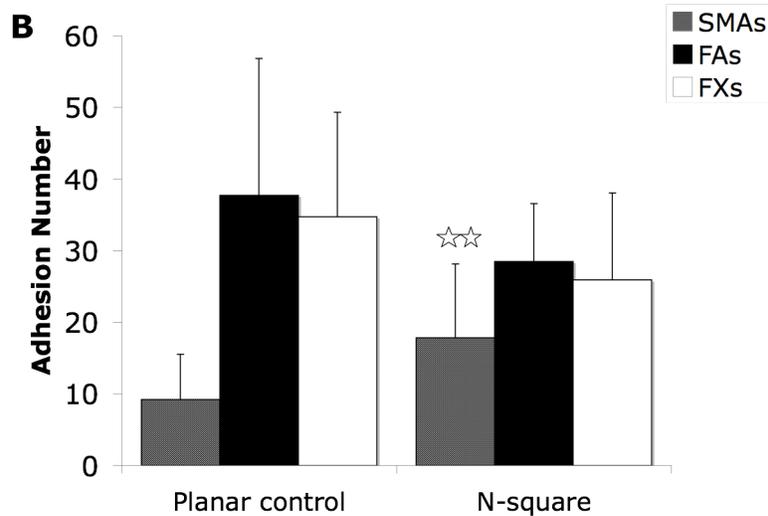
Fig. 3.8. Quantification of adhesion complex number in S-phase HOBs on near-square substrates. HOBs cultured on near-square (N-square) substrates formed decreased numbers of FXs and FAs relative to planar control substrates, however formation of SMAs was significantly increased. Difference of p < 0.01 denoted by ★★. Results are mean ± SD.

3.4. Further Protocol Refinement

It was decided to refine the automated image analysis methodology to sacrifice time for accuracy. To ensure that (A) all adhesions were detected and (B) that merged, or connected adhesions were distinguished from SMAs, manual rather than automated quantification procedures were used. After culture and immunolabelling using optimised protocols (described above) images of S-phase cells labelled for vinculin were exported to Photoshop® and adhesion complexes scored with an 8 pixel wide straight line on a layer superimposed onto the background image creating an adhesion schematic (fig. 3.9). Analysis of adhesion numbers per cell and adhesion length was performed by analysis of the adhesion schematic by ImageJ. Adhesion sub-grouping measurements were also revised. Adhesion complexes measuring less than 1 µm were assigned as FXs, while those from 1 – 5 µm were designated as FAs. Adhesion complexes over 5 µm in length were classified as SMAs. The adhesion frequency was measured as the average number of adhesions per cell that had a given adhesion length pertaining to an adhesion subtype. The bin size was 0.5 µm. Data was analysed using Kruskal-Wallis one-way ANOVA on ranks and since this is a non-parametric method, the Kruskal-Wallis test does not assume a normal population. Results of $p < 0.05$ were considered significant.
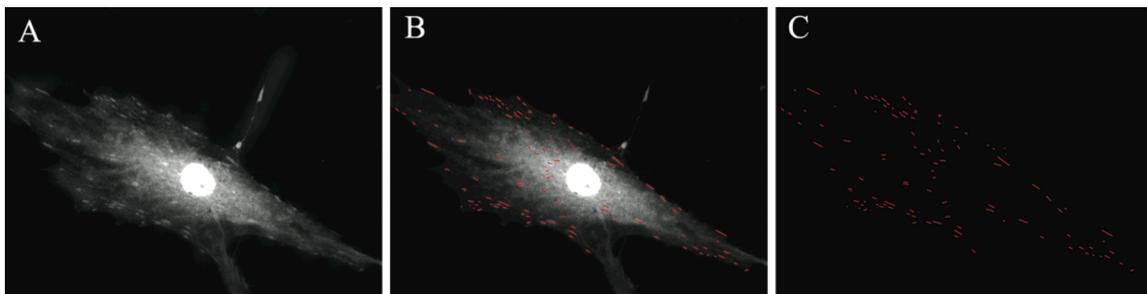

Fig. 3.9. Adhesion complex scoring and the quantification procedure in S-phase osteoblasts. (A) Adhesion sites and S-phase cells were identified by vinculin and BrdU immunofluorescent detection respectively. (B) Adhesions were scored with an 8 pixel wide straight line. (C) The background layer was subsequently removed before adhesion analysis.

3.5. Discussion

This preliminary experiment focused on the influence of an EBL fabricated nanopatterned substrate on primary S-phase HOB adhesion as determined by vinculin

mediated adhesion complex quantification as an exemplar. The methodology used was developed from that described by Owens and Meredith *et al.* (Meredith *et al.*, 2004). In their study, cells were studied using SEM after vinculin immunolabelling with simultaneous detection of S-phase nuclei using tritiated thymidine. Both techniques allow cells to be considered in a single phase on material surfaces. This is significant as cells are different sizes in different phases e.g. growth phase 1 (G1) compared to growth phase 2 (G2) and S-phase. The technique described here represents a significant advancement of the SEM technique as large numbers of cells can rapidly be analysed.

Past electron microscopical studies have relied on tritated thymidine detection coupled with a two-level vinculin detection system and subsequent resin embedding for dual S-phase, vinculin labelling (Meredith *et al.*, 2004, Owen *et al.*, 2002). This protocol was not only time consuming, but also involved nuclear emulsion development, resin curing and handling of radioisotopes, factors which have all been eliminated from the technique described herein. Many investigators have found BrdU to be as reliable in S-phase detection as tritated thymidine, and when incorporated into the cell nucleus is still a very stable antigen, giving a strong and reliable signal regardless of the fixation method or any further tissue processing (Mokry & Nemecek, 1995). For adequate immunodetection of nuclear associated BrdU, partial denaturation of the DNA helix, or scission of the total molecule must first occur for epitope exposure either by extreme pH (Yanai *et al.*, 1996), thermal denaturation (Beisker *et al.*, 1987) or DNase scission. Here both pH mediated denaturation and DNase scission were employed to investigate the effects of these techniques on the efficiency of both BrdU and vinculin immunolabelling efficiency.

The inhibitory effect of BrdU, after binding to the DNA, arrests the cell within S-phase. It has been suggested that during the cell cycle arrest the cytoplasmic cycle continues to proceed (Owen *et al.*, 2002). For this reason the total incubation time in BrdU was kept to just three hours before fixing in formaldehyde, this time is suitable for these experiments as DNA synthesis during S-phase has been shown to last approximately 7-8 hours (Bade *et al.*, 1966, Cameron & Greulich, 1963).

Highly-ordered nanopit symmetries have been shown to perturb cytoskeletal organisation and cellular adhesion in fibroblasts and epitenon cells (Dalby *et al.*, 2004a, Gallagher *et al.*, 2002). The mechanisms that lead to these physical alterations in cellular behaviour

are still largely unknown. This preliminary experiment has shown that nanotopographies can indeed affect adhesion formation in osteoblasts, in this case reducing total adhesion, but increasing in SMA formation. The experiment has demonstrated the optimisation of a robust high throughput protocol for the accurate quantification of integrin mediated adhesion sites *in vitro* with which to study the effects of nanomaterials on osteoblasts adhesion.

Furthermore, a further image analysis method has been detailed to reduce error and artefact with the sacrifice of speed to achieve highly accurate results.

3.5.1. Conclusion

A previously untested technique for the quantification of adhesion complex formation in a population of osteoblasts with synchronised nuclei was successfully optimised. The protocol facilitated the rapid quantification of adhesion formation in S-phase HOBs on planar and a nanopitted substrate. Near-square arrays induced increased SMA formation in HOBs, and mature cytoskeletal organisation. Such findings are intriguing as they are indicative of the potential influence of nanostructures on the mechanics of cell adhesion and subsequent cell function, as will be investigated in more depth in the next chapters.

CHAPTER IV

The Influence of Nanoscale Pits on

Osteoblasts Adhesion Formation and the

Functional Response of MSC Populations

4.1. General Introduction

The fabrication of experimental nanoscale substrates has been revolutionised by the development of focused charged beam machines that define a high-resolution pattern. EBL is one such advanced fabrication technique derived from technology originally developed for the microelectronics industry. The initial step in the design and production of a nanopatterned substrate is pattern definition in a radiation resistant substance. All patterns are initially designed in software before being transferred to a radiation-sensitive material (resist) by the action of a beam of focused electrons that is scanned over the resist and turned on and off as required (Wilkinson, 2004). Unlike photolithographic printing, a physical mask is not needed to pattern the surface with the beam of electrons. The resist is either developed in a chemical bath similar to photolithography, or the electron beam interacts with the material sufficiently to remove the resist material. The resolution of EBL depends on the electron beam spot size (4 nm in the latest machines) and electron scattering in the resist and backscattering from the substrate (Wilkinson, 2004); certainly resolution less than 10 nm can be obtained on silicon substrates. In conventional EBL arrays of dots are designed as an array of circles.

This relief pattern can be used as stencil for additive or a mask for subtractive pattern transfer. In this way, a die bearing the relief pattern is made that is used to transfer the pattern into substrates for experimental cellular studies via a hot embossing procedure. To investigate the interaction at the cell-substratum interface, topographies were fabricated with ordered arrays of nanopits in two different conformations – square and hexagonal. HOBs were cultured on these nanoscale topographies for 10 days. Adhesion formation was quantified only in S-phase cells identified by immunofluorescent detection of incorporated BrdU into total cell DNA. As described previously, this was to limit measurements to within the S-phase of the cell cycle, reducing variation in adhesion density caused by morphological changes within the cell cycle (Meredith *et al*., 2004). In order to investigate the hypothesis that adhesion modulation may be linked to osteogenic differentiation and influential in osteospecific function, MSCs were enriched by immunoselection using STRO-1 and cultured on experimental substrates for microarray analysis of modulations in gene expression.

4.2. Materials and Methodology

4.2.1 Experimental Substrates Fabricated by EBL

4.2.1.1. Original topography fabrication

Silicon wafers were cleaned under acetone in an ultrasonic bath for 5 minutes. They were then rinsed thoroughly in reverse osmosis water (ROH_2O) and blown dry with a filter-fitted air gun. Next, they were spun with primer for 30 seconds at 4000 revolutions per minute (rpm), then spun with the positive tone resist ZEP 520 (*Nippon Zeon, Tokyo, Japan*) for 30 seconds at 4000 rpm, and baked for 30 minutes at 90°C. The resulting layer was measured to be 1.8 μm thick. A Leica EBPG5-HR using an 80 nm spot size beam was used to write the pattern at 50 kV (fig. 4.1). The exposed samples were developed in o-xylene at 23°C for 60 seconds and rinsed in iso-2-propanol. Write fields were stitched together by mechanical movement of the stage. Substrate fabrication was originally by Dr. Nikolaj Gadegaard at the Dept. of electronic engineering, University of Glasgow.
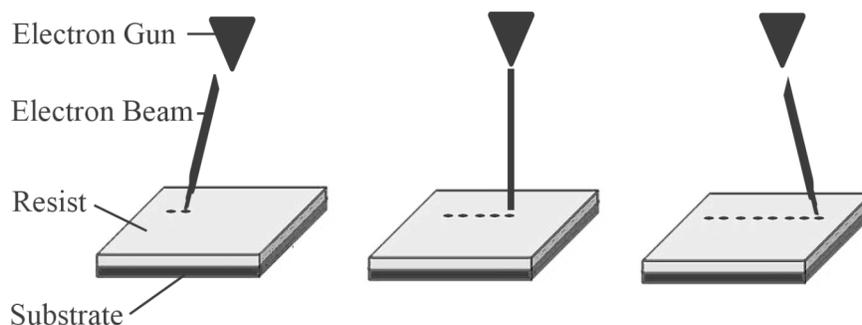
Fig. 4.1. EBL generation of nanoscale topographical features. The electron beam interacts with the underlying resist layer to form patterns of exposure that are soluble in xylene.

4.2.1.2. Nickel shim fabrication

To eliminate any variation in surface chemistry in the final substrates to be used for biological purposes, nickel shims for embossing were made directly from the patterned ZEP 520 resist. A thin (50 nm) seeding layer of Ni-V (7% vanadium) was sputter coated on both of the samples. The layer acted as an electrode in the galvanic bath where nickel was plated electrochemically on the Ni-V to a thickness of ca. 300 μm. Once returned from the plater, the nickel shims were cleaned by firstly stripping the polyurethane coating (used for protection during shipping) using chloroform in an ultrasound bath for

10-15 minutes. Secondly, silicon residue was stripped by being wet etched in 25% potassium hydroxide at 80°C for 1 hour. Shims were rinsed thoroughly in ROH_2O, air gun dried and were checked using AFM. Ni shims were kindly provided by John Pedersen (SDC Dandisc A/S, Denmark).

4.2.1.3. Final substrate preparation

The shims, patterned with an inverted replica of the nanotopography were finally trimmed to approximately 30 × 30 mm sizes using a metal guillotine. 1 cm^2 Imprints of the nickel shims were fabricated in molten pMMA (*Goodfellow, Cambridgeshire, UK*), achieved using an Obducat nanoimprinter (temperature = 180°C, pressure = 15 Bar, time = 300 seconds), and left to cool before separation. Planar pMMA was used as a control substrate as described in section 2.3. Polymeric replicas were kindly fabricated by Mrs. Mary Robertson and Ms. Sara McFarlane at the JWNC, University of Glasgow.

4.2.2. Cell Culture

Cell models and culture conditions were according to those described in section 2.2.1 and 2.2.2. Briefly HOBs derived from a femoral head biopsy of an 84 year old Caucasian female and a knee biopsy of a 74 year old Caucasian female (*PromoCell®, Heidelberg, Germany*). MSCs were enriched using STRO-1 antibody and magnetic cell sorting as described in section 2.2.2, from bone marrow samples obtained from haematologically normal patients undergoing routine hip replacement surgery. Both cell models were seeded onto untreated experimental, and planar control pMMA substrates. Prior to cell fixation, the cell cycle in HOB populations was synchronised and BrdU introduced into total cellular DNA as described in section 3.2.2.

4.2.3. Immunocytochemistry for Light Microscopy

Materials and methodology was according to those described in section 3.2.3. Briefly HOBs cultured on experimental and planar control pMMA substrates were fixed and subsequently incubated for 2 hours in an anti-BrdU/DNase-I solution including antibodies against one of; anti-vinculin monoclonal anti-human raised in mouse, clone hVin-1 (*1:200, Sigma, Poole, UK*), or anti-β-tubulin monoclonal anti-human raised in mouse, clone TUB 2.1 (*1:100, Sigma, Poole, UK*).

4.2.4. Immunocytochemistry for SEM

The immunolabelling method was a modified version of that first described by Richards *et al*. and described in full in section 2.4. Briefly, cells were stabilised in 4% paraformaldehyde and vinculin was labelled with goat anti-mouse 5 nm gold conjugate (*BB International, Cardiff, UK*) diluted 1:200 in PIPES buffer + 1% BSA + 0.1% Tween 20 overnight for 12 hours at 22°C. Gold probes were silver-enhanced with a silver developing solution for 7 minutes (*BBI International, Cardiff, UK*).

4.2.5. SEM

The cells were dehydrated through an ethanol series and with a SPI-DRY™ critical point dryer (*Structure Probe Inc., Leicestershire, UK*), before viewing with a Hitachi S-4700 field emission SEM as described in full in section 2.5.

4.2.6. Image Analysis

Experimental and planar control substrates were replicated 3 times and fluorescence images taken of HOBs on each (n = 15 per replicate) substrate were exported to Photoshop® and adhesion complexes scored with an 8 pixel wide straight line as described in section 3.4.

4.2.7. Plasmid Expansion and Cellular Transfection

Bacterial transformation, plasmid expansion and cellular transfection was accomplished using materials and methodology previously described in section 2.6. Briefly, a plasmid with an inserted sequence for vinculin plus a YFP tag was replicated by a population of *E. coli* cells. This plasmid was subsequently purified and transiently introduced into the HOB genome via electroporative transfection. Adhesion formation in these cells was studied via fluorescent live-cell imaging over a period of 36 hours.

4.2.8. RNA Isolation and Microarray Analysis

RNA extraction (n = 5), microarray hybridisation (n = 5) and gene data analysis was according to methodology previously described in section 2.7. Briefly, Individual gene expression detection was carried out with 1.7 K spotted DNA microarrays. The functional

and canonical analyses were generated through the use of IPA. Up and down regulated genes were associated with canonical pathways in the Ingenuity® Pathways knowledge base.

4.3. Results

4.3.1. Substrate Characterisation

The embossing process resulted in the fabrication of nanopit arrays in pMMA as verified by SEM (fig. 4.2 – 4.4). Substrates originally fabricated by EBL and transferred to pMMA replicas via a Ni intermediary were arrays of ordered pits which were 100 nm deep, 120 nm in diameter and possessed a centre – centre spacing of 300 nm. These EBL fabricated pits were arranged in square and hexagonal symmetries (fig. 4.2A and B). Material pit coverage was quantified as square, and hexagonal possessing 12.6% and 14.5% total pit coverage respectively. Nanopit substrates reproduced in pMMA were almost identical to the original master substrates writen in ZEP 520 photoresist. The planar pMMA control substrates possessed no visible topographical features under SEM and were verified to have an Ra of 1.2 nm over 10 mm^2 by AFM as described in section 2.3.
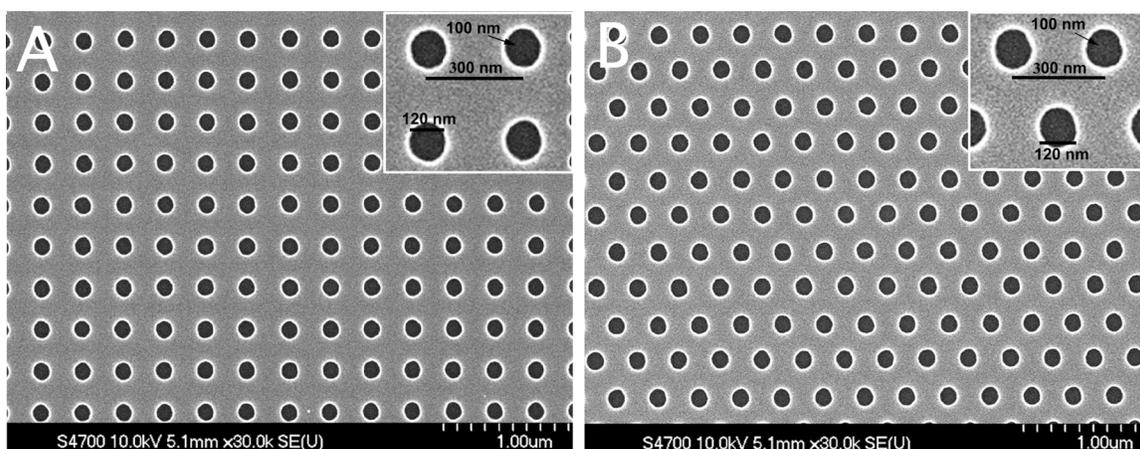
Fig. 4.2. Original substrate fabrication. Nanopit substrates were fabricated by EBL in ZEP 520 resist on silicone wafers (A) Square and (B) hexagonal nanopit arrays were identical in dimension and pitch. Pits were 100 nm deep, 120 nm in diameter and possessed a centre-to-centre spacing of 300 nm.
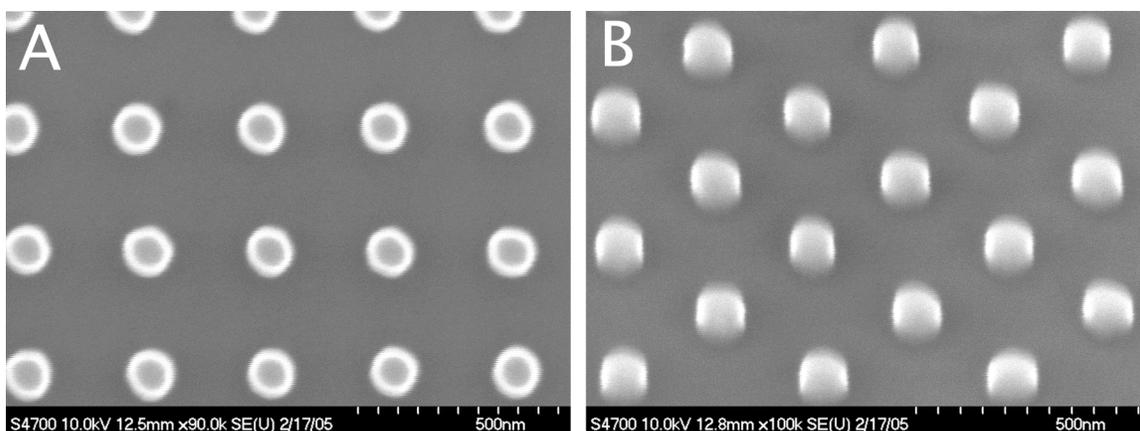
Fig. 4.3. Ni intermediary fabrication. (A) Square and (B) hexagonal negative shims we re fabricated from the original substrate via a sputtercoating process followed by electroplating with Ni.
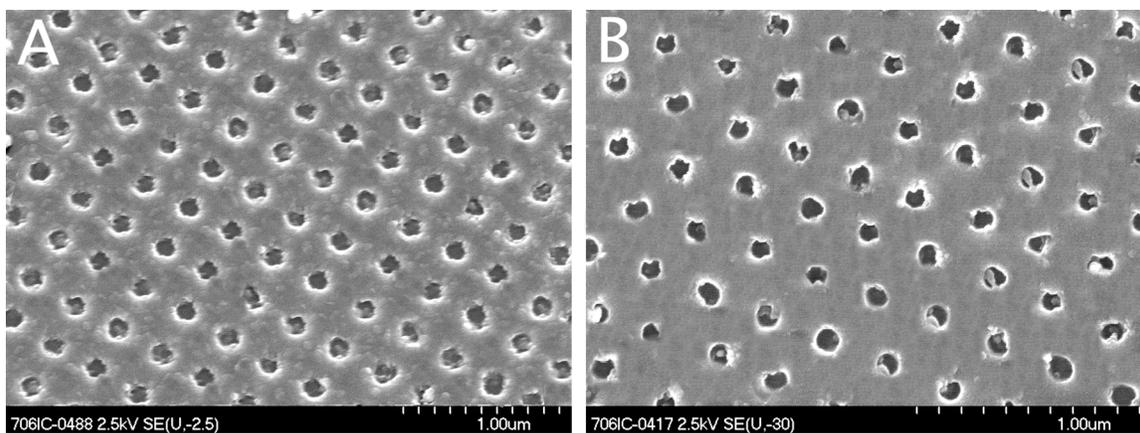
Fig. 4.4. Characterisation of pMMA replicates. (A) Square and (B) hexagonal relief nanopit arrays were transferred into a pMMA replicate via a hot embossing process.

4.3.2. HOB Morphology and Cytoskeletal Organisation

Experimental substrates modified S-phase HOB morphology and cytoskeletal organisation relative to planar controls. HOBs cultured on planar control substrates displayed extensive cell spreading and formed a substantial tubulin network (fig. 4.5A) that radiated from the perinuclear area to the cell periphery in prominent bundles surrounded by a more diffuse tubulin network. HOBs on square and hexagonal nanopit substrates adopted a polarised elongated morphology with reduced cell spreading. Cells were observed to form dense microtubule bundles that were orientated in the direction of cell polarity (fig. 4.5B and C) with reduced organisation relative to HOBs cultured on planar control substrates.
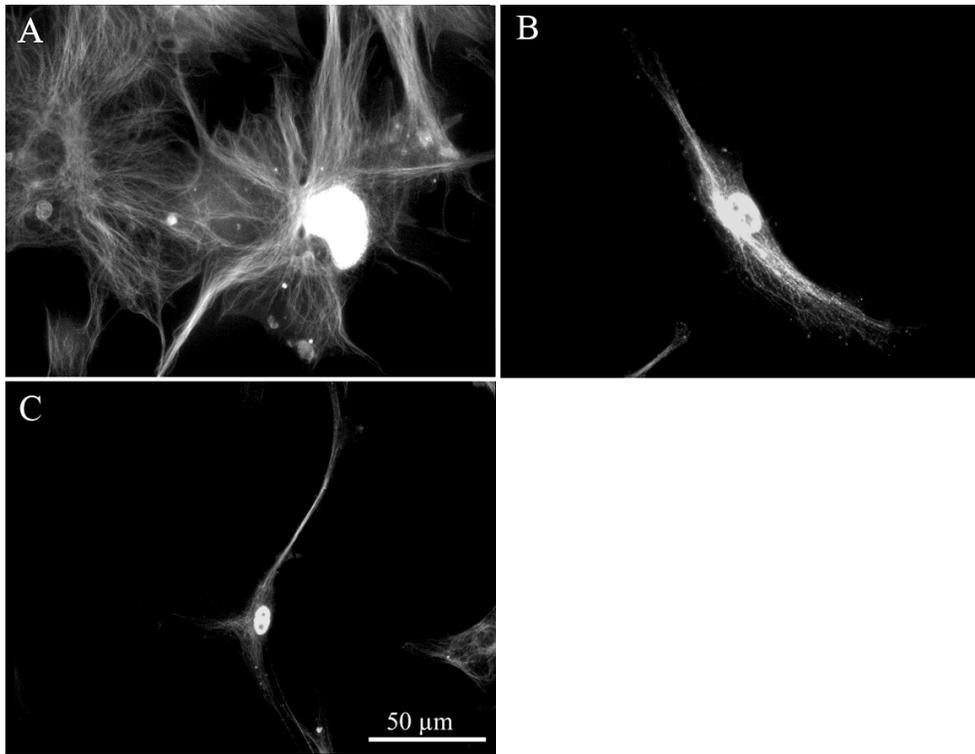
Fig. 4.5. Dual immunolabelling of the tubulin cytoskeleton and S-Phase nuclei of HOBs on nanopit substrates. (A) HOBs cultured on control substrates formed organised tubulin networks. Tubulin density decreased with increasing distance from the nucleus. (B) HOBs on square arrays were associated with decreased microtubule cytoskeleton organisation. The network was closely packed and orientated in the direction of cell polarity. (C) S-phase HOBs cultured on hexagonal nanopit arrays formed a dense and polarised microtubule network.

Actin cytoskeletal elements in S-phase HOBs on planar control substrates were prominent and organised into well-developed stress fibres, which typically spanned the entire cell body and were over 100 µm in length. Fibres (fig. 4.6A) terminated at adhesion sites. Cells on hexagonal and square nanopit substrates possessed reduced stress fibre organisation. These were elongated in the direction of cell polarity or identified as diffuse cytoplasmic staining (fig. 4.6B and C).

4.3.3. Adhesion Characterisation and Qualification

Characterisation of adhesion distribution by vinculin immunolabelling revealed significant differences in adhesion size and location in S-phase HOBs. HOBs on planar control substrates formed numerous adhesions of all subtypes.
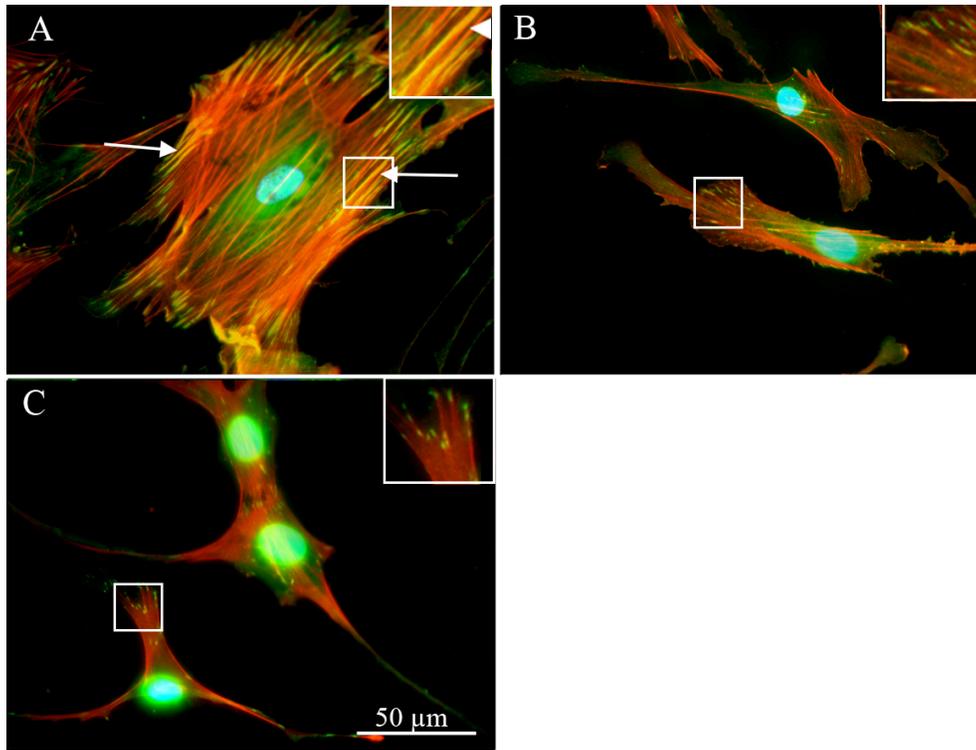
Fig. 4.6. Tri-fluorescent labelling of adhesion complexes and stress fibre organisation in S-Phase HOBs on nanopit substrates. (A) HOBs cultured on planar control substrates formed well-organised stress fibres and numerous adhesions. SMAs are indicated (arrows). (B) Square nanopit arrays disrupted actin cytoskeletal formation. Actin was concentrated in large polarising lamellipodia. Adhesion formation was reduced. (C) Hexagonal nanopit conformations disrupted actin stress fibre organisation. Adhesion formation was reduced and occurred predominantly at the polar regions. Red = actin, green = vinculin, blue = S-phase nuclei.

FXs and FAs were prominent at the region immediately preceding the leading edge and the extreme leading edge respectively. SMAs were located predominantly at the perinuclear region and non-advancing areas of the cell periphery (Fig. 4.6A and 4.7A). HOBs on square and hexagonal nanopit substrates were associated with reduced adhesion formation as identified by fluorescent and gold colloid labelling. FXs and FAs were localised predominantly at stress fibre terminations, SMA formation was not prevalent (fig. 4.6B and C) although when present was observed predominantly at the perinuclear region. FX and FA formation was disrupted by nanopit features and were observed predominantly within the interpit regions, extending between parallel arrays of pits (fig. 4.7B and C).
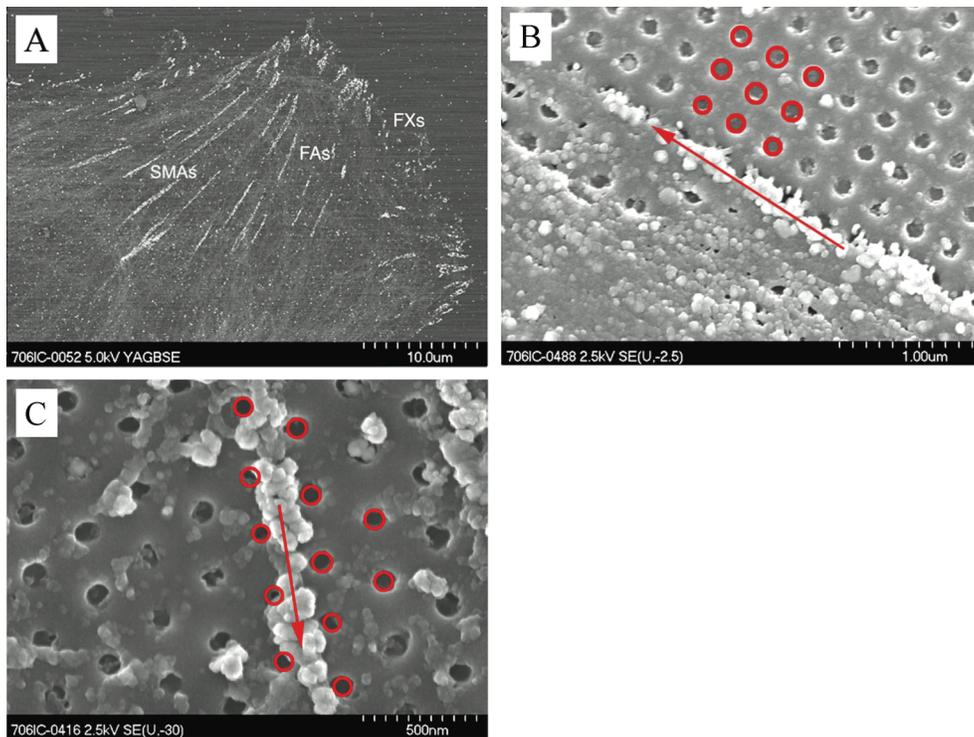
Fig. 4.7. Scanning electron immuno-labelling of adhesion complexes in HOBs on nanopit substrates.
(A) HOBs cultured on planar control substrates formed adhesions of all subtypes FXs were localised predominantly at the leading edge. FAs and SMAs were observed at both the cell periphery and the perinuclear region. (B) Square arrays of nanopits prevented direct adhesion complex formation. Adhesions were seen to align between parallel rows of pits (C) HOB adhesions formed predominantly at the interpit regions on hexagonal nanopit arrays. Adhesions were observed to extend between adjacent pit arrays Square and hexagonal configurations are indicated.

4.3.4. Adhesion Distribution and Quantification

Significant differences in the numbers of generated adhesion subtypes relative to planar control substrates were observed on both square and hexagonal nanopit topographies. HOBs on planar control substrates formed predominantly large FAs (mean 94.7) and SMA subtypes (mean 40.8) relative to the formation of FXs (mean 2.6) (fig. 4.9A and B). FX formation was predominant in HOBs cultured on both square and hexagonal topographies, accounting for approximately 22% and 16.5% respectively of all adhesions found in HOBs on these substrates (fig. 4.8).
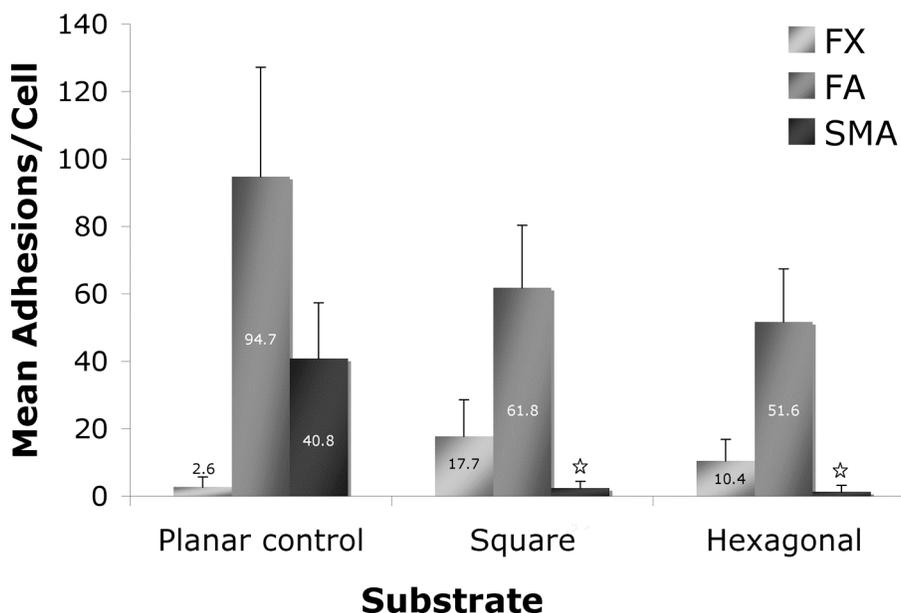
Fig. 4.8. Quantification of adhesion complex subtypes in S-phase HOBs on nanopit substrates. SMA formation was most prominent in HOBs on planar control substrates. FA incidence was decreased on all substrates relative to controls. FX incidence was greatest in HOBs on square and hexagonal nanoarrays. See Table 8.1 for relevant statistics. Included are mean values. Results are + standard deviation (STD), differences $p < 0.05$ denoted by ★

Planar control substrates produced an average of 40.8 SMAs per cell (STD 16.5). The occurrence of SMAs was greatly reduced on square and hexagonal nanopit substrates to less than 1 SMA per cell (STD 1.96 and 1.89 respectively). Very large SMAs (>10 μm) were only seen in HOBs grown on planar control substrates (fig. 4.9B).

Both nanopit topographies induced a decrease in FA formation in S-phase HOBs relative to controls, greatest decreases however were observed in HOBs cultured on hexagonal topographies. Relative to controls, FA formation on these substrates was reduced by approximately 47% and 55% respectively (fig. 4.8). Maximum adhesion frequency in HOBs cultured on both experimental substrates was at approximately 1.5 μm in length. This was increased to 2.5 μm in HOBs on planar control substrates. Adhesion frequency was observed to decline rapidly on nanopit substrates as adhesion length approached 3 μm (fig 4.9A)
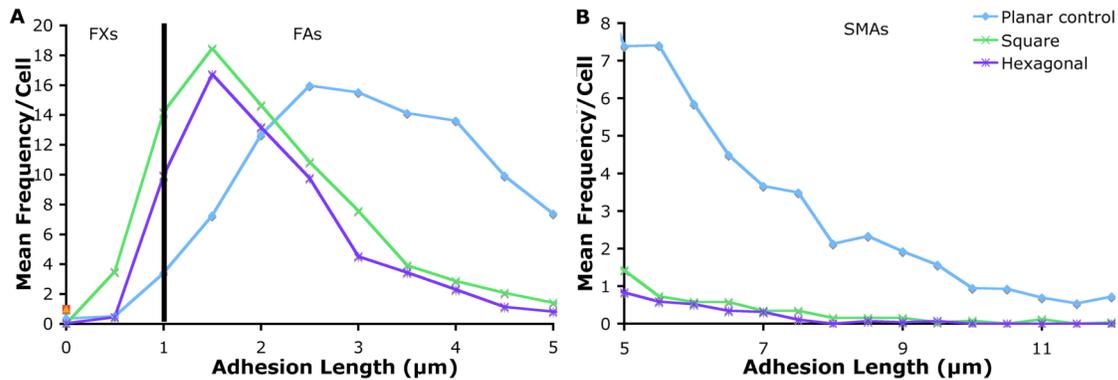
Fig. 4.9. Adhesion complex distribution in S-phase HOBs on nanopit substrates. (A) Focal FXs measuring < 1µm in length were most abundant in HOBs on square and hexagonal nanopit arrays. Distribution of FAs approaching 2 µm in length was increased on planar control substrates. both experimental substrates show a similar decline in adhesion complex distribution as FA lengths approach 3 µm. (B) Frequency of SMAs on nanopit arrays has an incidence of < 0.5 adhesions/cell. SMAs are most pronounced in HOBs cultured on control substrates. Square and hexagonal nanopit arrays show a sharp a similar decline in SMA incidence relative to planar controls.

4.3.5. Live Cell Adhesion Modulation

FA modulation as identified by YFP-vinculin live cell imaging allowed the dynamics of FA formation to be studied over a period of 36 hours following initial cell seeding onto experimental and planar control substrates.

HOBs on planar control substrates were seen to spread rapidly and form large FAs and SMAs 36 hours after HOB seeding. The smaller FXs present during initial cell adhesion were replaced by mature FAs during cell spreading (fig. 4.10). HOBs adopted a flattened and spread morphology following 36 hours of culture forming large peripheral focal and SMAs and sub-nuclear FAs at the ventral membrane. HOBs were seen to spread by rapid peripheral expanding followed by slow cytoplasmic flowing into the newly created intracellular void, as seen after 36 hours (fig. 4.10). Vinculin was observed to form non-adhesion associated cytoplasmic tracts. These were most prominent after 36 hours.
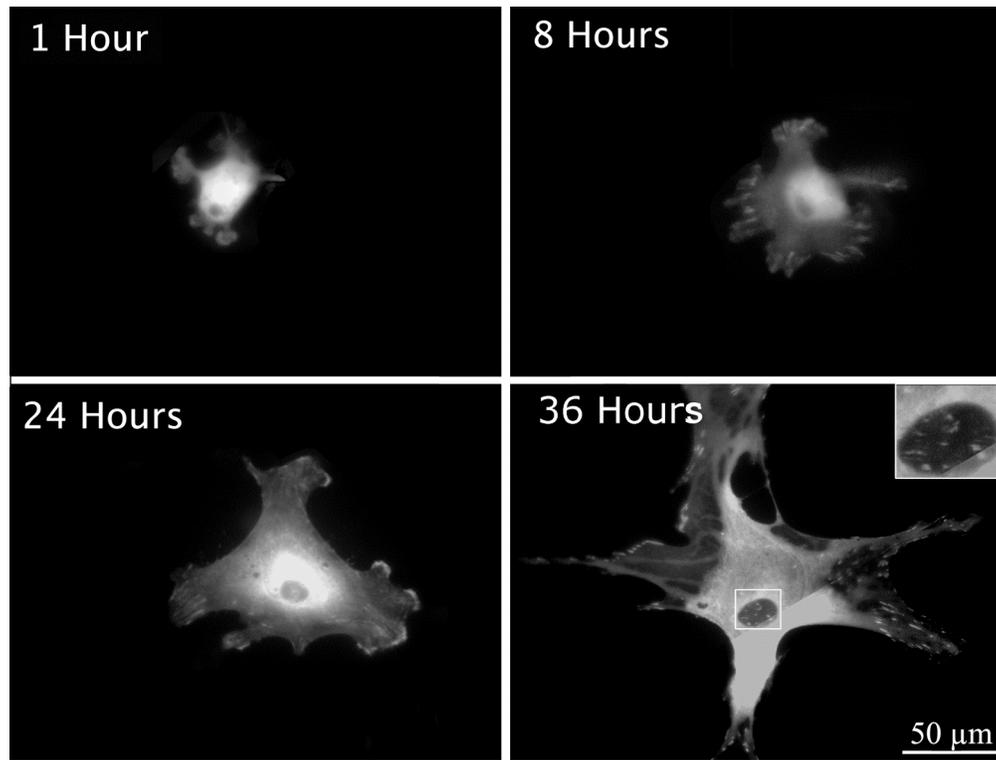
Fig. 4.10. YFP-vinculin analysis of the dynamics of adhesion formation in HOBs on planar substrates.
HOB spreading and adhesion formation was a dynamic process with HOBs on planar controls continually
forming and dissociating as cell spreading proceeded. FXs present at 8 hours are slowly replaced by FAs
and SMAs 36 hours following seeding. Sub-nuclear adhesion formation on the cellular ventral membrane
was also evident (boxed area). The mechanism of cellular spreading is observable at 36 hours. Here the
newly created intracellular void at the top centre of the image is slowly replaced with cytoplasm. Non-
adhesion associated vinculin tracts are also observable.

Square and hexagonal nanopit arrays retarded the cell-spreading process. HOBs were
observed to remain unspread on square nanopit arrays after 36 hours and adhesion
formation was significantly reduced relative to HOBs on planar controls. HOBs retained
a rounded morphology following 24 hours of culture. Observable vinculin positive
plaques were of the FX or FA subtype and localised predominantly in the slowly
extending lamellipodia after 36 hours (fig. 4.11).
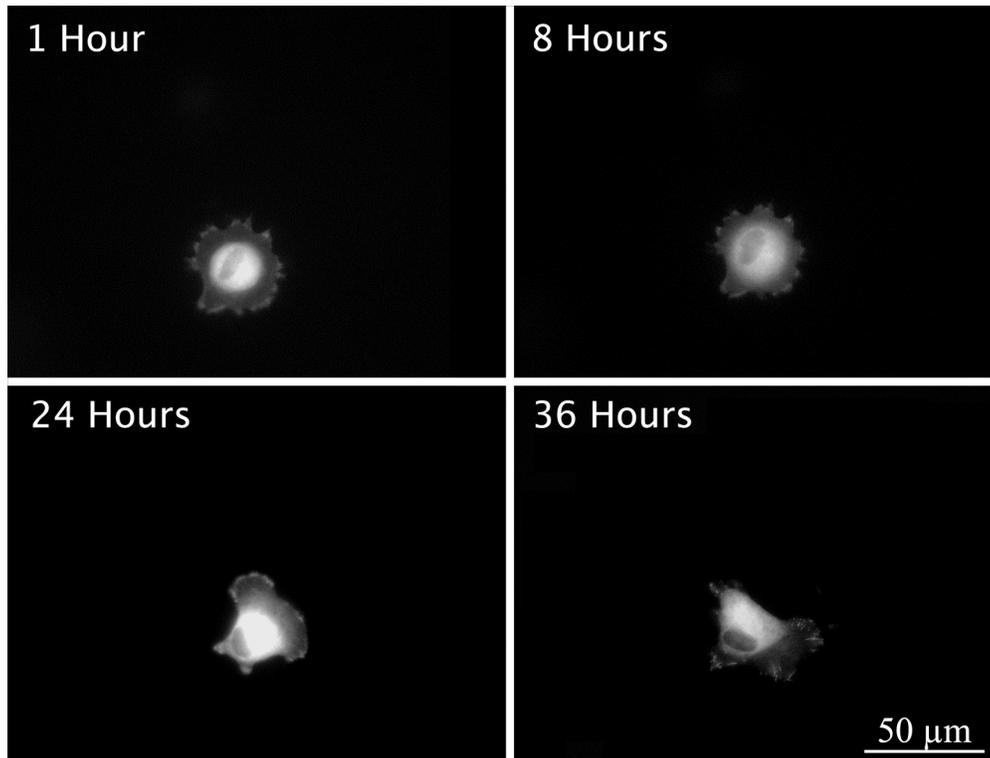
Fig. 4.11. YFP-vinculin analysis of the dynamics of adhesion formation in HOBs on square nanopit arrays. Square arrays of nanopits reduced the onset of cell-spreading. HOBs retained a rounded, unspread morphology after 24 hours forming dynamic FXs at the lamellipodia periphery after 36 hours.

Hexagonal nanopit arrays were also associated with a reduction in early spreading events in HOB populations. Again on this topography initial adhesion complex formation in HOBs was localised to peripheral lamellipodial extensions and adhesion complex maturation was not prominent after 24 hours. Following 36 hours of culture HOBs typically adopted an elongated morphology, indicative of a motile cellular phenotype (fig. 4.12).

4.3.6. Functional Response of STRO-1+ MSCs to Nanopits

Analysis of microarray data yielded significant alterations in broad functional signalling pathways in STRO-1+ MSCs. Canonical signalling pathways with the greatest number of modulated gene expression were associated with STRO-1+ MSCs cultured on nanopit topographies.
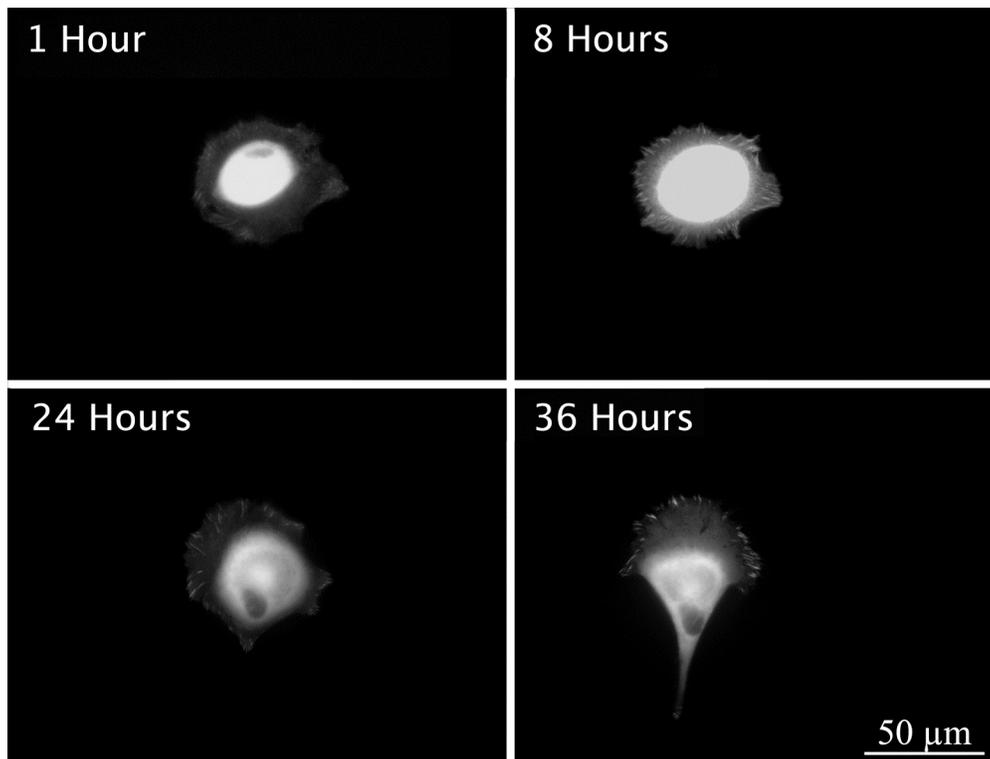
Fig. 4.12. YFP-vinculin analysis of the dynamics of adhesion formation in HOBs on hexagonal nanopit arrays. Hexagonal arrays of nanopits delayed the onset of cell-spreading. HOBs retained a rounded morphology after 24 hours adopting a polarised morphology after 36 hours.

Here on both nanopit arrays the modulation of 10-20% of gene expression was observable in vascular endothelial growth factor (VEGF), chemokine, p38-mitogen-activated protein kinase (p38-MAPK) and nuclear factor-kappa B (NF-kB) signalling pathways. Significant modulation was also observable in platelet derived growth factor (PDGF) and G-protein coupled receptor signalling in STRO-1+ populations cultured on square topographies (fig. 4.13A).

On nanopit substrates a general trend of genetic down-regulation of genes involved in multiple signalling pathways in STRO-1+ MSCs were linked to relatively large changes in multiple functional processes (fig. 4.13B). Genetic and signalling pathways involved in cell movement, cell signalling, cell growth and proliferation, and tissue development were significantly affected in STRO-1+ MSCs on both experimental substrates, corrolating with a reduction in adhesion subtype formation and cellular spreading in HOBs on nanopit substrates (fig. 4.5 - 4.13).
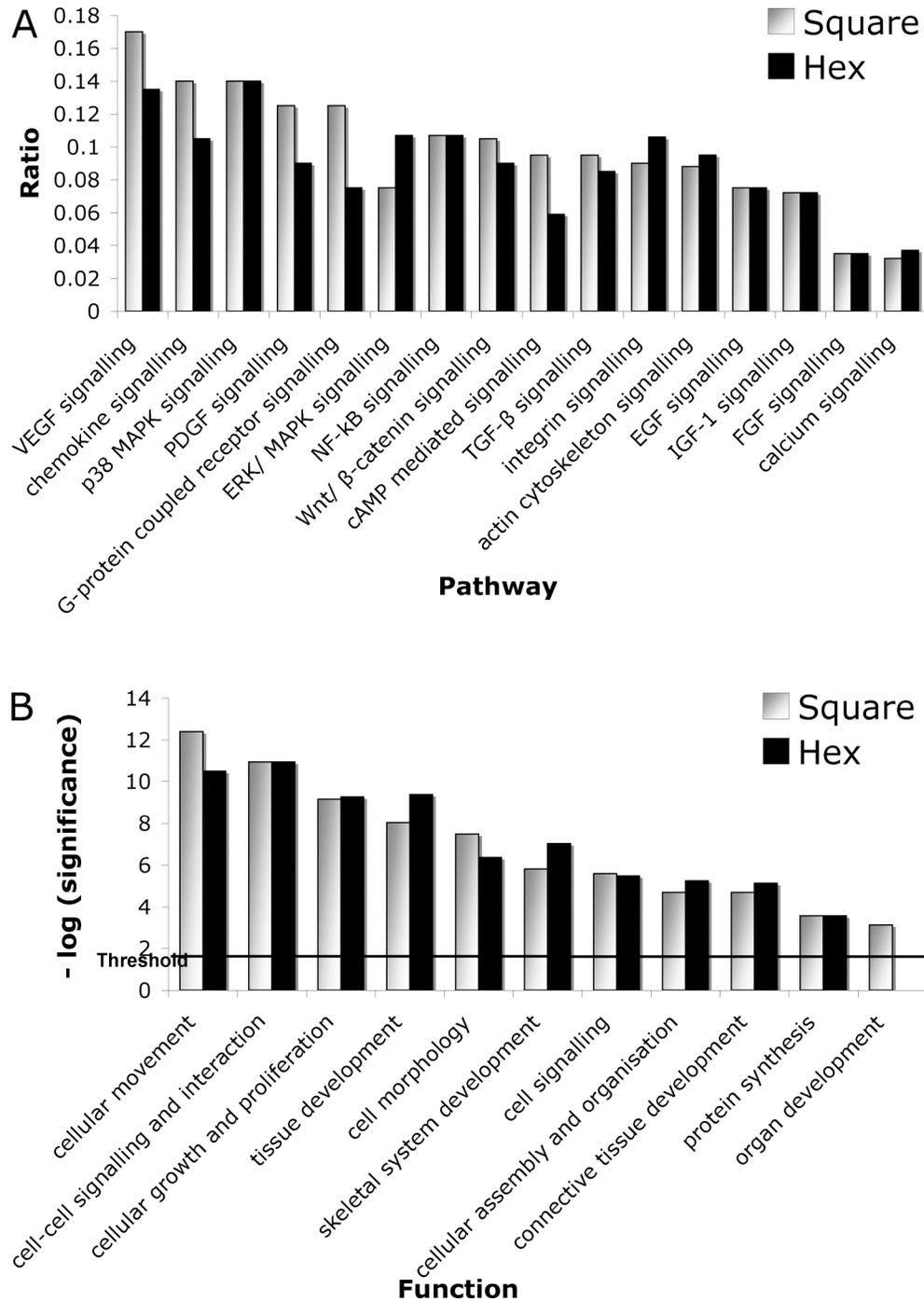
Fig. 4.13. Signalling pathway analysis of STRO-1+ MSCs on nanopit substrates. Canonical pathways analysis identified numerous well-defined signalling pathways that were most affected in these functional pathways. General trends showed the genes of interest within these pathways to be affected predominantly by down regulation on nanopit substrates. Functional Analysis of a network identified broad biological pathways that were most significantly affected by the nanopit topographies. MSCs cultured on hexagonal and square nanopit arrays were associated with significant changes in gene expression and function. A statistical threshold of p = 0.05 is indicated.

4.3.7. Wnt/β-Catenin Signalling

Canonical pathway analysis of STRO-1+ MSCs cultured on experimental substrates was correlated to significant modulation in genetic pathways linked to osteospecific function. Both nanopit topographies were associated with changes in approximately 10% of genes involved in Wnt/β-catenin signalling (fig. 4.13). An in-depth examination of these modulations revealed significant down-regulations in gene expression in STRO-1+ MSCs. STRO-1+ MSCs cultured on square (fig. 4.14A) and hexagonal (fig. 4.14B) nanopit arrays were both associated with increased transforming growth factor-β (TGF-β) expression, and multiple instances of down-regulated signalling molecule expression. On these substrates Wnt and cadherin expression was reduced relative to planar substrates as well as a number of associated signalling molecules.
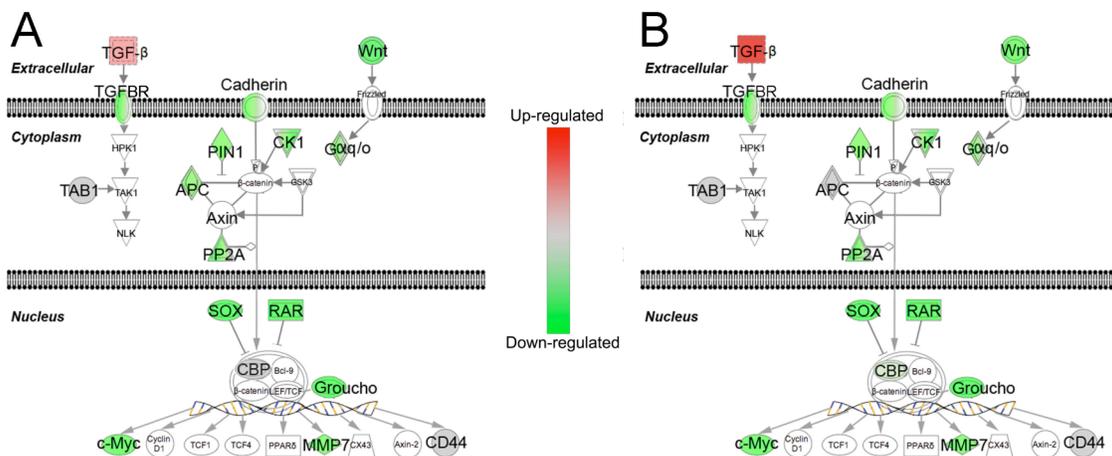
Fig. 4.14. Modulation of Wnt/β-catenin signalling in STRO-1+ MSCs on nanopit substrates. (A, B) Square and hexagonal nanopit substrates induced widespread modulation of Wnt/β-catenin signalling. Extensive down-regulation of signalling molecules was observed in STRO-1+ MSCs when cultured on nanopit substrates relative to cells cultured on planar controls. Red = up-regulation, green = down-regulation, grey = no change, colourless = not tested.

4.3.8. Integrin Signalling

Examination of integrin signalling revealed significant changes in gene expression in STRO-1+ MSCs cultured on experimental substrates relative to cells cultured on planar control substrates. Here both square and hexagonal substrates induced genetic modulation of approximately 10% of the genes involved in integrin signalling in STRO-1+ MSC populations (fig. 4.13). The majority of genes examined in the integrin signalling

pathway were down-regulated in MSCs cultured on both square (fig. 4.15A) and hexagonal (fig. 4.15B) nanopit arrays with exceptions observed in Rho expression. Down-regulation of FAK was prominent on both experimental topographies as were genes regulating the synthesis of adhesion associated proteins, notably the α and β integrins and the linker protein zyxin.
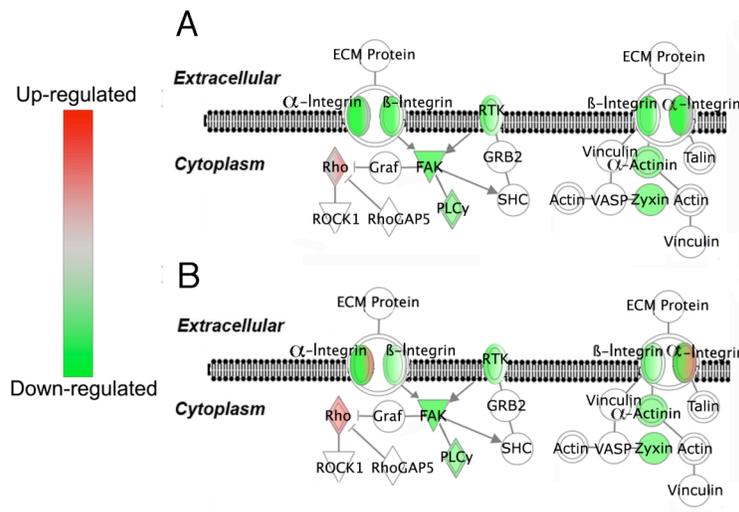
Fig. 4.15. Modulation of integrin signalling in STRO-1+ MSCs on nanopit substrates. Expression of genes involved in integrin signalling pathways were predominantly down-regulated in MSCs cultured on both (A) square and (B) hexagonal nanopit arrays. Red = Up-regulated, green = down-regulated, grey = no change, colourless = not tested.

4.4. Discussion

S-phase HOBs cultured on planar control substrates formed mature FAs and significantly higher numbers of SMAs than HOBs cultured on experimental substrates, indicating the disruptive affects that nanoscale pits can exert on mature adhesion formation. SEM revealed this perturbing effect to be a direct prevention of adhesion formation on the nanoscale pit features.

Relative to planar control substrates, experimental substrates induced changes in osteoblast cytoskeletal organisation, cellular morphology and adhesion formation, which were correlated to significant alterations in MSC genetic expression. It not possible at this point to dissect direct or indirect mechanotransductive pathways, although it seems possible that an interplay of both modalities influences changes in MSC genetic profiles. This is likely as firstly, reduced stress fibre and microtubule organisation is indicative of

a reduction in direct mechanotransduction, hence reduced genomic transcription seen on the nanopits and secondly, as demonstrated by microarray, a large number of indirect signalling pathways have been changed significantly.

In this chapter we have demonstrated that adhering osteoblast populations generate vinculin positive SMAs on planar control substrates and that cells on highly ordered nanopits are prevented from forming SMAs, structures analogous to elongated FAs and prominent in well spread cells. Real time observation of adhesion formation and cellular spreading allowed an insight into these processes over a finite time period. It was observed that adhesion formation is a continual dynamic process in HOBs cultured on planar and experimental substrates.

A reduction in adhesion formation in HOBs on nanopits was associated with significant decreases in expression of genes involved in fundamental signalling and functional pathways in MSCs. These findings highlight the existence of a possible relationship between adhesion formation and cellular spreading and the onset of cellular differentiation and function. Genes associated with Wnt/β-catenin and integrin signalling were significantly decreased in STRO-1+ MSCs on Nanopit topographies. The observable down-regulation of key genes involved in integrin signalling and signal transduction in MSC populations was correlated to a reduction in adhesion formation in osteoblast populations, possibly indicative of widespread reductions in intracellular signalling and subsequent differentiation in MSCs as induced by nanopit mediated adhesion perturbation.

4.4.1. Conclusion

The degree of topography order and feature dimensions can influence the generation of integrin mediated adhesions in S-phase HOBs as well as induce changes in gene profiles and influence functional pathways in MSCs. Ordered nanoscale pits prevent direct adhesion formation, instead inducing small FA and numerous FX formation at the interpit regions. These topographies also significantly reduced the expression of genes involved in many functional pathways in MSCs. These findings are intriguing as they indicate a critical size of nanofeature necessary to disrupt adhesion and subsequent cell function and may provide valuable insight for the production of next generation biomaterials where

cellular adhesion is unfavourable to device function or complicates its removal such as in temporary internal fixation.

CHAPTER V

The Influence of Random Nanoscale Islands and Craters on Osteoblast Adhesion Formation and the Functional Response of MSC Populations

5.1. General Introduction

To compare and contrast the effects of spatially random nanofeatures on osteospecific adhesion and function, nanoscale craters and islands were fabricated by polymer demixing. The surface of a solid amorphous polymer, or polymer mixture, is expected to be smooth and featureless. However, under certain circumstances marked topography can be obtained from a spontaneous demixing of the components of a binary blend, i.e. in thin films of certain polymer mixtures on selected substrates. The factors that determine demixing have been extensively studied. Principally, the mutual compatibility of the polymers controls the behaviour. The relationship between polymer compatibility and generation of topography in thin films of the blend is illustrated by examining a blend of poly(styrene) (pS) with a series of brominated polymers, poly(p-bromo-x-styrene) (pBrS), where x is the fraction of aromatic rings that are brominated, $0 \geq x \geq 1$. The compatibility of the brominated polymer with pS depends on the extent of bromination. When $x = 1$ the polymers are incompatible and the compatibility increases as $x \rightarrow 0$. Here we have used the fully brominated polymer, $x = 1$, in a study of cell interactions.

The interaction of the polymer components with the substrate and air during phase separation leads to a bilayer formation with a broad polymer-polymer interface. In this study we employed, pS/pBrS demixing, which is associated with a polymeric phase separation during a spin-casting process resulting in the spontaneous formation of nanoscale features. The shape of the topographic features (holes, ribbons or islands) can be controlled by varying the composition of the polymer mixture and the size of a particular feature by varying the concentration of the spin-casting solution (Affrossman *et al*. 1996, 1998; Affrossman & Stamm 2000) and finally by the spin-rate of the casting process.

The polymer de-mixed substrates were inevitably of mixed chemistry (and bromine containing). So the original samples were used for the replication of samples in biologically acceptable pMMA. Nanoscale craters and islands fabricated by polymer demixing were embossed into pMMA via intermediary Ni shims (Gadegaard *et al*., 2003b) for cell culture. This chapter is concerned with the affects of nanocraters and nanoislands fabricated by polymer demixing on osteoblast adhesion and morphology and

examines the functional modification of MSC populations on these topographies using both microscopical analysis and microarray gene profiling.

5.2. Materials and Methodology

5.2.1. Experimental Substrates Fabricated by Polymer Demixing

5.2.1.1. Original Topography Fabrication

Phase separation between pS and pBrS occurs and polymers demix when thin films of the blend are produced by spin casting. A graded series of structures may be obtained by varying the ratio of the polymers in the casting solution, the total polymer concentration, the solvent employed and the rate of spincasting. The range of structures varies from small islands to large islands, ribbons, large craters and, finally, to small pits. Substrates are fabricated by spin-casting a toluene solution containing 60% pBrS/40% pS weight per weight (w/w) blend on a silicone disk. After casting, the films were annealed above the glass transition temperature of pS, 103°C, so that the pS would become mobile and migrate to the surface. Two polymer concentrations and spin-casting speeds were selected for this study. Firstly a polymer film consisting of 1% w/w total pS and pBrS solution in toluene which was cast at 3000 rpm and secondly, a polymer film consisting of a 3% w/w total pS and pBrS solution in toluene which was cast at 1000 rpm. The dimensions of the resulting surface features were obtained by AFM using a NanoScope Dimension 3100 operating in tapping mode as SEM analysis is difficult to perform on the low aspect ratio features generated by polymer demixing. Original substrates were kindly fabricated by Dr. Stanley Affrossman at the Dept. of Pure and Applied Chemistry, University of Strathclyde.

5.2.1.2. Nickel shim fabrication

Ni shims fabrication is discussed in section 4.2.1.2 and reviewed by Gadegaard. (Gadegaard *et al*., 2003a).

5.2.1.3. Final substrate preparation

The embossing process is discussed in section 4.2.1.3. Planar pMMA was used as a control substrate as described in section 2.3.

5.2.2. Cell Culture

HOB and MSC cell models and culture conditions were according to those described in section 2.2.1 and 2.2.2. Briefly HOBs were derived from a femoral head biopsy of an 84 year old Caucasian female and a knee biopsy of a 74 year old Caucasian female (*PromoCell®, Heidelberg, Germany*). MSCs were enriched using STRO-1 antibody and magnetic cell sorting as described in section 2.2.2, from bone marrow samples obtained from haematologically normal patients undergoing routine hip replacement surgery. Both cell models were seeded onto untreated experimental, and planar control pMMA substrates. Prior to cell fixation, the cell cycle in HOB populations was synchronised and BrdU introduced into total cellular DNA as described in section 3.2.2.

5.2.3. Immunocytochemistry for Light Microscopy

Materials and methodology was according to those described in section 3.2.3. Briefly HOBs cultured on experimental and planar control pMMA substrates were fixed and subsequently incubated for 2 hours in an anti-BrdU/DNase-I solution including antibodies against one of; anti-vinculin monoclonal anti-human raised in mouse, clone hVin-1 (*1:200, Sigma, Poole, UK*), or anti-β-tubulin monoclonal anti-human raised in mouse, clone TUB 2.1 (*1:100, Sigma, Poole, UK*).

5.2.4. Immunocytochemistry for SEM

The immunolabelling method was a modified version of that first described by Richards *et al*. and described in full in section 2.4. Briefly, HOBs were stabilised in 4% paraformaldehyde and vinculin was labelled with goat anti-mouse 5 nm gold conjugate (*BB International, Cardiff, UK*) diluted 1:200 in PIPES buffer with 1% BSA and 0.1% Tween 20 overnight for 12 hours at 22°C. Gold probes were silver-enhanced with a silver developing solution for 7 minutes (*BBI International, Cardiff, UK*).

5.2.5. SEM

The HOBs were dehydrated through an ethanol series and with a SPI-DRY™ critical point dryer (*Structure Probe Inc., Leicestershire, UK*), before viewing with a Hitachi S-4700 field emission SEM as described in full in section 2.5.

5.2.6. Image Analysis

Experimental and planar control substrates were replicated 3 times and fluorescence images taken of HOBs on each (n = 15 per replicate) substrate were exported to Photoshop® and adhesion complexes scored with an 8 pixel wide straight line as described in section 3.4.

5.2.7. Plasmid Expansion and Cellular Transfection

Bacterial transformation, plasmid expansion and cellular transfection was accomplished using materials and methodology previously described in section 2.6. Briefly, a plasmid with an inserted sequence for vinculin plus a YFP tag was replicated by a population of *E. coli* cells. This plasmid was subsequently purified and transiently introduced into the HOB genome via electroporative transfection. Adhesion formation in these cells was studied via fluorescent live-cell imaging over a period of 36 hours.

5.2.8. RNA Isolation and Microarray Analysis

RNA extraction (n = 5), microarray hybridisation (n = 5) and gene data analysis was according to methodology previously described in section 2.7. Briefly, Individual gene expression detection was carried out with 1.7 K spotted DNA microarrays. The functional and canonical analyses were generated through the use of IPA Up and down regulated genes were associated with canonical pathways in the Ingenuity® Pathways knowledge base.

5.3. Results

5.3.1. Substrate Characterisation

Original substrates fabricated by polymer demixing possessed randomly displaced smooth island features as verified by AFM. Polymer-demixed substrates consisting of a 1% pS and pBrS solution in toluene which was spincast at 3000 rpm possessed densely packed island features with an average height of approximately 25-30 nm and were approximately 1.5 μm in width (fig. 5.1A). Polymer-demixed substrates consisting of a 3% pS and pBrS solution in toluene which was spincast at 1000 rpm possessed diffuse

island features with an average height of approximately 100 nm and were approximately 5 µm in width. These island features were surrounded by smaller column-like features (i.e. there was a bimodal feature distribution) that possessed an average height of approximately 60 nm and were approximately 2 µm in width (fig. 5.1B).
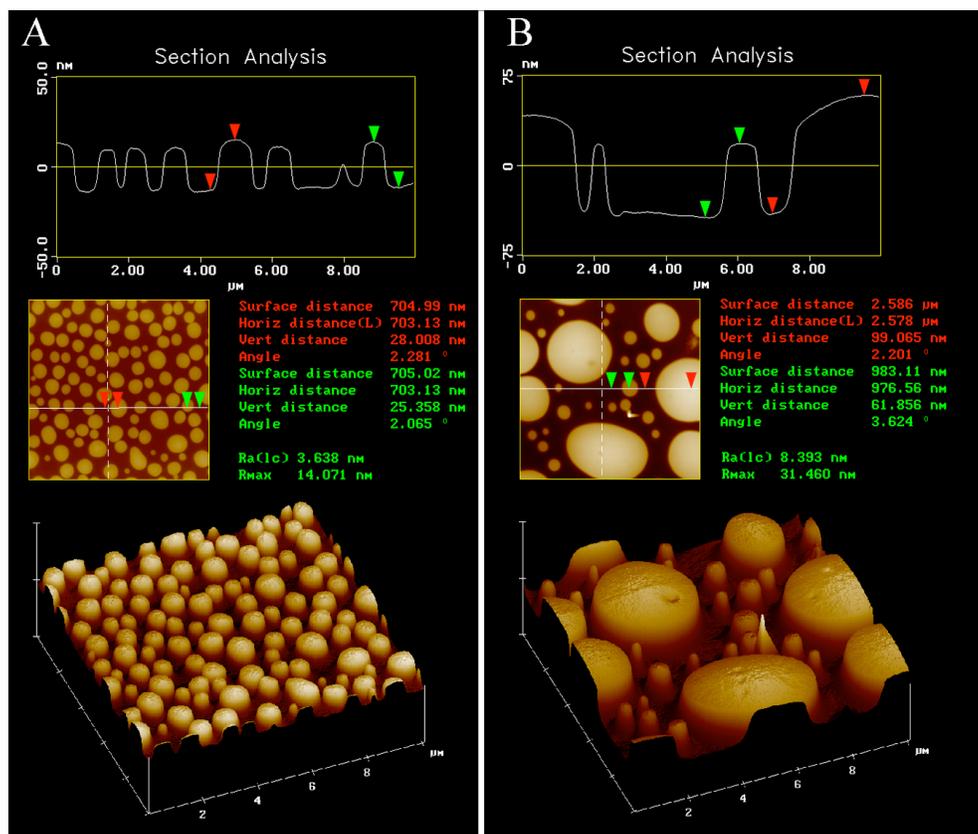
Fig. 5.1. Characterisation of original polymer demixed substrates. (A) Substrates fabricated from a blend of 1% pS and pBrS spincast at 3000 rpm possessed closely-packed island arrays with an average height and width of approximately 25-30 nm and 1.5 *µ*m respectively. **(B)** Substrates fabricated from a blend of 3% pS and pBrS spincast at 3000 rpm possessed diffuse island arrays with an average height and width of approximately 100 nm of 5 *µ*m respectively. These were interspersed with lesser nanocolumn features measuring 60 nm in height and 2 µm in width.

Nickel shims fabricated directly from the original substrates possessed an inverted and altered topography relative to the original polymer demixed substrates. Surface curvature of nanoisland features was obscured with sharp peaks. Island heights were diminished by approximately 65% on Polymer-demixed substrates consisting of a 1% pS and pBrS solution in toluene (fig. 5.2A), and by approximately 50% on Polymer-demixed substrates consisting of a 1% pS and pBrS solution in toluene (fig. 5.2B).
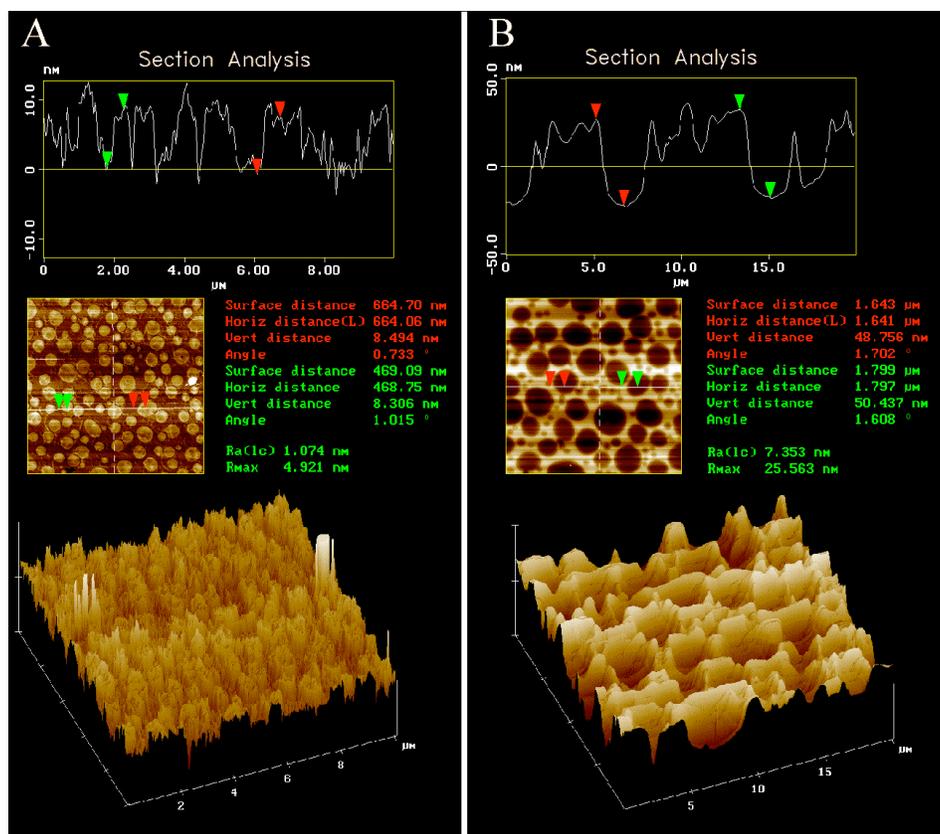
Fig. 5.2. *Characterisation of Ni shims derived from original polymer demixed substrates.* (A,B) Shims fabricated from both original pS and pBrS demixed substrates possessed irregular sharp peak features and were associated with diminished feature heights.

pMMA replicas of polymer-demixed substrates consisting of a 1% pS and pBrS solution in toluene, spincast at 3000 rpm possessed irregular, randomly displaced nanocraters, which were approximately 50 nm deep and 3 µm in diameter (fig 5.3A). Nanocraters were present within a rough matrix of 7.5 nm deep nanopits. pMMA replicas of Polymer-demixed substrates consisting of a 3% pS and pBrS solution in toluene, spincast at 1000

rpm possessed irregular, closely packed nanoislands, which were approximately 60 nm high, and 4 µm in diameter (fig. 5.3B). Although polymer demixed pMMA replicas differed significantly from original topographies, these were reproducible as embossing into pMMA was via the single Ni shim described herein (Dalby *et al*., 2006b). These topographies will hereon be referred to as nanocrater (fig 5.3A) and nanoisland (fig 5.3B) substrates respectively.
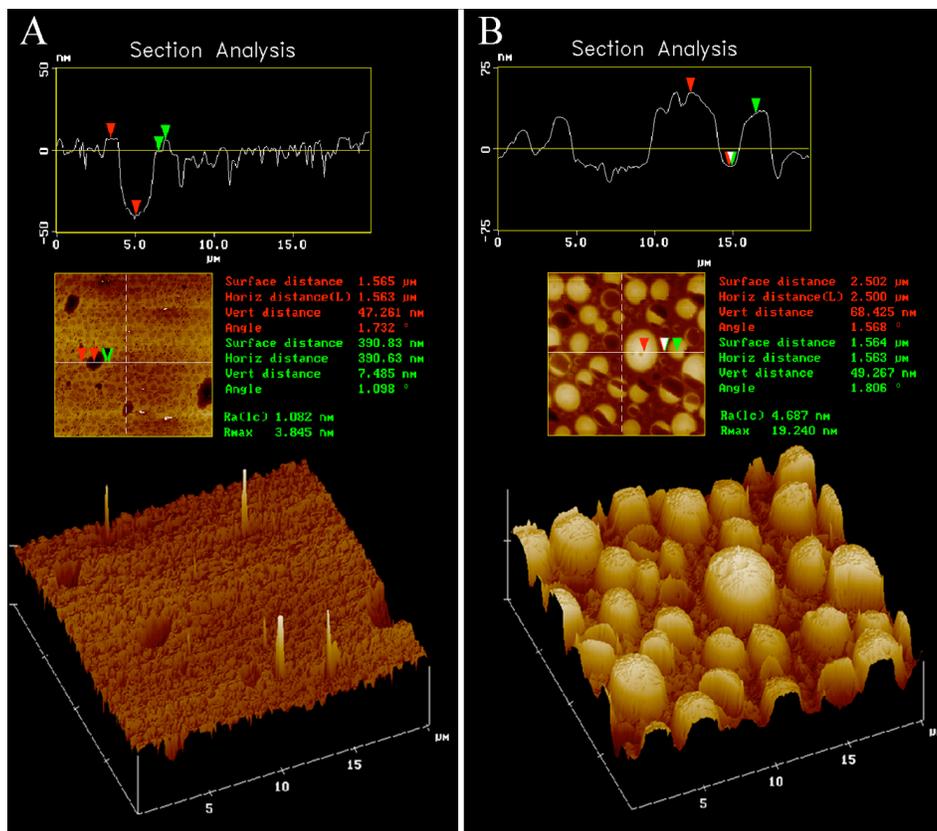
Fig. 5.3. Characterisation of pMMA embossed polymer demixed substrates. AFM revealed important data pertaining to surface Ra and feature dimensions. (A) Nanocrater features were approximately 50 nm deep and 3 µm wide. Craters were present within a matrix of nanopits approximately 10 nm deep. (B) Nanoisland features were approximately 60 nm in height and had an average diameter of approximately 4 µm.

The planar pMMA control substrates possessed no visible topographical features with SEM imaging and were verified to have an Ra of 1.2 nm over 10 mm^2 by AFM as described in section 2.3.

5.3.2. HOB Morphology and Cytoskeletal Organisation

Experimental nanosubstrates modified S-phase HOB morphology and cytoskeletal organisation relative to controls (for a detailed account of HOB morphology and cytoskeletal organisation on controls see section 4.3.2). HOBs cultured on nanocrater and nanoisland substrates displayed extensive cell spreading and formed a substantial tubulin network that became less dense with increasing distance from the nucleus, in a manner similar to HOBs on planar control substrates (fig. 5.4B and C). Stress fibre networks in osteoblasts on nanocrater and nanoisland substrates were comparable to HOBs on planar control substrates (fig. 5.5B and C).
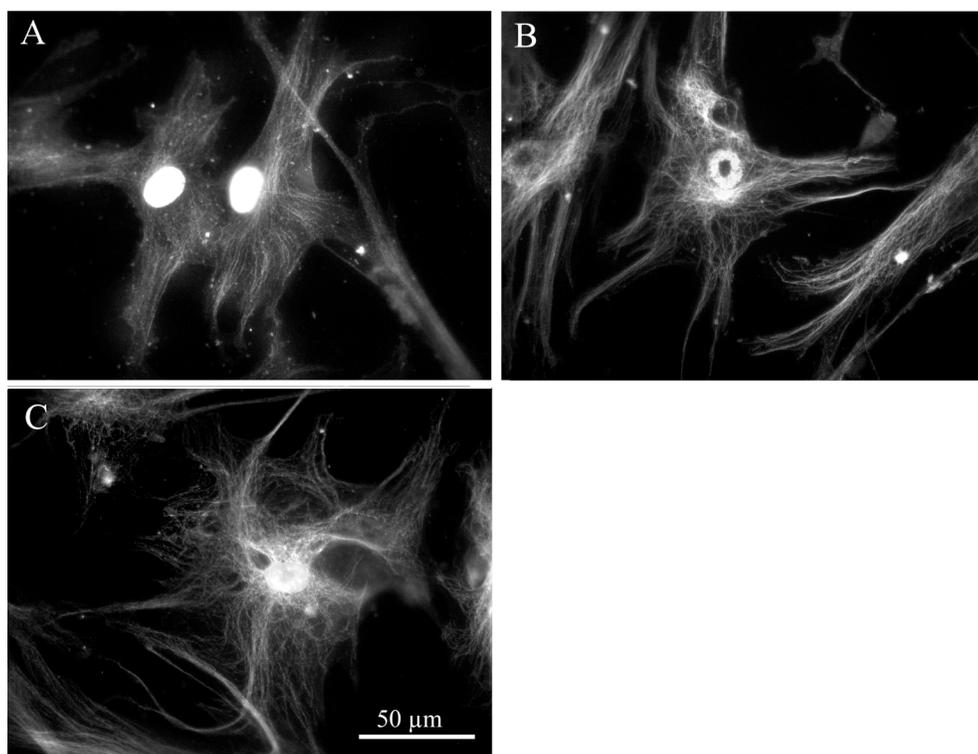
Fig. 5.4. Dual immunolabelling of the tubulin cytoskeleton and S-Phase nuclei of HOBs on polymer demixed substrates (A, B and C) HOBs cultured on control, nanocrater and nanoisland substrates formed organised tubulin networks. Tubulin density decreased with increasing distance from the nucleus and again extended into the cellular extensions.

5.3.3. Adhesion Characterisation and Qualification

Characterisation of adhesion distribution by vinculin immunolabelling revealed differences in adhesion size and location in S-phase HOBs on polymer demixed substrates relative to control substrates (see section 4.3.3). Both nanocrater and nanoisland substrates restricted the formation of FXs, identified by fluorescent and gold colloid labelling. FA and SMA formation was prevalent in HOBs on both topographies at the cell periphery and perinuclear region (fig. 5.5B and C and 5.6B and C). Although cellular spreading was comparable to HOBs cultured on planar control substrates, adhesion formation was not as prominent.
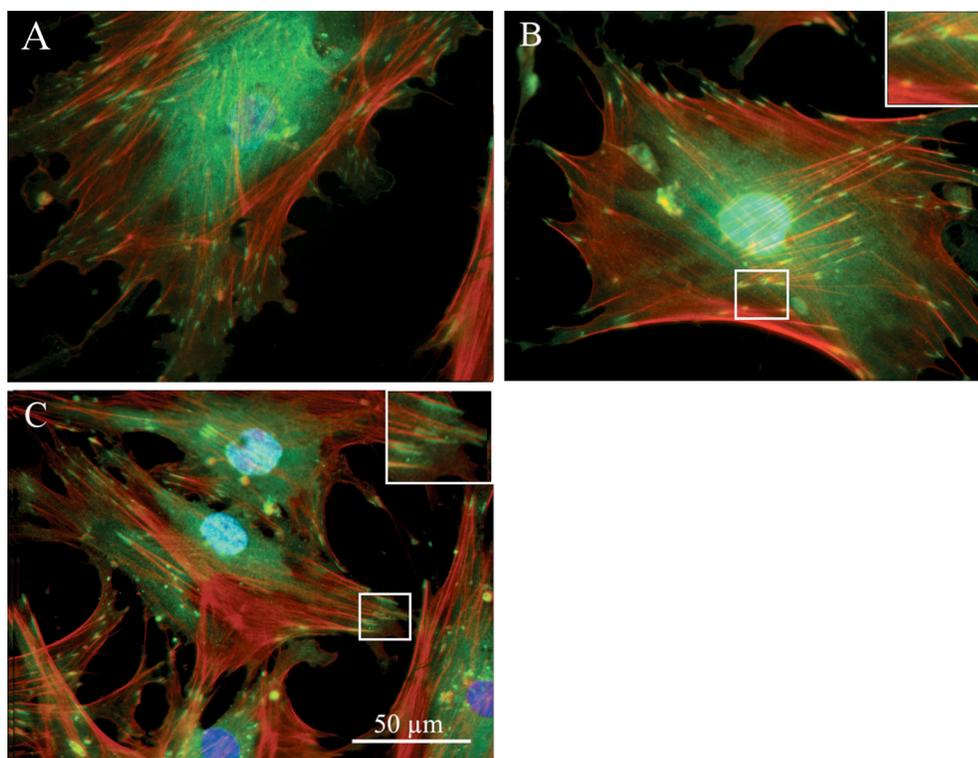
Fig. 5.5. Tri-fluorescent labelling of adhesion complexes and stress fibre organisation in S-Phase HOBs on polymer demixed substrates. (A) HOBs cultured on planar control substrates formed well-organised stress fibres and numerous adhesions, SMAs are indicated (arrows). (B) Osteoblasts on nanocraters possessed a well-developed actin cytoskeleton. Adhesions were less numerous and located both centrally and at the cell periphery. (C) HOBs cultured on nanoislands developed an organised actin cytoskeleton. Adhesion formation was reduced relative to planar control substrates. Red = actin, green = vinculin, blue = S-phase nuclei.
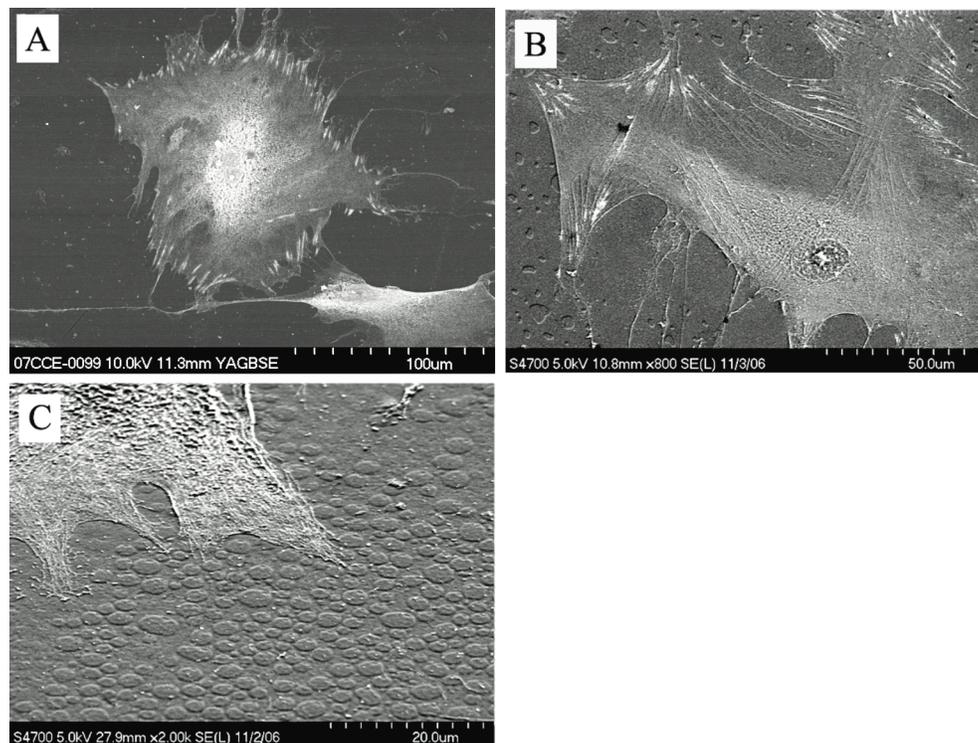
Fig. 5.6. Scanning electron immuno-labelling of adhesion complexes in HOBs on polymer demixed substrates. (A) HOBs cultured on planar control substrates formed numerous FXs, FAs and SMAs. (B) Nanocrater substrates accommodated focal and SMA formation within the craters and at intercrater regions. (C) Nanoisland substrates induced large lamellipodial extensions.

5.3.4. Adhesion Distribution and Quantification

Insignificant differences in the numbers of generated adhesion subtypes relative to planar control substrates were observed on both polymer demixed topographies. FX formation however, was not evident in HOBs on nanoisland and nanocrater substrates (fig. 5.7). S-phase HOBs cultured on nanocrater and nanoisland substrates formed predominantly large FAs and SMA subtypes relative to FX formation (fig. 5.8A and B). All topographies induced a decrease in FA formation in S-phase HOBs relative to controls, greatest decreases however were observed on nanoisland topographies. Relative to controls, FA formation on these substrates was reduced by approximately 47% (fig. 5.7). Adhesion distribution and quantification in HOBs cultured on planar control substrates is discussed in section 4.3.4. Adhesion complex frequency showed a similar trend to that of HOBs cultured on planar controls – i.e. a maximum was observed at 2.5 µm in length.
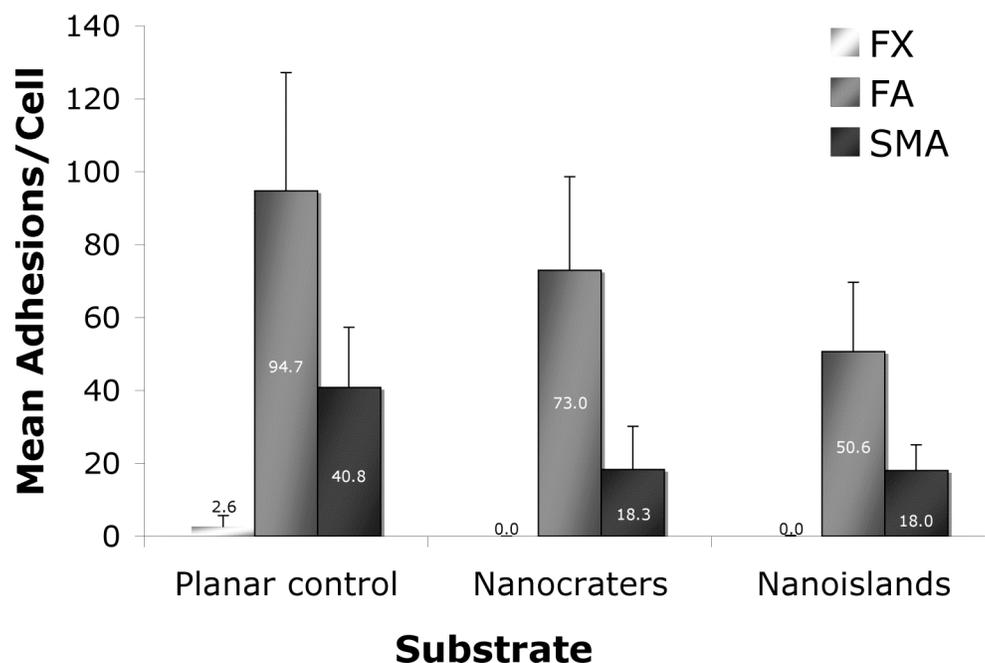
Fig. 5.7. Quantification of adhesion complex subtypes in S-phase HOBs on polymer demixed substrates.
SMA formation was most prominent in HOBs on planar control substrates. FA incidence was decreased on
all substrates relative to controls. FX incidence was not apparent in HOBs on experimental substrates. See
Table 8.1 for relevant statistics. Included are mean values. Results are + STD.
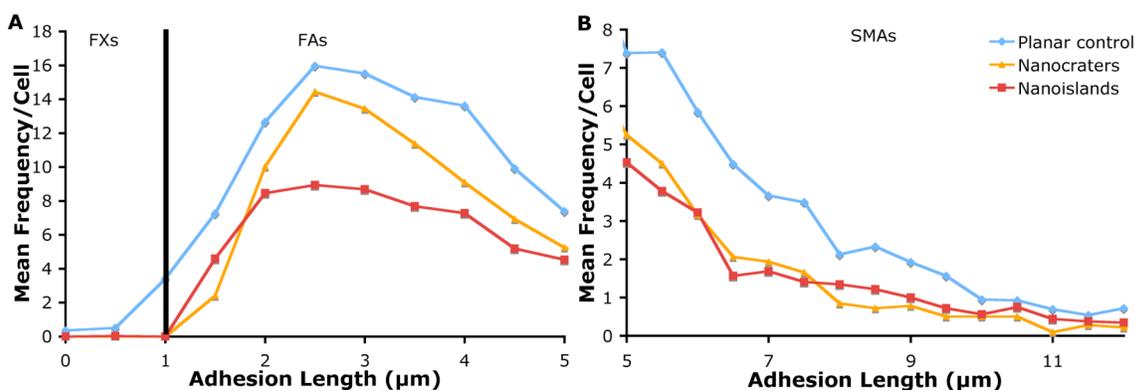
Fig. 5.8. Adhesion complex distribution in S-phase HOBs on polymer demixed substrates. (A)
Distribution of FXs were not noted in HOBs on both experimental topographies. FAs approaching 3 µm in
length was increased on planar control substrates and nanocrater substrates. All experimental substrates
show a similar decline in adhesion complex distribution as FA lengths approach 3 µm. (B) SMAs are most
pronounced in HOBs cultured on control substrates. HOBs cultured on planar control, nanoisland and
nanocrater substrates show a similar decline in SMAs incidence.

5.3.5. Live Cell Adhesion Modulation

FA modulation as identified by YFP-vinculin live cell imaging allowed the dynamics of FA formation to be studied over a period of 36 hours following initial cell seeding onto experimental and planar control substrates.

Adhesion formation in HOBs on nanocrater topographies occurred rapidly relative to planar controls. On this topography cellular spreading was more extensive following 1 hour of culture. Osteoblasts were seen to use FA associated filopodial extensions to increase cellular spreading. By 36 hours multiple FAs were observed to merge into larger SMAs (fig. 5.9).
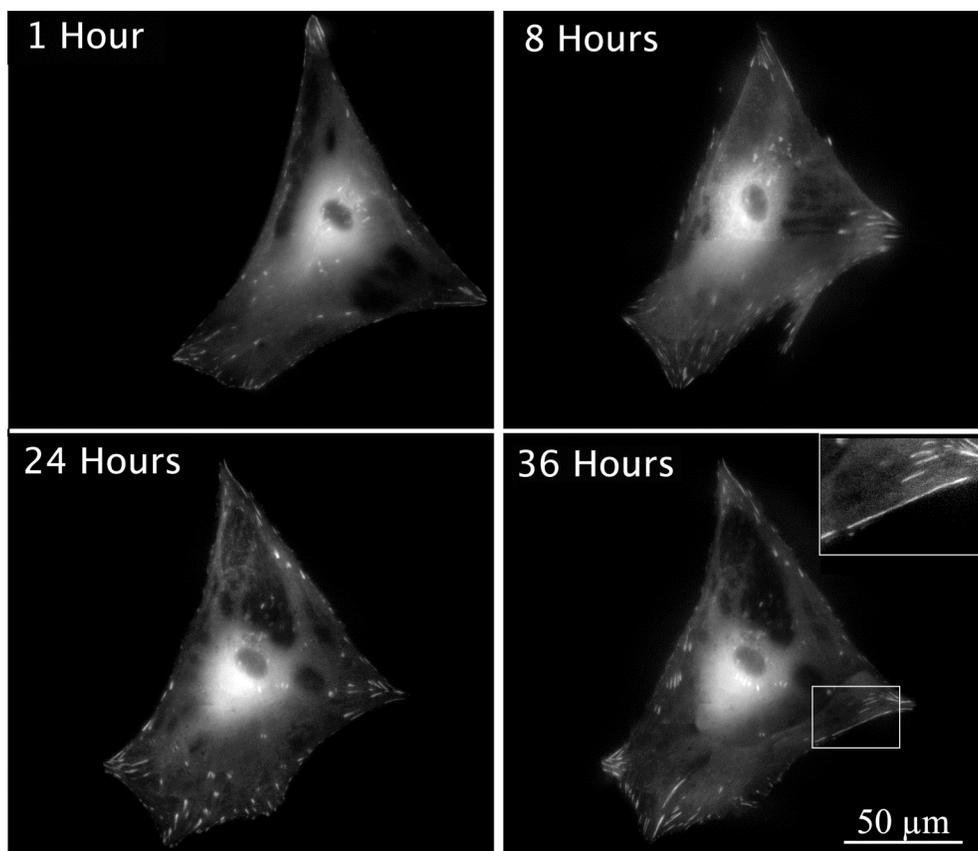
Fig. 5.9. YFP-vinculin analysis of the dynamics of adhesion formation in HOBs on nanocrater substrates. Cellular spreading was rapid following seeding, the mechanics of which are seen following 8 hours. Multiple FAs converge into SMAs by 36 hours of culture (boxed area).

Initial adhesion formation in HOBs on nanocrater topographies was comparable to planar control substrates. Following seeding, HOBs formed a circumferential network of FXs

seen after 1 hour. Increased cellular spreading was correlated to enhanced FA formation predominantly at the cell periphery. At 36 hours following osteoblast seeding, cellular spreading and pseudopodia formation were still prominent, however the frequency of FAs was reduced (fig. 5.10).

HOB live cell adhesion formation on planar control substrates is discussed in section 4.3.5.
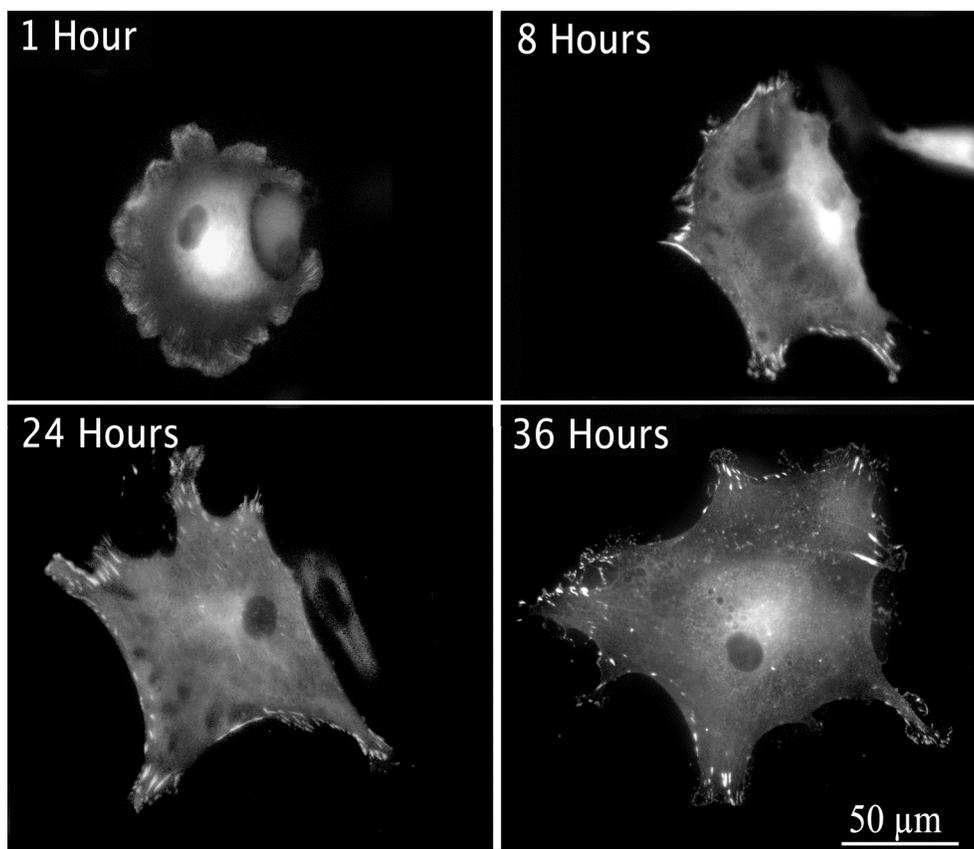
Fig. 5.10. YFP-vinculin analysis of the dynamics of adhesion formation in HOBs on nanoisland substrates. A circumferential network of FXs followed initial cell seeding. FA formation and cellular spreading both increased following 24 hours of culture, FA frequency was reduced following 36 hours of culture however.

5.3.6. Functional Response of STRO-1+ MSCs to Nanocraters and Nanoislands

Analysis of microarray data yielded significant alterations in canonical signalling pathways in STRO-1+ MSCs. Nanocrater and nanoisland substrates influenced minor changes in these canonical signalling pathways, (fig. 5.11A) by modulating the expression of relatively few pathway associated genes (fig. 5.12A and B and 5.13A and

B).

Both nanocrater and nanoisland topographies significantly influenced genetic pathways linked to p38-MAPK signalling. Here, more significant changes were noted in MSCs cultured on nanoisland topographies, on which the expression of approximately 5% of genes involved in this pathway were modulated relative to cells cultured on planar control substrates. Less significant changes were noted in MSCs cultured on nanocrater substrates, on which only 3% of associated genes were changes.

STRO-1+ MSCs cultured on nanoisland substrates also showed significant modulation of NF-kB signalling and Wnt/β-catenin signalling which were both associated with changes in 4-5% of the total genes involved in these signalling pathways. Relatively minor gene modulations were noted in STRO-1+ MSC populations cultured on nanocrater substrates however, which demonstrated 1-2% gene modulation in many canonical signalling pathways (fig. 5.11A).

Modulations in canonical signalling pathways were subsequently correlated to significant and broad changes in STRO-1+ MSC population function. Cellular growth and proliferation in STRO-1+ MSCs cultured on both polymer demixed substrates was significantly influenced by topographical features, however this was more than twice as significant on nanoisland substrates. Cell morphology was significantly affected on both substrates, correlating with cytoskeletal changes noted in HOBs on these substrates. Cellular movement, and cell-cell signalling were also both significantly modified in STRO-1+ MSCs cultured on nanocrater and nanoisland topographies. (fig. 5.11B).
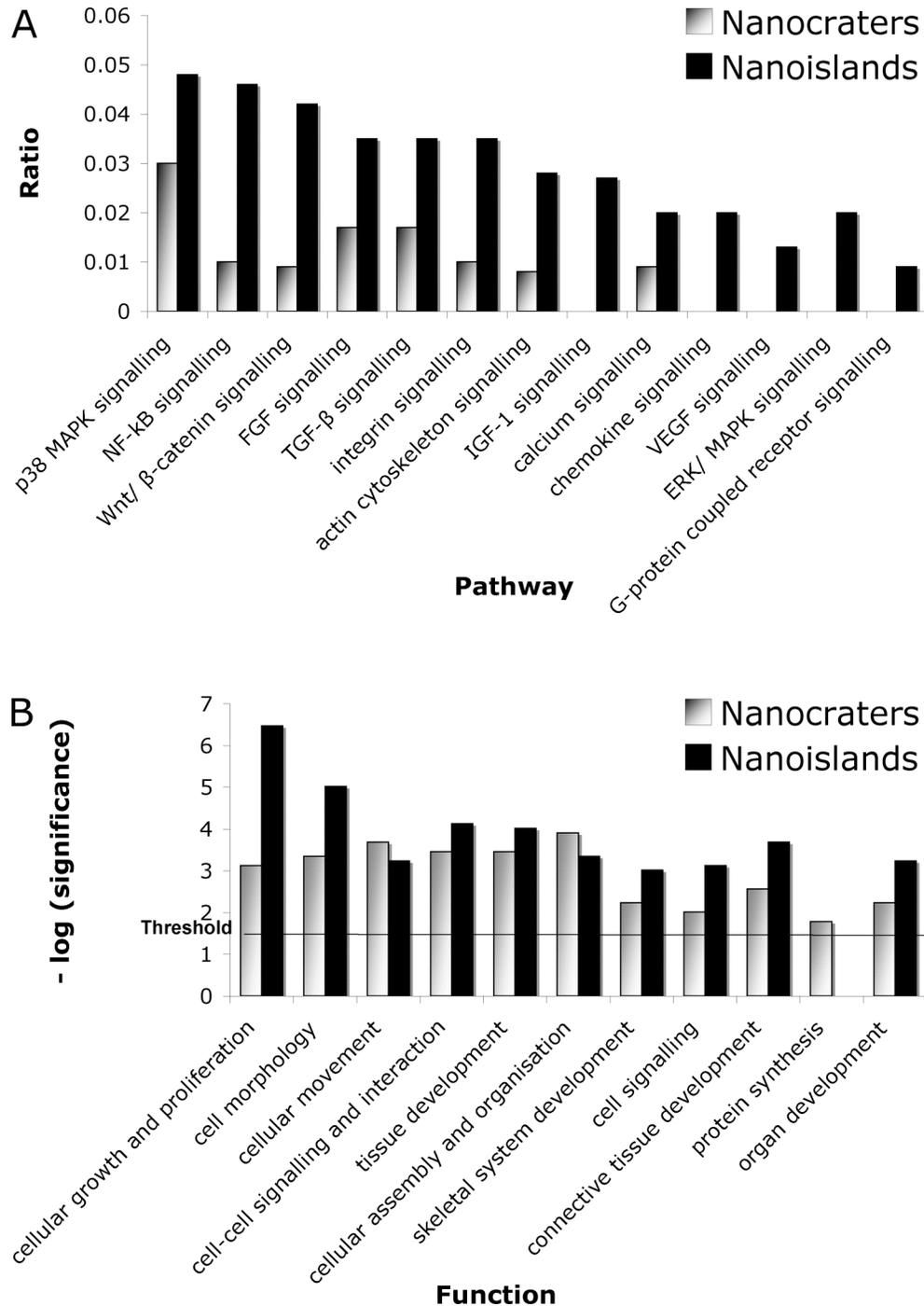
Fig. 5.11. Signalling pathway analysis of STRO-1+ MSCs on polymer demixed substrates. Canonical pathways analysis identified numerous well-defined signalling pathways that were most affected in MSCs cultured on experimental substrates. General trends showed the genes of interest within these pathways to be affected predominantly by minor up regulation on polymer demixed substrates. The Functional Analysis of a network identified biological pathways that were most significant to the genes in the network affected by the nanotopographies. MSCs cultured on experimental substrates were associated with minor changes in gene expression and function, however these were more pronounced in MSCs cultured on nanoisland topographies. A statistical threshold of p = 0.05 is indicated.

5.3.7. Wnt/β-Catenin Signalling

Canonical pathway analysis of STRO-1+ MSCs cultured on experimental substrates was correlated to significant modulation of genetic pathways linked to osteospecific function. Approximately 4% of genes involved in Wnt/β-Catenin Signalling were modulated in STRO-1+ MSC populations cultured on nanoisland topographies yet only 1% were affected in cells cultured on nanocrater topographies (fig. 5.11A). An in depth examination of Wnt/β-catenin signalling revealed changes in gene expression to be exclusively up-regulated or unchanged. Nanocrater substrates induced a minor up-regulation in transforming growth factor beta (TGF-β) expression yet no other changes were identified (fig. 5.12A). Increased TGF-β expression was also demonstrable in STRO-1+ MSCs cultured on nanoisland substrates, this was coupled with minor up-regulations in transforming growth factor-β activated kinase-1 binding protein (TAB1) and Ca^{2+}/cAMP-response elements binding protein (CPB) (fig. 5.12).
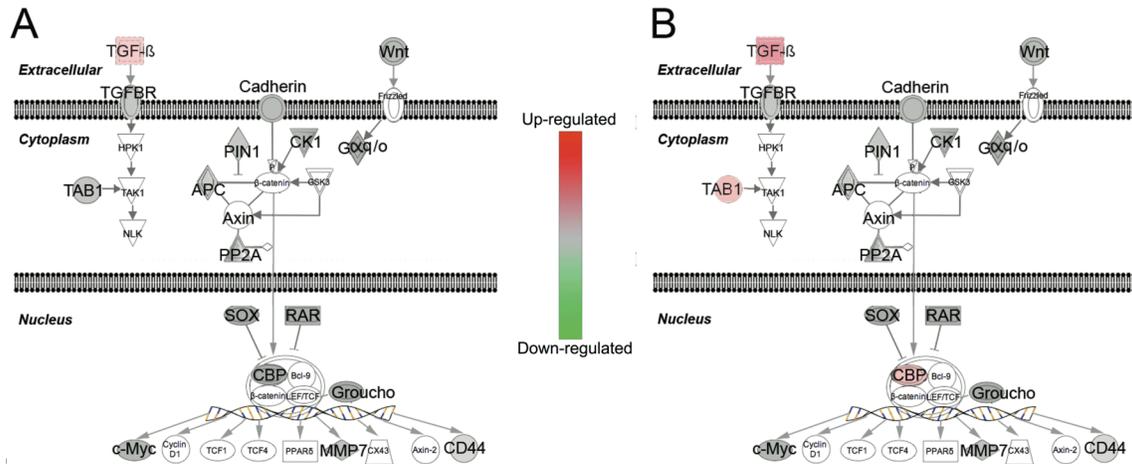
Fig. 5.12. Modulation of Wnt/β-catenin signalling in STRO-1+ MSCs on polymer demixed substrates. (A, B) Wnt/β-catenin signalling pathways were affected in STRO-1+ MSCs on nanocrater and nanoisland substrates respectively relative to planar controls. However, more changes in gene expression were noted in MSCs cultured on nanoisland topographies. Here gene modulation was restricted to minor up-regulations in TGF-β, TAB1 and CPB. Red = up-regulation, green = down-regulation, grey = no change, colourless = not tested.

5.3.8. Integrin Signalling

Examination of the integrin signalling pathway revealed only minor changes in gene expression in STRO-1+ MSCs cultured on experimental substrates relative to cells cultured on planar control substrates. Again the most changes were observed in MSCs cultured on nanoisland topographies. On this topography genetic expression of proteins involved in integrin signalling was modulated by 3.5%, whereas genetic modulation was only 1% in MSCs cultured on nanocrater topographies (fig. 5.11A). The majority of genes examined in the integrin signalling pathway were unchanged, however up-regulations in genes pertaining to α-integrin and Rho synthesis were identified in MSCs cultured on both nanocrater (fig. 5.13A) and nanoisland (fig. 5.13B) topographies.
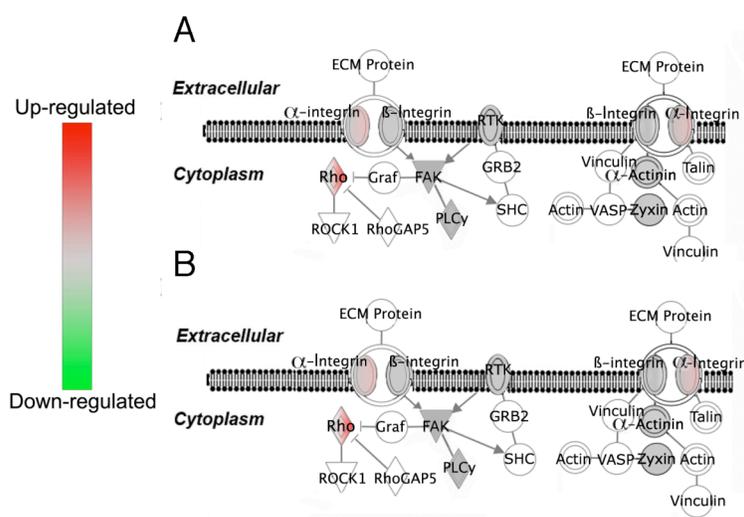
Fig. 5.13. Modulation of integrin signalling in STRO-1+ MSCs on polymer demixed substrates. Minor up-regulation in the expression of genes involved in integrin signalling pathways was noted in MSCs cultured on both (A) nanocrater and (B) nanoisland topographies. Red = Up-regulated, green = down-regulated, grey = no change, colourless = not tested.

5.4. Discussion

This chapter notes the influential role of nanoisland and nanocrater substrates fabricated by polymer demixing on osteoblast adhesion and STRO-1+ MSC function. The process of substrate fabrication allows rapid transformation of the chemical demixing process to substrates possessing random low-aspect ratio topography. Although the final substrates

topography differed significantly from the original substrates, typical when embossing low-aspect ratio nanofeatures (Dalby *et al.*, 2006b), polymeric replicates were shown to be reproducible. This reproducibility factor stemmed from the embossing process, which ensured that a single master template could produce near-identical replicates in pMMA.

The frequency of mature FAs and SMAs in S-phase HOBs cultured on planar control substrates was comparable to HOBs cultured on nanoisland and nanocrater substrates. Less extensive modulation of osteoblast adhesion was correlated to minor induced changes in osteoblast cytoskeletal organisation, cellular morphology and adhesion formation, which were further correlated to minor alterations (predominantly up-regulation) in MSC genetic expression.

Here again, the presence of vinculin positive SMAs on both experimental and planar control substrates was noted. A general trend of reduction regarding all adhesion subtypes was noted in HOBs on experimental substrates yet this reduced adhesion formation was seen to be more significant on nanoisland topographies, which were also associated with more significant changes in MSC function.

An interesting finding in adhesion modification on polymer demixed topographies was the absence of FXs at the time of S-phase HOB fixation (ten days). It can be reasoned that this absence in FXs is specific to the S-phase population, although a more obvious explanation is the presence of a topographically induced cessation of major cellular migration and the generation of stable sites of adhesion following ten days of culture.

It has been clearly shown that the features dimensions produced by polymer demixing induce filopodial and lamellipodial interaction, critical for increased cellular spreading and function. Early cellular spreading as identified in HOBs cultured on nanocrater topographies has been implicated in the onset of osteospecific differentiation (Kudelska-Mazur *et al.*, 2005). It appears that both topographically induced cellular spreading and mature adhesion plaque formation in the absence of migration are equally crucial for enhanced cell function and that these are causative factors in osteodifferentiation.

5.4.1. Conclusion

Due to the nanometric size of cellular components concerned with cell-biomaterial interactions, the surface structure of an implanted device influences cell adhesion processes when the surface topography is within nanometre range. The degree of topography order and feature dimension can influence the generation of integrin mediated adhesions in S-phase HOBs as well as induce changes in gene profiles and influence functional pathways in STRO-1+ MSCs. Random nanoislands and nanocraters formed by polymer demixing facilitated the formation and maturation of adhesion complexes in the absence of FX formation and were associated with a minor up-regulation of genes involved in many functional pathways. These findings are intriguing as they indicate topographical modification capable of reducing cell motility may increase osteospecific functionality.

CHAPTER VI

The Influence of 300 nm Deep Microgrooves on Osteoblast Adhesion Formation and the Functional Response of MSC Populations

6.1. General Introduction

The standard for fabricating microscale topographies is photolithography performed in the near-ultra violet (UV). This process involves exposing a silicon wafer coated with a photoresist to a near-UV light source (wavelength is typically 365 or 405 nm) through a mask that has the desired pattern on it. This mask selectively allows light through to the wafer thereby recreating the pattern in the photoresist. Subsequent development of the resist layer brings out the desired features. However, due to the inherent lower limit of this method (a function of the wavelength of light used) it is incompatible with creating nanometre-size features. This can be overcome to some degree by regulating the exposure of the resist layer to the photon source, thereby effectively controlling the feature height (Fukuda *et al.*, 1991) which was employed in this study. Photolithography was used to fabricate experimental topographies possessing arrays of repeating microscale grooves and ridges. As with other fabrication techniques described in section 4.1 and 5.1, samples were made in a three-step process of photolithography, nickel die fabrication and embossing, allowing for the fabrication of microgrooves with nanoscale depths in pMMA.

The phenomenon of cellular contact guidance on grooved topography has been well documented in the literature (den Braber *et al.*, 1998, Karuri *et al.*, 2004, Lenhert *et al.*, 2005). Nanoscale grooves with dimensions similar to those found in tissue *in vivo* have been shown to cause contact guidance and alignment *in vitro* in numerous studies involving human cell types, including corneal epithelial cells (Teixeira *et al.*, 2003), fibroblasts (Dalby *et al.*, 2003c) and osteoblasts (Lenhert *et al.*, 2005).

Here, photolithography was used to produce two grooved topographies of identical groove depths with different widths (10 and 100 μm repeat width, 300 nm approximate groove depth, 2 cm length). Again HOBs derived from femoral head and condyle biopsies, and STRO-1 immunoselected human MSCs isolated from the marrow of a femoral diaphysis were used as cell models to investigate the morphological and functional response respectively to grooved topographies. HOB adhesion complex formation was quantified and cytoskeletal morphology investigated with SEM and fluorescence microscopy. This was then followed up with Human 1718 gene cDNA microarrays to compare the reaction of STRO-1+ MSC to the nanogrooves with the

cellular response to planar control substrates at 21 days of cell culture. Data were then analysed by Inginuity® pathway analysis. Interesting changes were observed in the relative level of expression in genes involved in the areas of cell-cell signalling, cytoskeletal formation, ECM remodelling and adhesion associated signalling.

6.2. Materials and Methodology

6.2.1. Experimental Substrates Fabricated by Photolithography

6.2.1.1. Silicon preparation

Silicon wafers were cleaned under acetone in an ultrasonic bath for 5 minutes. They were then rinsed thoroughly in ROH_2O and blown dry with an air gun. Next, they were spun with primer for 30 seconds at 4000 rpm, then spun with S1818 photoresist (*Shipley, Marlborough, MA*) for 30 seconds at 4000 rpm, and baked for 30 minutes at 90°C. The resulting layer was measured BY AFM to be 1.8 μm thick. The photoresist layer was exposed to UV light through a chrome mask featuring an array of parallel slits on a Karl Suss MA6 mask aligner for 3.8 seconds. Then the resist layer was developed for 75 seconds in 50:50, Microposit developer: ROH_2O.

6.2.1.2. Silicon master fabrication

The specific design pattern, in this case rectangular grooves and ridges, was achieved by reactive ion etching using the exposed photoresist as a mask. The silicon substrate was etched in the silicon tetrachloride gas plasma of a Plasmalab System 100 machine (gas flow = 18 sccm, pressure = 9 mTorr, rf power = 250 Watts, DC bias = -330 Volts). The wafer was etched individually at 7 minutes at a nominal etch rate of 18 nm/minute. It was then stripped of resist in an acetone ultrasound bath for 5 minutes, followed by a 5 minute soak in concentrated sulphuric acid/hydrogen peroxide mixture before rinsing thoroughly in ROH_2O and drying in an air gun. The final silicon masters had 330 nm deep grooves that were either 10 μm or 100 μm in width. Substrates were kindly fabricated by Mrs. Mary Robertson and Ms. Sara McFarlane at the JWNC, University of Glasgow.

6.2.1.3. Nickel shim fabrication

Ni shims fabrication is discussed in section 4.2.1.2 and reviewed by Gadegaard. (Gadegaard *et al.*, 2003a).

6.2.1.4. Final substrate preparation

The embossing process is discussed in section 4.2.1.3. Planar pMMA was used as a control substrate as described in section 2.3.

6.2.2. Cell Culture

Cell models and culture conditions were according to those described in section 2.2.1. and 2.2.2. Briefly HOBs derived from a femoral head biopsy of an 84 year old Caucasian female and a knee biopsy of a 74 year old Caucasian female (*PromoCell®, Heidelberg, Germany*). MSCs were enriched using STRO-1 antibody and MACS as described in section 2.2.2, from bone marrow samples obtained from haematologically normal patients undergoing routine hip replacement surgery. Both cell models were seeded onto untreated experimental, and planar control pMMA substrates. Prior to cell fixation, the cell cycle in HOB populations was synchronised and BrdU introduced into total cellular DNA as described in section 3.2.2.

6.2.3. Immunocytochemistry for Light Microscopy

Materials and methodology was according to those described in section 3.2.3. Briefly HOBs cultured on experimental and planar control pMMA substrates were fixed and subsequently incubated for 2 hours in an anti-BrdU/DNase-I solution including antibodies against one of; anti-vinculin monoclonal anti-human raised in mouse, clone hVin-1 (*1:200, Sigma, Poole, UK*), or anti-β-tubulin monoclonal anti-human raised in mouse, clone TUB 2.1 (*1:100, Sigma, Poole, UK*).

6.2.4. Immunocytochemistry for SEM

The immunolabelling method was a modified version of that first described by Richards *et al*. and described in full in section 2.4. Briefly, cells were stabilised in 4% paraformaldehyde and vinculin was labelled with goat anti-mouse 5 nm gold conjugate (*BB International, Cardiff, UK*) diluted 1:200 in PIPES buffer + 1% BSA + 0.1% Tween 20 overnight for 12 hours at 22°C. Gold probes were silver-enhanced with a silver developing solution for 7 minutes (*BBI International, Cardiff, UK*).

6.2.5. SEM

The cells were dehydrated through an ethanol series and with a SPI-DRY^{TM} critical point dryer (*Structure Probe Inc., Leicestershire, UK*), before viewing with a Hitachi S-4700 field emission SEM as described in full in section 2.5.

6.2.6. Image Analysis

Experimental and planar control substrates were replicated 3 times and fluorescence images taken of HOBs on each (n = 15 per replicate) substrate were exported to Photoshop® and adhesion complexes scored with an 8 pixel wide straight line as described in section 3.4.

6.2.7. Plasmid Expansion and Cellular Transfection

Bacterial transformation, plasmid expansion and cellular transfection was accomplished using materials and methodology previously described in section 2.7. Briefly, a plasmid with an inserted sequence for vinculin plus a YFP tag was replicated by a population of *E. coli* cells. This plasmid was subsequently purified and transiently introduced into the HOB genome via electroporative transfection. Adhesion formation in these cells was studied via fluorescent live-cell imaging over a period of 36 hours.

6.2.8. RNA Isolation and Microarray Analysis

RNA extraction (n = 5), microarray hybridisation (n = 5) and gene data analysis was according to methodology previously described in section 2.5. Briefly, Individual gene expression detection was carried out with 1.7 K spotted DNA microarrays. The functional and canonical analyses were generated through the use of IPA Up and down regulated genes were associated with canonical pathways in the Ingenuity® Pathways knowledge base.

6.3. Results

6.3.1. Substrate Characterisation

Silicone substrates were destroyed during the nickel shim fabrication process. Nickel shims fabricated directly from the original substrates possessed an inverted topography relative to the original photolithography substrates. Nickel shims were verified by AFM to possess anisotrophic arrays of grooves/ridges measuring either 10 or 100 µm in width. 10 µm wide grooves were verified by AFM to be approximately 310 nm in depth and 100 µm wide grooves approximately 300 nm in depth (fig. 6.1). Ra on both 10 µm wide and 100 µm wide grooved substrates was 37.5 and 58.5 nm over 10 mm^2 respectively.
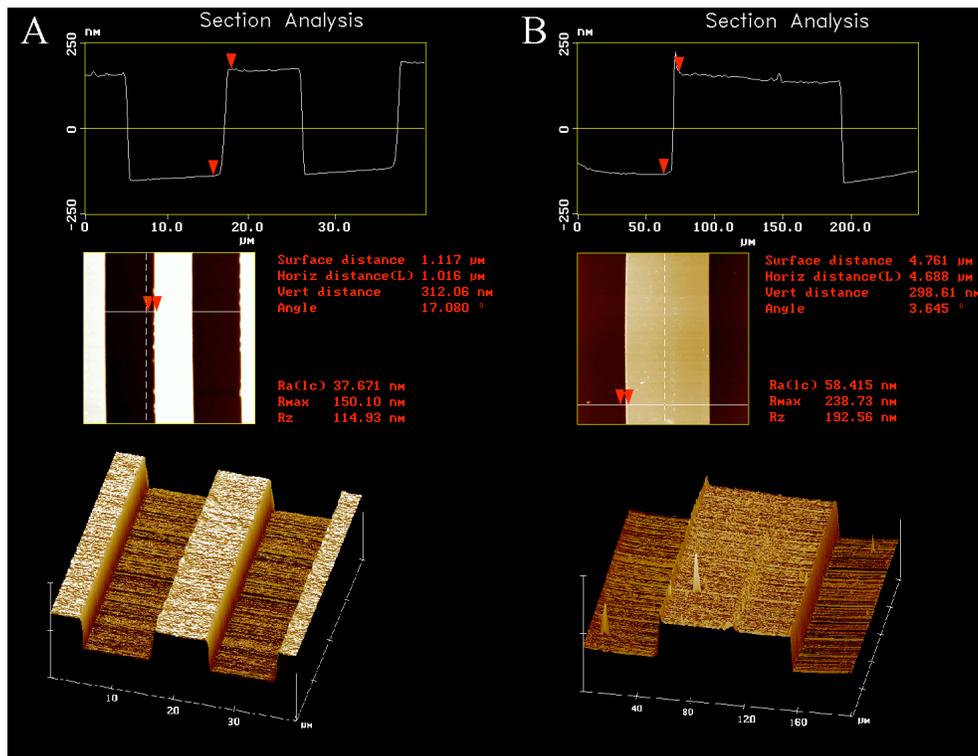
Fig. 6.1. Characterisation of Ni shims derived from original photolithography substrates. AFM analysis revealed Ni Substrates to possess an inverted topography of the original substrates fabricated in silicone. Groove/ridge arrays were (A) 10 µm in width and 310 nm in depth, or (B) 100 µm and 300 nm in depth.

The embossing process resulted in the fabrication of two groove/ridge topographies possessing repeating grooves and ridges with identical depths and periodicity as verified by AFM (fig. 6.2). Topographies possessed either 10 µm wide groove/ridge arrays which were approximately 308 nm deep/high or 100 µm wide groove/ridge arrays which were 292 nm deep/high.

Planar control substrates had an Ra of 1.2 nm over 10 mm^2 as verified by AFM (fig. 2.1).
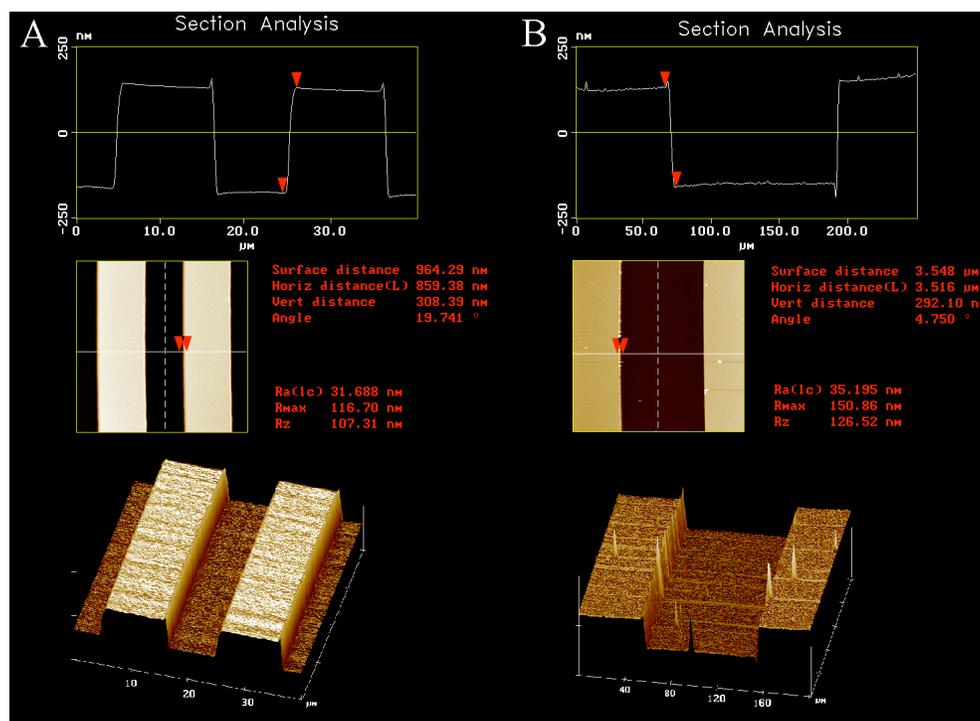
Fig. 6.2. Characterisation of pMMA embossed photolithography substrates. Groove/ridged arrays embossed into pMMA substrates were shown by AFM to be almost identical to nickel shims, i.e. approximately 300 nm deep and (A) 10 µm or (B) 100 µm in width.

6.3.2. HOB Morphology and Cytoskeletal Organisation

HOBs cultured on 10 µm grooves formed dense microtubule bundles that were orientated in the direction of cell polarity (fig. 6.3B). Cells cultured on 100 µm groove/ridge arrays possessed a well-developed microtubule network that appeared similar to HOBs cultured on planar control substrates (fig. 6.3A and C). Here the microtubule network was observed to radiate outwards from the microtubule dense perinuclear area to the cell perhiphery.
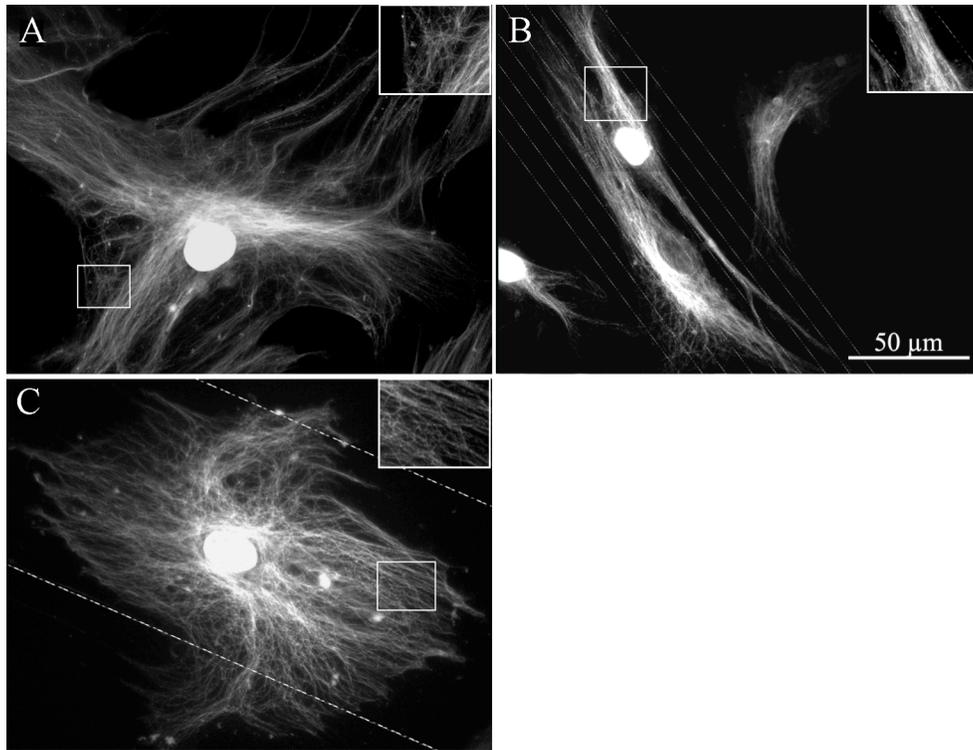
Fig. 6.3. Duel immunolabelling of the tubulin cytoskeleton and S-Phase nuclei of HOBs on microgrooved substrates. (A and C) HOBs cultured on control and 100 µm groove substrates formed organised tubulin networks. Tubulin density decreased with increasing distance from the nucleus. (B) Contact guidance was increased in cells on 10 µm groove substrates. S-phase HOBs formed a dense and polarised microtubule network.

Nanogroove substrates modified S-phase HOB morphology and cytoskeletal organisation relative to planar control substrates. HOBs cultured on both experimental substrates experienced cellular alignment, which was inversely proportional to groove/ridge width (fig. 6.3 and 6.4 and 6.5). HOBs on 10 µm groove/ridge topographies adopted a non-spread or a polarised elongated morphology, demonstrating contact guidance (fig. 6.3B, 6.4B and 6.5B). Actin fibres in HOBs on 10 µm groove/ridge arrays could be seen to run either perpendicular or parallel to the grooves, but stress fibres arranged both parallel and perpendicular to groove direction rarely occurred in a single cell (fig. 6.4). Cellular spreading and stress fibre networks in HOBs on 100 µm groove/ridge arrays appeared similar to cells on planar controls.

Planar control morphology and cytoskeletal organisation is discussed in section 4.3.2.

129
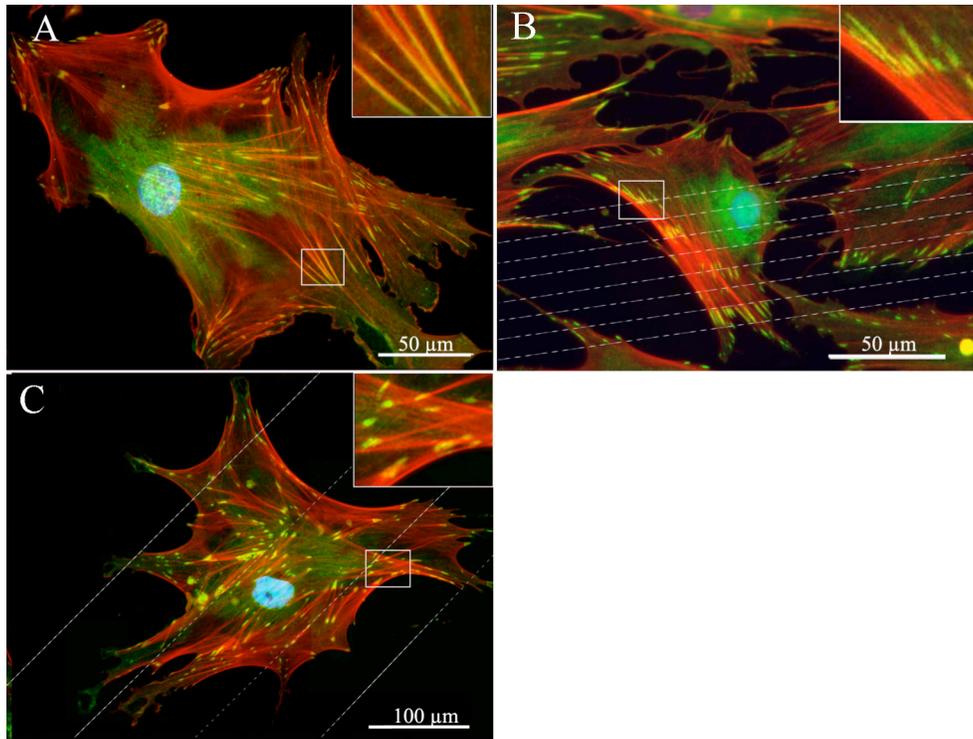
Fig. 6.4. Tri-fluorescent labelling of adhesion complexes and stress fibre organisation in S-Phase HOBs on microgrooved substrates. (A) HOBs cultured on planar control substrates formed well-organised stress fibres and numerous SMAs (boxed area). (B) Osteoblasts on 100 µm grooves possessed a well-developed actin cytoskeleton. Adhesions were large and numerous. (C) 10 µm groove arrays disrupted cellular spreading and adhesion formation. Adhesion formation was influenced by groove orientation. Red = actin, green = vinculin, blue = S-phase nuclei.

6.3.3. Adhesion Characterisation and Qualification

Vinculin immunolabelling revealed significant differences in adhesion formation in S-phase HOBs on nanogrooved substrates relative to control substrates (see section 4.3.3). Orientation and location of adhesions was significantly effected in HOBs on 10 µm groove/ridge arrays (fig. 6.4B and 6.5B). Adhesion formation occurred predominantly on top of the ridge structures and were observed to form either parallel or perpendicular to the groove angle. Adhesion formation in HOBs on 100 µm groove/ridge substrates was similar to that of HOBs on planar control substrates (fig. 6.4C and 6.5C), unlike adhesion formation in HOBs cultured on 10 µm wide grooves, adhesion location and orientation was not significantly affected by this topography.
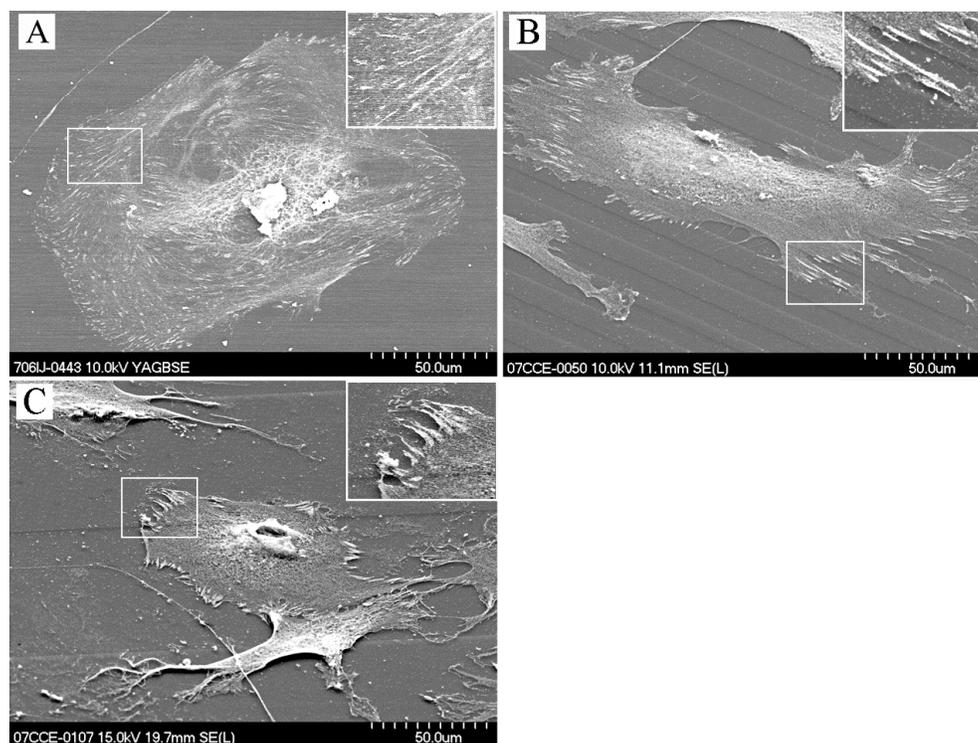
Fig. 6.5. Scanning electron immuno-labelling of adhesion complexes in HOBs on microgrooved substrates. (A) HOBs cultured on planar control substrates formed adhesion complexes of all subtypes. (B) 10 µm groove/ridge arrays influenced cellular alignment and adhesion orientation. Cells adopted a polarised morphology. (C) 100 µm grooves provided a step topography, which did not significantly affect adhesion formation or cellular orientation.

6.3.4. Adhesion Distribution and Quantification

Significant differences in the numbers of generated adhesion subtypes were observed on 10 µm groove/ridge arrays relative to both control and 100 µm grooves. FXs were the least prominent adhesion subtype present in HOBs cultured on planar control and experimental substrates (fig. 6.6 and 6.7A). FAs were the predominant adhesion sub-type in HOBs on planar control substrates and experimental substrates. However, HOBs cultured on the 10 µm grooves formed significantly fewer FAs than cells cultured on control and 100 µm grooves (100 µm grooves showed no significant difference from control). HOBs cultured on the 100 µm groove substrates formed on average 83.8 FAs per cell. This was reduced on 10 µm groove/ridge topographies to just 45 per cell. Adhesion distribution and quantification in HOBs cultured on planar control substrates is discussed in section 4.3.4.
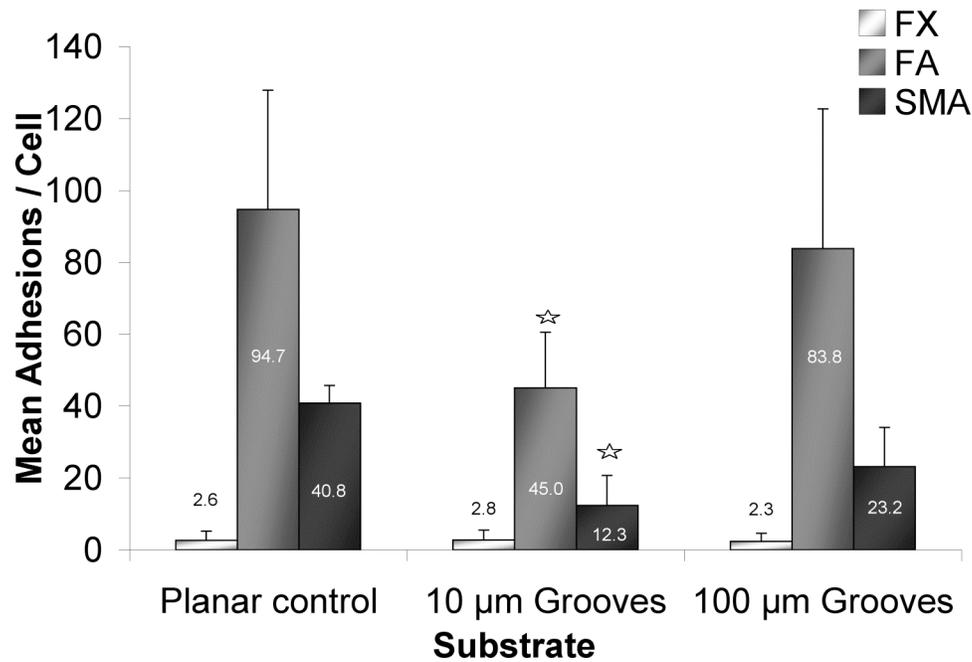
Fig. 6.6. Quantification of adhesion complex subtypes in S-phase HOBs on microgrooved substrates.
SMA formation was greatest in HOBs on planar control substrates. SMA formation was significantly
reduced in cells on 10 μm grooves. FA incidence was significantly decreased only in HOBs on 10 μm
substrates. See Table 8.1 for relevant statistics. Included are mean values. Results are + STD. $p < 0.05$
denoted by ★

SMA incidence was reduced (almost halved) on 100 μm groove/ridge arrays (23.2)
relative to control substrates and significantly reduced (halved again) on 10 μm
groove/ridge arrays (12.3). The frequency of SMAs > 8 μm in length was less than 1 per
cell in HOBs cultured on 10 μm groove/ridge arrays. Very large SMAs (>10 μm) were
only observed in HOBs cultured on planar control substrates and 100 μm groove/ridge
topographies (fig. 6.7B). Adhesion distribution was moderately shifted to the left on
experimental substrates relative to planar control substrates. Maximum FA frequency was
found to occur at 2 μm in length. This was increased to 2.5 μm on planar control
substrates.
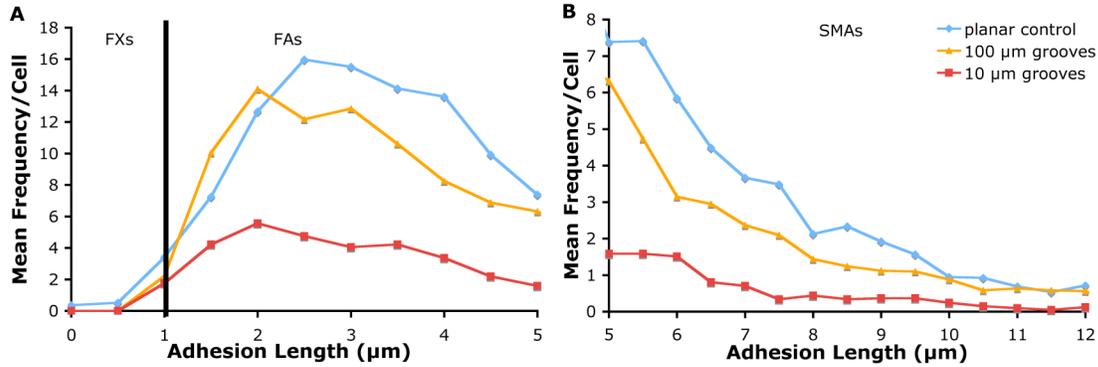
Fig. 6.7. Adhesion complex distribution in S-phase HOBs on microgrooved substrates. Adhesion distribution was left-shifted on experimental substrates. (A) Frequency of FAs approaching 2 μm in length was increased on flat and 100 μm groove substrates. All experimental substrates show a similar decline in adhesion complex distribution as FA lengths approach 3 μm. (B) SMAs are most numerous in HOBs cultured on control substrates. SMA frequency declines on all substrates as length increases.

6.3.5. Adhesion Orientation

Planar controls, and 100 μm groove/ridge topographies did not significantly affect adhesion orientation. Adhesion orientation was dictated by cellular morphology and stress fibre formation on planar and 100 μm groove/ridge arrays. Adhesion alignment in HOBs cultured on 10 μm groove/ridge arrays however was significantly influenced. Here 20% of all adhesions were parallel with respect to the groove orientation (fig. 6.8).
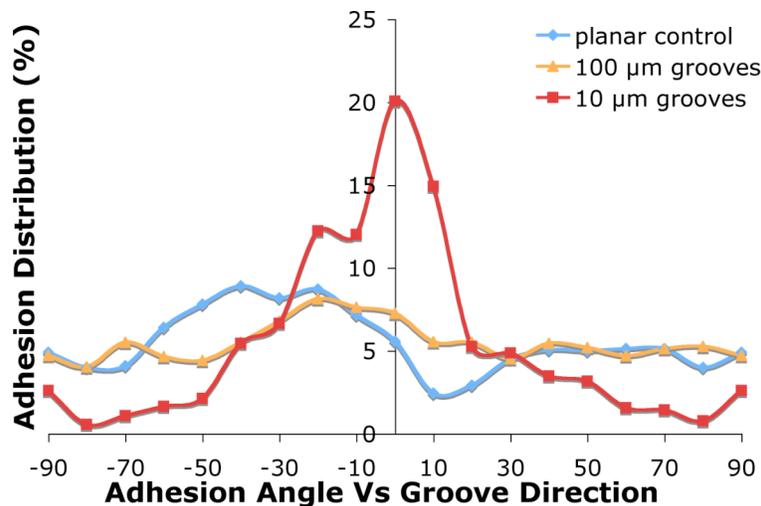
Fig. 6.8. Adhesion complex alignment on microgrooved substrates. Adhesion complex alignment was only affected by 10 μm groove substrates. The majority of adhesions on this topography deviated less than 30 degrees from the groove direction. Approximately 20% of adhesions were aligned parallel with the grooves.

133

6.3.6. Live Cell Adhesion Modulation

FA modulation as identified by YFP-vinculin live cell imaging allowed the dynamics of FA formation to be studied over a period of 36 hours. HOBs on 10 μm groove/ridge arrays rapidly aligned to the topography demonstrating contact guidance, a polarised morphology and formed FXs at the leading edge. FXs were replaced by FAs following 8 hours of culture, which were more prevalent at the leading edge. Following 36 hours of culture HOBs were significantly elongated and maintained a similar distribution of adhesion formation. Adhesion formation was predominantly parallel to the groove orientation in HOBs following 8 hours after cell seeding, following 24 hours however adhesions approximately perpendicular to the groove orientation were also prevalent (fig. 6.9).
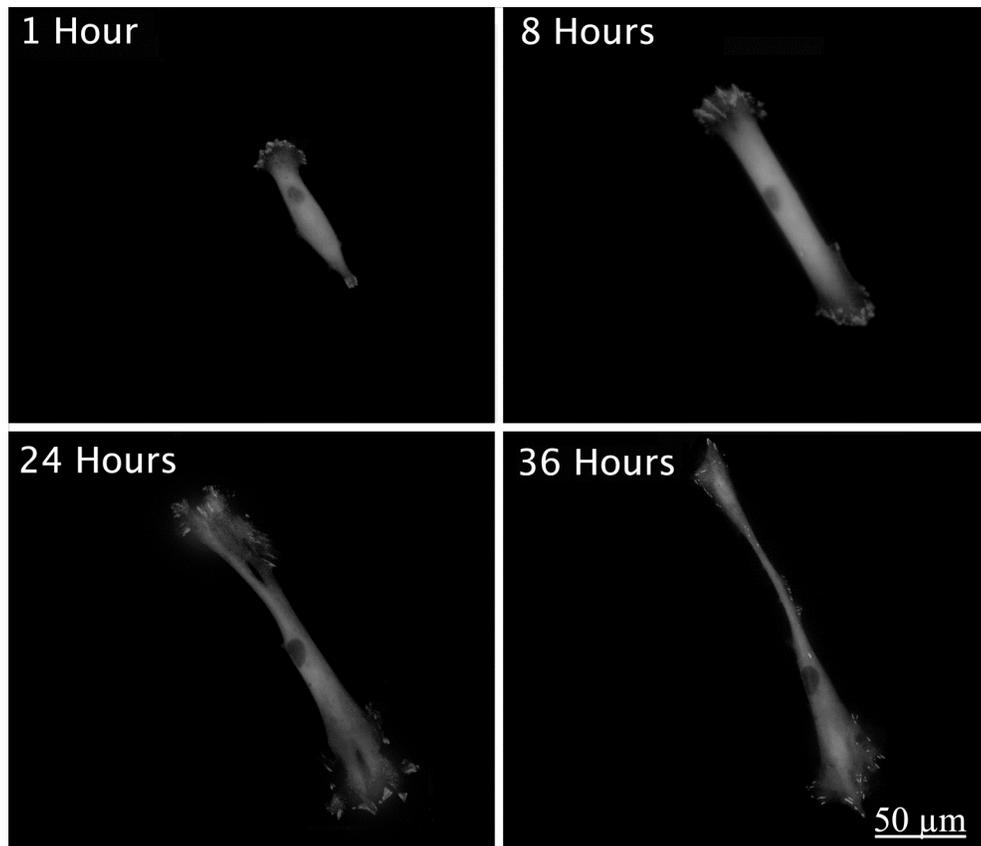
Fig. 6.9. YFP-vinculin analysis of the dynamics of adhesion formation in HOBs on 10 μm groove substrates. HOBs exhibited contact guidance 1 hour following cell seeding. FA formation occurred predominantly at the polar extremes of the cell and were aligned with or perpendicular to the groove orientation**.**

HOBs on 100 µm groove/ridge arrays did not demonstrate significant contact guidance or cellular alignment. HOBs formed large lamellipodia associated with peripheral FA formation following 8 hours of culture. Rapid cellular spreading was evident by 24 hours of culture, also accompanied by extensive mature adhesion formation. HOBs adopted a flattened and spread morphology following 36 hours of culture forming large peripheral focal and SMAs. Topographical influence over adhesion plaque orientation was not evident, however adhesion formation was common at the step interface (fig. 6.10). HOB live cell adhesion formation on planar control substrates is discussed in section 4.3.5.
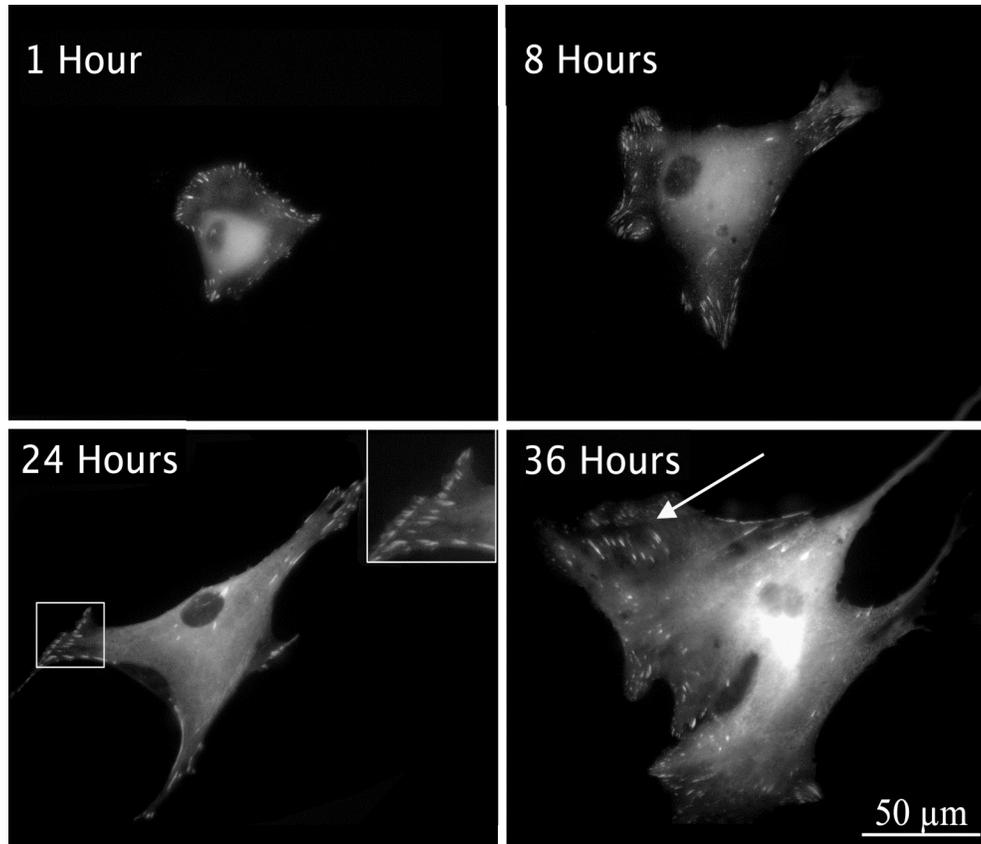
Fig. 6.10. YFP-vinculin analysis of the dynamics of adhesion formation in HOBs on 100 µm groove topography. Filopodia extensions present at t=1 hour were replaced with lamellipodia following 8 hours culture. Adhesions were not aligned by groove orientation but formed rows, which abutted at the topographical steps by 24 hours (boxed areas). Cellular spreading and adhesion formation increased with time up to 36 hours of culture. Arrow indicates underlying topographical step and abutting adhesions.

6.3.7. The Functional Response of STRO-1+ MSCs to Grooved Topographies

Analysis of microarray data revealed significant changes in canonical genetic pathways of STRO-1+ MSCs cultured on both nanogrooved substrates which were dependant on groove width (fig. 6.11A). These gene expression changes were linked to several well-defined canonical pathways.

Both 10 μm and 100 μm groove/ridge arrays significantly influenced genetic pathways linked to STRO-1+ MSC signalling pathways and cellular function (fig. 6.11A). Of most significance were relative changes in p38-MAPK signalling in cells cultured on experimental topographies. Here the expression of approximately 8% of genes involved in this pathway were modulated in STRO-1+ MSCs cultured on 10 μm groove/ridge arrays and approximately 10% of genes in this pathway modulated in STRO-1+ MSCs cultured on 100 μm groove/ridge arrays.

STRO-1+ MSCs cultured on 10 μm groove/ridge arrays also showed significant modulation of VEGF signalling. Here 7% of genes involved in this signalling pathway were modulated relative to cells cultured on planar controls. MSCs cultured on 100 μm grooves however, were associated with a significant changes in expression of the genes responsible for transcription of PDGF signalling pathway proteins. Here 9% of genes involved in this pathway were changed relative to planar control substrates. Both groove/ridge topographies were observed to modulate chemokine signalling in approximately 7% of the total genes involved with this pathway.
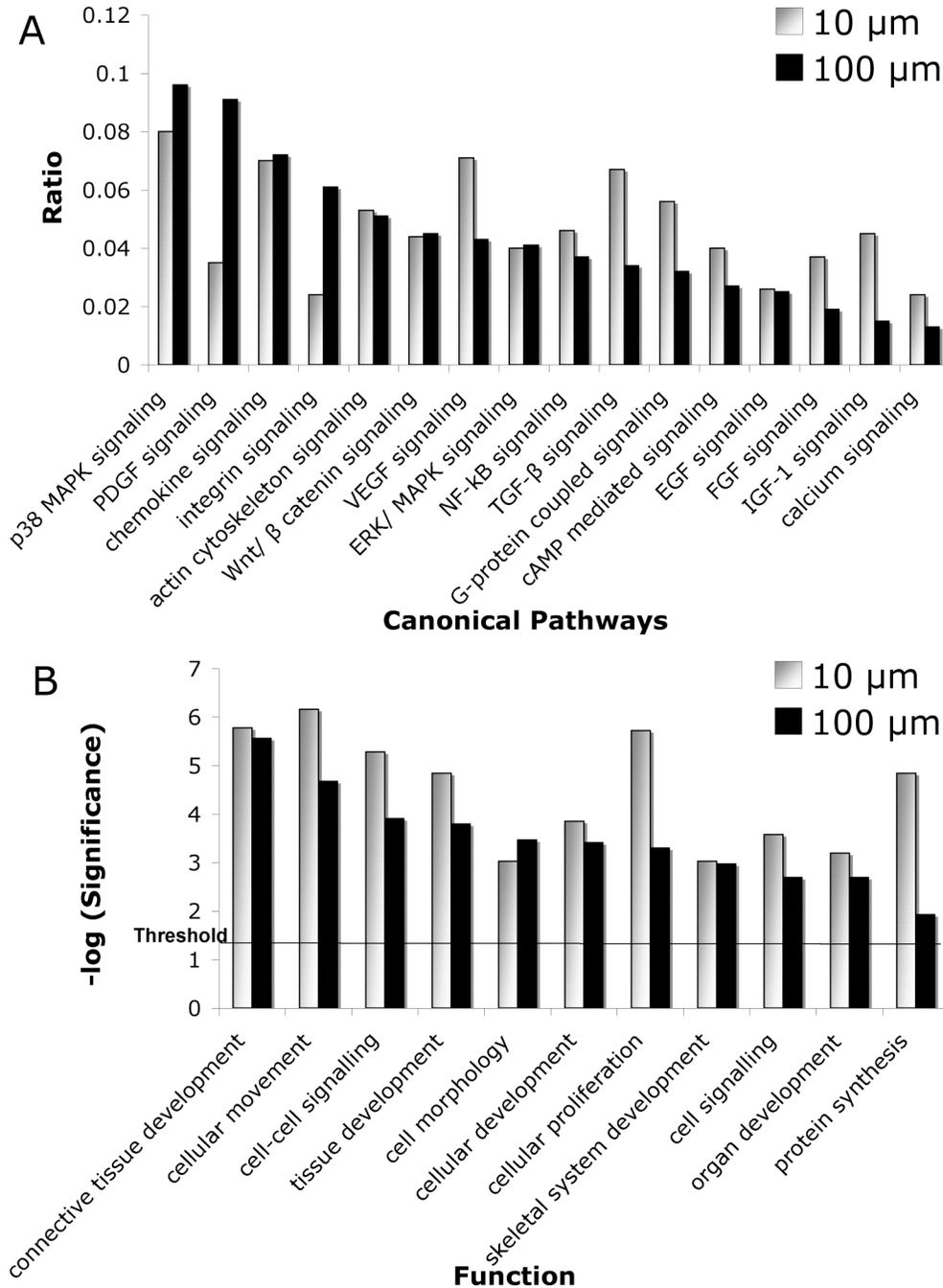
Fig. 6.11. Signalling pathway analysis of STRO-1+ MSCs on microgrooved substrates. (A) Canonical pathway analysis of STRO-1+ MSCs on experimental substrates identified numerous well-defined signalling pathways that were most affected in cells cultured on groove/ridge substrates. Significant changes in canonical p38-MAPK signalling were induced by both experimental topographies. Canonical VEGF signalling and PDGF signalling was significantly affected by 10 µm and 100 µm groove/ridge arrays respectively. (B) The Functional Analysis of a network of identified biological pathways that were most significant to the genes in the network affected by the groove/ridge topographies. MSCs cultured on both 10 and 100 µm groove arrays were associated with significant changes in cell function, in particular connective tissue development and cellular proliferation. A statistical threshold of significance p = 0.05 indicates the probability that the association between the genes in the dataset canonical pathway is explained by chance alone.

Modulations of canonical signalling pathways were subsequently correlated to large functional changes in STRO-1+ MSC populations. Connective tissue development in STRO-1+ MSCs cultured on both grooved substrates was significantly influenced. Trends indicate significant down-regulations in gene expression occurred in STRO-1+ MSCs cultured on 10 μm groove/ridge arrays and predominant genetic up-regulations occurred in STRO-1+ MSCs cultured on 100 μm groove/ridge arrays. Cellular movement and protein synthesis pathways were also significantly modified in STRO-1+ MSCs cultured on 10 μm groove/ridge topographies. Cell morphology was significantly affected on both substrates, correlating with the cytoskeletal changes noted in HOBs cultured on groove/ridge arrays. Furthermore, significant down-regulations in cell proliferation pathways were seen in cells cultured on the 10 μm groove/ridge arrays.

6.3.8. Wnt/β-Catenin Signalling

Canonical pathway analysis of STRO-1+ MSCs cultured on experimental substrates was correlated to significant modulation in genetic pathways linked to osteospecific function. An in depth examination of Wnt/β-catenin signalling revealed significant changes in expression of multiple genes involved in this pathway. 10 μm wide groove/ridge substrates induced down-regulations in 5% of the total genes that regulate the synthesis of proteins involved with Wnt/β-catenin signalling, including membrane associated Wnt and the cadherins. The transcription factors, sex determining region Y-like, high mobility group box (SOX) and retinoic acid receptor (RAR) of the nuclear compartment were also down-regulated on 10 μm groove/ridge arrays (fig. 6.12A).

An up-regulation in expression of 5% of total genes involved in Wnt/β-catenin signalling was observed in STRO-1+ MSCs cultured on 100 μm substrates. Up-regulations were noted in transforming growth factor beta receptor (TGFBR) coupled with minor up-regulations in cytoplasmic casein kinase 1 (CK1) and the G-protein Gαq/0. The majority of up-regulations were noted in genes encoding transcription factors, including SOX, RAR, CPB and Groucho (fig. 6.12B).
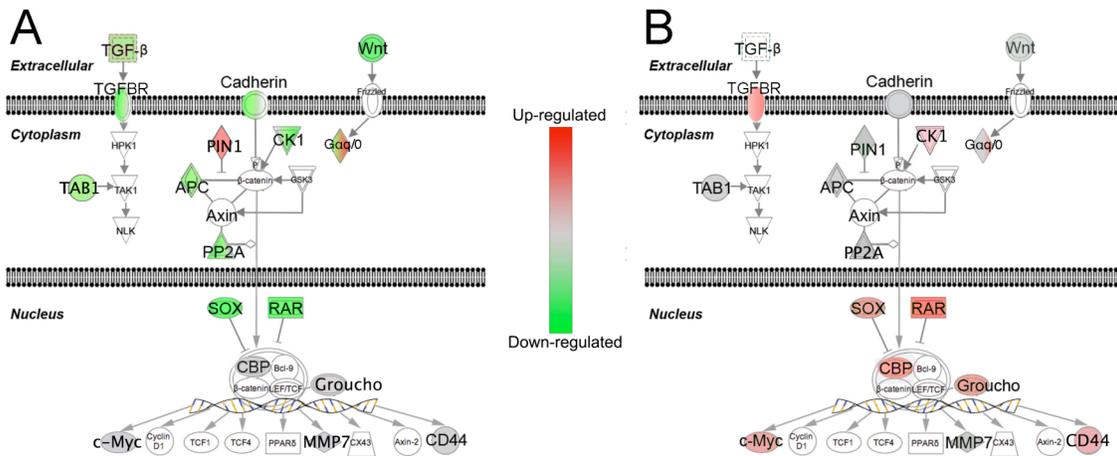
***Fig. 6.12. Modulation of Wnt/β-catenin signalling in STRO-1+* MSCs *on microgrooved substrates.* (A)** Significant numbers of down-regulations in genes associated with Wnt/β-catenin signalling were noted in STRO-1+ MSCs cultured on 10 µm groove/ride substrates. The majority of these being cytoplasmic associated. (B) The majority of affected genes in STRO-1+ cells on 100 µm groove/ride substrates were nucleus associated up-regulations. Red = Up-regulated, green = down-regulated, grey = no change, colourless = not tested.

6.3.9. Integrin Signalling

Analysis of transmembrane integrin signalling revealed contrasting modulation of STRO-1+ MSCs function when cultured on 10 µm or 100 µm groove/ridge arrays. Canonical pathway analysis revealed that 2% of genes involved in integrin signalling were significantly modulated in STRO-1+ MSCs cultured on 10 µm groove/ridge arrays (fig. 6.12A), down-regulations included genes coding for the adhesions plaque associated proteins α-integrin and α-actinin and the Rho proteins. Up-regulations were only noted in Genes responsible for FAK and receptor tyrosine kinase (RTK) synthesis (fig. 6.13A).

There were notable modulations in STRO-1+ MSCs cultured on 100 µm groove/ridge arrays. Here 6% of total genes involved in the integrin signalling pathway were changed relative to MSCs cultured on planar controls (fig. 6.12B). Up-regulation of adhesion associated α and ß-integrin expression and α-actinin were noted as well as a corresponding up-regulation in Rho expression (fig. 6.13B).
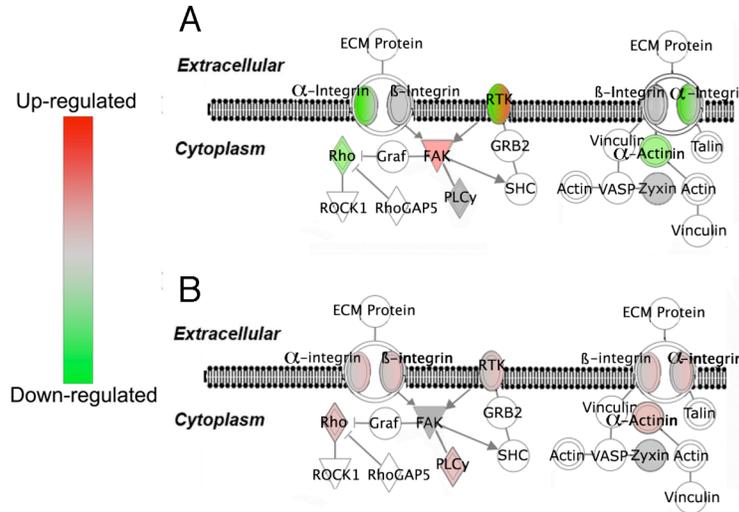
Fig. 6.13. Modulation of integrin signalling in STRO-1+ MSCs on microgrooved substrates. (A) Expression of genes involved in adhesion formation and cytoskeletal strengthening were down-regulated in MSCs cultured on 10 µm grooves. (B) Conversely, up-regulations in similar genes were noted in MSCs cultured on 100 µm grooves. Red = Up-regulated, green = down-regulated, grey = no change, colourless = not tested.

6.4. Discussion

Previous studies have concluded that the interplay between both groove depth and width modulate cellular response and induce contact guidance (Sutherland *et al.*, 2005). We hypothesised that topography with both nanoscale and microscale dimensions, which closely approximate the size of *in vivo* topographical features found in mineralised tissues, would better support osteoblast adhesion and STRO-1+ MSC function. The experimental methods outlined in this chapter utilise photolithography to create anisotropic topographies of grooves and ridges possessing microscale widths and a constant nanoscale depth.

In this chapter vinculin positive SMAs were again noted in primary human osteoblasts on nanogroove and planar substrates. Well-spread osteoblasts such as those found on control and 100 µm groove/ridge substrates contained many of these super-long adhesions. It is hypothesised that the mechanosensory function of FAs facilitates increased intracellular tension on these substrates and anisotropic protein recruitment at the adhesion plaque resulting in the generation of elongated adhesions.

S-phase HOBs cultured on planar control substrates formed predominantly mature FAs

and SMAs, indicative of a well-adhered, well-spread phenotype. HOBs cultured on experimental substrates, demonstrated varying degrees of contact guidance and adhesion formation dependent on groove width. Adhesion complex formation was most perturbed in HOBs cultured on 10 μm groove/ridge arrays. Here frequency of both FAs and SMAs was reduced. Immuno-SEM revealed adhesion formation of all subtypes to occur predominantly on the top of the ridge structures, a phenomenon previously reported by Teixeira *et al*. (Teixeira *et al*., 2003). Groove regions facilitated focal and SMA formation in the direction of groove propagation, aligning both osteoblasts and peripheral adhesions with groove orientation (fig. 6.6B).

Nanogrooves induced changes in osteoblast cytoskeletal organisation, cellular morphology and primarily, adhesion formation, which were correlated to significant alterations in MSC gene expression (fig. 6.11). Gene expression was seen to be modified extensively with increasing cellular alignment, which specifically induced a significant decrease in the expression of the transcription factors RAR and SOX (fig 6.12), both of which play important roles in a variety of developmental processes, particularly during organogenesis (Chen *et al*., 2008, Koopman *et al*., 2004). It appears that nanogroove substrates act as mediators of cellular function through both the regulation of adhesion formation and subsequent signalling pathways activated/deactivated by cellular elongation and alignment.

α-Actinin expression was increased in MSCs cultured on 100 μm and reduced in cells cultured on 10 μm groove/ridge topographies. α-Actinin is a major stress fibre associated protein that plays a key role in bundling and maintaining the stability of the stress fibres (Burridge *et al*., 1988, Byers *et al*., 1984). In addition to functioning as a organiser of stress fibres, α-Actinin also directly connects the stress fibres to FAs via the structural protein vinculin (Katoh *et al*., 2007). A down regulation in α-Actinin expression will result in deceased tension dependent adhesion growth, cellular tension and subsequent adhesion mediated cellular signalling as noted in cells cultured on 10 μm groove/ridge arrays. It appears that nanogroove substrates act as mediators of cellular function through both the regulation of adhesion formation and subsequent signalling pathways activated/ deactivated by cellular elongation.

It has been shown that contact guidance reduces the scaffolding of FAs through reduction of proteins such as RACK 1. RACK 1 helps stabilise FAs and hence the formation of large adhesions. If RACK 1 is over-expressed, contact guidance is reduced, if it is under-expressed, super-aligned cells are seen. Thus, it appears that small adhesions are a pre-requisite for contact guidance. This is sensible if physiological roles for contact guidance are considered, i.e. travel of fibroblasts to sites of wound healing. For this process, alignment and motility are required, which relies upon remodelling of small FXs (Dalby *et al*., 2008c).

6.4.1. Conclusion

Dynamic regulation of FA structure and the integrin-cytoskeleton associations modulating cellular function, plays a central role in balancing adhesive and migratory stimuli in the cell (Cohen *et al*., 2004). Nanogroove feature dimension influence the generation of adhesion complex subtypes in S-phase HOBs as well as modulating functional response in STRO-1+ MSC populations. Increasing groove width is associated with reduced contact guidance and increased adhesion formation and osteospecific function. Conversely decreased nanogroove widths were associated with increased contact guidance, reduced adhesion formation and reduction in osteospecific function. These findings are intriguing as they indicate a critical frequency of nanofeatures is necessary to modulate cellular adhesion and subsequent cellular function and may provide valuable insight for the fabrication of osteoinductive biomaterials with significant clinical implications.

CHAPTER VII

Discussion

7.1. General Introduction

The biological interactions occurring at the cell/implant interface are decisive for the clinical success of an implant. The topographical characteristics of an implant material are important mediators of cellular adhesion, spreading, migration of cells, and their differentiated cell functions (Diehl *et al*., 2005, Kudelska-Mazur *et al*., 2005, Lim *et al*., 2007, Loesberg *et al*., 2007). Cell cytocompatibility as a product of adhesion is mediated by transmembrane integrins at sites of adhesion; which bind to adsorbed ECM proteins secreted by the cell.

Topographical modification of an orthopaedic implant may be a viable method to guide tissue integration and has been shown *in vitro* to dramatically influence osseogenesis, inhibit bone resorption (Marchisio *et al*., 2005, Santiago *et al*., 2005) and regulate cell adhesion (Dalby *et al*., 2003b). Non-adhesive surface modification (Pearce *et al*., 2008) is of great potential benefit in the design of orthopaedic implants, in particular where internal fixation devices have been reported to induce latent pain (Brown *et al*., 2001) and complications warranting device removal, i.e. infection (Islamoglu *et al*., 2002) or excessive migration (Baums *et al*., 2006). Osteoblast adhesion and bony tissue mineralisation can, for example, complicate the removal of plating systems, increasing removal torque and predisposing screw damage and bone refracture (Jago & Hindley, 1998, Sanderson *et al*., 1992)

Prosthetic joint articulation such as that occurring at the acetabular cup – femoral head interface, relies on the high durability and low friction properties of the internal components to prevent wear particle formation, aseptic loosening and subsequent prosthesis failure (Grobler *et al*., 2005, Kim *et al*., 2005b). Cellular migration and adhesion within this compartment can result in fibrous tissue formation and mineralisation initialising inflammation and immunologic response (Konttinen *et al*., 2005), ultimately resulting in pain and a reduction in the degree of available motion. Thus, anti-adhesive substrates (e.g. Square and Hex nanopatterned materials) could be useful in the fabrication of implantable devices that depend on minimal cellular adhesion. Conversely, materials that promote osteoblast specific adhesion may enhance functional differentiation (Kalajzic *et al*., 2005) resulting in the neogenesis of mineralised matrix, bony tissue formation and deposition. Because polymeric bone cements do not promote a

biological secondary fixation, topographically induced tissue neogenesis such as that observed on nanocrater and nanoisland substrates greatly aids in implant stability and integration, extremely desirable in joint replacement strategies to prevent aseptic loosening and device failure.

Thus the manipulation of a substrate's topography to affect its adhesive potential and the ability of cells to adhere at the cell-substrate interface may be viewed as an approach to direct and organise the adhesion and differentiation of migrating cells in bone repair.

The importance of topographical modification in regulating cell-biomaterial interactions and subsequent signal transduction processes has been shown experimentally throughout this thesis. Although previous studies have shown nanotopographical structures to affect the expression level of adhesion components like integrin, paxillin, and phosphorylated FAK in the cell, (Heydarkhan-Hagvall *et al.*, 2007, Karuri *et al.*, 2006) the regulation mechanisms of these processes still remain undiscovered. Biophysical signals arising at the cell/substratum interface are thought to regulate cell function by mechanotransductive mechanisms. One hypothesis is that integrins not only induce intracellular signalling but also function as force dependant mechanotransducers, acting via the actin cytoskeleton to translate tension applied at the tissue level to changes in cellular function.

In order to elucidate the effects of topographical cues on primary human osteoblast populations, biologically relevant nanoscale substrates were used to examine cell-substratum adhesion in osteoblasts and the functional response of STRO-1+ MSCs. Here, it has been shown that topography with both nanoscale and microscale dimensions, which closely approximate the size of *in vivo* topographical features, better supports osteoblast adhesion and osteospecific STRO-1+ MSC function.

To ensure that only topographical effects are recorded, shims were used to emboss the designs into a substrate with stiffness comparable with that of trabecular bone, pMMA was chosen for its physical characteristics as well as chemical properties, an amorphous stiff polymer with an elastic modulus of approximately 3 GPa. No satisfactory conclusions have been reached regarding the elastic properties of bone tissue, however current literature places the elastic modulus of trabecular bone between 10 and 20 GPa, depending on the experimental procedure (Yamashita *et al.*, 2002).

7.2. Subsequent Protocol Development

A novel technique has been developed in this thesis for the duel immunofluorescent detection of vinculin and nuclear localised BrdU to identify sites of FA and S-phase cells respectively. This technique was both accurate and rapid to perform and, when coupled with the meticulous image analysis technique described in section 3.4, allowed sensitive quantification of adhesion formation.

The rationale behind selective S-phase adhesion quantification arises from findings that S-phase cells undergo extreme flattening (Cross & ap Gwynn, 1987, Hunter *et al*., 1995). Non-S-phase cells display a more spherical morphology with less contact area with the substrate surface compared to S-phase cells (Meredith *et al*., 2004). In addition there is little sample variation with respect to adhesion density measurements in S-phase cells. Thus when measuring S-phase cell adhesion, changes observed are directly linked to the material surface properties and culture environment, rather than the cell cycle phase and, in the case of this study, are directly related to topography.

The inhibitory effect of the presence of the nucleotide analogue BrdU, after its binding to the DNA, arrests the cell within S-phase. It has been suggested that during this cell cycle arrest the nuclear cycle continues to proceed (Owen *et al*., 2002). For this reason the total incubation time in BrdU was kept to three hours before immediate fixing in formaldehyde.

The ability to immunolabel for two separate antigens is reliant on being able to discern visually between the structures being labeled or between the two labels themselves. The technique described herein is only possible due to the distinct morphological characteristics of the nucleus and the FA. The method is extremely fast compared to the previous methods (Owen *et al*., 2002) but does have the disadvantage that it cannot visualise FAs below the nucleus, or in very thick (rounded) cell types.

An interesting future development could be the use of proliferating cell nuclear antigen (PCNA). PCNA may offer a reliable alternative to BrdU nuclear detection of S-phase cells. PCNA is detectable by immunocytochemically during late G1- and S-phase and can be used as a naturally occurring marker for cell proliferation (Hall & Woods, 1990). PCNA is detectable only in the nucleus (Lorz *et al*., 1994), thus immunolabelling of such a naturally occurring nuclear constituent may negate the need for invasive toxic

substances such as tritated thymidine and BrdU for cell cycle phase determination.

SEM studies utilising duel vinculin and S-phase nuclei labelling theoretically improve on immunofluorescent methods by allowing regulation of depth of signal formation, increasing the spatial resolution available and facilitating the simultaneous visualisation of topography, whole cells and adhesion sites (fig. 7.1). To investigate the efficiency of such a technique the immunofluorescent protocol was adapted for SEM analysis of adhesion sites in S-phase cells.
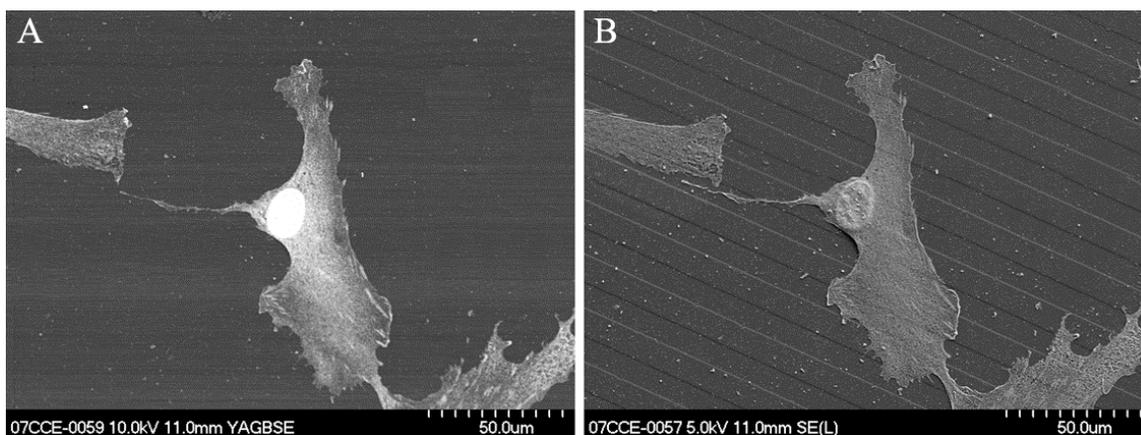
Fig. 7.1. SEM analysis of adhesion formation in S-phase HOBS on 10 μm groove/ridge nanoarrays (Biggs et al., 2008). (A) BSE mode was used for the visualisation of adhesion sites and S-phase nuclei in HOBs on 10 μm grooved topographies. (B) SE mode allowed visualisation of topographical structure.

Although this technique was not used for quantitative or qualitative purposes throughout this thesis, it has since been shown to be as accurate a technique for adhesion quantification in a synchronised population of cells as immunofluorescent protocols and allows high magnification analysis of adhesion nanofeature interactions. If time was allowing, this would thus be a natural evolution for this study.

To allow S-phase nuclei labelling in cells fixed for SEM the diameter of the colloid probe was reduced from 4 nm to 1.4 nm. Previously problems with signal intensity have arisen with the use of colloids < 2 nm in diameter. Owen *et al*. hypothesise that failure of these colloids is due to impaired silver enhancement, as the colloid becomes enveloped by the anti-vinculin IgG, effectively adsorbing a layer of protein that resists silver reduction at the colloid surface (Owen *et al*., 2001). Here the problem of small colloid probe

envelopment was overcome by the use of a three level detection system where the tertiary gold colloid was conjugated to a streptavidin molecule. Streptavidin is smaller than a whole IgG molecule and does not aggregate (Laitinen *et al.*, 2006), allowing penetration of the nucleus to reach antigens inaccessible to larger gold probes.

A combination of a soluble silver compound and a reducing agent induces the deposition of silver onto the gold probe. This process, termed autometallography enhancement (Christensen *et al.*, 1992, Weipoltshammer *et al.*, 2000), permits the user to benefit from the low steric hindrance of small colloidal gold markers and the increased sample penetration, whilst still being able to visualise the markers at low magnification. The 1.4 nm gold colloid retains rapid nuclear penetration and high label efficiency (Richards *et al.*, 2001a) yet is available following antigen binding for subsequent enlargement via silver deposition.

7.3. Nanotopography Influences Osteoblast Adhesion Formation

S-phase HOBs cultured on all experimental substrates demonstrated a modulation in adhesion formation. Recent studies have shown that integrin-mediated adhesions are not all alike and different molecular and cellular variants may be distinguished. Because adhesion formation is a dynamic and complex process, valuable information was generated through subgrouping these cellular adhesions into three forms, representing different stages of cell-substratum interaction and also possibly differential cellular function.

HOBs cultured on planar control substrates formed predominantly mature FAs and SMAs, indicative of a well-adhered, well-spread phenotype. It can be hypothesised that the mechanosensory function of FAs facilitates increased intracellular tension and anisotropic protein recruitment at the adhesion plaque resulting in the generation of elongated adhesions. These SMAs although morphologically fibrillar, are distinct from the fibronectin organising fibrillar adhesion (fig. 7.2) and retain the molecular composition of classic FAs, such as proteins associated with transductive pathways including vinculin and FAK (Cukierman *et al.*, 2001, Zamir *et al.*, 2000). Indeed SMA formation has be correlated to an increase in the association of vinculin and talin to the

adhesion plaque which has been shown to activate adhesion elongation and interfere with vinculin turn-over, ultimately leading to hypertrophy of the adhesion (Cohen *et al.*, 2005). It is probable that the generation of these SMAs and the conservation of FA associated proteins, most notably FAK, induces increased up-regulation in many major survival and osteoinductive signalling pathways (Kim *et al.*, 2007, Leucht *et al.*, 2007, Liu *et al.*, 2008a, Liu *et al.*, 2008b).

The work outlined in this thesis identified HOBs cultured on nanopit substrates to be associated with an increase in FX formation coupled with a disruption of mature adhesion formation. HOBs formed significantly more FXs then cells cultured on planar control substrates. FXs are nascent integrin-mediated adhesions formed during early lamellipodial activity at the cell periphery and the leading edge (Zaidel-Bar *et al.*, 2004). These only transform into FAs proper following integrin clustering coupled with increased intracellular tension. These complexes play a role in motility, providing short lived anchoring sites to the ECM, allowing the contractile actomyosin machinery to pull the cell body and trailing edge forward (Nicolas *et al.*, 2004, Zamir *et al.*, 2000). An increase in FX formation is strongly indicative of a decrease in total cellular adhesion by disruption of FA maturation.

That FAs were predominantly reduced in length indicates an increase in dynamic FX turnover and cellular motility. Once formed, FXs either turnover or undergo maturation. The molecular basis of this process has received a great deal of attention over the last several years because of its central role in cell migration. In particular, locally regulated FAK appears to be a key trigger for adhesion turnover as will be discussed in section 7.5.

Nanopit type substrates have consistently been shown to reduce cellular adhesion *in vitro* (Biggs *et al.*, 2006, Martines *et al.*, 2004), although a decrease in protein adsorption may be a regulatory factor and has been shown to influence cellular migration through adhesion modulation (Xia *et al.*, 2008).

SMA formation was significantly reduced in S-phase HOBs on nanopit substrates, shown by SEM to be caused by direct nanopit disruption of adhesion formation. It can be postulated that pits of this scale could have an effect on the physical properties of the substrate, affecting surface free energy and hence potential surface wettability. This has been demonstrated to occur on nanofabricated substrates, whereby ordered

nanotopography can induce a state of 'superhydrophobicity' on a material surface (Martines *et al.*, 2005). This in turn results in decreased protein adsorption (Hornekaer *et al.*, 2005, Keselowsky *et al.*, 2004), as well as conformational changes in integrin specific ECM protein binding domains (Keselowsky *et al.*, 2003).
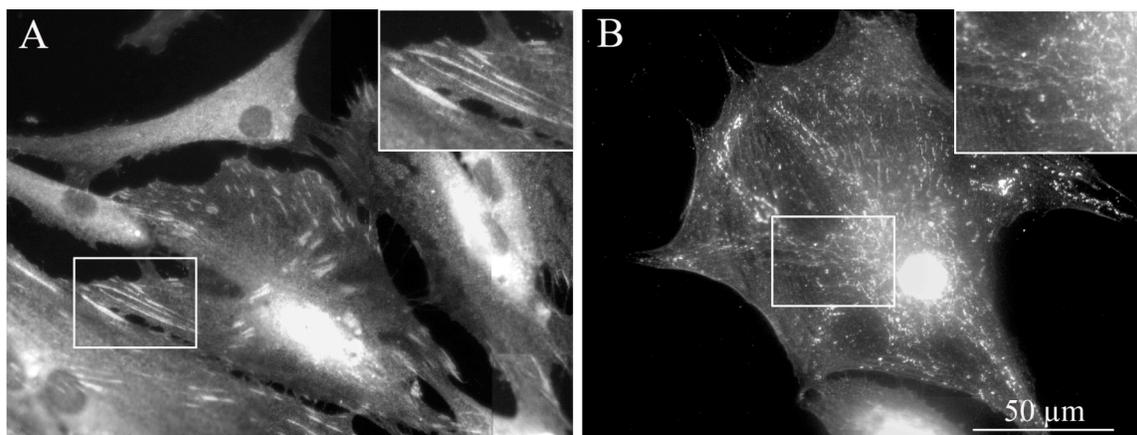
Fig 7.2. Super-mature adhesions are distinct from fibrillar adhesions (Biggs unpublished data). FA elongation is either associated with (A) SMA formation (vinculin label) or (B) fibrillar adhesion formation (tensin label). These structures are morphologically and biochemically distinct and play individual roles in cellular adhesion and tissue formation respectively.

It is hypothesised here that nanopits reduce SMA formation by directly inhibiting integrin clustering, which occurs in FA at the range of 5–200 nm (Arnold *et al.*, 2004, Eisenbarth *et al.*, 2006). Thus it seems conceivable that nanopit dimensions (120 nm diameter) disrupt the elongation of FXs into mature FAs by inhibiting protein recruitment at the adhesion site. Recent findings by Cavalacanti-Adam *et al.* indicate that indeed defects of 100 nm do inhibit integrin clustering, adhesion formation and cellular spreading (Cavalcanti-Adam *et al.*, 2007). Furthermore, Dalby *et al.* used immuno-transmission electron microscopy (TEM) of vinculin to show that adhesions could not form directly over the square arrays of nanopits investigated in this thesis (Dalby *et al.*, 2006a).

Conversely, polymer demixed nanocraters and nanoislands were shown experimentally to significantly disrupt the formation of FXs in S-phase HOBs and also reduce the formation of SMAs. It can be hypothesised that polymer demixed features reduce adhesion number but increase cell spreading and osteospecific function by providing both disruptive and adherent features. It can be reasoned that in this case, whilst an increase in SMAs was not

observed, topographically induced cessation of cellular migration through disruption of FXs produces a similar result.

It has been reported that the dorsal (and also likely the ventral) surface of the FA has a corrugated dorsal surface formed by filamentous structures spaced by an average of 127 nm and protruding by 10 to 40 nm over the interadjacent areas (Franz & Muller, 2005). It may be that these dimensions place a limit on the minimum feature size which may perturb adhesion formation by direct means. Polymer demixed topographies were shown to exhibit a bimodal feature distribution. It is feasible that the large lateral dimensions of the polymer demixed islands and lacuni features are perceived by cells as essentially planar and therefore favorable for adhesion and it is in fact the stimuli from the second phase smaller features that influence cellular adhesion.

Focal and SMA formation in HOBs cultured on polymer demixed topographies was comparable to cells cultured on planar control substrates, indicating the predominant effects of polymer demixed topographies to be on FX formation. Although it was unascertained whether polymer demixed topographies influence protein adsorption, a similar study by Lim *et al* has shown that substrates produced by polymer demixing affected surface wettability dependant on nanoisland height. The smaller the nanoislands, the smaller the water contact angle and accordingly, the more cellular adhesion observed (Lim *et al.*, 2005b). It could be that this reduction in surface wettability was responsible for the minor reductions in adhesion formation observed in HOBs on polymer demixed substrates and that the polymer demixed features themselves act as adhesive stimuli, while the trapped air between the features is responsible for the reduction in surface wettability, protein adsorption and HOB adhesion. Indeed nanotopographical substrates with true pillar structures which increase the potential for trapped air have been shown to dramatically reduce cellular adhesion (Kim *et al.*, 2005a).

HOBs cultured on nanogrooved substrates, demonstrated varying degrees of contact guidance and adhesion formation dependent on groove width. Adhesion complex formation was most perturbed in HOBs cultured on 10 μm groove/ridge arrays. Here frequency of both FAs and SMAs was reduced. Immuno-SEM revealed adhesion formation of all subtypes to occur predominantly on the top of the ridge structures, a phenomenon previously reported by Teixeira *et al.* (Teixeira *et al.*, 2003) Adhesion to the

ridge surface was prevalent in HOBs cultured on 10 groove/ridge arrays but was absent in HOBs on 100 µm groove/ridge topographies, as increased inter-ridge area facilitated increased osteoblast spreading on both ridge and groove areas.

FA alignment also occurred in the absence of cellular alignment, a phenomenon previously observed only on microgroove topographies (Richards *et al*., 1997). It has been suggested that the geometrical dimensions of the FA plaque facilitate its formation and forced alignment within the microscale topographical ridges (Ohara & Buck, 1979). FAs are shown to decrease in width from 2 µm at the peripheral terminal to about 0.5 µm at the stress-fibre-associated end (Franz & Muller, 2005) which maybe forces adhesions to form within the grooves and accounts for the adhesion alignment noted on 10 µm groove/ridge arrays.

Mineralised tissues can be viewed as a dynamic system of self-regulating nanostructures containing grooves and ridges imparted by the collagen and mineral constituents. Previous studies have concluded that the interplay between both groove depth and width modulate cellular response and induce contact guidance (Sutherland *et al*., 2005). Here it is hypothesised that topography with both nanoscale and microscale dimensions, which closely approximate the size of *in vivo* topographical features are capable of modifying cellular adhesion and cellular morphology, which in turn alters cellular function.

Groove regions facilitated focal and SMA formation in the direction of groove propagation, aligning both osteoblasts and peripheral adhesions with groove orientation. FAs show highly anisotropic growth dynamics in which the additional proteins are mostly accumulated in the direction of the force exerted by the cytoskeleton on the FAs (Besser & Safran, 2006). Cell and cytoskeletal alignment has generally been found to be more pronounced on patterns with ridge widths between 1 and 5 µm than on grooves and ridges with larger lateral dimensions (Karuri *et al*., 2004, Matsuzaka *et al*., 2000, Teixeira *et al*., 2003) such as those used in this study. However, this may be dependant on cell type and size and whilst most studies of contact guidance have studies smaller fibroblasts, here larger osteoblasts and MSCs were used and the 10 µm grooves did efficiently align the cells. The 100 µm grooves, however, may be better described as step cues, where a cell will normally only contact one edge.

7.4. Nanotopography Influences Osteoblast Morphology

YFP-vinculin experiments indicate that adhesion dependant cellular spreading and hence intracellular generated tensional forces are perturbed on nanopit topographies compared to cells on planar control and polymer demixed substrates. Here cellular spreading seemed to be dependant on intracellular tension. It is hypothesised that intracellular tension gradually builds within the stress fibres by the action of myosin II and adhesion strengthening by integrin clustering. Increased tension results in a rapid expansion of the cellular periphery mediated by contractile forces of the peripheral stress fibres and the spontaneous generation of intracellular-voids, which are slowly replaced by the flow of cytoplasm. This modality of cellular spreading is inhibited on the nanopit arrays as both adhesion and subsequent intracellular tension is disrupted.

Early cellular spreading coupled with mature adhesion formation noted in HOBs cultured on both nanocrater and nanoisland topographies has been shown to prevent adhesion dependant apoptosis (Frisch *et al*., 1996). This specialised programmed cell death termed anoikis involves cellular detachment from the substrate or inhibition of adhesion formation. Recent studies have shown that changes in cell shape (Flusberg *et al*., 2001) or the presence of unoccupied integrins (Stupack *et al*., 2001) can induce anoikis. The established role of integrins in regulating survival signals (Frisch & Ruoslahti, 1997, Meerovitch *et al*., 2003, Zhang *et al*., 1995) and the role of FA-associated proteins in anoikis resistance (Attwell *et al*., 2000, Xia *et al*., 2004) suggest that mature adhesion formation and cellular spreading events are important for cell survival.

Early cell spreading may also be an indicator of further expression of osteoblast phenotype. A study by Kudelska-Mazur *et al* demonstrated a correlation between increased adhesion formation, cell spreading and osteospecific function. In particular osteocalcin, ALP and collagen synthesis were shown to be elevated in well-spread cells (Kudelska-Mazur *et al*., 2005), again alluding to the osteogenic potential of nanocrater and nanoisland substrates as modulators of adhesion formation and cellular spreading.

Cytoskeletal elements were shown to be similar in HOBs cultured on planar control substrates and in HOBs cultured on both polymer demixed topographies, while the cytoskeleton remained unorganised on nanopit substrates. The interactions between FAs and the actin network is complex, due to the fact that actin network in most migrating

cells is not stationary with respect to the substrate, but moves away from the leading edge of the cell in a process known as retrograde flow (Cramer, 1997, Harris, 1994), thought to be a consequence of the pressure of actin assembly against the membrane and contractile forces in the actin network (Suter & Forscher, 2000). It is this flow that is reportedly responsible for the ruffling of the leading edge immediately prior to adhesion formation (Alexandrova *et al*., 2008). This dynamic mobility of the actin network and increased retrograde flow may account for the lack of microfilament organisation observed in HOBs on nanopit arrays.

The phenomenon of cellular contact guidance on grooved topography has been well documented in literature (den Braber *et al*., 1998, Karuri *et al*., 2004, Lenhert *et al*., 2005). Nanoscale grooves with dimensions similar to those found in tissue *in vivo* have been shown to cause contact guidance and alignment in numerous studies involving human cell types, including corneal epithelial cells (Teixeira *et al*., 2003), fibroblasts (Dalby *et al*., 2003c) and osteoblasts (Lenhert *et al*., 2005). Andersson *et al* reported on the evidence that cell alignment and elongation increase with groove depth rather than groove width (Andersson *et al*., 2003). Jayaraman *et al* have reported on the importance of microtexture in dental implant osseointegration in which grooved surfaces permitted attachment of more cells than a smooth surface and that cell shape and cytoskeleton alignment all indicated increased cellular adhesion (Jayaraman *et al*., 2004). Both cellular alignment and adhesion can viewed as desirable elicited responses for successful implant integration, however this is implant specific and one may take preference over the other. Narrow grooved substrates may enhance the migration and alignment of fibroblasts during the wound healing response, leading to enhanced ECM organisation. Conversely increased groove width may induce enhanced cellular adhesion and osteospecific function, desirable features of orthopaedic devices. Furthermore, it could be postulated that if stem cells take on the bipolar morphology imposed by a high degree of contact guidance it is likely they will act as fibroblasts, whereas if they are allowed to take on a well-spread, polygonal morphology, they may develop into osteoblasts.

Loesberg *et al* hypothesised that a cellular ''point break'' is reached, with decreasing nanogroove width, where cells no longer display contact guidance (Loesberg *et al*., 2007) this cut off point was found to be 100 nm in width and 35 nm in depth. A study by Hu *et*

al also on ~300 nm deep grooves concluded that the efficiency of smooth muscle cell alignment and elongation increases monotonically with the decrease of groove pitch, indicating that nanoscale structures produce cellular alignment and elongation by a different modality than microscale grooves (Hu *et al.*, 2005). It may be that on micron sized grooves contact guidance is predominantly mechanical – i.e. the cell is forced along a topographical edge via a containment effect. On nanometric grooves alignment may be more biological, occurring as a consequence of ECM alignment followed by adhesion alignment which subsequently direct the cell body/nucleus to align.

As well as actin cytoskeletal elements, microtubules were also affected in HOBs cultured on experimental substrates. Studies indicate that motile cells possess two distinct microtubule networks. The majority of their microtubules comprise a highly dynamic subset, whose distal plus ends are positioned randomly throughout the cell periphery (Salaycik *et al.*, 2005). By contrast, a more stable (less dynamic) subset is typically arrayed between the nucleus and its leading edge (Gundersen & Bulinski, 1988). Tubulin subunits become stabilised by acetylation along the entire length of the microtubule and the acetylation state of the stable microtubules may imbue them with special functional properties (Westermann & Weber, 2003). For instance, this increased stability has been shown to increase the FA size *in vitro* (Tran *et al.*, 2007). HOBs observed to possess a well defined microtubule network, i.e. on planar control, polymer demixed, and 100 μm wide groove/ridge arrays were also associated with mature adhesion formation, and a well organised stress fibre network. It can be reasoned that this well developed microtubule network is contributing to the stability of the adhesion sites and facilitating SMA generation.

Nanotopographical mediated changes in cytoskeletal morphology have led to the question of whether topography directly nanoimprints onto the cell structure and somehow influences the propagation of signal transduction. Evidence presented from SEM, TEM and fluorescent microscopy detection show that the arrangements of cytoskeletal components are consistent with the underlying nanotopography and this has implication for cytoskeleton related signalling (Wood *et al.*, 2008). Time-lapse video studies of cells moving from areas bearing nanotopography to flat areas and vice versa suggests that the nanoimprinting takes 1–6 hours to manifest in the cytoskeleton (Curtis *et al.*, 2006).

Studies have further shown that this nanoimprinting is driven by the β_3 integrin subunit rather than the β_1 subunit (Wood *et al.*, 2007). This nanoimprinting of cells may be a novel type of cell signalling so far neglected and may contribute to direct mechanosignalling. Here modification of cytoskeletal elements in tensegrity units and their interactions with the nucleus, may cause organisational changes within the interphase nucleus (Dalby *et al.*, 2007c, Ingber, 2006). Nanoimprinting may also modulate indirect signalling by influencing cytoskeleton related signalling molecules e.g. extracellular signal-regulated kinases (ERK), FAK and MAPK. Examples of cytoskeletal nanoimprinting of HOBs on grooves are shown in fig 7.3.
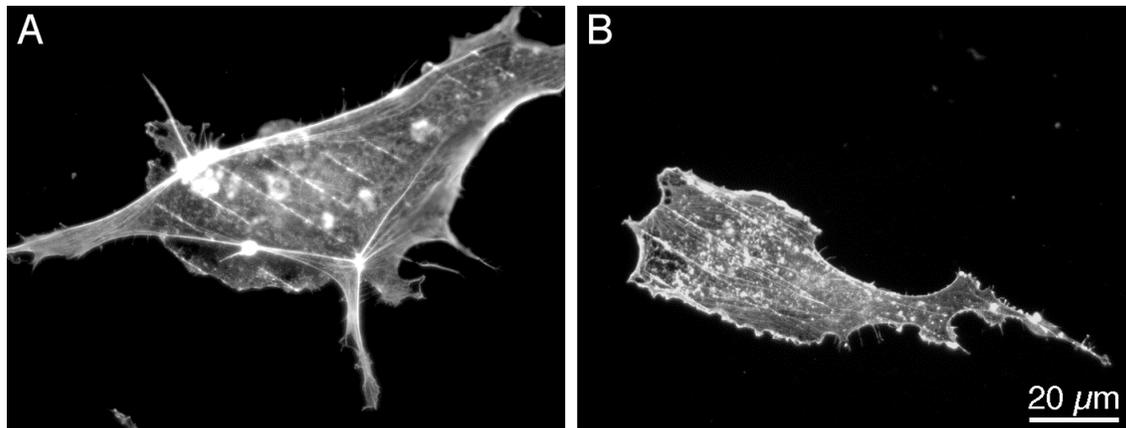
Fig 7.3. Nanoimprinting of grooves onto the cell cytoskeleton (Biggs unpublished data). (A,B) The nanogroove topography is visibly reproduced within the filaments of the actin cytoskeleton in endothelial cells.

7.5. Nanotopography Influences MSC Function

The major event that triggers osteogenesis is the transition of MSCs into bone-forming, differentiated osteoblast cells and is controlled by sequential activation of diverse transcription factors that regulate the expression of specific genes. In addition to their adhesive functions, integrins mediate bi-directional signalling between the ECM and the cell interior and are crucial in cell survival and differentiation (Attwell *et al.*, 2000, Grigoriou *et al.*, 2005, Stupack *et al.*, 2001). Although integrin molecules provide a platform for intracellular signalling, they do not have intrinsic enzymatic activities in their cytoplasmic domains (Liu *et al.*, 2000). Therefore, downstream signalling is mediated by non-receptor tyrosine kinases (Schaller *et al.*, 1992). Interestingly integrin

receptors have been shown *in vitro* to be spatially associated with the STRO-1 membrane receptor (Gronthos *et al.*, 2001), which perhaps indicates another possible mode of integrin mediated differentiation in MSC populations, as undifferentiated cells no longer express the STRO-1 surface antigen.

β_1 integrins have been shown to be the predominant adhesion receptor subfamily utilised by stromal precursor cells for adhesion formation *in vitro* although, as has been discussed, β_2 integrins have been implicated in mediating cellular attachment to nanostructured substrates (Wood *et al.*, 2008) and it has been suggested they are important in the differentiation of stromal precursor cells into functional osteoblast-like cells (Gronthos *et al.*, 2001). Only STRO-1 MSCs cultured on nanopit topographies were shown to undergo a down-regulation in β-integrin expression, again indicative of both reduced cell adhesion and osteospecific function. Integrin mediated attachment activates FAK autophosphorylation, which provides a binding site for the Src family kinase (Src) (Chan *et al.*, 1994) and promotes FAK binding to a number of signalling molecules (Klemke *et al.*, 1997) including talin and paxillin (Chen *et al.*, 1995), which link the integrin–FAK signalling complex to the actin cytoskeleton (Kim *et al.*, 2007).

FAK has been shown in previous studies to be an important mediator of adhesion turnover and is well established as a regulator of the actin cytoskeleton and cell motility, particularly in invasive metastasis (Behmoaram *et al.*, 2008). Indeed, FAK-null cells assemble large and stable adhesion complexes leading to a reduction in cell migration (Sieg *et al.*, 1999). Curiously although HOBs cultured on nanopit topographies were associated with small FX formation, STRO-1+ MSCs cultured on nanopit topographies were associated with a decrease in FAK synthesis. This may be indicative of a general reduction in FX turnover, suggesting that perhaps cellular motility is not increased on this topography as previously speculated, rather HOBs adopt an elongated morphology in response to FA perturbation. In agreement to this, it is has been seen in RACK1 knockout cells, where large FAs cannot be formed, that elongated cell morphologies spontaneously form on planar materials (Dalby *et al.*, 2008c).

Furthermore, a study by Leucht *et al* demonstrated that a down-regulation of FAK expression reduces the cellular response to physical stimuli. It was noted that bone marrow cells in which FAK activity was knocked-down no longer up-regulated

skeletogenic genes, collagen fibrils remained disorganised and the mechanically-induced osteogenic response was lost (Leucht *et al*., 2007).

Conversely, MSCs cultured on 10 μm groove/ridge arrays were associated with an increase in FAK expression. Here cells also adopted a polarised morphology and increased total FX formation, suggesting a true increase in FX turnover. Indeed, many previous studies have shown grooved topographies to be associated with an increase in cell motility (Kaiser *et al*., 2006). As would be expected in cells that form stable and even SMAs, FAK expression was not modulated on the 100 μm groove topographies or on both polymer demixed substrates – topographies shown to reduce FX turnover.

Force application to bound integrins promotes FA assembly by activating the small guanosine triphosphatase Rho and stimulating its downstream targets mammalian diaphanous protein 1 (mDia1) and Rho-associated kinase (ROCK) which interplay to promote actin filament polymerisation, induce cytoskeletal tension and regulate ECM organisation (Bhadriraju *et al*., 2007, Yoneda *et al*., 2007). Studies indicate that FAK can negatively regulate Rho activity, which was up-regulated in STRO-1+ MSCs cultured on nanopit substrates. This can probably be explained by an increase in lamellipodia formation and has been shown previously that RhoA activity is decreased on nanostructured topographies relative to planar substrates (Hu *et al*., 2008).

Conversely, inhibition of Rho activity reduces cell spreading and FA organisation and has been shown to promote the formation of unusual arborised cell projections (Anastasiadis *et al*., 2000, Noren *et al*., 2000). STRO-1+ MSCs cultured on 10 μm nanogroove topographies demonstrated decreased Rho expression coupled with this reduction in FA formation and cell spreading, typical in cells undergoing increased cell migration, when FXs and lamellipodia are more prominent than FAs and stress fibres (Bershadsky *et al*., 2003). Rho expression was increased on 100 μm groove/ridge topographies and both polymer demixed topographies correlating to an increase in FA formation, stress fibre formation and cell spreading.

As well as integrin mediated signalling, complex signalling pathways of osteospecific interest were modulated by experimental topographies. The canonical Wnt/β-catenin signalling pathway has recently been found to play an essential role in osteogenesis, bone development and postnatal maintenance of bone mass (Day *et al*., 2005, Hill *et al*., 2005,

Krishnan *et al*., 2006). Wnts are secreted growth factors, of which there are 19 Wnt family proteins in total. Canonical Wnts transduce their signals through intracellular beta-catenin. Importantly, Wnt signalling has previously been shown to be regulated by cellular adhesion and to control the ubiquitination and stability of the FA proteins (Deng *et al*., 2008, Piters *et al*., 2008).

The modulation in expression of transcription factors RAR and SOX by the Wnt signalling pathway indicates that topography can induce an epigenetic modulation of the commitment to a skeletogenic lineage (Leucht *et al*., 2007). Translation assays show that both RAR and SOX can repress translation, and move mRNA away from polysomes, consistent with prevention of translation initiation (Chen *et al*., 2008, Takash *et al*., 2001). Conversely both RAR and SOX transcription factors are also able to bind to promoter regions of DNA to activate the transcription of target genes (Kamachi *et al*., 1999, Mendelsohn *et al*., 1991). There is growing appreciation that simultaneous activation and repression of gene expression is a feature of multiple developmental signalling pathways and importantly it is this crosstalk between Wnt signalling and other developmental pathways that regulates transcriptional events.

STRO-1+ MSCs cultured on both nanopit and 10 μm nanogroove topographies were associated with a general reduction in Wnt/β-catenin signalling culminating in a general reduction of cellular transcription, suggesting that these experimental substrates may prevent the onset of osteospecific differentiation by the prevention of cellular adhesion and spreading (Kudelska-Mazur *et al*., 2005). Such a scenario also points to a possible role of FX formation in cellular de-differentiation. It may also be conceived that cellular alignment may be associated with fibrospecific differentiation.

It can be further postulated that the onset of MSC differentiation occurs following cessation of cellular migration. *In vivo* bone tissue regeneration is characterised by sequential stages that start with osteoblast proliferation, followed by their differentiation and finally mineralisation of the ECM, produced as the endpoint of osteoblast phenotypic expression. This scenario is associated with an observed increase in focal and SMA formation; cellular spreading and a reduction in FX turnover as identified in HOBs cultured on polymer demixed and 100 μm grooved topographies. This up-regulation in Wnt signalling has been observed previously in preosteoblastic cells cultured on

hydroxyapatite substrates, where a 4.4-fold increase in SOX9 expression was noted (Song *et al.*, 2008).

Although analysis of the Wnt/beta-catenin signalling pathway revealed significant modulation of gene expression, the experimental work of this thesis identified the p38–MAPK pathway as one that was most significantly modulated by experimental substrates (fig. 7.4-7.6). p38–MAPK signalling, acting through tissue-specific transcription factors, may generally control progenitor/stem cell lineage processes in mesenchymal tissues and has been shown to positively regulate osteogenic differentiation through bone morphological proteins and other growth factors (Ge *et al.*, 2007). Here significant changes in p38–MAPK signalling in MSC populations were identified as being caused by modulation of transforming growth factor (TGF)β expression.

From recent reports TGF-β exerts its effects on MAPK-dependent signalling through phosphorylation of p38 and activation of transcription factors that have binding sites in DNA, inducing an immediate increase in differential function (Oka *et al.*, 2007, Woodman *et al.*, 2008). TGF-β is the most abundant growth factor in bone and has been shown to be important in osteogenesis during mandibular development (Oka *et al.*, 2007). In addition to a proliferative effect on osteoblast function, TGF-β controls bone resorption by inducing the formation of osteoclasts (Fox & Lovibond, 2005).

TGF-β expression was effected in STRO-1+ MSC populations on all experimental substrates except 100 µm groove/ridge topographies. The observed down-regulation of TGF-β in STRO-1+ populations cultured on 10 µm wide grooves, combined with a fusiform morphology may be indicative of a more fibroblastic phenotype. Interestingly, modulated TGF-β expression was associated with both up and down-regulation of p38–MAPK signalling proteins. This suggests that an interplay of multiple signalling pathways controls the topographical modulation of MSC function and perhaps indicates that the indirect mechanotransductive signalling pathways discussed above may be complemented by direct mechanotransductive mechanisms to regulate progenitor cell function.

Direct mechanotransduction is thought to occur as surfaces change adhesion morphology and hence regulate gross cellular morphology (as can be seen in this thesis). The

inhomogenity that the cytoskeleton provides to the cytoplasm is thought to allow such changes in cellular morphology to be conveyed to the nucleus (i.e. as the cell changes shape so will the nucleus) (Wang & Suo, 2005). It is presently not understood how this mechanical linkage from adhesion to nucleus works, but it is generally considered that an interconnected percolation network (Forgacs, 1995), possibly as a specialised tensegrity structure (Ingber, 2003), links microfilaments directly tethered to adhesions via interaction with microtubules and intermediate filament to the nucleus as cytoskeltal intermediate filaments directly associate with nucleoskeletal intermediate filaments (lamins). It is further likely that this works through tension with rounded cells being relaxed and then spreading passing tensile forces to the nucleus. This is considered to be the case as it would be hard to push (i.e. apply compression) through the rather stringy cytoskeleton and also as the lamins cannot be compressed as they are very dense when relaxed, but can be expanded (Dahl *et al.*, 2004).

It is now accepted that interphase chromosomes occupy discrete territories within the nucleus. These territories are complex folded structures with interchromatin channels penetrating into the territory interior and allowing diffusion of transcriptional activators (Cremer & Cremer, 2001). The telomeric ends of the interphase chromosomes are linked to the lamins and should thus be responsive to tension and it has been shown that cells responding to topography and changing morphology will change the relative positioning of their centromeres (Dalby *et al.*, 2006a, Dalby *et al.*, 2007c). Such changes in chromosomal morphology may: change the ability of transcription factors to penetrate the territories, alter the proximity of genes to polymerase rich transcription factories (Osborne *et al.*, 2004) or even stall polymerase motors in response to changes in DNA tension (Bryant *et al.*, 2003),
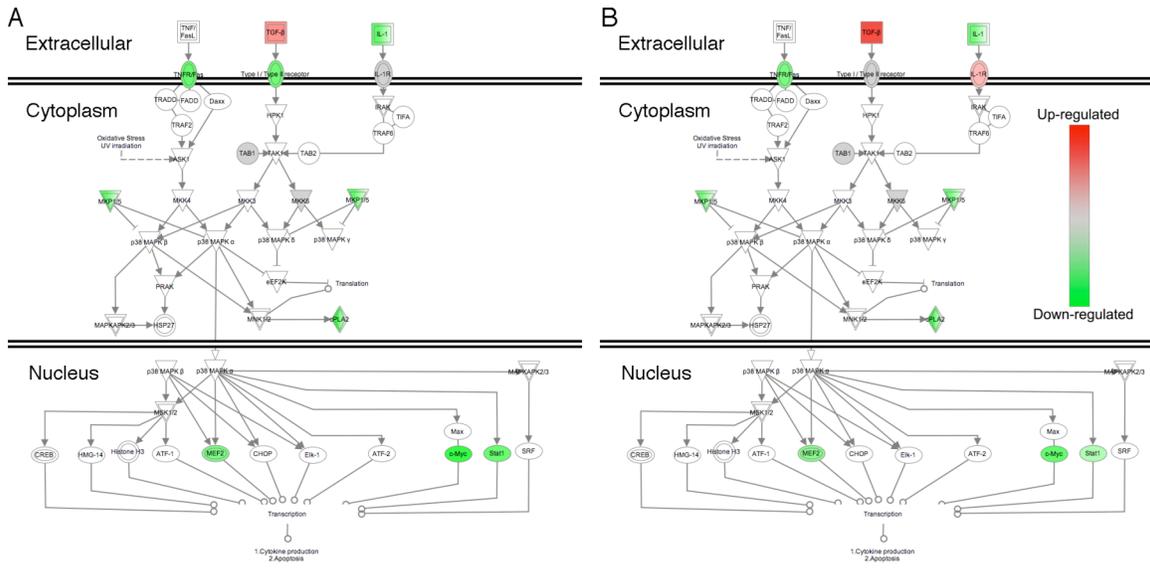
Fig. 7.4. p38–MAPK signalling in MSC populations cultured on nanopit substrates. STRO-1+ MSCs cultured on both nanopit topographies demonstrated significant up-regulation of TGF-β expression. This was coupled to widespread down-regulations in the p38–MAPK signalling pathway. (A) Square nanopit arrays, (B) hexagonal nanopit arrays.
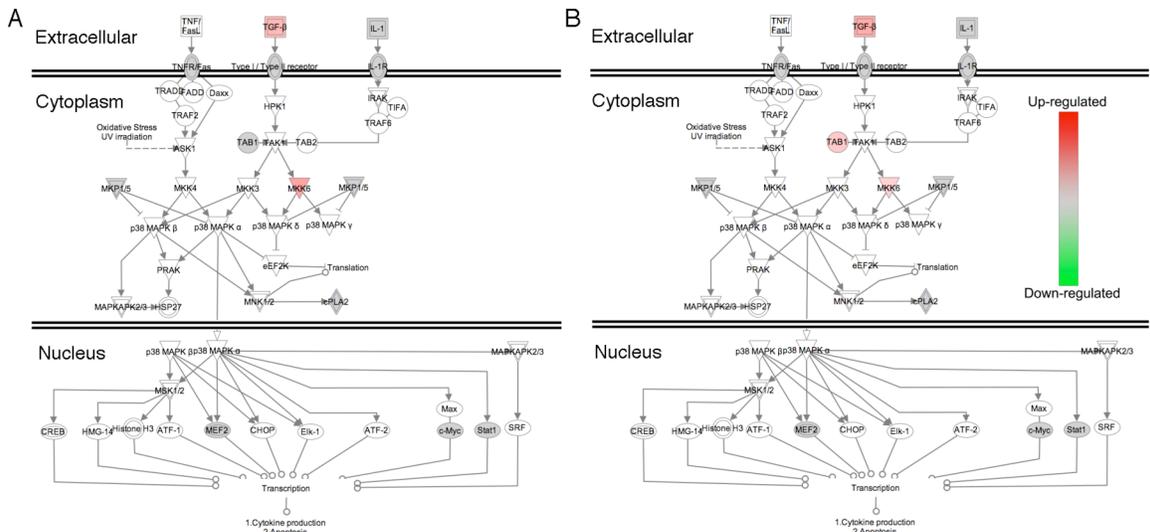
Fig. 7.5. p38–MAPK signalling in MSC populations cultured on polymer demixed substrates. Polymers demixed substrates were associated with significant up-regulation in TGF-β expression in STRO-1+ MSC populations, however further downstream signalling processes and transcriptional events were only minimally affected. (A) Nanocraters, (B) nanoislands.
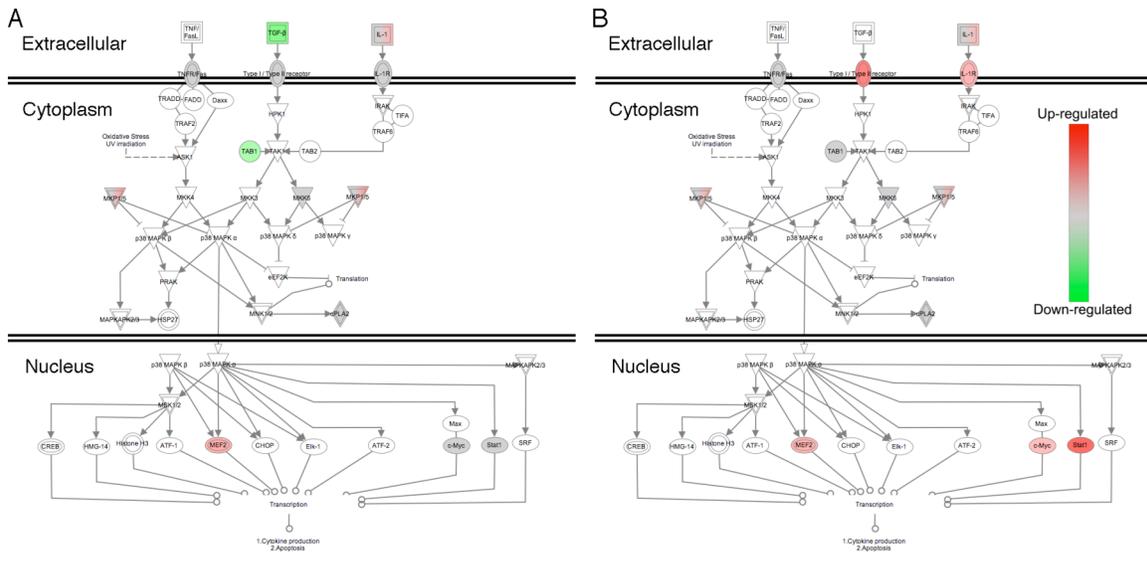
Fig. 7.6. p38–MAPK signalling in MSC populations cultured on nanogroove substrates. p38–MAPK signalling was markedly changed by varying the groove width. (A) 10 µm grooves were associated with a down-regulation in TGF-β expression. (B) 100 µm grooves induced an up-regulation in TGF-β receptors as well as a number of transcription factors.

7.6. Summary

In the developed world in 1950, there were 9.3 people under 20 years old living for every person over 65, by 2025 this ratio is forecast to be 0.59 people under 20 years old for every person older than 65. Currently surgeons face a mounting pressure due to an aging population and associated problems of rheumatoid arthritis as well as a more sports active younger populations and problems associated with osteoarthritis. Due to the present lifespan of many orthopaedic procedures (The 10 year failure rate for revision hip surgery was 26% in a Norwegian study of 4762 operations) (Lie *et al.*, 2004) patients will have to wait longer with pain before surgeons will consider operations. Metallic devices can be hard to work with due their material properties and so success *to date* with surface treatments to encourage direct bone growth and hence develop implants for life has been limited.

It was hypothesised in this thesis that nanoscale topographical features are important mediators of cellular adhesion and subsequent cellular function, and that surface modification is a potent tool for enhancing cytocompatability with an aim to improving

orthopaedic device functionality by regulating cell-substratum interactions. The scope of this thesis was twofold. Firstly to investigate the interactions of osteoblast populations with polymeric nanoscale topographies, with an aim to understanding how integrin mediated adhesion is modulated by nanotopographical structures. Secondly, to correlate these modulations in adhesion formation to functional responses, and in particular MSC differentiation.

Ordered nanoscale pits fabricated by EBL significantly modulated both cellular adhesion and function. These pits were shown to prevent direct adhesion formation in cellular populations, instead HOBs cultured on these topographies formed small FAs and numerous FXs at the interpit regions. Nanopits also significantly reduced the expression of genes involved in many functional pathways in MSC osteodifferentiation.

Random nanoislands and nanocraters fabricated by polymer demixing were also seen to affect cellular function. Both topographies induced the formation and maturation of adhesion complexes and were associated with a minor up-regulation of genes involved in many functional pathways. These findings are intriguing as they indicate topographical modification capable of reducing cell motility may increase cellular functionality.

Finially nanogroove substrates were fabricated by photolithography. Groove width was shown to influence the generation of adhesion complex subtypes in S-phase HOBs as well as modulate functional response in STRO-1+ MSC populations. Increasing the groove width was associated with reduced contact guidance and increased adhesion formation and osteospecific function. Conversely decreased nanogroove widths were associated with increased contact guidance, reduced adhesion formation and reduction in osteospecific function.

The findings presented within this thesis indicate that cellular populations do react to topographical features and that a device may be fabricated with topographical cues capable of regulating both cellular adhesion and MSC function. Furthermore, these topographically modified devices may have critical implications for enhanced bone repair and the potential for future clinical translation.

7.7. Future Work

7.7.1. Undercut Features and Cell Adhesion

As already stated, a major issue with orthopaedic joint prosthesis is to establish their permanent fixation to the adjacent bone. Nanotopographical features have been shown in this thesis to regulate cell adhesion at the cellular level by modulating integrin mediated adhesion formation at the cell-substratum interface. When designing a device which relies on permanent fixation it would be beneficial to enhance increased adhesion at the cellular level and also promote a physical interlocking of the device with the surrounding tissue.

Internal fixation stability can be achieved by either the application of a cement between bone and prosthesis, or by encouraging bone growth into to the prosthesis surfaces. The use of topographical modification for increased biologic attachment of implants offers a valuable alternative to pMMA bone cement as a means of fixation. Undercut surface features may be one methodology for further increasing cellular adhesion (by steric hindrance) at the tissue-device interface (Curodeau *et al*., 2000). Undercutting describes a tapering of a topographical feature towards the opening, which in effect allows bone and ECM infiltration but dramatically increased interlocking by restricting tissue-implant separation.

One of the unique advantages of high-resolution top-down techniques in substrate fabrication is the ability to couple these with advanced etching techniques that allows re-entrant features such as undercuts and overhangs within the topographical features. Interestingly, a recent study by Ogawa *et al* has demonstrated that the strength of osseointegration was increased by a factor of three by the inclusion of nanoundercut features (Ogawa *et al*., 2008). One intriguing question that this raises is whether single cell adhesion, rather than whole tissue invasion would be modified if a level of undercut was introduced to the topographical features outlined in this thesis? Although it seems unlikely that undercut would increase adhesion on nanopit array substrates as these were shown to prevent direct cell-substratum interactions, it may be possible that introducing a level of undercut to the nanopit substrates could further diminish cellular adhesion formation by trapping air more efficiently and increasing hydrophobicity. Conversely undercutting may also enhance protein adsorption by trapping and thus increase cellular

adhesion.

Undercut may be of benefit when combined with groove/ridge topographical features. Grooves 100 μm in width were shown to increase osteospecific differentiation in MSC populations while facilitating cellular spreading and adhesion formation. This increased cellular adhesion may be complemented by fabricating the grooves to resemble base-up anisotropic prisms. Certainly, at whole tissue level, this topographical modification would increase pull-out forces 90° to the implant surface as well as dramatically restrict lateral movements in one plane (fig. 7.7). Increasing the contact forces in two dimensions would be of great benefit in load-bearing prosthesis design, particularly hip replacement, which are associated with forces parallel to, as well as 90° to the implant.
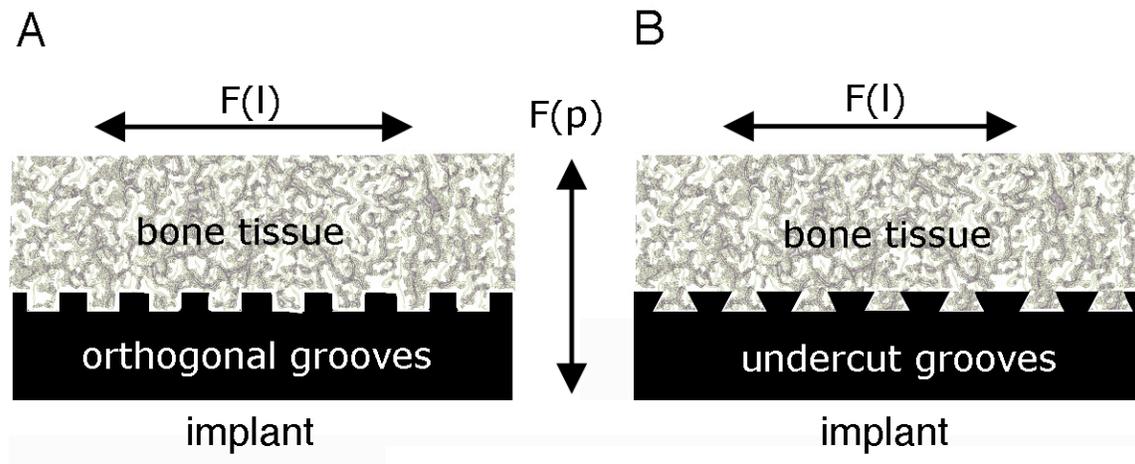
Fig 7.7. Topographical undercut grooves may increase implant stability. (A) Orthogonal arrays of grooves/ridges increase surface area and increase the force required for lateral movements to occur relative to planar surfaces F(l). (B) Undercut features also increase this lateral inertia but simultaneously increase the pull-out force relative to orthogonal groove/ridge arrays F(p).

The investigation into the effect of undercut nanoscale features on cell adhesion is at present very much neglected. It has already been documented that minute changes in the order of nanoscale features greatly effect the cell response (Dalby *et al.*, 2007d), it seems reasonable that minor changes in the morphology of a specific nanofeature, by introducing undercut, may also modulate the cellular response as well as promote greater tissue adhesion.

7.7.2. Podosome Formation

Podosomes are ring-like structures formed on the ventral surface of the plasma membrane that appear to be involved in a wide range of physiological and pathological aspects such as sealing-ring formation in osteoclasts. Podosomes are self-organised, dynamic, actin-containing structures that adhere to the ECM via integrins (Collin *et al*., 2006, Linder, 2007). Like FAs, podosomes are dynamic microstructures whose known functions include both mechanotransduction (Collin *et al*., 2008) and local ECM degradation. Of five different integrin-dependent adhesions (FAs, FXs, fibrillar adhesions, SMAs and podosomes), podosomes are the least understood in terms of dynamics and physical features. Podosomes are characterised by a dense central column of Filamentous-actin, the actin core, which is surrounded by a loosely organised actin meshwork, called the podosome cloud (Collin *et al*., 2006) which co-localises with adaptor and regulatory proteins such as vinculin and the integrins. Podosomes are small, highly dynamic, dot-like structures that have a similar size-range as that of FXs (0.5–1 μm). Indeed podosomes have been observed to initiate from FAs due to changes in the phosphorylation status of adhesion plaque proteins, most notably Src, which, as previously discussed, is an important binding partner of FAK (Oikawa *et al*., 2008). A recent study by Destaing *et al* indicates that Src null osteoclasts have fewer podosomes than normal cells and that these podosomes have a longer life span, suggesting that Src promotes both the initiation of podosome formation and podosome disassembly (Destaing *et al*., 2008). In osteoblasts, podosomes are thought to play a dual role in cell proliferation and bone mineralisation and have been shown to be dynamic mechanosensors and sensitive to substrate stiffness (Collin *et al*., 2008, Furlan *et al*., 2007), although the exact mechanisms of this process and whether podosome formation is sensitive to topographical cues is still under investigation.

7.7.3. Transient Receptor Potential Channels

Although integrin mediated adhesion sites are central to the transduction of mechanical forces by both direct and indirect mechanisms, other mediators of transduction may also play important roles in the modification of cellular function by mechanical stimuli. Most notably transmembrane pores are increasingly being recognised as potential

mechanotransductive structures in skeletal cells. In the initial phase of mechanotransduction, deformation of the cell membrane by stretch as well as shear stress results in the mechanical opening of transmembrane ion channels (Hughes *et al.*, 2005). Recently, proteins in the transient receptor potential (TRP) families have been identified as being involved with signalling in a variety of mechanosensory cells, mediating calcium entry and downstream signalling cascades in response to mechanical stimuli and altered cellular morphology (Kindt *et al.*, 2007). TRP channels form pores in the lipid bilayer of the plasma membrane, regulating ion fluxes across the membrane.

Presently, TRP channels are known to comprise a superfamily of proteins subdivided into at least seven different subfamilies; furthermore these TRP channels have been shown to be regulated by integrin mediated adhesion formation (Davis *et al.*, 2002). In particular TRP vanilloid type 4 channel receptors have been shown to play a function in signal transduction in response to flow or shear stress and may be important in nanotopographical mediated mechanotransduction. A preliminary study of these receptors has shown that they are highly expressed in endothelial cell aligned on nanogrooved topographies and further to this they are located extensively on cellular filopodial extensions (fig.7.8).
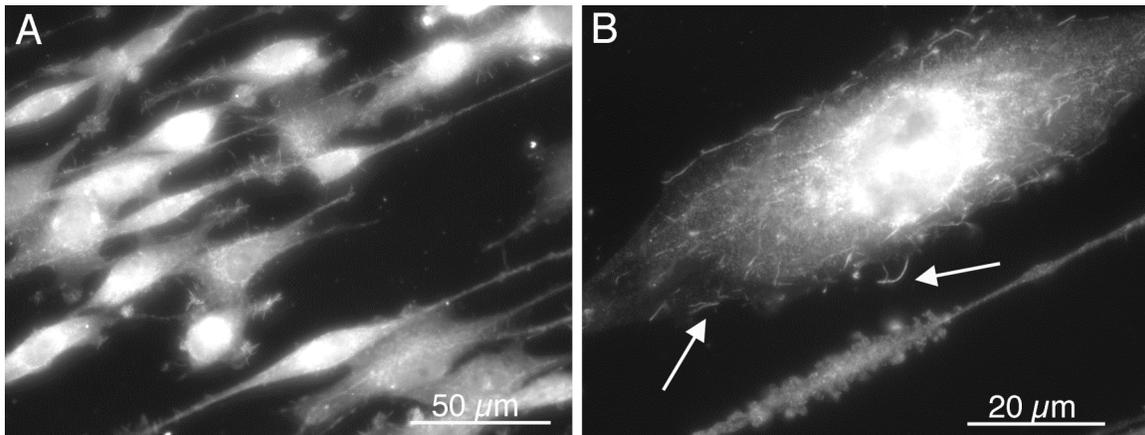
Fig 7.8. TRPV4 expression in endothelial cells aligned on a nanogrooved topography (Biggs unpublished data). (A) High levels of TRPV4 expression were noted in endothelial cells aligned by nanoscale grooves. (B) Cellular filopodia were associated with a high density of TRPV4 channels (white arrows).

7.7.4. Translation to the Clinic

It is predicted that the percentage of persons over 50 years of age affected by bone diseases will double by 2020 (Navarro *et al.*, 2008). Clearly this represents a need for permanent, temporary or biodegradable orthopaedic devices that are designed to substitute or guide bone repair. When a polymeric device can provide mechanical fixation comparable to metallic materials, the use of bioresorbable polymeric implants has several advantages over the use of traditional metallic fixation. For example, biodegradable implants reduce bone resorbtion via stress shielding and eliminate subsequent surgeries that may be necessary to remove metallic implants. They also aid in post-operative diagnostic imaging, avoiding artefact and obscuring from metal implants.

Initial uncertainty regarding the adequacy of biodegradable materials to withstand functional stresses obliged clinicians to implement these biomaterials in non-load-bearing applications such as fixation of the maxillofacial skeleton (Cutright & Hunsuck, 1972). Of all fractures of the maxillofacial skeleton, those of the mandible place the greatest demands on internal fixation devices and internal fixation (even with metal devices) is complicated by the highest failure rate in the maxillofacial skeleton. Modification by self-reinforcing (SR) techniques (Suuronen, 1993), has allowed progressive extension of bioabsorbable fixation to fractures of the maxillofacial skeleton subject to greater functional loading. This approach consists of reinforcing the polymer matrix with oriented fibres or fibrils of the same material. Recent studies indicate that SR bioresorbable devices support healing of mandibular fractures, in a manner comparable to that of titanium fixation (Ashammakhi *et al.*, 2004, Ferretti, 2008, Yerit *et al.*, 2002).
Orthopaedic biomaterials for CMF fixation should be designed with optimal physical and chemical properties to promote tissue regeneration as well as bioactivity to induce specific cellular responses at the molecular level and modulate cellular function. It can be hypothesised that third generation biomaterials, in particular SR biodegradable devices may be modified to control cellular interactions with an aim to enhancing bone union. Recently SR composites have been modified to contain osteoconductive elements (Niemela *et al.*, 2005) which could effectively accelerate bone tissue healing. In particular bioactive polymer-hydroxyapatite composites have been shown to promote osteoblast adhesion and differentiation *in vitro* and hold great promise for the fabrication

of CMF devices (Zhang *et al.*, 2007). The next stage then in the evolution of polymeric fixation may rely on the topographical modification of self-reinforced resorbable polymers encompassing a bioactive phase, with an aim to regulating cellular adhesion and differentiation followed by controlled construct resorbtion.

The fabrication of complex three-dimensional polymeric devices to include nanoscale features is a complicated process associated with low reproducibility. However, the fabrication of next-generation orthopaedic devices may be facilitated by upscaling through injection moulding. Large-scale replication of nanostructures into polymer surfaces by injection moulding is already demonstrated for mass storage applications (CD/DVD). The main advantages of injection moulding in comparison to hot embossing include its 10 to 1000-fold shorter production cycle time (seconds), its ability to shape surface structure in a single process, and its allowance for simultaneous surface structuring of all object faces (Gadegaard *et al.*, 2003a), advantageous properties for the fabrication of three-dimensional orthopaedic devices. Recently the fabrication process for the nanoscale pit arrays used in this thesis has been up-scaled by injection moulding for cell studies (Hart *et al.*, 2007) indicating that injection moulding may facilitate the production of orthopaedic devices fabricated to include topographical structures.

8.1. Statistical Table

Table 8.1. Statistically significant data pertaining to adhesion subtype quantification. Kruskal-Wallis one-way ANOVA was used to estimate equality of population medians among substrate groups. Rank differences were generated between FX, FA and SMA formation on experimental substrates. The largest rank difference was seen in SMA formation on planar and hexagonal nanopit groups. Data group comparisons indicate a significance of $p < 0.05$.

Comparison	Diff. of Ranks
Control SMA vs Hex SMA	232.262
Control SMA vs Square SMA	204.42
Square FX vs Nanolacuni FX	178.404
Square FX vs Nanoisland FX	176.747
Nanoisland SMA vs Hex SMA	145.39
Nanolacuni SMA vs Hex SMA	138.223
Hex FX vs Nanolacuni FX	137.828
Hex FX vs Nanoisland FX	136.170
Control FA vs 10 μm grooves FA	125.878
Control SMA vs 10 μm grooves SMA	117.018

Abercrombie, M., Heaysman, J. E. & Pegrum, S. M. (1970). The locomotion of fibroblasts in culture. 3. Movements of particles on the dorsal surface of the leading lamella. *Exp Cell Res* **62**, 389-98.

Abrams, G. A., Goodman, S. L., Nealey, P. F., Franco, M. & Murphy, C. J. (2000). Nanoscale topography of the basement membrane underlying the corneal epithelium of the rhesus macaque. *Cell Tissue Res* **299**, 39-46.

Adams, J. C. (2002). Regulation of protrusive and contractile cell-matrix contacts. *J Cell Sci* **115**, 257-65.

Affrossman, S., Jerome, R., O'Neill, S. A., Schmitt, T. & Stamm, M. (2000). Surface Structure of Thin Film Blends of Polystyrene and Poly(n-butyl methacrylate). *Colloid & Polymer Sci* **278**, 993-999.

Affrossman, S., Kiff, F. T., O'Neill, S. A., Pethrick, R. A. & Richards, R. W. (1998). Topography and surface composition of thin films of blends of PMMA and PEO. *Macromolecules* **32**, 2721–2730.

Affrosman, S., Henn, G., O' Niell, S. A., Pethrick, R. A. & Stamm, M. (1996). Surface topography and composition of deuterated polystyrene-poly(bromostyrene) blends. *Macromoleculaes* **29**, 5010-5016.

Akisaka, T., Yoshida, H. & Suzuki, R. (2006). The ruffled border and attachment regions of the apposing membrane of resorbing osteoclasts as visualized from the cytoplasmic face of the membrane. *J Electron Microsc (Tokyo)* **55**, 53-61.

Alexandrova, A. Y., Arnold, K., Schaub, S., Vasiliev, J. M., Meister, J. J., Bershadsky, A. D. & Verkhovsky, A. B. (2008). Comparative dynamics of retrograde actin flow and focal adhesions: formation of nascent adhesions triggers transition from fast to slow flow. *PLoS ONE* **3**, e3234.

Anastasiadis, P. Z., Moon, S. Y., Thoreson, M. A., Mariner, D. J., Crawford, H. C., Zheng, Y. & Reynolds, A. B. (2000). Inhibition of RhoA by p120 catenin. *Nat Cell Biol* **2**, 637-44.

Andersson, A. S., Brink, J., Lidberg, U. & Sutherland, D. S. (2003). Influence of systematically varied nanoscale topography on the morphology of epithelial cells. *IEEE Trans Nanobioscience* **2**, 49-57.

Andersson, M., Suska, F., Johansson, A., Berglin, M., Emanuelsson, L., Elwing, H. & Thomsen, P. (2007). Effect of molecular mobility of polymeric implants on soft tissue reactions: An in vivo study in rats. *J Biomed Mater Res A* **84A**, 652-660.

Arnold, M., Cavalcanti-Adam, E. A., Glass, R., Blummel, J., Eck, W., Kantlehner, M., Kessler, H. & Spatz, J. P. (2004). Activation of integrin function by nanopatterned adhesive interfaces. *Chemphyschem* **5**, 383-8.

Aroush, R. B. & Wagner, H. D. (2006). Shear-Stress Profile along a Cell Focal Adhesion. *Adv Mater* **18**, 1537-1540.

Artico, M., Ferrante, L., Pastore, F. S., Ramundo, E. O., Cantarelli, D., Scopelliti, D. & Iannetti, G. (2003). Bone autografting of the calvaria and craniofacial skeleton: historical background, surgical results in a series of 15 patients, and review of the literature. *Surg Neurol* **60**, 71-9.

Ashammakhi, N., Renier, D., Arnaud, E., Marchac, D., Ninkovic, M., Donaway, D., Jones, B., Serlo, W., Laurikainen, K., Tormala, P. & Waris, T. (2004). Successful use of biosorb osteofixation devices in 165 cranial and maxillofacial cases: a multicenter report. *J Craniofac Surg* **15**, 692-701; discussion 702.

Attwell, S., Roskelley, C. & Dedhar, S. (2000). The integrin-linked kinase (ILK) suppresses anoikis. *Oncogene* **19**, 3811-5.

Bade, E. G., Sadnik, I. L., Pilgrim, C. & Maurer, W. (1966). Autoradiographic study of DNA-synthesis in the regenerating liver of the mouse. *Exp Cell Res* **44**, 676-8.

Badylak, S. F. (2002). The extracellular matrix as a scaffold for tissue reconstruction. *Semin Cell Dev Biol* **13**, 377-83.

Bakker, A., Klein-Nulend, J. & Burger, E. (2004). Shear stress inhibits while disuse promotes osteocyte apoptosis. *Biochem Biophys Res Commun* **320**, 1163-8.

Balaban, N. Q., Schwarz, U. S., Riveline, D., Goichberg, P., Tzur, G., Sabanay, I., Mahalu, D., Safran, S., Bershadsky, A., Addadi, L., Geiger, B. (2001). Force and focal adhesion assembly: a close relationship studied using elastic micropatterned substrates. *Nat Cell Biol* **3**, 466-72.

Bar-Shavit, Z. (2007). The osteoclast: a multinucleated, hematopoietic-origin, bone-resorbing osteoimmune cell. *J Cell Biochem* **102**, 1130-9.

Barry, F. P., Boynton, R. E., Haynesworth, S., Murphy, J. M. & Zaia, J. (1999). The monoclonal antibody SH-2, raised against human mesenchymal stem cells, recognizes an epitope on endoglin (CD105). *Biochem Biophys Res Commun* **265**, 134-9.

Baums, M. H., Zelle, B. A., Schultz, W., Ernstberger, T. & Klinger, H. M. (2006). Intraarticular migration of a broken biodegradable interference screw after anterior cruciate ligament reconstruction. *Knee Surg Sports Traumatol Arthrosc* **14**, 865-8.

Baxter, L. C., Frauchiger, V., Textor, M., ap Gwynn, I. & Richards, R. G. (2002). Fibroblast and osteoblast adhesion and morphology on calcium phosphate surfaces. *Eur Cell Mater* **4**, 1-17.

Behmoaram, E., Bijian, K., Jie, S., Xu, Y., Darnel, A., Bismar, T. A. & Alaoui-Jamali, M. A. (2008). Focal Adhesion Kinase-Related Proline-Rich Tyrosine Kinase 2 and Focal Adhesion Kinase Are Co-Overexpressed in Early-Stage and Invasive ErbB-2-Positive Breast Cancer and Cooperate for Breast Cancer Cell Tumorigenesis and Invasiveness. *Am J Pathol* **173**, 1540-50.

Beirne, J. C., Barry, H. J., Brady, F. A. & Morris, V. B. (1996). Donor site morbidity of the anterior iliac crest following cancellous bone harvest. *Int J Oral Maxillofac Surg* **25**, 268-71.

Beisker, W., Dolbeare, F. & Gray, J. W. (1987). An improved immunocytochemical procedure for high-sensitivity detection of incorporated bromodeoxyuridine. *Cytometry* **8**, 235-9.

Bernard, G. W. & Pease, D. C. (1969). An electron microscopic study of initial intramembranous osteogenesis. *Am J Anat* **125**, 271-90.

Berry, C. C., Dalby, M. J., Oreffo, R. O., McCloy, D. & Affrosman, S. (2006). The interaction of human bone marrow cells with nanotopographical features in three dimensional constructs. *J Biomed Mater Res A* **79**, 431-9.

Bershadsky, A., Kozlov, M. & Geiger, B. (2006a). Adhesion-mediated mechanosensitivity: a time to experiment, and a time to theorize. *Curr Opin Cell Biol* **18**, 472-81.

Bershadsky, A. D., Balaban, N. Q. & Geiger, B. (2003). Adhesion-dependent cell mechanosensitivity. *Annu Rev Cell Dev Biol* **19**, 677-95.

Bershadsky, A. D., Ballestrem, C., Carramusa, L., Zilberman, Y., Gilquin, B., Khochbin, S., Alexandrova, A. Y., Verkhovsky, A. B., Shemesh, T. & Kozlov, M. M. (2006b). Assembly and mechanosensory function of focal adhesions: experiments and models. *Eur J Cell Biol* **85**, 165-73.

Bershadsky, A. D., Tint, I. S., Neyfakh, A. A., Jr. & Vasiliev, J. M. (1985). Focal contacts of normal and RSV-transformed quail cells. Hypothesis of the transformation-induced deficient maturation of focal contacts. *Exp Cell Res* **158**, 433-44.

Besser, A. & Safran, S. A. (2006). Force-induced adsorption and anisotropic growth of focal adhesions. *Biophys J* **90**, 3469-84.

Bevelander, G. & Johnson, P. L. (1950). A histochemical study of the development of membrane bone. *Anat Rec* **108**, 1-21.

Bhadriraju, K., Yang, M., Alom Ruiz, S., Pirone, D., Tan, J. & Chen, C. S. (2007). Activation of ROCK by RhoA is regulated by cell adhesion, shape, and cytoskeletal tension. *Exp Cell Res* **313**, 3616-23.

Biggs, M. J., Richards, R. G., Gadegaard, N., Wilkinson, C. D. & Dalby, M. J. (2006). Regulation of implant surface cell adhesion: characterization and quantification of S-phase primary osteoblast adhesions on biomimetic nanoscale substrates. *J Orthop Res* **25**, 273-282.

Biggs, M. J., Richards, R. G., Gadegaard, N., Wilkinson, C. D. & Dalby, M. J. (2007). The effects of nanoscale pits on primary human osteoblast adhesion formation and cellular spreading. *J Mater Sci Mater Med* **18**, 399-404.

Biggs M. J., Richards, R. G., Gadegaard, N., Wilkinson, C. D. & Dalby, M. J. (2008). Focal adhesion interactions with topographical structures: a novel method for immuno-SEM labelling of focal adhesions in S-phase cells. *J Microsc* **231,** 28-37.

Birch de, B. (1880). The Constitution and Relations of Bone Lamellae, Lacunae, and Canaliculi, and some Effects of Trypsin Digestion on Bone. *J Physiol* **2**, 360-446 7.

Bloom, S., Lockard, V. G. & Bloom, M. (1996). Intermediate filament-mediated stretch-induced changes in chromatin: a hypothesis for growth initiation in cardiac myocytes. *J Mol Cell Cardiol* **28**, 2123-7.

Blumer, M. J., Schwarzer, C., Perez, M. T., Konakci, K. Z. & Fritsch, H. (2006). Identification and location of bone-forming cells within cartilage canals on their course into the secondary ossification centre. *J Anat* **208**, 695-707.

Boyan, B. D., Lossdorfer, S., Wang, L., Zhao, G., Lohmann, C. H., Cochran, D. L. & Schwartz, Z. (2003). Osteoblasts generate an osteogenic microenvironment when grown on surfaces with rough microtopographies. *Eur Cell Mater* **6**, 22-7.

Bozec, L., de Groot, J., Odlyha, M., Nicholls, B. & Horton, M. A. (2005). Mineralised tissues as nanomaterials: analysis by atomic force microscopy. *IEE Proc Nanobiotechnol* **152**, 183-6.

Bozec, L. & Horton, M. A. (2006). Skeletal tissues as nanomaterials. *J Mater Sci Mater Med* **17**, 1043-8.

Brabazon, D., Naher, S. & Biggs, P. (2008). Glazing of tool dies for semi-solid steel forming. *Int J Mater Form*. **In Press**, DOI: 10.1007/s12289-008-0223-9

Brodsky, B. & Persikov, A. V. (2005). Molecular structure of the collagen triple helix. *Adv Protein Chem* **70**, 301-39.

Brody, S., Anilkumar, T., Liliensiek, S., Last, J. A., Murphy, C. J. & Pandit, A. (2006). Characterizing nanoscale topography of the aortic heart valve basement membrane for tissue engineering heart valve scaffold design. *Tissue Eng* **12**, 413-21.

Brown, O. L., Dirschl, D. R. & Obremskey, W. T. (2001). Incidence of hardware-related pain and its effect on functional outcomes after open reduction and internal fixation of ankle fractures. *J Orthop Trauma* **15**, 271-4.

Bryant, Z., Stone, M. D., Gore, J., Smith, S. B., Cozzarelli, N. R. & Bustamante, C. (2003). Structural transitions and elasticity from torque measurements on DNA. *Nature* **424**, 338-41.

Buchel, P., Rahal, A., Seto, I. & Iizuka, T. (2005). Reconstruction of orbital floor fracture with polyglactin 910/polydioxanon patch (ethisorb): a retrospective study. *J Oral Maxillofac Surg* **63**, 646-50.

Burridge, K., Fath, K., Kelly, T., Nuckolls, G. & Turner, C. (1988). Focal adhesions: transmembrane junctions between the extracellular matrix and the cytoskeleton. *Annu Rev Cell Biol* **4**, 487-525.

Byers, H. R., White, G. E. & Fujiwara, K. (1984). Organization and function of stress fibers in cells in vitro and in situ. A review. *Cell Muscle Motil* **5**, 83-137.

Cameron, I. L. & Greulich, R. C. (1963). Evidence for an essentially constant duration of DNA synthesis in renewing epithelia of the adult mouse. *J Cell Biol* **18**, 31-40.

Campbell, I. D. (2008). Studies of focal adhesion assembly. *Biochem Soc Trans* **36**, 263-6.

Carragher, N. O. & Frame, M. C. (2004). Focal adhesion and actin dynamics: a place where kinases and proteases meet to promote invasion. *Trends Cell Biol* **14**, 241-9.

Carvalho, R. S., Kostenuik, P. J., Salih, E., Bumann, A. & Gerstenfeld, L. C. (2003). Selective adhesion of osteoblastic cells to different integrin ligands induces osteopontin gene expression. *Matrix Biol* **22**, 241-9.

Cattaruzza, M., Lattrich, C. & Hecker, M. (2004). Focal adhesion protein zyxin is a mechanosensitive modulator of gene expression in vascular smooth muscle cells. *Hypertension* **43**, 726-30.

Cavalcanti-Adam, E. A., Volberg, T., Micoulet, A., Kessler, H., Geiger, B. & Spatz, J. P. (2007). Cell spreading and focal adhesion dynamics are regulated by spacing of integrin ligands. *Biophys J* **92**, 2964-74.

Chan, P. Y., Kanner, S. B., Whitney, G. & Aruffo, A. (1994). A transmembrane-anchored chimeric focal adhesion kinase is constitutively activated and phosphorylated at tyrosine residues identical to pp125FAK. *J Biol Chem* **269**, 20567-74.

Charnley, J. (1960). Anchorage of the femoral head prosthesis to the shaft of the femur. *J Bone Joint Surg Br* **42-B**, 28-30.

Chen, H. C., Appeddu, P. A., Parsons, J. T., Hildebrand, J. D., Schaller, M. D. & Guan, J. L. (1995). Interaction of focal adhesion kinase with cytoskeletal protein talin. *J Biol Chem* **270**, 16995-9.

Chen, N., Onisko, B. & Napoli, J. L. (2008). The nuclear transcription factor RARalpha associates with neuronal RNA granules and suppresses translation. *J Biol Chem* **283**, 20841-7.

Chesnick, I. E., Mason, J. T., Giuseppetti, A. A., Eidelman, N. & Potter, K. (2008). Magnetic resonance microscopy of collagen mineralization. *Biophys J* **95**, 2017-26.

Chicurel, M. E., Chen, C. S. & Ingber, D. E. (1998). Cellular control lies in the balance of forces. *Curr Opin Cell Biol* **10**, 232-9.

Chou, L., Firth, J. D., Uitto, V. J. & Brunette, D. M. (1995). Substratum surface topography alters cell shape and regulates fibronectin mRNA level, mRNA stability, secretion and assembly in human fibroblasts. *J Cell Sci* **108 (Pt 4)**, 1563-73.

Christensen, M. M., Danscher, G., Ellermann-Eriksen, S., Schionning, J. D. & Rungby, J. (1992). Autometallographic silver-enhancement of colloidal gold particles used to label phagocytic cells. *Histochemistry* **97**, 207-11.

Ciapetti, G., Ambrosio, L., Marletta, G., Baldini, N. & Giunti, A. (2006). Human bone marrow stromal cells: In vitro expansion and differentiation for bone engineering. *Biomaterials* **27**, 6150-60.

Clark, P., Connolly, P., Curtis, A. S., Dow, J. A. & Wilkinson, C. D. (1987). Topographical control of cell behaviour. I. Simple step cues. *Development* **99**, 439-48.

Clark, P., Connolly, P., Curtis, A. S., Dow, J. A. & Wilkinson, C. D. (1990). Topographical control of cell behaviour: II. Multiple grooved substrata. *Development* **108**, 635-44.

Clark, P., Connolly, P., Curtis, A. S., Dow, J. A. & Wilkinson, C. D. (1991). Cell guidance by ultrafine topography in vitro. *J Cell Sci* **99 (Pt 1)**, 73-7.

Cohen, D. M., Chen, H., Johnson, R. P., Choudhury, B. & Craig, S. W. (2005). Two distinct head-tail interfaces cooperate to suppress activation of vinculin by talin. *J Biol Chem* **280**, 17109-17.

Cohen, D. M., Kutscher, B., Chen, H., Murphy, D. B. & Craig, S. W. (2006). A conformational switch in vinculin drives formation and dynamics of a talin-vinculin complex at focal adhesions. *J Biol Chem* **281**, 16006-15.

Cohen, M., Joester, D., Geiger, B. & Addadi, L. (2004). Spatial and temporal sequence of events in cell adhesion: from molecular recognition to focal adhesion assembly. *Chembiochem* **5**, 1393-9.

Coleman, R. E. (2006). Clinical features of metastatic bone disease and risk of skeletal morbidity. *Clin Cancer Res* **12**, 6243s-6249s.

Collin, O., Na, S., Chowdhury, F., Hong, M., Shin, M. E., Wang, F. & Wang, N. (2008). Self-organized podosomes are dynamic mechanosensors. *Curr Biol* **18**, 1288-94.

Collin, O., Tracqui, P., Stephanou, A., Usson, Y., Clement-Lacroix, J. & Planus, E. (2006). Spatiotemporal dynamics of actin-rich adhesion microdomains: influence of substrate flexibility. *J Cell Sci* **119**, 1914-25.

Conrad, C. & Huss, R. (2005). Adult stem cell lines in regenerative medicine and reconstructive surgery. *J Surg Res* **124**, 201-8.

Cool, S. M. & Nurcombe, V. (2005). The osteoblast-heparan sulfate axis: Control of the bone cell lineage. *Int J Biochem Cell Biol* **37**, 1739-45.

Cramer, L. P. (1997). Molecular mechanism of actin-dependent retrograde flow in lamellipodia of motile cells. *Front Biosci* **2**, d260-70.

Cremer, T. & Cremer, C. (2001). Chromosome territories, nuclear architecture and gene regulation in mammalian cells. *Nat Rev Genet* **2**, 292-301.

Cross, S. J. & ap Gwynn, I. (1987). Adhesion and the cell cycle in cultured L929 and CHO cells. *Cytobios* **50**, 41-62.

Cukierman, E., Pankov, R., Stevens, D. R. & Yamada, K. M. (2001). Taking cell-matrix adhesions to the third dimension. *Science* **294**, 1708-12.

Curodeau, A., Sachs, E. & Caldarise, S. (2000). Design and fabrication of cast orthopedic implants with freeform surface textures from 3-D printed ceramic shell. *J Biomed Mater Res* **53**, 525-35.

Curtis, A. (2004). Tutorial on the biology of nanotopography. *IEEE Trans Nanobioscience* **3**, 293-5.

Curtis, A. S. (1964). The Mechanism Of Adhesion Of Cells To Glass. A Study By Interference Reflection Microscopy. *J Cell Biol* **20**, 199-215.

Curtis, A. S., Casey, B., Gallagher, J. O., Pasqui, D., Wood, M. A. & Wilkinson, C. D. (2001). Substratum nanotopography and the adhesion of biological cells. Are symmetry or regularity of nanotopography important? *Biophys Chem* **94**, 275-83.

Curtis, A. S., Dalby, M. J. & Gadegaard, N. (2006). Nanoprinting onto cells. *J R Soc Interface* **3**, 393-8.

Curtis, A. S. G., Gadegaard, N., Dalby, M. J., Riehle, M. O., Wilkinson, C. D. W. & Aitchison, G. (2004). Cells react to nanoscale order and symmetry in their surroundings. *IEEE Trans Nanobioscience* **3**, 61-65.

Cutright, D. E. & Hunsuck, E. E. (1972). The repair of fractures of the orbital floor using biodegradable polylactic acid. *Oral Surg Oral Med Oral Pathol* **33**, 28-34.

Dahl, K. N., Kahn, S. M., Wilson, K. L. & Discher, D. E. (2004). The nuclear envelope lamina network has elasticity and a compressibility limit suggestive of a molecular shock absorber. *J Cell Sci* **117**, 4779-86.

Dalby, M. J., Andar, A., Nag, A., Affrossman, S., Tare, R., McFarlane, S. & Oreffo, R. O. (2008a). Genomic expression of mesenchymal stem cells to altered nanoscale topographies. *J R Soc Interface* **5**, 1055-65.

Dalby, M. J., Biggs, M. J., Gadegaard, N., Kalna, G., Wilkinson, C. D. & Curtis, A. S. (2006a). Nanotopographical stimulation of mechanotransduction and changes in interphase centromere positioning. *J Cell Biochem* **100**, 326-338.

Dalby, M. J., Biggs, M. J. P., Gadegaard, N., Kalna, G., Wilkinson, C. D. W. & Curtis, A. S. G. (2007a). Nanotopographical Stimulation of Mechanotransduction and Changes in Interphase Centromere Positioning. *Journal of Cellular Biochemistry* **100**, 326-338.

Dalby, M. J., Childs, S., Riehle, M. O., Johnstone, H. J., Affrossman, S. & Curtis, A. S. (2003a). Fibroblast reaction to island topography: changes in cytoskeleton and morphology with time. *Biomaterials* **24**, 927-35.

Dalby, M. J., Gadegaard, N., Curtis, A. S. & Oreffo, R. O. (2007b). Nanotopographical control of human osteoprogenitor differentiation. *Curr Stem Cell Res Ther* **2**, 129-38.

Dalby, M. J., Gadegaard, N., Herzyk, P., Sutherland, D., Agheli, H., Wilkinson, C. D. & Curtis, A. S. (2007c). Nanomechanotransduction and interphase nuclear organization influence on genomic control. *J Cell Biochem* **102**, 1234-44.

Dalby, M. J., Gadegaard, N., Riehle, M. O., Wilkinson, C. D. & Curtis, A. S. (2004a). Investigating filopodia sensing using arrays of defined nano-pits down to 35 nm diameter in size. *Int J Biochem Cell Biol* **36**, 2005-15.

Dalby, M. J., Gadegaard, N., Tare, R., Andar, A., Riehle, M. O., Herzyk, P., Wilkinson, C. D. & Oreffo, R. O. (2007d). The control of human mesenchymal cell differentiation using nanoscale symmetry and disorder. *Nat Mater* **6**, 997-1003.

Dalby, M. J., Gadegaard, N. & Wilkinson, C. D. (2008b). The response of fibroblasts to hexagonal nanotopography fabricated by electron beam lithography. *J Biomed Mater Res A* **84**, 973-9.

Dalby, M. J., Hart, A. & Yarwood, S. J. (2008c). The effect of the RACK1 signalling protein on the regulation of cell adhesion and cell contact guidance on nanometric grooves. *Biomaterials* **29**, 282-9.

Dalby, M. J., McCloy, D., Robertson, M., Agheli, H., Sutherland, D., Affrossman, S. & Oreffo, R. O. (2006b). Osteoprogenitor response to semi-ordered and random nanotopographies. *Biomaterials* **27**, 2980-7.

Dalby, M. J., Riehle, M. O., Johnstone, H., Affrossman, S. & Curtis, A. S. (2004b). Investigating the limits of filopodial sensing: a brief report using SEM to image the interaction between 10 nm high nano-topography and fibroblast filopodia. *Cell Biol Int* **28**, 229-36.

Dalby, M. J., Riehle, M. O., Johnstone, H. J., Affrossman, S. & Curtis, A. S. (2003b). Nonadhesive nanotopography: fibroblast response to poly(n-butyl methacrylate)-poly(styrene) demixed surface features. *J Biomed Mater Res A* **67**, 1025-32.

Dalby, M. J., Riehle, M. O., Yarwood, S. J., Wilkinson, C. D. & Curtis, A. S. (2003c). Nucleus alignment and cell signaling in fibroblasts: response to a micro-grooved topography. *Exp Cell Res* **284**, 274-82.

Dalby, M. J., Yarwood, S. J., Riehle, M. O., Johnstone, H. J., Affrossman, S. & Curtis, A. S. (2002). Increasing fibroblast response to materials using nanotopography: morphological and genetic measurements of cell response to 13-nm-high polymer demixed islands. *Exp Cell Res* **276**, 1-9.

Danen, E. H., Sonneveld, P., Brakebusch, C., Fassler, R. & Sonnenberg, A. (2002). The fibronectin-binding integrins alpha5beta1 and alphavbeta3 differentially modulate RhoA-GTP loading, organization of cell matrix adhesions, and fibronectin fibrillogenesis. *J Cell Biol* **159**, 1071-86.

Davies, J. E. (2007). Bone bonding at natural and biomaterial surfaces. *Biomaterials* **28**, 5058-67.

Davies, P. F., Robotewskyj, A. & Griem, M. L. (1993). Endothelial cell adhesion in real time. Measurements in vitro by tandem scanning confocal image analysis. *J Clin Invest* **91**, 2640-52.

Davis, M. J., Wu, X., Nurkiewicz, T. R., Kawasaki, J., Gui, P., Hill, M. A. & Wilson, E. (2002). Regulation of ion channels by integrins. *Cell Biochem Biophys* **36**, 41-66.

Day, T. F., Guo, X., Garrett-Beal, L. & Yang, Y. (2005). Wnt/beta-catenin signaling in mesenchymal progenitors controls osteoblast and chondrocyte differentiation during vertebrate skeletogenesis. *Dev Cell* **8**, 739-50.

Day, T. F. & Yang, Y. (2008). Wnt and hedgehog signaling pathways in bone development. *J Bone Joint Surg Am* **90 Suppl 1**, 19-24.

De Jong, K. L., MacLeod, H. C., Norton, P. R. & Petersen, N. O. (2006). Fibronectin organization under and near cells. *Eur Biophys J* **35**, 695-708.

den Braber, E. T., de Ruijter, J. E., Ginsel, L. A., von Recum, A. F. & Jansen, J. A. (1998). Orientation of ECM protein deposition, fibroblast cytoskeleton, and attachment complex components on silicone microgrooved surfaces. *J Biomed Mater Res* **40**, 291-300.

Deng, Z. L., Sharff, K. A., Tang, N., Song, W. X., Luo, J., Luo, X., Chen, J., Bennett, E., Reid, R., Manning, D., Xue, A., Montag, A. G., Luu, H. H., Haydon, R. C. & He, T. C. (2008). Regulation of osteogenic differentiation during skeletal development. *Front Biosci* **13**, 2001-21.

Dennis, J. E., Carbillet, J. P., Caplan, A. I. & Charbord, P. (2002). The STRO-1+ marrow cell population is multipotential. *Cells Tissues Organs* **170**, 73-82.

Deshpande, V. S., McMeeking, R. M. & Evans, A. G. (2006). A bio-chemo-mechanical model for cell contractility. *Proc Natl Acad Sci U S A* **103**, 14015-20.

Destaing, O., Sanjay, A., Itzstein, C., Horne, W. C., Toomre, D., De Camilli, P. & Baron, R. (2008). The tyrosine kinase activity of c-Src regulates actin dynamics and organization of podosomes in osteoclasts. *Mol Biol Cell* **19**, 394-404.

Dettin, M., Bagno, A., Gambaretto, R., Iucci, G., Conconi, M. T., Tuccitto, N., Menti, A. M., Grandi, C., Di Bello, C., Licciardello, A. & Polzonetti, G. (2008). Covalent surface modification of titanium oxide with different adhesive peptides: Surface characterization and osteoblast-like cell adhesion. *J Biomed Mater Res A*.

Dettin, M., Conconi, M. T., Gambaretto, R., Bagno, A., Di Bello, C., Menti, A. M., Grandi, C. & Parnigotto, P. P. (2005). Effect of synthetic peptides on osteoblast adhesion. *Biomaterials* **26**, 4507-15.

Diehl, K. A., Foley, J. D., Nealey, P. F. & Murphy, C. J. (2005). Nanoscale topography modulates corneal epithelial cell migration. *J Biomed Mater Res A* **75**, 603-11.

Dulgar-Tulloch, A. J., Bizios, R. & Siegel, R. W. (2008). Human mesenchymal stem cell adhesion and proliferation in response to ceramic chemistry and nanoscale topography. *J Biomed Mater Res A*. **In Press**, DOI: 10.1002/jbm.a.32116.

Durieux, A. C., Desplanches, D., Freyssenet, D. & Fluck, M. (2007). Mechanotransduction in striated muscle via focal adhesion kinase. *Biochem Soc Trans* **35**, 1312-3.

Ebraheim, N. A., Elgafy, H. & Xu, R. (2001). Bone-graft harvesting from iliac and fibular donor sites: techniques and complications. *J Am Acad Orthop Surg* **9**, 210-8.

Eghbali-Fatourechi, G. Z., Lamsam, J., Fraser, D., Nagel, D., Riggs, B. L. & Khosla, S. (2005). Circulating osteoblast-lineage cells in humans. *N Engl J Med* **352**, 1959-66.

Eisenbarth, E., Velten, D., Muller, M., Thull, R. & Breme, J. (2006). Nanostructured niobium oxide coatings influence osteoblast adhesion. *J Biomed Mater Res A* **79**, 166-75.

Engler, A. J., Sweeney, H. L., Discher, D. E. & Schwarzbauer, J. E. (2007). Extracellular matrix elasticity directs stem cell differentiation. *J Musculoskelet Neuronal Interact* **7**, 335.

Everhart, L. P., Jr. & Rubin, R. W. (1974). Cyclic changes in the cell surface. I. Change in thymidine transport and its inhibition by cytochalasin B in Chinese hamster ovary cells. *J Cell Biol* **60**, 434-41.

Fang, T. C., Otto, W. R., Rao, J., Jeffery, R., Hunt, T., Alison, M. R., Cook, H. T., Wright, N. A. & Poulsom, R. (2008). Haematopoietic lineage-committed bone marrow cells, but not cloned cultured mesenchymal stem cells, contribute to regeneration of renal tubular epithelium after HgCl(2)-induced acute tubular injury. *Cell Prolif* **41,** 575-91.

Fayet, C., Bendeck, M. P. & Gotlieb, A. I. (2007). Cardiac valve interstitial cells secrete fibronectin and form fibrillar adhesions in response to injury. *Cardiovasc Pathol* **16**, 203-11.

Fell, H. B. & Robison, R. (1934). The development of the calcifying mechanism in avian cartilage and osteoid tissue. *Biochem J* **28**, 2243-53.

Ferretti, C. (2008). A prospective trial of poly-L-lactic/polyglycolic acid co-polymer plates and screws for internal fixation of mandibular fractures. *Int J Oral Maxillofac Surg* **37**, 242-8.

Fisher, R. A. (1922). On the interpretation of X from contingency tables, and the calculation of P. *J. R. Statist. Soc.* **85**, 87-94.

Flusberg, D. A., Numaguchi, Y. & Ingber, D. E. (2001). Cooperative control of Akt phosphorylation, bcl-2 expression, and apoptosis by cytoskeletal microfilaments and microtubules in capillary endothelial cells. *Mol Biol Cell* **12**, 3087-94.

Forgacs, G. (1995). On the possible role of cytoskeletal filamentous networks in intracellular signaling: an approach based on percolation. *J Cell Sci* **108 (Pt 6)**, 2131-43.

Fox, S. W. & Lovibond, A. C. (2005). Current insights into the role of transforming growth factor-beta in bone resorption. *Mol Cell Endocrinol* **243**, 19-26.

Franz, C. M. & Muller, D. J. (2005). Analyzing focal adhesion structure by atomic force microscopy. *J Cell Sci* **118**, 5315-23.

Frenot, A. & Chronakis, I. S. (2003). Polymer nanofibers assembled by electrospinning. *Curr. Opin. Colloid interface Sci* **8**, 64-75.

Friedenstein, A. J. (1995). Marrow stromal fibroblasts. *Calcif Tissue Int* **56 Suppl 1**, S17.

Frisch, S. M. & Ruoslahti, E. (1997). Integrins and anoikis. *Curr Opin Cell Biol* **9**, 701-6.

Frisch, S. M., Vuori, K., Ruoslahti, E. & Chan-Hui, P. Y. (1996). Control of adhesion-dependent cell survival by focal adhesion kinase. *J Cell Biol* **134**, 793-9.

Fukuda, H., Imai, A., Terasawa, T. & Okazaki, S. (1991). New approach to resolution limit and advanced image formation techniques in optical lithography. *IEEE Trans Electron Devices* **38**, 67-75.

Furlan, F., Galbiati, C., Jorgensen, N. R., Jensen, J. E., Mrak, E., Rubinacci, A., Talotta, F., Verde, P. & Blasi, F. (2007). Urokinase plasminogen activator receptor affects bone homeostasis by regulating osteoblast and osteoclast function. *J Bone Miner Res* **22**, 1387-96.

Gadegaard, N., Mosler, M. & Larsen, M. B. (2003a). Biomimetic polymer nanostructures by injection molding. *Macromolecular Materials and Engineering* **288**, 76-83.

Gadegaard, N., Thoms, S., Macintyre, D. S., Mcghee, K., Gallagher, J., Casey, B. & Wilkinson, C. D. W. (2003b). Arrays of Nano-dots for Cellular Engineering. *Microelectronic Engineering* **67-68**, 126-168.

Gallagher, J. O., McGhee, K. F., Wilkinson, C. D. W. & Riehle, M. O. (2002). Intraction of Animal Cells with Ordered Nanotopography. *IEEE Trans Nanobioscience* **1**, 24-28.

Garcia, A. J. (2005). Get a grip: integrins in cell-biomaterial interactions. *Biomaterials* **26,** 7525-9.

Ge, C., Xiao, G., Jiang, D. & Franceschi, R. T. (2007). Critical role of the extracellular signal-regulated kinase-MAPK pathway in osteoblast differentiation and skeletal development. *J Cell Biol* **176**, 709-18.

Gear, A. J., Apasova, E., Schmitz, J. P. & Schubert, W. (2005). Treatment modalities for mandibular angle fractures. *J Oral Maxillofac Surg* **63**, 655-63.

George-Weinstein, M., Gerhart, J., Mattiacci-Paessler, M., Simak, E., Blitz, J., Reed, R. & Knudsen, K. (1998). The role of stably committed and uncommitted cells in establishing tissues of the somite. *Ann N Y Acad Sci* **842**, 16-27.

Giraud-Guille, M. M. (1988). Twisted plywood architecture of collagen fibrils in human compact bone osteons. *Calcif Tissue Int* **42**, 167-80.

Griesbeck, O., Baird, G. S., Campbell, R. E., Zacharias, D. A. & Tsien, R. Y. (2001). Reducing the environmental sensitivity of yellow fluorescent protein. Mechanism and applications. *J Biol Chem* **276**, 29188-94.

Grigoriou, V., Shapiro, I. M., Cavalcanti-Adam, E. A., Composto, R. J., Ducheyne, P. & Adams, C. S. (2005). Apoptosis and survival of osteoblast-like cells are regulated by surface attachment. *J Biol Chem* **280**, 1733-9.

Grobler, G. P., Learmonth, I. D., Bernstein, B. P. & Dower, B. J. (2005). Ten-year results of a press-fit, porous-coated acetabular component. *J Bone Joint Surg Br* **87**, 786-9.

Gronthos, S., Chen, S., Wang, C. Y., Robey, P. G. & Shi, S. (2003). Telomerase accelerates osteogenesis of bone marrow stromal stem cells by upregulation of CBFA1, osterix, and osteocalcin. *J Bone Miner Res* **18**, 716-22.

Gronthos, S., Simmons, P. J., Graves, S. E. & Robey, P. G. (2001). Integrin-mediated interactions between human bone marrow stromal precursor cells and the extracellular matrix. *Bone* **28**, 174-81.

Gronthos, S. & Zannettino, A. C. (2008). A method to isolate and purify human bone marrow stromal stem cells. *Methods Mol Biol* **449**, 45-57.

Guarino, M. (1995). Epithelial-to-mesenchymal change of differentiation. From embryogenetic mechanism to pathological patterns. *Histol Histopathol* **10**, 171-84.

Gundersen, G. G. & Bulinski, J. C. (1988). Selective stabilization of microtubules oriented toward the direction of cell migration. *Proc Natl Acad Sci U S A* **85**, 5946-50.

Guo, W. H., Frey, M. T., Burnham, N. A. & Wang, Y. L. (2006). Substrate rigidity regulates the formation and maintenance of tissues. *Biophys J* **90**, 2213-20.

Gupton, S. L. & Waterman-Storer, C. M. (2006). Spatiotemporal feedback between actomyosin and focal-adhesion systems optimizes rapid cell migration. *Cell* **125**, 1361-74.

Gustafson, T. & Wolpert, L. (1961). Cellular mechanisms in the morphogenesis of the sea urchin larva. The formation of arms. *Exp Cell Res* **22**, 509-20.

Hall, P. A. & Woods, A. L. (1990). Immunohistochemical markers of cellular proliferation: achievements, problems and prospects. *Cell Tissue Kinet* **23**, 505-22.

Hamilton, D. W., Chehroudi, B. & Brunette, D. M. (2007). Comparative response of epithelial cells and osteoblasts to microfabricated tapered pit topographies in vitro and in vivo. *Biomaterials* **28**, 2281-93.

Han, Y., Cowin, S. C., Schaffler, M. B. & Weinbaum, S. (2004). Mechanotransduction and strain amplification in osteocyte cell processes. *Proc Natl Acad Sci U S A* **101**, 16689-94.

Hanarp, P., Sutherland, D., Gold, J. & Kasemo, B. (1999). Nanostructured model biomaterial surfaces prepared by colloidal lithography. *Nanostruct. Mater* **12**, 429-432.

Harris, A. K. (1994). Locomotion of tissue culture cells considered in relation to ameboid locomotion. *Int Rev Cytol* **150**, 35-68.

Hart, A., Gadegaard, N., Wilkinson, C. D., Oreffo, R. O. & Dalby, M. J. (2007). Osteoprogenitor response to low-adhesion nanotopographies originally fabricated by electron beam lithography. *J Mater Sci Mater Med* **18**, 1211-8.

Hautamaki, M. P., Aho, A. J., Alander, P., Rekola, J., Gunn, J., Strandberg, N. & Vallittu, P. K. (2008). Repair of bone segment defects with surface porous fiber-reinforced polymethyl methacrylate (PMMA) composite prosthesis: histomorphometric incorporation model and characterization by SEM. *Acta Orthop* **79**, 555-64.

Hench, L. L. & Polak, J. M. (2002). Third-generation biomedical materials. *Science* **295**, 1014-7.

Hermanto, U., Zong, C. S., Li, W. & Wang, L. H. (2002). RACK1, an insulin-like growth factor I (IGF-I) receptor-interacting protein, modulates IGF-I-dependent integrin signaling and promotes cell spreading and contact with extracellular matrix. *Mol Cell Biol* **22**, 2345-65.

Hernandez, C. J., Majeska, R. J. & Schaffler, M. B. (2004). Osteocyte density in woven bone. *Bone* **35**, 1095-9.

Herrmann, H., Bar, H., Kreplak, L., Strelkov, S. V. & Aebi, U. (2007). Intermediate filaments: from cell architecture to nanomechanics. *Nat Rev Mol Cell Biol* **8**, 562-73.

Heydarkhan-Hagvall, S., Choi, C. H., Dunn, J., Heydarkhan, S., Schenke-Layland, K., MacLellan, W. R. & Beygui, R. E. (2007). Influence of systematically varied nano-scale topography on cell morphology and adhesion. *Cell Commun Adhes* **14**, 181-94.

Hill, T. P., Spater, D., Taketo, M. M., Birchmeier, W. & Hartmann, C. (2005). Canonical Wnt/beta-catenin signaling prevents osteoblasts from differentiating into chondrocytes. *Dev Cell* **8**, 727-38.

Hirayama, Y. & Sumpio, B. E. (2007). Role of ligand-specific integrins in endothelial cell alignment and elongation induced by cyclic strain. *Endothelium* **14**, 275-83.

Hornekaer, L., Baurichter, A., Petrunin, V. V., Luntz, A. C., Kay, B. D. & Al-Halabi, A. (2005). Influence of surface morphology on D2 desorption kinetics from amorphous solid water. *J Chem Phys* **122**, 124701.

Howard, A. & Pelc, S. R. (1951). Synthesis of nucleoprotein in bean root cells. *Nature* **167**, 599-600.

Hu, J., Liu, X. & Ma, P. X. (2008). Induction of osteoblast differentiation phenotype on poly(L-lactic acid) nanofibrous matrix. *Biomaterials* **29**, 3815-21.

Hu, S., Chen, J. & Wang, N. (2004a). Cell spreading controls balance of prestress by microtubules and extracellular matrix. *Front Biosci* **9**, 2177-82.

Hu, S., Eberhard, L., Chen, J., Love, J. C., Butler, J. P., Fredberg, J. J., Whitesides, G. M. & Wang, N. (2004b). Mechanical anisotropy of adherent cells probed by a three-dimensional magnetic twisting device. *Am J Physiol Cell Physiol* **287**, C1184-91.

Hu, W., Yim, E. K. F., Reano, R. M., Leong, K. W. & Pang, S. W. (2005). Effects of nanoimprinted patterns in tissue-culture polystyrene on cell behavior. *J. Vasc. Sci. Technol. B* **23**, 2984-2989.

Hubbell, J. A. (2003). Materials as morphogenetic guides in tissue engineering. *Curr Opin Biotechnol* **14**, 551-8.

Hughes, S., El Haj, A. J. & Dobson, J. (2005). Magnetic micro- and nanoparticle mediated activation of mechanosensitive ion channels. *Med Eng Phys* **27**, 754-62.

Hunter, A., Archer, C. W., Walker, P. S. & Blunn, G. W. (1995). Attachment and proliferation of osteoblasts and fibroblasts on biomaterials for orthopaedic use. *Biomaterials* **16**, 287-95.

Husheem, M., Nyman, J. K., Vaaraniemi, J., Vaananen, H. K. & Hentunen, T. A. (2005). Characterization of circulating human osteoclast progenitors: development of in vitro resorption assay. *Calcif Tissue Int* **76**, 222-30.

Huxley-Jones, J., Robertson, D. L. & Boot-Handford, R. P. (2007). On the origins of the extracellular matrix in vertebrates. *Matrix Biol* **26**, 2-11.

Ingber, D. E. (2003). Tensegrity II. How structural networks influence cellular information processing networks. *J Cell Sci* **116**, 1397-408.

Ingber, D. E. (2006). Cellular mechanotransduction: putting all the pieces together again. *Faseb J* **20**, 811-27.

Ingber, D. E., Prusty, D., Sun, Z., Betensky, H. & Wang, N. (1995). Cell shape, cytoskeletal mechanics, and cell cycle control in angiogenesis. *J Biomech* **28**, 1471-84.

Isaac, J., Loty, S., Hamdan, A., Kokubo, T., Kim, H. M., Berdal, A. & Sautier, J. M. (2008). Bone-like tissue formation on a biomimetic titanium surface in an explant model of osteoconduction. *J Biomed Mater Res A*. **In Press**, DOI: 0.1002/jbm.a.31993

Islamoglu, K., Coskunfirat, O. K., Tetik, G. & Ozgentas, H. E. (2002). Complications and removal rates of miniplates and screws used for maxillofacial fractures. *Ann Plast Surg* **48**, 265-8.

Ismail, F. S., Rohanizadeh, R., Atwa, S., Mason, R. S., Ruys, A. J., Martin, P. J. & Bendavid, A. (2007). The influence of surface chemistry and topography on the contact guidance of MG63 osteoblast cells. *J Mater Sci Mater Med* **18**, 705-14.

Jago, E. R. & Hindley, C. J. (1998). The removal of metalwork in children. *Injury* **29**, 439-41.

Jayaraman, M., Meyer, U., Buhner, M., Joos, U. & Wiesmann, H. P. (2004). Influence of titanium surfaces on attachment of osteoblast-like cells in vitro. *Biomaterials* **25**, 625-31.

Jean, R. P., Gray, D. S., Spector, A. A. & Chen, C. S. (2004). Characterization of the nuclear deformation caused by changes in endothelial cell shape. *J Biomech Eng* **126**, 552-8.

Jin, C. Y., Zhu, B. S., Wang, X. F., Lu, Q. H., Chen, W. T. & Zhou, X. J. (2008). Nanoscale surface topography enhances cell adhesion and gene expression of madine darby canine kidney cells. *J Mater Sci Mater Med* **19**, 2215-22.

Kaiser, J. P., Reinmann, A. & Bruinink, A. (2006). The effect of topographic characteristics on cell migration velocity. *Biomaterials* **27**, 5230-41.

Kalajzic, I., Staal, A., Yang, W. P., Wu, Y., Johnson, S. E., Feyen, J. H., Krueger, W., Maye, P., Yu, F., Zhao, Y., Kuo, L., Gupta, R. R., Achenie, L. E., Wang, H. W., Shin, D. G. & Rowe, D. W. (2005). Expression profile of osteoblast lineage at defined stages of differentiation. *J Biol Chem* **280**, 24618-26.

Kamachi, Y., Cheah, K. S. & Kondoh, H. (1999). Mechanism of regulatory target selection by the SOX high-mobility-group domain proteins as revealed by comparison of SOX1/2/3 and SOX9. *Mol Cell Biol* **19**, 107-20.

Karamichos, D., Brown, R. A. & Mudera, V. (2007). Collagen stiffness regulates cellular contraction and matrix remodeling gene expression. *J Biomed Mater Res A* **83**, 887-94.

Karuri, N. W., Liliensiek, S., Teixeira, A. I., Abrams, G., Campbell, S., Nealey, P. F. & Murphy, C. J. (2004). Biological length scale topography enhances cell-substratum adhesion of human corneal epithelial cells. *J Cell Sci* **117**, 3153-64.

Karuri, N. W., Porri, T. J., Albrecht, R. M., Murphy, C. J. & Nealey, P. F. (2006). Nano- and microscale holes modulate cell-substrate adhesion, cytoskeletal organization, and -beta1 integrin localization in SV40 human corneal epithelial cells. *IEEE Trans Nanobioscience* **5**, 273-80.

Kasperk, C., Schneider, U., Sommer, U., Niethard, F. & Ziegler, R. (1995a). Differential effects of glucocorticoids on human osteoblastic cell metabolism in vitro. *Calcif Tissue Int* **57**, 120-6.

Kasperk, C., Wergedal, J., Strong, D., Farley, J., Wangerin, K., Gropp, H., Ziegler, R. & Baylink, D. J. (1995b). Human bone cell phenotypes differ depending on their skeletal site of origin. *J Clin Endocrinol Metab* **80**, 2511-7.

Katoh, K., Kano, Y. & Ookawara, S. (2007). Rho-kinase dependent organization of stress fibers and focal adhesions in cultured fibroblasts. *Genes Cells* **12**, 623-38.

Keselowsky, B. G., Collard, D. M. & Garcia, A. J. (2003). Surface chemistry modulates fibronectin conformation and directs integrin binding and specificity to control cell adhesion. *J Biomed Mater Res A* **66**, 247-59.

Keselowsky, B. G., Collard, D. M. & Garcia, A. J. (2004). Surface chemistry modulates focal adhesion composition and signaling through changes in integrin binding. *Biomaterials* **25**, 5947-54.

Khatiwala, C. B., Peyton, S. R., Metzke, M. & Putnam, A. J. (2007). The regulation of osteogenesis by ECM rigidity in MC3T3-E1 cells requires MAPK activation. *J Cell Physiol* **211**, 661-72.

Kim, D. H., Kim, P., Suh, K., Kyu Choi, S., Ho Lee, S. & Kim, B. (2005a). Modulation of adhesion and growth of cardiac myocytes by surface nanotopography. *Conf Proc IEEE Eng Med Biol Soc* **4**, 4091-4.

Kim, H. J., Kim, U. J., Kim, H. S., Li, C., Wada, M., Leisk, G. G. & Kaplan, D. L. (2008). Bone tissue engineering with premineralized silk scaffolds. *Bone* **42**, 1226-34.

Kim, J. B., Leucht, P., Luppen, C. A., Park, Y. J., Beggs, H. E., Damsky, C. H. & Helms, J. A. (2007). Reconciling the roles of FAK in osteoblast differentiation, osteoclast remodeling, and bone regeneration. *Bone* **41**, 39-51.

Kim, S. O., Solak, H. H., Stoykovich, M. P., Ferrier, N. J., De Pablo, J. J. & Nealey, P. F. (2003). Epitaxial self-assembly of block copolymers on lithographically defined nanopatterned substrates. *Nature* **424**, 411-4.

Kim, Y. G., Kim, S. Y., Kim, S. J., Park, B. C., Kim, P. T. & Ihn, J. C. (2005b). The use of cementless expansion acetabular component and an alumina-polyethylene bearing in total hip arthroplasty for osteonecrosis. *J Bone Joint Surg Br* **87**, 776-80.

Kimura, W., Yasugi, S., Stern, CD. & Fukuda, K. (2006). Fate and plasticity of the endoderm in the early chick embryo. *Gene Expr Patterns* **6**, 783-93.

Kinder, M., Chislock, E., Bussard, K. M., Shuman, L. & Mastro, A. M. (2008). Metastatic breast cancer induces an osteoblast inflammatory response. *Exp Cell Res* **314**, 173-83.

Kindt, K. S., Viswanath, V., Macpherson, L., Quast, K., Hu, H., Patapoutian, A. & Schafer, W. R. (2007). Caenorhabditis elegans TRPA-1 functions in mechanosensation. *Nat Neurosci* **10**, 568-77.

Klemke, R. L., Cai, S., Giannini, A. L., Gallagher, P. J., de Lanerolle, P. & Cheresh, D. A. (1997). Regulation of cell motility by mitogen-activated protein kinase. *J Cell Biol* **137**, 481-92.

Kline, R. M., Jr. & Wolfe, S. A. (1995). Complications associated with the harvesting of cranial bone grafts. *Plast Reconstr Surg* **95**, 5-13; discussion 14-20.

Knothe Tate, M. L. (2003). "Whither flows the fluid in bone?" An osteocyte's perspective. *J Biomech* **36**, 1409-24.

Konttinen, Y. T., Zhao, D., Beklen, A., Ma, G., Takagi, M., Kivela-Rajamaki, M., Ashammakhi, N. & Santavirta, S. (2005). The microenvironment around total hip replacement prostheses. *Clin Orthop Relat Res* **430**, 28-38.

Koopman, P., Schepers, G., Brenner, S. & Venkatesh, B. (2004). Origin and diversity of the SOX transcription factor gene family: genome-wide analysis in Fugu rubripes. *Gene* **328**, 177-86.

Kosaka, M., Miyanohara, T., Wada, Y. & Kamiishi, H. (2003a). Intracranial migration of fixation wires following correction of craniosynostosis in an infant. *J Craniomaxillofac Surg* **31**, 15-9.

Kosaka, M., Uemura, F., Tomemori, S. & Kamiishi, H. (2003b). Scanning electron microscopic observations of 'fractured' biodegradable plates and screws. *J Craniomaxillofac Surg* **31**, 10-4.

Krasteva, N., Seifert, B., Albrecht, W., Weigel, T., Schossig, M., Altankov, G. & Groth, T. (2004). Influence of polymer membrane porosity on C3A hepatoblastoma cell adhesive interaction and function. *Biomaterials* **25**, 2467-76.

Krishnan, V., Bryant, H. U. & Macdougald, O. A. (2006). Regulation of bone mass by Wnt signaling. *J Clin Invest* **116**, 1202-9.

Kudelska-Mazur, D., Lewandowska-Szumiel, M., Mazur, M. & Komender, J. (2005). Osteogenic cell contact with biomaterials influences phenotype expression. *Cell Tissue Bank* **6**, 55-64.

Kveiborg, M., Flyvbjerg, A., Rattan, S. I. & Kassem, M. (2000). Changes in the insulin-like growth factor-system may contribute to in vitro age-related impaired osteoblast functions. *Exp Gerontol* **35**, 1061-74.

Kveiborg, M., Rattan, S. I., Clark, B. F., Eriksen, E. F. & Kassem, M. (2001). Treatment with 1,25-dihydroxyvitamin D3 reduces impairment of human osteoblast functions during cellular aging in culture. *J Cell Physiol* **186**, 298-306.

Laing, P. G. (1979). Clinical experience with prosthetic materials: historical perspectives, current problems, and future directions. *ASTM-STP* **684**, 199-211.

Laitinen, O. H., Hytonen, V. P., Nordlund, H. R. & Kulomaa, M. S. (2006). Genetically engineered avidins and streptavidins. *Cell Mol Life Sci* **63**, 2992-3017.

Leclerc, E., David, B., Griscom, L., Lepioufle, B., Fujii, T., Layrolle, P. & Legallaisa, C. (2006). Study of osteoblastic cells in a microfluidic environment. *Biomaterials* **27**, 586-95.

Lenhert, S., Meier, M. B., Meyer, U., Chi, L. & Wiesmann, H. P. (2005). Osteoblast alignment, elongation and migration on grooved polystyrene surfaces patterned by Langmuir-Blodgett lithography. *Biomaterials* **26**, 563-70.

Leucht, P., Kim, J. B., Currey, J. A., Brunski, J. & Helms, J. A. (2007). FAK-Mediated mechanotransduction in skeletal regeneration. *PLoS ONE* **2**, e390.

Li, F., Li, B., Wang, Q. M. & Wang, J. H. (2008). Cell shape regulates collagen type I expression in human tendon fibroblasts. *Cell Motil Cytoskeleton* **65**, 332-41.

Liao, H., Andersson, A. S., Sutherland, D., Petronis, S., Kasemo, B. & Thomsen, P. (2003). Response of rat osteoblast-like cells to microstructured model surfaces in vitro. *Biomaterials* **24**, 649-54.

Lie, S. A., Havelin, L. I., Furnes, O. N., Engesaeter, L. B. & Vollset, S. E. (2004). Failure rates for 4762 revision total hip arthroplasties in the Norwegian Arthroplasty Register. *J Bone Joint Surg Br* **86**, 504-9.

Lim, J. Y., Dreiss, A. D., Zhou, Z., Hansen, J. C., Siedlecki, C. A., Hengstebeck, R. W., Cheng, J., Winograd, N. & Donahue, H. J. (2007). The regulation of integrin-mediated osteoblast focal adhesion and focal adhesion kinase expression by nanoscale topography. *Biomaterials* **28**, 1787-97.

Lim, J. Y., Hansen, J. C., Siedlecki, C. A., Hengstebeck, R. W., Cheng, J., Winograd, N. & Donahue, H. J. (2005a). Osteoblast adhesion on poly(L-lactic acid)/polystyrene demixed thin film blends: effect of nanotopography, surface chemistry, and wettability. *Biomacromolecules* **6**, 3319-27.

Lim, J. Y., Hansen, J. C., Siedlecki, C. A., Runt, J. & Donahue, H. J. (2005b). Human foetal osteoblastic cell response to polymer-demixed nanotopographic interfaces. *J R Soc Interface* **2**, 97-108.

Linder, S. (2007). The matrix corroded: podosomes and invadopodia in extracellular matrix degradation. *Trends Cell Biol* **17**, 107-17.

Little, K. (1973). Observations on the nature and production of proteins in the intercellular matrices of connective tissues. *J Pathol* **110**, 1-12.

Liu, G., Meng, X., Jin, Y., Bai, J., Zhao, Y., Cui, X., Chen, F. & Fu, S. (2008a). Inhibitory role of focal adhesion kinase on anoikis in the lung cancer cell A549. *Cell Biol Int* **32**, 663-70.

Liu, S., Calderwood, D. A. & Ginsberg, M. H. (2000). Integrin cytoplasmic domain-binding proteins. *J Cell Sci* **113 (Pt 20)**, 3563-71.

Liu, Z., Zhang, H. M., Yuan, J., Lim, T., Sall, A., Taylor, G. A. & Yang, D. (2008b). Focal adhesion kinase mediates the IGTP-induced PI3K/Akt survival pathway and further initiates a positive feedback loop of NF-kappaB activation. *Cell Microbiol* **10**, 1787-800.

Loesberg, W. A., te Riet, J., van Delft, F. C., Schon, P., Figdor, C. G., Speller, S., van Loon, J. J., Walboomers, X. F. & Jansen, J. A. (2007). The threshold at which substrate nanogroove dimensions may influence fibroblast alignment and adhesion. *Biomaterials* **28**, 3944-51.

Lorz, M., Meyer-Breiting, E. & Bettinger, R. (1994). Proliferating cell nuclear antigen counts as markers of cell proliferation in head and neck cancer. *Eur Arch Otorhinolaryngol* **251**, 91-4.

Lotz, M. M., Burdsal, C. A., Erickson, H. P. & McClay, D. R. (1989). Cell adhesion to fibronectin and tenascin: quantitative measurements of initial binding and subsequent strengthening response. *J Cell Biol* **109**, 1795-805.

Lu, J., Rao, M. P., MacDonald, N. C., Khang, D. & Webster, T. J. (2008). Improved endothelial cell adhesion and proliferation on patterned titanium surfaces with rationally designed, micrometer to nanometer features. *Acta Biomater* **4**, 192-201.

Mack, P. J., Kaazempur-Mofrad, M. R., Karcher, H., Lee, R. T. & Kamm, R. D. (2004). Force-induced focal adhesion translocation: effects of force amplitude and frequency. *Am J Physiol Cell Physiol* **287**, C954-62.

Mann, V., Huber, C., Kogianni, G., Jones, D. & Noble, B. (2006). The influence of mechanical stimulation on osteocyte apoptosis and bone viability in human trabecular bone. *J Musculoskelet Neuronal Interact* **6**, 408-17.

Marchisio, M., Di Carmine, M., Pagone, R., Piattelli, A. & Miscia, S. (2005). Implant surface roughness influences osteoclast proliferation and differentiation. *J Biomed Mater Res B Appl Biomater* **75**, 251-6.

Martines, E., McGhee, K., Wilkinson, C. & Curtis, A. (2004). A parallel-plate flow chamber to study initial cell adhesion on a nano-featured surface. *IEEE Trans Nanobioscience* **3**, 90-95.

Martines, E., Seunarine, K., Morgan, H., Gadegaard, N., Wilkinson, C. D. & Riehle, M. O. (2005). Superhydrophobicity and superhydrophilicity of regular nanopatterns. *Nano Lett* **5**, 2097-103.

Matsuzaka, K., Walboomers, F., de Ruijter, A. & Jansen, J. A. (2000). Effect of microgrooved poly-l-lactic (PLA) surfaces on proliferation, cytoskeletal organization, and mineralized matrix formation of rat bone marrow cells. *Clin Oral Implants Res* **11**, 325-33.

McCreadie, B. R., Hollister, S. J., Schaffler, M. B. & Goldstein, S. A. (2004). Osteocyte lacuna size and shape in women with and without osteoporotic fracture. *J Biomech* **37**, 563-72.

McCulloch, E. A., Till, J. E. & Siminovitch, L. (1965). The role of independent and dependent stem cells in the control of hemopoietic and immunologic responses. *Wistar Inst Symp Monogr* **4**, 61-8.

Meerovitch, K., Bergeron, F., Leblond, L., Grouix, B., Poirier, C., Bubenik, M., Chan, L., Gourdeau, H., Bowlin, T. & Attardo, G. (2003). A novel RGD antagonist that targets both alphavbeta3 and alpha5beta1 induces apoptosis of angiogenic endothelial cells on type I collagen. *Vascul Pharmacol* **40**, 77-89.

Mendelsohn, C., Ruberte, E., LeMeur, M., Morriss-Kay, G. & Chambon, P. (1991). Developmental analysis of the retinoic acid-inducible RAR-beta 2 promoter in transgenic animals. *Development* **113**, 723-34.

Meredith, D. O., Owen, G. R., ap Gwynn, I. & Richards, R. G. (2004). Variation in cell-substratum adhesion in relation to cell cycle phases. *Exp Cell Res* **293**, 58-67.

Meyer, P. C. (1956). The histological identification of osteoid tissue. *J Pathol Bacteriol* **71**, 325-33.

Milner, K. R. & Siedlecki, C. A. (2007). Submicron poly(L-lactic acid) pillars affect fibroblast adhesion and proliferation. *J Biomed Mater Res A* **82**, 80-91.

Mirmalek-Sani, S. H., Tare, R. S., Morgan, S. M., Roach, H. I., Wilson, D. I., Hanley, N. A. & Oreffo, R. O. (2006). Characterization and multipotentiality of human fetal femur-derived cells: implications for skeletal tissue regeneration. *Stem Cells* **24**, 1042-53.

Mokry, J. & Nemecek, S. (1995). Immunohistochemical detection of proliferative cells. *Sb Ved Pr Lek Fak Karlovy Univerzity Hradci Kralove* **38**, 107-13.

Montjovent, M. O., Burri, N., Mark, S., Federici, E., Scaletta, C., Zambelli, P. Y., Hohlfeld, P., Leyvraz, P. F., Applegate, L. L. & Pioletti, D. P. (2004). Fetal bone cells for tissue engineering. *Bone* **35**, 1323-33.

Mulari, M. T., Qu, Q., Harkonen, P. L. & Vaananen, H. K. (2004). Osteoblast-like cells complete osteoclastic bone resorption and form new mineralized bone matrix in vitro. *Calcif Tissue Int* **75**, 253-61.

Narayanan, N., Jones, D. L., Xu, A. & Yu, J. C. (1996). Effects of aging on sarcoplasmic reticulum function and contraction duration in skeletal muscles of the rat. *Am J Physiol* **271**, C1032-40.

Navarro, M., Michiardi, A., Castano, O. & Planell, J. A. (2008). Biomaterials in orthopaedics. *J R Soc Interface* **5**, 1137-58.

Nicolas, A., Geiger, B. & Safran, S. A. (2004). Cell mechanosensitivity controls the anisotropy of focal adhesions. *Proc Natl Acad Sci U S A* **101**, 12520-5.

Niemela, T., Niiranen, H., Kellomaki, M. & Tormala, P. (2005). Self-reinforced composites of bioabsorbable polymer and bioactive glass with different bioactive glass contents. Part I: Initial mechanical properties and bioactivity. *Acta Biomater* **1**, 235-42.

Noren, N. K., Liu, B. P., Burridge, K. & Kreft, B. (2000). p120 catenin regulates the actin cytoskeleton via Rho family GTPases. *J Cell Biol* **150**, 567-80.

Norman, J. J. & Desai, T. A. (2006). Methods for fabrication of nanoscale topography for tissue engineering scaffolds. *Ann Biomed Eng* **34**, 89-101.

Ogawa, T., Saruwatari, L., Takeuchi, K., Aita, H. & Ohno, N. (2008). Ti nano-nodular structuring for bone integration and regeneration. *J Dent Res* **87**, 751-6.

Ohara, P. T. & Buck, R. C. (1979). Contact guidance in vitro. A light, transmission, and scanning electron microscopic study. *Exp Cell Res* **121**, 235-49.

Oikawa, T., Itoh, T. & Takenawa, T. (2008). Sequential signals toward podosome formation in NIH-src cells. *J Cell Biol* **182**, 157-69.

Oka, K., Oka, S., Sasaki, T., Ito, Y., Bringas, P., Jr., Nonaka, K. & Chai, Y. (2007). The role of TGF-beta signaling in regulating chondrogenesis and osteogenesis during mandibular development. *Dev Biol* **303**, 391-404.

Oleschuk, R. D., McComb, M. E., Chow, A., Ens, W., Standing, K. G., Perreault, H., Marois, Y. & King, M. (2000). Characterization of plasma proteins adsorbed onto biomaterials. By MALDI-TOFMS. *Biomaterials* **21**, 1701-10.

Oreffo, R. O., Cooper, C., Mason, C. & Clements, M. (2005). Mesenchymal stem cells: lineage, plasticity, and skeletal therapeutic potential. *Stem Cell Rev* **1**, 169-78.

Orgel, J. P., Irving, T. C., Miller, A. & Wess, T. J. (2006). Microfibrillar structure of type I collagen in situ. *Proc Natl Acad Sci U S A* **103**, 9001-5.

Ormo, M., Cubitt, A. B., Kallio, K., Gross, L. A., Tsien, R. Y. & Remington, S. J. (1996). Crystal structure of the Aequorea victoria green fluorescent protein. *Science* **273**, 1392-5.

Osborne, C. S., Chakalova, L., Brown, K. E., Carter, D., Horton, A., Debrand, E., Goyenechea, B., Mitchell, J. A., Lopes, S., Reik, W. & Fraser, P. (2004). Active genes dynamically colocalize to shared sites of ongoing transcription. *Nat Genet* **36**, 1065-71.

Ottani, V., Martini, D., Franchi, M., Ruggeri, A. & Raspanti, M. (2002). Hierarchical structures in fibrillar collagens. *Micron* **33**, 587-96.

Owen, G. R., Meredith, D. O., Ap Gwynn, I. & Richards, R. G. (2001). Enhancement of immunogold-labelled focal adhesion sites in fibroblasts cultured on metal substrates: problems and solutions. *Cell Biol Int* **25**, 1251-9.

Owen, G. R., Meredith, D. O., ap Gwynn, I. & Richards, R. G. (2002). Simultaneously identifying S-phase labelled cells and immunogold-labelling of vinculin in focal adhesions. *J Microsc* **207**, 27-36.

Palumbo, C., Ferretti, M. & Marotti, G. (2004). Osteocyte dendrogenesis in static and dynamic bone formation: an ultrastructural study. *Anat Rec A Discov Mol Cell Evol Biol* **278**, 474-80.

Pancer, Z., Kruse, M., Muller, I. & Muller, W. E. (1997). On the origin of Metazoan adhesion receptors: cloning of integrin alpha subunit from the sponge Geodia cydonium. *Mol Biol Evol* **14**, 391-8.

Pavalko, F. M., Norvell, S. M., Burr, D. B., Turner, C. H., Duncan, R. L. & Bidwell, J. P. (2003). A model for mechanotransduction in bone cells: the load-bearing mechanosomes. *J Cell Biochem* **88**, 104-12.

Pawlicki, R. (1975). Bone canaliculus endings in the area of the osteocyte lacuna. Electron-microscopic studies. *Acta Anat (Basel)* **91**, 292-304.

Pearce, A. I., Pearce, S. G., Schwieger, K., Milz, S., Schneider, E., Archer, C. W. & Richards, R. G. (2008). Effect of surface topography on removal of cortical bone screws in a novel sheep model. *J Orthop Res* **26**, 1377-83.

Pelc, S. R. & Howard, A. (1952). Techniques of autoradiography and the application of the stripping-film method to problems of nuclear metabolism. *Br Med Bull* **8**, 132-5.

Pellegrin, S. & Mellor, H. (2007). Actin stress fibres. *J Cell Sci* **120**, 3491-9.

Perkins, S. J., Nealis, A. S., Dudhia, J. & Hardingham, T. E. (1989). Immunoglobulin fold and tandem repeat structures in proteoglycan N-terminal domains and link protein. *J Mol Biol* **206**, 737-53.

Pfeilschifter, J., Diel, I., Pilz, U., Brunotte, K., Naumann, A. & Ziegler, R. (1993). Mitogenic responsiveness of human bone cells in vitro to hormones and growth factors decreases with age. *J Bone Miner Res* **8**, 707-17.

Piters, E., Boudin, E. & Van Hul, W. (2008). Wnt signaling: A win for bone. *Arch Biochem Biophys* **473**, 112-6.

Pollard, T. D. (2003). The cytoskeleton, cellular motility and the reductionist agenda. *Nature* **422**, 741-5.

Prendergast, F. G. & Mann, K. G. (1978). Chemical and physical properties of aequorin and the green fluorescent protein isolated from Aequorea forskalea. *Biochemistry* **17**, 3448-53.

Quarto, R., Mastrogiacomo, M., Cancedda, R., Kutepov, S. M., Mukhachev, V., Lavroukov, A., Kon, E. & Marcacci, M. (2001). Repair of large bone defects with the use of autologous bone marrow stromal cells. *N Engl J Med* **344**, 385-6.

Quattrocchi, C. C., Piciucchi, S., Sammarra, M., Santini, D., Vincenzi, B., Tonini, G., Grasso, R. F. & Zobel, B. B. (2007). Bone metastases in breast cancer: higher prevalence of osteosclerotic lesions. *Radiol Med (Torino)* **112**, 1049-59.

Race, A., Miller, M. A. & Mann, K. A. (2008). A modified PMMA cement (Sub-cement) for accelerated fatigue testing of cemented implant constructs using cadaveric bone. *J Biomech* **41**, 3017-23.

Raghoebar, G. M., Louwerse, C., Kalk, W. W. & Vissink, A. (2001). Morbidity of chin bone harvesting. *Clin Oral Implants Res* **12**, 503-7.

Rho, J. Y., Kuhn-Spearing, L. & Zioupos, P. (1998). Mechanical properties and the hierarchical structure of bone. *Med Eng Phys* **20**, 92-102.

Ricard-Blum, S. & Ruggiero, F. (2005). The collagen superfamily: from the extracellular matrix to the cell membrane. *Pathol Biol (Paris)* **53**, 430-42.

Richards, R. G. & Ap Gwynn, I. (1995). Backscattered electron imaging of the undersurface of resin-embedded cells by field emission scanning electron microscopy. **177**, 43-52.

Richards, R. G., Lloyd, P. C., Rahn, B. A. & Gwynn, I. A. (1993). A new method for investigating the undersurface of cell monolayers by scanning electron microscopy. *J Microsc* **171**, 205-13.

Richards, R. G., Rahn, B. A. & ap Gwynn, I. (1997). A quantitative method of measuring cell adhesion areas. Review. *Cells and Materials* **7**, 15-30.

Richards, R. G., Stiffanic, M., Owen, G. R., Riehle, M., Ap Gwynn, I. & Curtis, A. S. (2001a). Immunogold labelling of fibroblast focal adhesion sites visualised in fixed material using scanning electron microscopy, and living, using internal reflection microscopy. *Cell Biol Int* **25**, 1237-49.

Richards, R. G., Stiffanic, M., Owen, G. R., Riehle, M., Ap Gwynn, I. & Curtis, A. S. (2001b). Immunogold labelling of fibroblast focal adhesion sites visualised in fixed material using scanning electron microscopy, and living, using internal reflection microscopy. *Cell Biol Int.* **25**, 1237-49.

Ring, D. (2008). Displaced, unstable fractures of the radial head: Fixation vs. replacement-What is the evidence? *Injury* **39**, 1329-37.

Ripamonti, U., Richter, P. W., Nilen, R. W. & Renton, L. (2008). The induction of bone formation by smart biphasic hydroxyapatite tricalcium phosphate biomimetic matrices in the non-human primate Papio ursinus. *J Cell Mol Med*. **In Press**, DOI: 10.1111/j.1582-4934.2008.00312.x.

Rubin, M. A., Rubin, J. & Jasiuk, I. (2004). SEM and TEM study of the hierarchical structure of C57BL/6J and C3H/HeJ mice trabecular bone. *Bone* **35**, 11-20.

Ruppel, M. E., Miller, L. M. & Burr, D. B. (2008). The effect of the microscopic and nanoscale structure on bone fragility. *Osteoporos Int* **19**, 1251-65.

Saez, A., Ghibaudo, M., Buguin, A., Silberzan, P. & Ladoux, B. (2007). Rigidity-driven growth and migration of epithelial cells on microstructured anisotropic substrates. *Proc Natl Acad Sci U S A* **104**, 8281-6.

Salaycik, K. J., Fagerstrom, C. J., Murthy, K., Tulu, U. S. & Wadsworth, P. (2005). Quantification of microtubule nucleation, growth and dynamics in wound-edge cells. *J Cell Sci* **118**, 4113-22.

San Thian, E., Ahmad, Z., Huang, J., Edirisinghe, M. J., Jayasinghe, S. N., Ireland, D. C., Brooks, R. A., Rushton, N., Bonfield, W. & Best, S. M. (2008). The role of electrosprayed apatite nanocrystals in guiding osteoblast behaviour. *Biomaterials* **29**, 1833-43.

Sanderson, P. L., Ryan, W. & Turner, P. G. (1992). Complications of metalwork removal. *Injury* **23**, 29-30.

Santiago, A. S., Santos, E. A., Sader, M. S., Santiago, M. F. & Soares Gde, A. (2005). Response of osteoblastic cells to titanium submitted to three different surface treatments. *Pesqui Odontol Bras* **19**, 203-8.

Sathananthan, A. H. & Trounson, A. (2005). Human embryonic stem cells and their spontaneous differentiation. *Ital J Anat Embryol* **110**, 151-7.

Sato, M., Aslani, A., Sambito, M. A., Kalkhoran, N. M., Slamovich, E. B. & Webster, T. J. (2008). Nanocrystalline hydroxyapatite/titania coatings on titanium improves osteoblast adhesion. *J Biomed Mater Res A* **84**, 265-72.

Schaller, M. D., Borgman, C. A., Cobb, B. S., Vines, R. R., Reynolds, A. B. & Parsons, J. T. (1992). pp125FAK a structurally distinctive protein-tyrosine kinase associated with focal adhesions. *Proc Natl Acad Sci U S A* **89**, 5192-6.

Schlunck, G., Han, H., Wecker, T., Kampik, D., Meyer-ter-Vehn, T. & Grehn, F. (2008). Substrate rigidity modulates cell matrix interactions and protein expression in human trabecular meshwork cells. *Invest Ophthalmol Vis Sci* **49**, 262-9.

Schneider, G. B., Zaharias, R., Seabold, D., Keller, J. & Stanford, C. (2004). Differentiation of preosteoblasts is affected by implant surface microtopographies. *J Biomed Mater Res A* **69**, 462-8.

Schwarz, U. S., Erdmann, T. & Bischofs, I. B. (2006). Focal adhesions as mechanosensors: the two-spring model. *Biosystems* **83**, 225-32.

Seebeck, J., Goldhahn, J., Morlock, M. M. & Schneider, E. (2005). Mechanical behavior of screws in normal and osteoporotic bone. *Osteoporos Int* **16 Suppl 2**, S107-11.

Shi, S., Gronthos, S., Chen, S., Reddi, A., Counter, C. M., Robey, P. G. & Wang, C. Y. (2002). Bone formation by human postnatal bone marrow stromal stem cells is enhanced by telomerase expression. *Nat Biotechnol* **20**, 587-91.

Shibahara, T., Noma, H., Furuya, Y. & Takaki, R. (2002). Fracture of mandibular reconstruction plates used after tumor resection. *J Oral Maxillofac Surg* **60**, 182-5.

Sieg, D. J., Hauck, C. R. & Schlaepfer, D. D. (1999). Required role of focal adhesion kinase (FAK) for integrin-stimulated cell migration. *J Cell Sci* **112 (Pt 16)**, 2677-91.

Simmons, P. J. & Torok-Storb, B. (1991). Identification of stromal cell precursors in human bone marrow by a novel monoclonal antibody, STRO-1. *Blood* **78**, 55-62.

Smith, L. L., Niziolek, P. J., Haberstroh, K. M., Nauman, E. A. & Webster, T. J. (2007). Decreased fibroblast and increased osteoblast adhesion on nanostructured NaOH-etched PLGA scaffolds. *Int J Nanomedicine* **2**, 383-8.

Song, J. H., Kim, J. H., Park, S., Kang, W., Kim, H. W., Kim, H. E. & Jang, J. H. (2008). Signaling responses of osteoblast cells to hydroxyapatite: the activation of ERK and SOX9. *J Bone Miner Metab* **26**, 138-42.

Steinhardt, Y., Aslan, H., Regev, E., Zilberman, Y., Kallai, I., Gazit, D. & Gazit, Z. (2008). Maxillofacial-Derived Stem Cells Regenerate Critical Mandibular Bone Defect. *Tissue Eng Part A* **14**, 1763-73.

Stenderup, K., Justesen, J., Eriksen, E. F., Rattan, S. I. & Kassem, M. (2001). Number and proliferative capacity of osteogenic stem cells are maintained during aging and in patients with osteoporosis. *J Bone Miner Res* **16**, 1120-9.

Steven, F. S. (1972). Current concepts of collagen structure. *Clin Orthop Relat Res* **85**, 257-74.

Stupack, D. G., Puente, X. S., Boutsaboualoy, S., Storgard, C. M. & Cheresh, D. A. (2001). Apoptosis of adherent cells by recruitment of caspase-8 to unligated integrins. *J Cell Biol* **155**, 459-70.

Suh, C. W., Kim, M. Y., Choo, J. B., Kim, J. K., Kim, H. K. & Lee, E. K. (2004). Analysis of protein adsorption characteristics to nano-pore silica particles by using confocal laser scanning microscopy. *J Biotechnol* **112**, 267-77.

Suska, F., Emanuelsson, L., Johansson, A., Tengvall, P. & Thomsen, P. (2007). Fibrous capsule formation around titanium and copper. *J Biomed Mater Res A* **85**, 888-96.

Suter, D. M. & Forscher, P. (2000). Substrate-cytoskeletal coupling as a mechanism for the regulation of growth cone motility and guidance. *J Neurobiol* **44**, 97-113.

Sutherland, J., Denyer, M. & Britland, S. (2005). Contact guidance in human dermal fibroblasts is modulated by population pressure. *J Anat* **206**, 581-7.

Suuronen, R. (1993). Biodegradable fracture-fixation devices in maxillofacial surgery. *Int J Oral Maxillofac Surg* **22**, 50-7.

Tabata, Y. (2001). Recent progress in tissue engineering. *Drug Discov Today* **6**, 483-487.

Tabata, Y. (2004). Tissue regeneration based on tissue engineering technology. *Congenit Anom (Kyoto)* **44**, 111-24.

Takash, W., Canizares, J., Bonneaud, N., Poulat, F., Mattei, M. G., Jay, P. & Berta, P. (2001). SOX7 transcription factor: sequence, chromosomal localisation, expression, transactivation and interference with Wnt signalling. *Nucleic Acids Res* **29**, 4274-83.

Tamkun, J. W., DeSimone, D. W., Fonda, D., Patel, R. S., Buck, C., Horwitz, A. F. & Hynes, R. O. (1986). Structure of integrin, a glycoprotein involved in the transmembrane linkage between fibronectin and actin. *Cell* **46**, 271-82.

Tan, J. L., Tien, J., Pirone, D. M., Gray, D. S., Bhadriraju, K. & Chen, C. S. (2003). Cells lying on a bed of microneedles: an approach to isolate mechanical force. *Proc Natl Acad Sci U S A* **100**, 1484-9.

Tanaka, M., Takayama, A., Ito, E., Sunami, H., Yamamoto, S. & Shimomura, M. (2007). Effect of pore size of self-organized honeycomb-patterned polymer films on spreading, focal adhesion, proliferation, and function of endothelial cells. *J Nanosci Nanotechnol* **7**, 763-72.

Tanaka, Y., Nakayamada, S. & Okada, Y. (2005). Osteoblasts and osteoclasts in bone remodeling and inflammation. *Curr Drug Targets Inflamm Allergy* **4**, 325-8.

Tare, R. S., Babister, J. C., Kanczler, J. & Oreffo, R. O. (2008). Skeletal stem cells: phenotype, biology and environmental niches informing tissue regeneration. *Mol Cell Endocrinol* **288**, 11-21.

Teixeira, A. I., Abrams, G. A., Bertics, P. J., Murphy, C. J. & Nealey, P. F. (2003). Epithelial contact guidance on well-defined micro- and nanostructured substrates. *J Cell Sci* **116**, 1881-92.

Teixeira, A. I., McKie, G. A., Foley, J. D., Bertics, P. J., Nealey, P. F. & Murphy, C. J. (2006). The effect of environmental factors on the response of human corneal epithelial cells to nanoscale substrate topography. *Biomaterials* **27**, 3945-54.

Teixeira, A. I., Nealey, P. F. & Murphy, C. J. (2004). Responses of human keratocytes to micro- and nanostructured substrates. *J Biomed Mater Res A* **71**, 369-76.

Tran, A. D., Marmo, T. P., Salam, A. A., Che, S., Finkelstein, E., Kabarriti, R., Xenias, H. S., Mazitschek, R., Hubbert, C., Kawaguchi, Y., Sheetz, M. P., Yao, T. P. & Bulinski, J. C. (2007). HDAC6 deacetylation of tubulin modulates dynamics of cellular adhesions. *J Cell Sci* **120**, 1469-79.

Triplett, J. W. & Pavalko, F. M. (2006). Disruption of alpha-actinin-integrin interactions at focal adhesions renders osteoblasts susceptible to apoptosis. *Am J Physiol Cell Physiol* **291**, C909-21.

Turvey, T. A., Bell, R. B., Tejera, T. J. & Proffit, W. R. (2002). The use of self-reinforced biodegradable bone plates and screws in orthognathic surgery. *J Oral Maxillofac Surg* **60**, 59-65.

Vakonakis, I. & Campbell, I. D. (2007). Extracellular matrix: from atomic resolution to ultrastructure. *Curr Opin Cell Biol* **19**, 578-83.

Wagner, H. D. & Weiner, S. (1992). On the relationship between the microstructure of bone and its mechanical stiffness. *J Biomech* **25**, 1311-20.

Wan, Y., Wang, Y., Liu, Z., Qu, X., Han, B., Bei, J. & Wang, S. (2005). Adhesion and proliferation of OCT-1 osteoblast-like cells on micro- and nano-scale topography structured poly(l-lactide). *Biomaterials* **26**, 4453-9.

Wang, N. & Suo, Z. (2005). Long-distance propagation of forces in a cell. *Biochem Biophys Res Commun* **328**, 1133-8.

Ward, M. D & Hammer, W. A. (1993). A theoretical analysis for the effect of focal contact formation on cell-substrate attachment strength. *Biophys J* **64**, 936-59.

Watanabe, H. (1965). Electron microscopic studies on the ossification in chick tibia. I. Endochondral ossification. *Kumamoto Med J* **18**, 45-63.

Weinger, J. M. & Holtrop, M. E. (1974). An ultrastructural study of bone cells: the occurrence of microtubules, microfilaments and tight junctions. *Calcif Tissue Res* **14**, 15-29.

Weipoltshammer, K., Schofer, C., Almeder, M. & Wachtler, F. (2000). Signal enhancement at the electron microscopic level using Nanogold and gold-based autometallography. *Histochem Cell Biol* **114**, 489-95.

Westermann, S. & Weber, K. (2003). Post-translational modifications regulate microtubule function. *Nat Rev Mol Cell Biol* **4**, 938-47.

Wilkinson, C. D. (2004). Making structures for cell engineering. *Eur Cell Mater* **8**, 21-6.

Wiltfang, J., Kessler, P., Buchfelder, M., Merten, H. A., Neukam, F. W. & Rupprecht, S. (2004). Reconstruction of skull bone defects using the hydroxyapatite cement with calvarial split transplants. *J Oral Maxillofac Surg* **62**, 29-35.

Wojciak-Stothard, B., Curtis, A., Monaghan, W., MacDonald, K. & Wilkinson, C. (1996). Guidance and activation of murine macrophages by nanometric scale topography. *Exp Cell Res* **223**, 426-35.

Wolter, J. R. & Meyer, R. F. (1984). Sessile macrophages forming clear endothelium-like membrane on inside of successful keratoprosthesis. *Trans Am Ophthalmol Soc* **82**, 187-202.

Wood, M. A. (2007). Colloidal lithography and current fabrication techniques producing in-plane nanotopography for biological applications. *J R Soc Interface* **4**, 1-17.

Wood, M. A., Bagnaninchi, P. & Dalby, M. J. (2008). The beta integrins and cytoskeletal nanoimprinting. *Exp Cell Res* **314**, 927-35.

Woodman, L., Siddiqui, S., Cruse, G., Sutcliffe, A., Saunders, R., Kaur, D., Bradding, P. & Brightling, C. (2008). Mast cells promote airway smooth muscle cell differentiation via autocrine up-regulation of TGF-beta1. *J Immunol* **181**, 5001-7.

Wozniak, M. A., Modzelewska, K., Kwong, L. & Keely, P. J. (2004). Focal adhesion regulation of cell behavior. *Biochim Biophys Acta* **1692**, 103-19.

Xia, H., Nho, R. S., Kahm, J., Kleidon, J. & Henke, C. A. (2004). Focal adhesion kinase is upstream of phosphatidylinositol 3-kinase/Akt in regulating fibroblast survival in response to contraction of type I collagen matrices via a beta 1 integrin viability signaling pathway. *J Biol Chem* **279**, 33024-34.

Xia, N., Thodeti, C. K., Hunt, T. P., Xu, Q., Ho, M., Whitesides, G. M., Westervelt, R. & Ingber, D. E. (2008). Directional control of cell motility through focal adhesion positioning and spatial control of Rac activation. *Faseb J* **22**, 1649-59.

Xu, L. C. & Siedlecki, C. A. (2007). Effects of surface wettability and contact time on protein adhesion to biomaterial surfaces. *Biomaterials* **28**, 3273-83.

Yamaguchi, M., Shinbo, T., Kanamori, T., Wang, P. C., Niwa, M., Kawakami, H., Nagaoka, S., Hirakawa, K. & Kamiya, M. (2004). Surface modification of poly(L:-lactic acid) affects initial cell attachment, cell morphology, and cell growth. *J Artif Organs* **7**, 187-93.

Yamashita, J., Li, X., Furman, B. R., Rawls, H. R., Wang, X. & Agrawal, C. M. (2002). Collagen and bone viscoelasticity: a dynamic mechanical analysis. *J Biomed Mater Res* **63**, 31-6.

Yanai, T., Matsumoto, C., Takashima, H., Yoshida, K., Sakai, H., Isowa, K., Iwasaki, T., Sato, Y. & Masegi, T. (1996). Immunohistochemical demonstration of S-phase cells by anti-bromodeoxyuridine monoclonal antibody in cattle tissues. *J Comp Pathol* **114**, 265-72.

Yang, X., Walboomers, X. F., van den Beucken, J. J., Bian, Z., Fan, M. & Jansen, J. A. (2008). Hard Tissue Formation of STRO-1-Selected Rat Dental Pulp Stem Cells In Vivo. *Tissue Eng Part A*. **In Press**, DOI: 10.1089/ten.tea.2008.0133.

Yerit, K. C., Enislidis, G., Schopper, C., Turhani, D., Wanschitz, F., Wagner, A., Watzinger, F. & Ewers, R. (2002). Fixation of mandibular fractures with biodegradable plates and screws. *Oral Surg Oral Med Oral Pathol Oral Radiol Endod* **94**, 294-300.

Yim, E. K., Pang, S. W. & Leong, K. W. (2007). Synthetic nanostructures inducing differentiation of human mesenchymal stem cells into neuronal lineage. *Exp Cell Res* **313**, 1820-9.

Yoneda, A., Ushakov, D., Multhaupt, H. A. & Couchman, J. R. (2007). Fibronectin matrix assembly requires distinct contributions from Rho kinases I and -II. *Mol Biol Cell* **18**, 66-75.

You, L. D., Weinbaum, S., Cowin, S. C. & Schaffler, M. B. (2004). Ultrastructure of the osteocyte process and its pericellular matrix. *Anat Rec A Discov Mol Cell Evol Biol* **278**, 505-13.

Zaffe, D., Bertoldi, C. & Consolo, U. (2003). Element release from titanium devices used in oral and maxillofacial surgery. *Biomaterials* **24**, 1093-9.

Zagris, N. (2001). Extracellular matrix in development of the early embryo. *Micron* **32**, 427-38.

Zaidel-Bar, R., Cohen, M., Addadi, L. & Geiger, B. (2004). Hierarchical assembly of cell-matrix adhesion complexes. *Biochem Soc Trans* **32**, 416-20.

Zamir, E., Katz, M., Posen, Y., Erez, N., Yamada, K. M., Katz, B. Z., Lin, S., Lin, D. C., Bershadsky, A., Kam, Z. & Geiger, B. (2000). Dynamics and segregation of cell-matrix adhesions in cultured fibroblasts. *Nat Cell Biol* **2**, 191-6.

Zannettino, A. C., Harrison, K., Joyner, C. J., Triffitt, J. T. & Simmons, P. J. (2003). Molecular cloning of the cell surface antigen identified by the osteoprogenitor-specific monoclonal antibody, HOP-26. *J Cell Biochem* **89**, 56-66.

Zhang, Y., Tanner, K. E., Gurav, N. & Di Silvio, L. (2007). In vitro osteoblastic response to 30 vol% hydroxyapatite-polyethylene composite. *J Biomed Mater Res A* **81**, 409-17.

Zhang, Z., Vuori, K., Reed, J. C. & Ruoslahti, E. (1995). The alpha 5 beta 1 integrin supports survival of cells on fibronectin and up-regulates Bcl-2 expression. *Proc Natl Acad Sci U S A* **92**, 6161-5.

Zhu, B., Lu, Q., Yin, J., Hu, J. & Wang, Z. (2005). Alignment of osteoblast-like cells and cell-produced collagen matrix induced by nanogrooves. *Tissue Eng* **11**, 825-34.

Zhu, B., Zhang, Q., Lu, Q., Xu, Y., Yin, J., Hu, J. & Wang, Z. (2004). Nanotopographical guidance of C6 glioma cell alignment and oriented growth. *Biomaterials* **25**, 4215-23.

Ziegler, W. H., Gingras, A. R., Critchley, D. R. & Emsley, J. (2008). Integrin connections to the cytoskeleton through talin and vinculin. *Biochem Soc Trans* **36**, 235-9.

Zimerman, B., Volberg, T. & Geiger, B. (2004). Early molecular events in the assembly of the focal adhesion-stress fiber complex during fibroblast spreading. *Cell Motil Cytoskeleton* **58**, 143-59.

Zinger, O., Anselme, K., Denzer, A., Habersetzer, P., Wieland, M., Jeanfils, J., Hardouin, P. & Landolt, D. (2004). Time-dependent morphology and adhesion of

osteoblastic cells on titanium model surfaces featuring scale-resolved topography. *Biomaterials* **25**, 2695-711.